KU LEUVEN

ARENBERG DOCTORAL SCHOOL
Faculty of Engineering Science

Dynamic analysis of a wind turbine gearbox

Towards prediction of mechanical tonalities

Frederik Vanhollebeke

Dissertation presented in partial fulfillment of the requirements for the degree of Doctor in Engineering

January 2015

Dynamic analysis of a wind turbine gearbox

Towards prediction of mechanical tonalities

Frederik VANHOLLEBEKE

Examination committee:
Prof. dr. ir. P. Wollants, chair
Prof. dr. ir. W. Desmet, supervisor
Prof. dr. ir. D. Vandepitte, co-supervisor
Prof. dr. ir. P. Sas
Prof. dr. ir. K. Meerbergen
Dr. ir. J. Peeters
Prof. dr. ir. H. Van Der Auweraer

Prof. dr. ir. G. Jacobs
(CWD - RWTH Aachen University)

Dissertation presented in partial fulfillment of the requirements for the degree of Doctor in Engineering

January 2015

ISBN 978-94-6018-942-5

D/2015/7515/2

Preface

In 2007 startte ik mijn loopbaan bij het toenmalige Hansen Transmissions in de Technology groep van Roger Bogaert. Samen met m'n meest directe collega's Joris, Ben en Sonja zetten we onze schouders onder alles wat te maken had met loads, dynamica, trillingen en geluid van windturbine tandwielkasten. Het was vooral dit laatste wat me uitermate aansprak: trillingen en geluid en dit toegepast in een nieuw domein namelijk de windturbine industrie. Een doctoraat had ik na mijn studies wel overwogen, maar aan de kant geschoven wegens naar mijn eigen mening te academisch en te weinig toegepast. Toen Bert Pluymers me inlichtte over de mogelijkheden van een Baekeland doctoraat was ik onmiddellijk verkocht: het praktische en toegepaste uit de industrie combineren met diepgaande inzichten en ondersteuning vanuit de academische wereld om een praktisch en relevant vraagstuk op te lossen. Ik denk dat dit onderzoek ook zonder Baekeland mandaat uitgevoerd zou worden, maar ben er zeker van dat de combinatie van industrie en academische wereld dit doctoraat, met deze tekst als één van de resultaten, diepgaander en relevanter gemaakt heeft. Aan het begin van deze tekst zou ik graag een oprecht woord van dank richten aan iedereen die me hierbij geholpen heeft.

Vooreerst wil ik mijn beide promotoren Joris Peeters en Wim Desmet bedanken. Joris, bedankt om me op een zondagnamiddag in januari 2007 op te bellen om me te informeren over een job opportuniteit bij Hansen Transmissions, een kans die ik met beide handen gegrepen heb. Dank voor het vertrouwen die je in me gesteld hebt en de kansen die je me gegeven hebt, je was voor mij de ideale industriële promotor, mentor, collega en baas. Wim, dank je wel voor onze interessante discussies en meetings, dank je wel voor de grote vrijheid en academische ondersteuning die je me gegeven hebt tijdens mijn onderzoek. Ik voelde me naast Hansen en later ZF-medewerker ook echt lid van je, aanvankelijk kleine, maar later grote multibody groep, en wist dat ik altijd op je kon rekenen. Daarnaast wil ik ook mijn co-supervisor Dirk Vandepitte en mijn assessoren Paul Sas en Karl Meerbergen bedanken voor alle input, correcties en suggesties

bij het nalezen van deze tekst. Furthermore I would like to thank, next to my promotors, copromotor and assessors, also Prof. Dr. Ir. Georg Jacobs and Prof. Dr. Ir Herman Van Der Auweraer for being part of my jury, and also the IWT who funded this research.

Zowel voor als tijdens mijn doctoraat was ik in eerste plaats ZF-medewerker. Er zijn dus heel wat ZF-collega's die op directe of indirecte wijze bijgedragen hebben aan de resultaten van dit doctoraat. Allereerst wil ik Joris Peeters en Stefan Lammens, toenmalig CTO bedanken. Zij maakten het mogelijk dat mijn doctoraat zowel bij het IWT als intern in ZF goedgekeurd werd. Sonja, dank je wel voor het nalezen en corrigeren van al m'n papers en het in goede banen leiden van ALARM. Ben, dank je wel voor de goede samenwerking. We hebben al veel dingen ontdekt en geleerd omtrent dynamica van windturbine aandrijflijnen, ik hoop dat we nog lang op deze manier kunnen verderwerken. Kris Inghelbrecht en Roger Bogaert, dank je wel voor de vele interessante discussies omtrent dynamica, trillingen en geluid en om me steeds te wijzen op de praktische haalbaarheid van m'n ideeën. Daarnaast wil ik ook nog al m'n andere collega's uit Gent, Kontich en Lommel bedanken voor de toffe werksfeer die er binnen ZF heerst.

Although I eventually did not spend that much time in my office at PMA, I enjoyed every minute of it, especially the non-technical discussions during lunch. It furthermore proved to be a good location to hide myself from my other obligations at ZF and allowed me to completely focus on my PhD. Jan Helsen and Pepijn Peeters, thanks for all the interesting discussions we had about gearboxes and noise and vibrations. Jan Croes, Daniele Brandolisio and Pepijn Peeters, thanks for the help with the experimental validation campaigns. Jean-Pierre Merckx, thanks for all the support, repair and insurance regarding the equipment for the experimental validation campaigns. Bert Pluymers, thanks for informing me about the IWT Baekeland funding mechanism during lunch at some project meeting. If it was not for this over noon discussion this dissertation would never have existed. I would also like to thank you for your technical support when performing both simulations and measurements.

I would also like to thank a lot of fellow researchers working at LMS who I consider as colleagues. Bart Peeters, *friendly by default*, thank you for introducing me into the world of noise and vibrations during my internship and thesis at LMS. This internship and thesis were the start of my interest in noise and vibrations, and will probably determine the rest of my professional career. I really enjoy working together. I would also like to thank Karl Janssens, Wim Hendricx, Herman Van Der Auweraer, Gert Heirman, Simone Manzato

and Emilio Di Lorenzo for all the joined efforts, interesting discussions and assistance in numerous projects, masters theses and measurement campaigns.

Furthermore I would like to thank all the partners of the ALARM project and Alexander Ribbentrop, Christian Schönke and Marcel thor Straten of Senvion in particular. Thanks for giving me more insight in wind turbines, wind turbine control and wind turbine dynamics. I appreciated our open way of working, and hope that we continue working in such an atmosphere.

Last, but certainly not least wil ik ook m'n familie bedanken voor al de kansen die ze me gegeven hebben. Stefan, dank je wel voor de gevarieerde afleiding, gaande van boekhouding tot renovatiewerken. Ook wil ik graag m'n schoonfamilie bedanken om op de kindjes te passen als ik weer eens laat thuis kwam omwille van een conferentie of vergadering. Babs, bedankt voor wie je bent en voor alles wat je voor mij en ons gezinnetje gedaan hebt! Door je vele uitstapjes met de kids kon ik thuis verder werken aan deze opdracht. Dank je wel! Louise, Leonie en Vic, in jullie bijzijn een thesis schrijven was niet echt haalbaar, bedankt om af en toe jullie rustige kamer ter beschikking te stellen! Nu mijn '*boekje*' eindelijk af is, kijk ik er naar uit om samen een mooie speeltoren voor jullie te bouwen!

Fred.
2015

Abstract

This dissertation describes the development of a methodology and modelling approach to lower the mechanical noise of the drive train of a modern wind turbine with a strong focus on the wind turbine gearbox. Although this mechanical noise is not the main noise source from a wind turbine, it could - especially when it contains audible tonal components - result in non-conformity to local noise regulations. This becomes more stringent when wind turbines are installed closer to urbanised areas. This research is motivated by inefficiencies in a cost and time consuming reactive trial and error approach to reduce or remove audible mechanical tonalities from the wind turbine noise.

This dissertation focusses on the mechanical tonalities linked with the wind turbine gearbox. This mechanical noise originates from the interaction between the gears inside the gearbox, and then propagates directly airborne through the air or indirectly structure-born through the other wind turbine components to the outside. Two fundamental approaches exist to reduce or to remove a mechanical tonality. The first approach attempts to reduce the noise source by optimising the gears for low-noise. The second approach modifies the propagation path, also called transfer path from the source to the listener, such that the noise originating from the noise source is not amplified or even attenuated when it reaches the listener. The methodology proposed in this dissertation focusses on the second approach: using virtual prototyping models to assess and to optimise these transfer paths.

The development of this methodology consists of 3 main parts: firstly individual components of the wind turbine gearbox are investigated in detail and if necessary experimentally validated. Secondly these individual components are assembled into a wind turbine gearbox model. The impact of these individual components on the global eigenmodes of the gearbox are investigated, and the model of the complete gearbox is experimentally validated by performing an

experimental modal analysis. Lastly a model of two gearboxes on the end-of-line test rig is generated, investigated and also experimentally validated. This step-by-step approach, including the numerous experimental validation cases, resulted in a significant increase in both insight and confidence in the dynamic behaviour predicted by these virtual prototyping models.

This dissertation demonstrates this methodology and modelling approach by performing two optimisation cases. The first optimisation case focusses on the impact of the bearings on the resulting vibrations. The second optimisation case modifies the flexible gearbox housing, which is considered the most dominant component, to shift an important eigenmode out of the operating range of the wind turbine. Both these optimisation cases clearly illustrate the potential of pro-actively using virtual simulation models to optimise the noise and vibration behaviour of the wind turbine gearbox during its design.

Beknopte samenvatting

Dit proefschrift bespreekt de ontwikkeling van een methodologie en modelleer aanpak met als doel het mechanisch geluid te reduceren van een moderne windturbine aandrijflijn, met een sterke focus op de windturbine tandwielkast. Alhoewel het mechanische geluid niet de dominante geluidsbron van een windturbine is, kan dit mechanisch geluid, in het bijzonder als het hoorbaar is en een uitgesproken tonaal karakter heeft, leiden tot non-conformiteit ten opzichte van de geldende regelgeving omtrent windturbine geluid. Dit weegt des te zwaarder door naarmate de windturbines dichter bij (dicht) bewoonde gebieden geplaatst worden. Dit onderzoek is ontstaan vanuit de kostelijke en tijdsrovende trail-and-error aanpak die momenteel veelvuldig gebruikt wordt om hoorbare mechanische tonaliteiten te verzwakken of te verwijderen.

Dit proefschrift focust op de mechanische tonaliteiten afkomstig van de windturbine tandwielkast. Deze mechanische tonaliteiten ontstaan door de interactie van de verschillende tandwielen intern in de tandwielkast en propageren zich, ofwel rechtstreeks door de lucht, ofwel door andere structurele windturbine componenten zoals de toren en de bladen naar buiten. Een mechanische tonaliteit kan op twee verschillende manieren aangepakt worden. De eerste manier probeert de tonaliteit te verzwakken door de bron, in dit geval de vertanding, te optimaliseren. De tweede manier beïnvloed het propagatie of transfer pad van de bron naar de ontvanger zodanig dat de mechanische tonaliteit door dit transfer pad niet versterkt maar verzwakt wordt. Dit proefschrift onderzoekt de tweede aanpak: het gebruik van virtuele prototype modellen om deze transfer paden te beoordelen en te optimaliseren.

De ontwikkeling van deze methodology kan opgesplitst worden in 3 grote stukken. Eerst worden de individuele componenten van de wind turbine tandwielkast in detail onderzocht en indien nodig experimenteel gevalideerd. Daarna worden deze individuele componenten samengevoegd om zo het model

van de volledige windturbine tandwielkast te vormen. De impact van deze individuele componenten op de globale eigenmodes van de tandwielkast worden onderzocht, en daarenboven wordt dit model van de windturbine tandwielkast ook experimenteel gevalideerd. Ten laatste wordt een model van de proefstand met twee tandwielkasten opgesteld. Ook dit model wordt onderzocht en experimenteel gevalideerd. Deze stap voor stap aanpak, alsook de vele experimentele validatie metingen zorgen voor een beduidende stijging in het inzicht en het vertrouwen in het dynamisch gedrag voorspeld door deze virtuele prototype modellen.

Dit proefschift demonstreert deze methodology en modelleer aanpak met behulp van twee optimalisaties. De eerste optimalisatie onderzoekt de invloed van de lagers op de resulterende trillingen, terwijl de tweede optimalisatie de tandwielkast behuizing aanpast om een hoorbare resonantie uit het werkingsgebied van de windturbine te verplaatsen. Beide optimalisaties tonen duidelijk de kracht en het potentieel om pro-aktief, tijdens het ontwikkelprocess van de windturbine tandwielkast, virtuele prototype modellen te gebruiken om zo het geluids- en trillingsgedrag te optimaliseren.

Acronyms

AM amplitude modulation. 22, 25, 28

AML automatic matched layer. 131

APDL Ansys parametric design language. 73, 81

ASV averaged surface velocity. 54, 132

ATV acoustic transfer vector. 133–135, 140, 181

BE boundary element. 11, 12, 56, 131

CMS component mode synthesis. 54, 55, 62, 65, 72, 80, 81, 91, 135, 141

DOF degree of freedom. xxi, 48–51, 53, 56, 57, 61, 80, 81, 83, 91, 142, 154, 178, 180, 187

EMA experimental modal analysis. 65–67, 70, 75, 77, 80, 83, 104, 109, 112, 117, 127, 139, 143, 148, 149, 153, 154, 181, 187

EOL end of line. 3, 5, 9, 12, 145, 146, 148, 153, 180, 182, 184, 185

FE finite element. 6, 7, 9, 10, 51, 54–57, 60, 62, 65, 67, 68, 71–73, 77, 80–84, 90, 92, 96, 99, 104, 114, 123, 130–132, 134, 140, 141, 153, 154, 157, 170, 180–183, 187, 188, 197

FRF frequency response function. 66, 67, 75, 77, 83, 97, 98, 113, 127, 129, 163, 164, 189

GHG greenhouse gass. 14, 15

GRC Gearbox Reliability Collaborative. 52, 53

HSH high speed housing. 11, 64, 65, 67–69, 71, 72, 74, 80, 104, 108, 112–116, 119, 120, 128, 137–139, 153, 154, 180, 181

HS-IG high speed intermediate gear. 109, 112, 115, 120, 128, 138

HS-IS high speed intermediate shaft. 96, 108, 112, 121, 128, 166

HS-IS-GS high speed intermediate shaft bearing, generator side. xxv, 125, 165, 168, 169, 171–173

HS-IS-RS high speed intermediate shaft bearing, rotor side. xxv, 88, 125, 168–170, 173

HSS high speed shaft. 96, 108, 112, 121, 128, 134

HSS-GS high speed shaft bearing, generator side. 93, 165, 168, 169

HSS-RS high speed shaft bearing, rotor side. 92, 168, 169

IBH ISS intermediate bearing housing, intermediate speed side. 64, 74, 173

IBH LSS intermediate bearing housing, low speed side. 63, 65, 67, 68, 71, 93, 173

IPCC intergovernmental panel on climate change. 13, 44

ISRW intermediate speed ring wheel. 63

ISS-PC intermediate speed stage planet carrier. 82–84, 86, 119, 120, 127, 138, 140

ISS-PC-GS intermediate speed stage planet carrier bearing, generator side. 164

LF low frequency. 22, 24, 30

LSRW low speed ring wheel. 63, 65, 67, 68, 71, 93

LSS-PC low speed stage planet carrier. 82, 84, 86, 104, 119–121, 125, 128, 138

LSS-PC-RS low speed stage planet carrier bearing, rotor side. 92, 93, 95, 105, 125

LSS-SU low speed stage sun. 83, 86

MAC modal assurance criterion. 68, 69, 77, 92, 113, 115, 143, 187

MATV modal acoustic transfer vector. 133–136, 140, 157, 181

MB multi body. 7, 9–12, 50–53, 56, 57, 59–62, 80–83, 87, 88, 98, 107, 109, 115, 123, 127, 131, 132, 137, 140, 148, 163, 164, 173, 179, 182–184, 187, 197

MBS multi body simulation. 6, 60, 115

MC main cover. 11, 64, 65, 67–69, 71, 72, 74, 80, 104, 108, 112–116, 119, 120, 128, 137–139, 153, 154, 180, 181

MPC multi point constraint. 65, 90, 91

MPF modal participation factor. 80, 81, 132–135, 157, 181

NASA National Aeronautics and Space Administration. 54–58, 130, 179

NREL National Renewable Energy Laboratory. 52

NV noise & vibration. 3, 5, 47, 56, 98

TA torque arm. 63, 65, 67, 68, 71, 72, 93, 97, 120, 125, 128, 138, 180

TE transmission error. 39, 97, 98, 103, 105, 157, 181

TE-FRF transmission error frequency response function. 97, 98, 103, 105, 157, 175, 181

TPA transfer path analysis. 161–163, 165, 169

Contents

List of Figures

List of Tables

Chapter 1

Introduction

To reach the stringent but necessary climate targets, more and more investments are made in clean and renewable energy sources. Over the last ten years this has resulted in an increase of more than 700% of installed wind energy power. As a consequence of this, more and more wind turbines are not only put up in remote areas, but also within the vicinity of urban zones, and care should be taken that those newly installed wind turbines do not cause additional nuisance for the closely living habitants. Noise from wind turbines is such an item. Even though the total noise level of a wind turbine is rather low (see figure 1.1), the noise from a wind turbine may have some characteristics which render it annoying. As a result, wind turbine manufacturers are challenged with high requirements regarding noise emissions. Official regulations aim at keeping wind turbine noise levels low to protect the inhabitants. Compliance with noise emission criteria is crucial for wind turbine start-up permission.

Noise from wind turbines can be subdivided in two distinct categories: aeroacoustic noise and mechanical noise. The aeroacoustic noise originates from the interaction between the air and the rotating blades, tower and nacelle, and depends heavily on the rotational speed and size of rotor as well as on the actual blade design. Aeroacoustic noise of the wind turbine is broadband of nature and is considered as the dominant noise source of a wind turbine. Mechanical noise on the other hand originates from the mechanical components inside the wind turbine such as the generator, the gearbox, the yaw and pitch drives, ... Noise from these mechanical components is, in contrast with the broadband aeroacoustic noise, mainly tonal of nature.

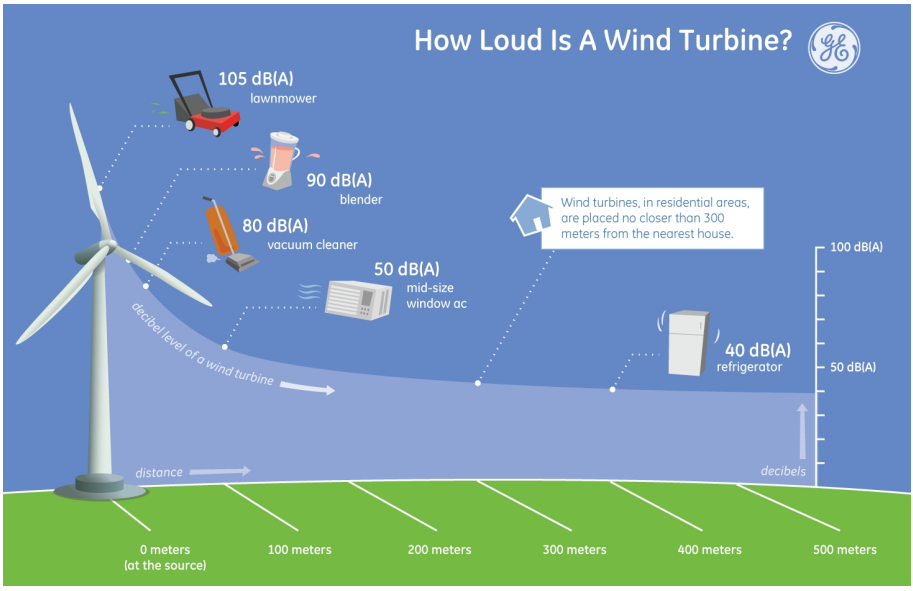

Figure 1.1: Sound pressure level of a typical wind turbine in function of the distance compared with typical household appliances. (Source: GE Global Research; National institute of Deafness and Other Communication Disorders (NIDCD part of NIH). Retrieved from `http://www.gereports.com/post/92442325225/how-loud-is-a-wind-turbine` on August, 13th, 2014)

Although this mechanical noise is not considered as the dominant source of the wind turbine noise, it can that these tonal components become audible when they rise above the surrounding broadband aeroacoustic noise. As the human hearing is very sensitive to such tonal components, their presence may render the total wind turbine noise annoying. Techniques to reduce the global wind turbine noise level, such as optimising the blade design or reducing the rotational speed of the rotor, have no significant impact on the produced mechanical noise, and may therefore result in even higher tonal levels compared with the aeroacoustic background noise leading to an even more annoying wind turbine noise. Furthermore the presence of these tonal components may result in additional penalties on the total noise level of the wind turbine and may lead to non-conformity to local noise regulations.

A significant amount of effort is spent to reduce the aeroacoustic noise of a wind turbine consisting of computational fluid dynamics (CFD) calculations,

wind tunnel testing, and testing on actual operating wind turbines. These efforts are rather easily managed during the design process of a wind turbine as it is mainly the design of the rotor blades which affects the aeroacoustic noise.

Optimisation of the wind turbine design to reduce the mechanical noise is rather new and unknown. For a long time it was believed that the resulting audible level of the mechanical noise from the gearbox solely depends on the gear design and quality. It was tried to characterise and to limit the resulting noise and vibrations from the gears by imposing hard limits on the end of line (EOL) test rig. These hard limits could however not guarantee low mechanical noise levels once the gearbox was mounted in the wind turbine. It was only recently recognised that not only the gear design and quality has a huge impact on the mechanical noise level, but also the design of the gearbox housing, the design of the bed plate, the design of the gearbox supporting system, including the ability of the supporting bushings to isolate the gearbox, ... as these components can amplify or reduce the noise originating from e.g. the gears. Furthermore, all these components have an impact on each other: a gearbox which does not produce audible mechanical noise in one wind turbine may lead to tonal noise in a different wind turbine. A multidisciplinary co-operation of the different parties involved in the development process is therefore uttermost necessary to attempt to reduce the mechanical noise.

Up to now, the wind turbine gearbox, which is an integral part of the wind turbine drive train, is designed without taking the dynamics of the entire wind turbine drive train into account. The resulting mechanical noise behaviour can therefore only be assessed once the gearbox is installed in the wind turbine during the final stage of the design process: the prototype field validation. Non-compliance with requirements at this stage of the development process implies high costs of rework and unwanted delay in product introduction for both wind turbine and gearbox. This research is motivated by inefficiencies in a cost and time consuming reactive trial and error approach to reduce or remove audible mechanical tonalities from the wind turbine noise.

1.1 Research objectives

The study in this dissertation starts from an investigation into the state-of-the-art in the simulation of wind turbine drive train noise & vibration (NV). From this overview, the need for experimentally validated virtual prototyping models, capable of accurately predicting the dynamic behaviour of a wind turbine drive

train, is expressed. This need is translated into the development of the wind turbine gearbox, resulting in following key objectives for this dissertation:

1. develop a methodology / modelling approach to assess the vibro-acoustic behaviour of a wind turbine gearbox in the frequency area covering all relevant gear excitation frequencies. Focus of this methodology should be on the structural transfer path translating the gear excitation forces into resulting vibrations or audible noise levels, but not on the gear excitation mechanism itself;
2. experimentally validate this modelling approach;
3. get insight in which components are dominant for the dynamic behaviour;
4. get insight in which components are dominant for model accuracy;
5. use this methodology to shorten the trajectory to meet the noise and vibration requirements by a factor of 2, either by pro-active support to the design teams, or by reactive troubleshooting support during the prototype validation; and
6. use this methodology to reduce the investment cost of reactive troubleshooting on an existing product by 30%.

Key objectives 1 through 4 are explicitly addressed in this dissertation in chapters 4, 5 and 6. Key objectives 5 and 6 are the result of using the methodology and modelling approach during the design of the gearbox, and are touched upon by chapter 8, but are not calculated in detail.

1.2 Scope definition

Figure 1.2 sets the scope for these objectives: the methodology presented to predict mechanical tonalities is valid for the complete wind turbine. The presented modelling approach can be used on the complete wind turbine for both the structure-born vibrations and the airborne noise. The scope of this dissertation for the modelling approach is however limited to investigations and experimentally validations on a wind turbine gearbox. Furthermore it should be noted that this dissertation is based on several models and experiments on large wind turbine gearboxes. Most of the modelling approach however was validated on one gearbox in particular, resulting in some conclusions which could be specific to this wind turbine gearbox. However, due to the huge

similarity between different wind turbine gearboxes, very similar results are expected. Furthermore, the proposed methodology and modelling approach can be utilised to gain insight in the NV behaviour of various mechanical systems.

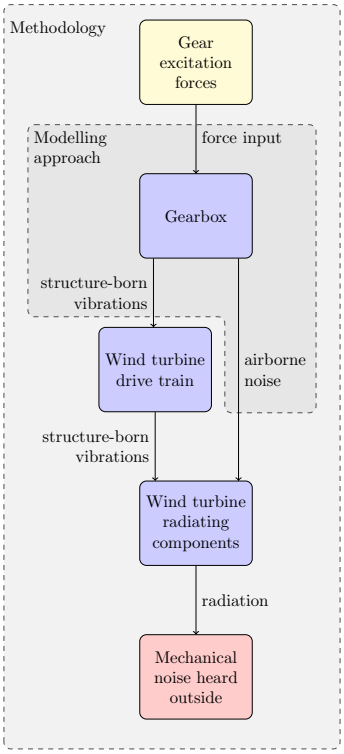

Figure 1.2: Scope of this dissertation.

1.3 Research facilitators

The research presented in this dissertation was conducted in a close co-operation between the KU Leuven and ZF Wind Power Antwerpen NV. This resulted in a dissertation with both an academic, but also with a strong industrial / practical point of view on the issues. This furthermore implies that all measurement results are real life measurements conducted on real wind turbine gearboxes, on real wind turbine gearboxes on the EOL test rig (including the 13.2MW dynamic

R&D test rig) or on individual parts of wind turbine gearboxes, and that all models used throughout this dissertation are models of a real operational multi megawatt wind turbine gearbox, or its parts, making this work as relevant as possible. As a consequence however, some measurement and model results such as eigenfrequencies are confidential and are only partially reported.

The research conducted in this dissertation should be considered a fundamental building block in the framework of a bigger project called the ALARM project which focusses on modelling and validating the parts of the drive train and wind turbine which fall out of the scope of this dissertation. More information about the ALARM project can be found in [39, 2].

1.4 Research strategy

Chapter 3 defines the need for experimentally validated accurate noise and vibration models tailored for the wind turbine drive train application. This results in two important topics throughout this dissertation: modelling and experimental validation.

1.4.1 Modelling

Throughout this dissertation two modelling techniques are constantly used for structural calculations: the finite element (FE) modelling technique and the flexible multi body simulation (MBS) technique. Choice between those two techniques depends on the questions to be solved: while the FE modelling technique is easy to use and gives detailed insight in single components, the flexible MBS technique is more appropriate when interested in the dynamic interaction of several flexible components. More details about these two techniques is given in the chapters utilising these techniques.

1.4.2 Experimental validation

The high level of complexity in the presented models requires a thorough validation strategy. A multi-level validation strategy is chosen for this purpose. This increases confidence in smaller parts of the complete model first and allows to better identify typical uncertainties in those models. This is valuable insight and can avoid similar extensive measurements for future models. Because the

multi body (MB) model of the gearbox is afterwards mainly used to identify critical eigenfrequencies, the experimental validation campaign focuses purely on the comparison of the modal behaviour of the gearbox component or (sub)model compared with its experimentally characterised modal behaviour.

Figure 1.3 graphically illustrates this validation strategy. It is composed of 5 levels:

1. component level
2. empty gearbox housing level
3. gearbox assembly level
4. gearbox on test rig level
5. wind turbine level

In the first level, the component level, the FE models of the individual components are validated. In the second level, multiple individual components are assembled to form the flexible housing of the gearbox. Validation in this level focuses on how these individual components are bolted together and how this affects the dynamic properties of the gearbox housing. The objective of level 3 is to validate the resulting MB model of the gearbox, which is done in two steps. Level 4 validates this gearbox model on the test rig, and validation level 5 focuses on the structural and acoustic behaviour of the total wind turbine. This dissertation focuses on the first four levels of validation. The last validation level is a task for the ALARM project.

1.4.3 Used software

Throughout this dissertation multiple software packages are used (in alphabetical order):

- ANSYS Inc., Ansys to generate and dynamically reduce the flexible bodies used in the MB model.
- Dassault Systèmes - SIMPACK AG, Simpack to generate and analyse the MB models used to investigate the dynamic behaviour of the wind turbine gearbox throughout this dissertation.

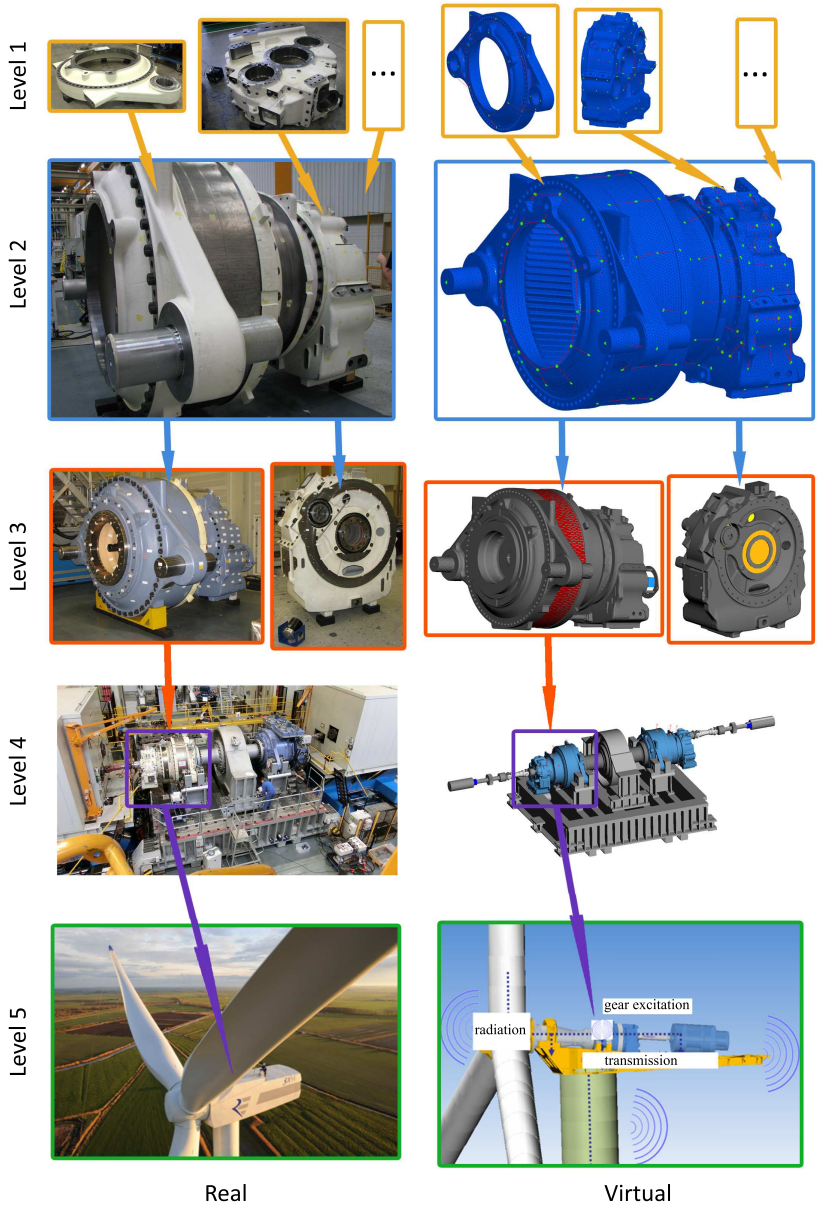

Figure 1.3: Graphical representation of the multi-level validation strategy

- Dynamic Design Solutions N.V., Femtools to compute correlations between FE models, MB models and experimental validation results, and to perform sensitivity studies, design of experiments and modal updates on both FE and MB models. For more information see Appendix A
- Siemens PLM Software - LMS, Test.LAB to perform the numerous validation measurements throughout this dissertation, and to perform the transfer path analysis on simulated gearbox data (section 8.1)
- Siemens PLM Software - LMS, Virtual.LAB to perform the acoustic radiation calculations of the gearbox.
- The MathWorks, Inc., Matlab to perform optimisations, automations, conversions, ... on all kinds of experimental data, models and simulation results.

1.5 Main contributions

The main contributions of this dissertation to the current state-of-the-art and to the current state-of-the-use include:

- an in-depth experimental validation of individual components of a wind turbine gearbox, a sub-assembly of a wind turbine gearbox, a complete assembled gearbox, and of two assembled gearboxes on the EOL test rig
- insight in the dynamic behaviour of wind turbine gearboxes and wind turbine gearboxes on the EOL test rig
- insight in the required model detail necessary to accurately predict the dynamic behaviour of wind turbine gearboxes
- insight in the sensitivities of individual components of the wind turbine gearbox on the resulting dynamic behaviour
- insight in the impact of the non-constant bearing stiffness on the dynamic behaviour of the wind turbine gearbox
- insight in the impact of the modelling approach used for introducing gear forces into large flexible ring wheels on the accuracy of resulting vibration amplitudes

1.6 Overview of the dissertation

This dissertation comprises 9 chapters. **Chapter 2** gives an introduction to modern wind turbines and wind turbine noise. It starts with a short introduction on the climate change and the need for renewable energy. It then continues with a small historical overview on wind turbines and how a modern wind turbine is constructed. It gives insight in the individual wind turbine noise sources, how this noise is perceived, how it is regulated by local governments and how it impacts wind turbine farm planning. This section concludes with an introduction on wind turbine gearboxes, the noise originating from those wind turbine gearboxes and how this and other noise sources can propagate to the outside world.

Chapter 3 describes the state-of-the-art with respect to drive train modelling with a strong focus on the dynamic behaviour of the wind turbine drive train. It gives an overview on literature of wind turbine drive train design load models, and gearbox noise and vibration models for both wind turbine gearboxes and non wind turbine gearboxes. It then highlights the limitations of these approaches with respect to a wind turbine drive train and justifies the need for the key objectives investigated in this dissertation.

Chapter 4 is the first of four chapters which form the essence of this dissertation. In this chapter the individual components of the gearbox are investigated, modelled and experimentally validated (level 1 and level 2 in figure 1.3). It starts with a short introduction on the main modelling technique used throughout this dissertation: the flexible MB technique and then focusses on these individual components:

1. The **gearbox housing** is one of the most important components determining the global gearbox dynamics. In a first step the individual castings and ring wheels which form the gearbox housing are investigated and experimentally validated. In a second step these validated individual components are joined to form the gearbox housing model. Again this step is experimentally validated giving insight in the accuracy of the resulting gearbox housing. This section ends with an overview on how this FE model of the gearbox housing is incorporated in the MB model of the complete gearbox.
2. For the **planet carriers** a somewhat simpler approach is used: modelling of the planet carriers and experimental validation of these planet carriers is performed in only one step.

3. Two aspects of the **bearings** are investigated: the actual stiffness calculation of the bearing, and the way how this bearing stiffness is introduced in the flexible housing affects the global eigenmodes of this flexible housing.

4. **Shafts** are only minimally investigated as their flexibility contributes only to a lesser amount to the global dynamics of the wind turbine gearbox. Although excitation mechanisms of the **gears** are not the focus in this dissertation, the impact on how these gear excitation forces should be introduced in the flexible gearbox housing is investigated.

This chapter ends with a general conclusion regarding the accuracy and impact of these individual gearbox components on the overall gearbox dynamics.

In **Chapter 5** the individual gearbox components which were investigated in the previous chapter are combined to form both the structural MB model and the acoustic boundary element (BE) model of the gearbox. This chapter contains three parts:

1. First a model is constructed of the high speed housing (HSH) and main cover (MC) including shafts and gear. A sensitivity study is performed to investigate the impact of the gearbox housing, the bearing stiffness values and the gear wheel inertia. Furthermore the impact of bearing pre-load on the global dynamics is investigated. The accuracy of this model of the HSH and MC is investigated by performing a correlation of this model with an experimental characterisation of the dynamic behaviour of this sub assembly (level 3 in figure 1.3).

2. Secondly a model of the complete gearbox is constructed containing all shafts, gears, planet carriers, etc... Similarly with the model of the HSH and MC, a sensitivity study is performed to investigate the impact of the gearbox housing, the bearing stiffness values, the gear wheel inertia and the inertia and stiffness of both planet carriers. Also the effect of bearing pre-load on this model is investigated. As the flexible gearbox housing has the highest impact on the global dynamics of the complete gearbox, a sensitivity study is performed to investigate the impact of the most important individual castings, which form the complete gearbox housing, on the overall dynamic behaviour of the complete gearbox. This section then continues to investigate the accuracy of this model by correlating it with an experimental validation campaign on this gearbox (level 3 in figure 1.3).

3. The last part argues why advanced acoustic models are necessary to accurately predict the radiated noise of a wind turbine gearbox, it gives

insight in the acoustic BE model used in this dissertation, and ends with a procedure how to use the results from the structural MB model of the gearbox as an input for the BE model to predict the radiated noise.

This chapter ends with formulating the main conclusions concerning the modelling and accuracy of a wind turbine gearbox.

Chapter 6 investigates the behaviour of the wind turbine gearbox on the EOL test rig. This chapter starts with an overview of the model used to assess the dynamic behaviour of two wind turbine gearboxes on the EOL test rig. It then continues with an investigation on the impact of both the flexible supporting structure and the load on the global dynamics of this test setup. Again, a sensitivity study is performed to gain insight in the effect of the gear stiffness, the supporting structure stiffness, the torque arm bushing stiffness and the low speed coupling stiffness on the resulting eigenmodes of the two gearboxes on the test rig. This chapter then continues with the measurement campaign performed on the EOL test rig and the correlation of the experimentally obtained eigenmodes of the test rig setup with the MB model (level 4 in figure 1.3). This chapter ends with the main conclusions concerning the modelling and the experimental validation of the EOL test rig setup.

Chapter 7 proposes a virtual prototyping methodology to pro-actively prevent tonal wind turbine noise. Firstly, based on the insights gathered from previous chapters, it lists the requirements for such a virtual prototyping model, for both the structural and acoustic model. Secondly, the analysis procedure to actually calculate the mechanical tones is discussed, and an example is given.

Chapter 8 presents two optimisation cases which focus on the wind turbine gearbox. The first optimisation case investigates the impact of the bearings on the resulting vibration amplitudes by using the transfer path analysis technique and numerical sensitivity studies. In the second optimisation case the gearbox housing is modified resulting in the shift of a resonance out of the operating range.

Chapter 9 summarises the main conclusions of this dissertation and lists some suggestions for future research.

Chapter 2

Introduction to wind turbines and wind turbine noise

2.1 Introduction

This chapter gives an overview on wind turbines and wind turbine noise related matters. It starts with a short overview on the climate change, and how renewable energy can mitigate the effects. It then continues with a brief description of the history of wind turbines and an overview on the most important components of a wind turbine. It then introduces wind turbine noise: its different sources, its specific characteristics, how wind turbine noise is perceived, and when it is considered as annoying. A brief overview on regulations on wind turbine noise is given and their impact on wind turbine farm planning. This section then continues with an introduction in wind turbine gearboxes and its noise sources. This section ends with a description on how the noise and vibrations from the wind turbine gearbox can propagate to the outside world.

2.2 Climate change and renewable energy

In April 2014 the intergovernmental panel on climate change (IPCC) published the long-awaited draft of the last part of their fifth assessment report (AR5). The complete assessment report consists of three parts. The first part, published in 2013, focusses mainly on the physical basis and proves that human activity is the main cause of global heating and unprecedented changes over decades to

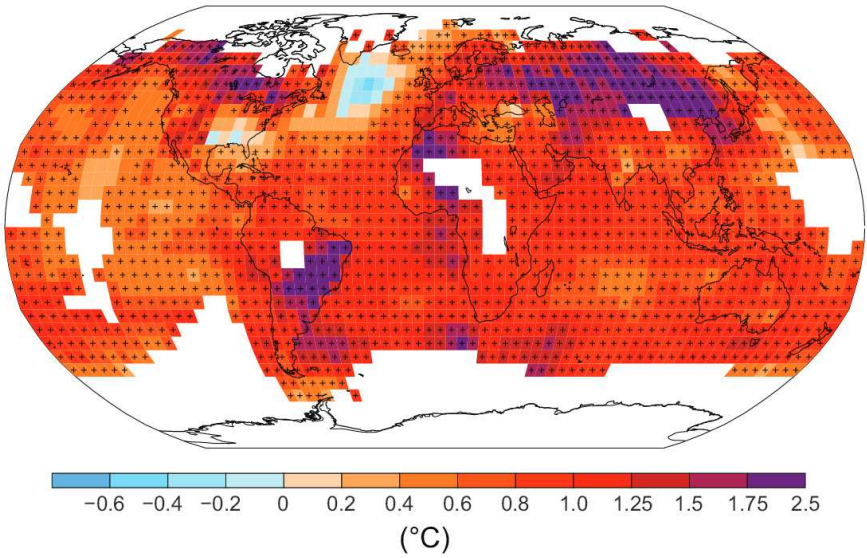

Figure 2.1: map of the observed surface temperature change from 1901 to 2012. Reproduced from [161], Figure SPM1

millennia in all components of the climate system: warming of the atmosphere and the ocean (see figure 2.1), diminishing snow and ice, rising sea levels and increasing concentrations of greenhouse gases [161].

> Human influence on the climate system is clear. This is evident from the increasing greenhouse gass (GHG) concentrations in the atmosphere, positive radiative forcing, observed warming, and understanding of the climate system.
>
> (IPCC, WG I, AR5, Summary for Policymakers. [161])

Part two of this report addresses Impacts, Adaptation, and Vulnerability [33, 7]. Depending on the region (see figure 2.2) threats include loss of livelihoods, settlements, infrastructure to increased flood damage, increased threat for waterborne diseases, increased water restrictions, increased risks from wildfires, heat-related human mortality, ... It is clear that these are real threats, but the impact and severity of these threats luckily still depends heavily on how we react to these forecasts and on our efforts to reduce the GHG emissions to mitigate these harmful effects. Multiple strategies and the required efforts

to mitigate these effects are addressed in the third part of this comprehensive report:

> Scenarios reaching atmospheric concentration levels of about 450 ppm CO_2 equivalent by 2100 (consistent with a likely chance to keep temperature change below 2°C relative to pre-industrial levels) include substantial cuts in anthropogenic GHG emissions by mid-century through large-scale changes in energy systems and potentially land use *(high confidence)*. Scenarios reaching these concentrations by 2100 are characterized by lower global GHG emissions in 2050 than in 2010, 40% to 70% lower globally, and emissions levels near zero gigatonnes CO_2 equivalent or below in 2100.
> In scenarios reaching 500 ppm CO_2 equivalent by 2100, 2050 emissions levels are 25% to 55% lower than in 2010 globally. In scenarios reaching 550 ppm CO_2 equivalent, emissions in 2050 are from 5% above 2010 levels to 45% below 2010 levels globally. At the global level, scenarios reaching 450 ppm CO_2 equivalent **are also characterized by more rapid improvements of energy efficiency, a tripling to nearly a quadrupling of the share of zero- and low-carbon energy supply from renewables, nuclear energy and fossil energy with carbon dioxide capture and storage (CCS), or bioenergy with CCS (BECCS) by the year 2050**. These scenarios describe a wide range of changes in land use, reflecting different assumptions about the scale of bioenergy production, afforestation, and reduced deforestation. All of these emissions, energy, and land-use changes vary across regions. Scenarios reaching higher concentrations include similar changes, but on a slower timescale. On the other hand, scenarios reaching lower concentrations require these changes on a faster timescale.

(IPCC, WG III, AR5, Summary for Policymakers. [31])

It needs little or no arguments that wind energy can significantly attribute to the goal of tripling to nearly quadrupling the share of renewable energy supply. National and regional policy are however still the main drivers for wind energy deployment which can easily be seen for e.g. North America in figure 2.3 which has undergone an unsteady policy with respect to renewables. A more steady and global approach is necessary to widespread adopt renewable energy and to

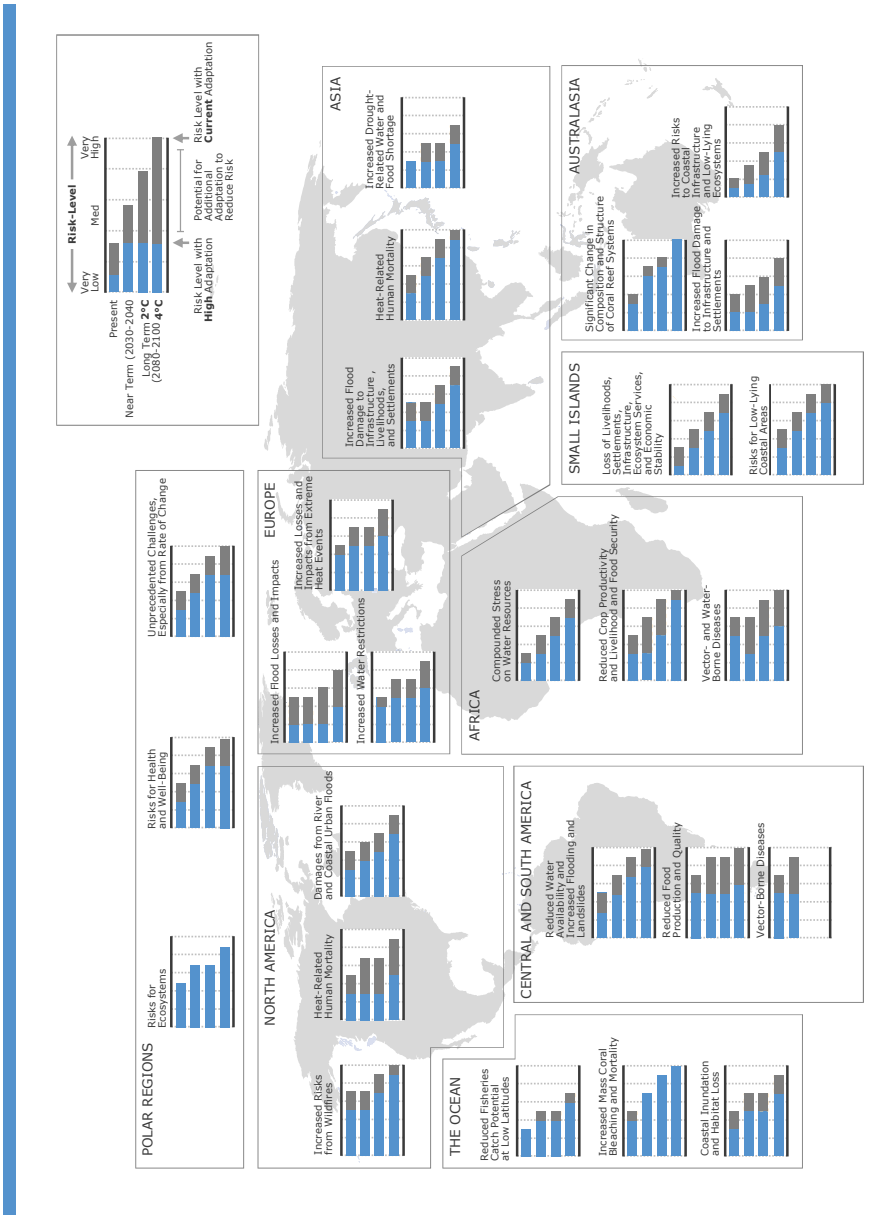

Figure 2.2: Impacts caused by climate changes by region. Retrieved from `http://ipcc-wg2.gov/AR5/images/uploads/WGIIAR5-Slides-June_12_2014.pptx` on August, 13th, 2014

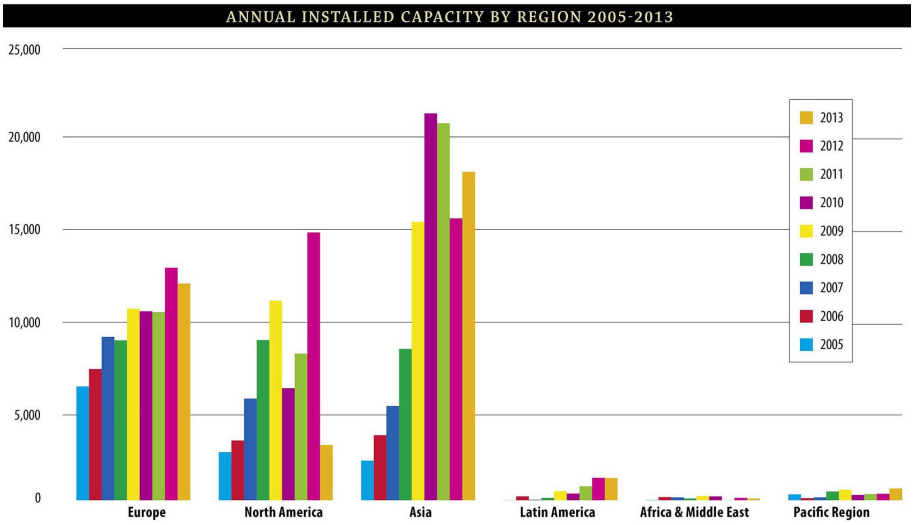

Figure 2.3: Annually installed wind energy capacity by region. (Source: Global Wind Energy Councel (www.gwec.net))

mitigate the climate changes.

Noise from wind turbines may reduce or slow down this highly necessary and widespread adoption as noise issues for on-shore wind turbines are sometimes the reason why a wind turbine or a wind turbine farm is not erected (after protest from closely living residents, with possible noise issues being one of the arguments), why less turbines are placed in a farm (because total noise levels are limited by legislation), or why a wind turbine is running in a so-called 'silent' mode with a reduced rotor speed resulting in a lower power output.

2.3 Wind turbines

First records of windmills date back to the 7th century in Persia were windmills were used for grinding grain and for pumping water. Around the 14th century windmills became a major source of power, and have been used for grinding, pumping, sawing, ... In 1887 prof James Blyth constructed the first wind turbine: a windmill utilised to generate electricity to charge accumulators [139].

Figure 2.4 shows a larger wind turbine engineered by Charles F. Brush erected in the winter of 1888, with a rated power of 12kW.

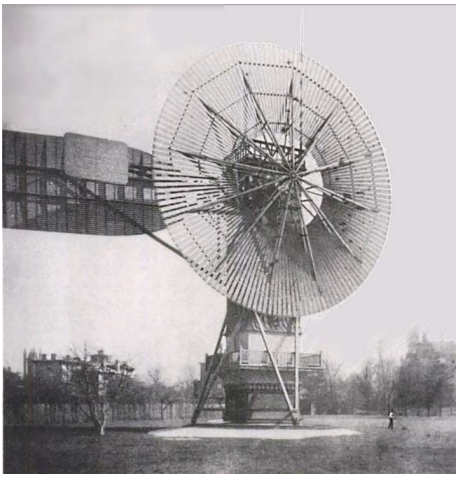

Figure 2.4: Charles Brush's windmill of 1888, used for generating electricity. Reproduced from: Robert W. Righter (1996) Wind Energy in America: A History, University of Oklahoma Press, page 44 Retrieved on 27 December 2008

Popularity of using wind energy to produce electricity has always and is still largely linked with the fluctuating price of fossil fuels: when fuel prices drop, interest in wind energy also drops, when fuel prices rize so does the interest in wind energy. Since the first wind turbine of James Blyth and on the pace of the fossil fuel price wind turbines were further developed and evolved into the modern wind turbines which are known today. Most common used wind turbines today are wind turbines with a horizontal axis with the rotor mounted on the upwind side. A more elaborate history on the historical development of wind turbines can be found in [99].

2.3.1 Layout

Figure 2.5 shows the layout of a state-of-the-art wind turbine. The blades (2) convert the kinetic wind energy to torque and are mounted on the hub (3). To control the energy capture from the wind, the blades can be rotated along their axis using the pitch system (4). The power from the wind is transferred from the hub through the main shaft (8) to the gearbox (9) which increases the rotational speed and lowers the torque. The gearbox connects through a high speed coupling (10) to the generator (11) converting the mechanical power into

electrical energy. Both gearbox, main bearings and generator are supported on the mainframe (5) which in its turn is supported by the tower (1) and can point itself in or out of the wind using the yaw system (7). This entire process is controlled using the controller (12). The nacelle cover (6) is the outer enclosure of the wind turbine. A more in-depth description of all individual components can be found in [132].

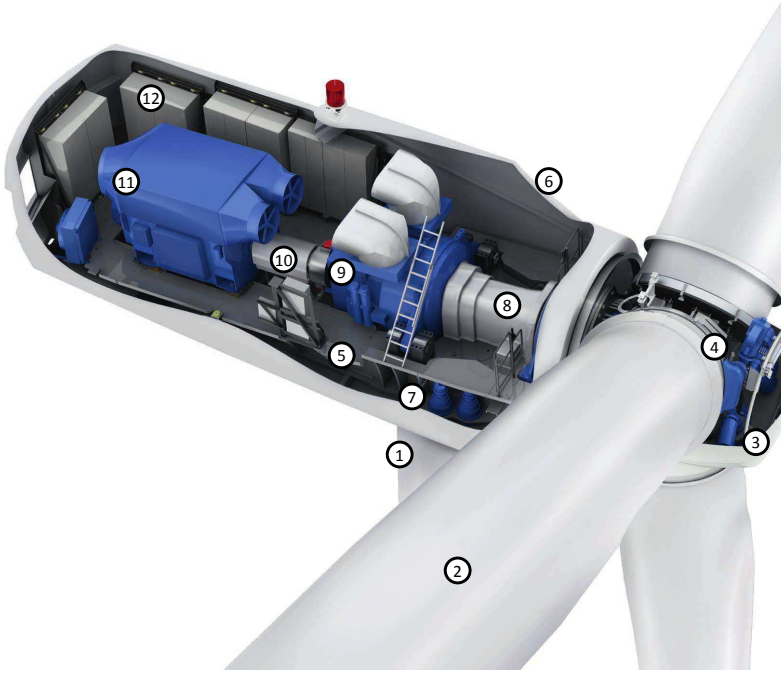

Figure 2.5: Internal layout of a modern wind turbine. Senvion 3X.M Series wind turbine, reproduced from [151].

2.3.2 Operating range

Most often a synchronous or a doubly fed induction generator is used to convert the mechanical power into electrical energy. Main advantage of the doubly fed induction generator is that the wind turbine is not bound to a specific operating speed: the controller is able to set the operating condition of the generator at any rotational speed, optimising the energy output of the wind turbine. Figure 2.6 shows a fictional, but typical operating curve of a wind turbine. Next to the

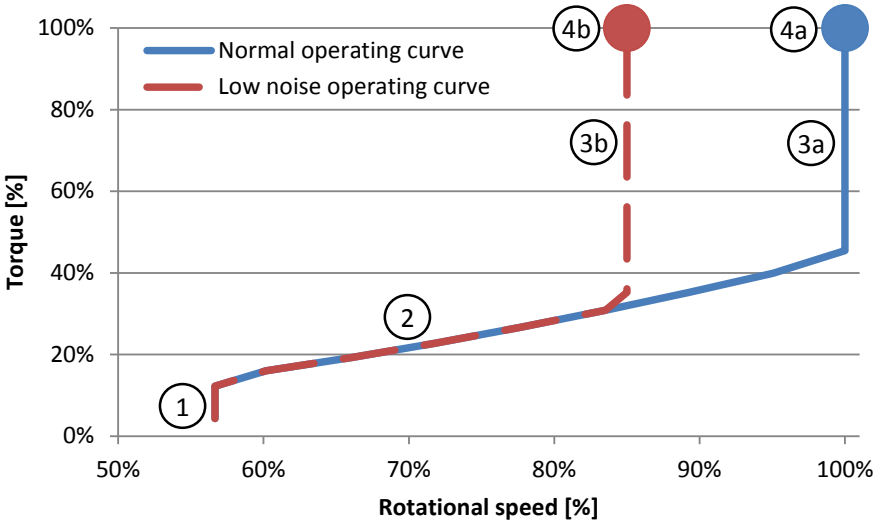

Figure 2.6: Typical operating curve of a fictional wind turbine. Blue: normal operating curve, red: low-noise operating curve.

normal operating curve, also the low-noise operating curve is given[1]. Figure 2.7 shows the same information, but plotted with respect to the wind speed. Several typical regions exist in such an operating curve (see figure 2.6):

(1) Wind turbine start-up: at a wind speed of approximately 4 m/s, the wind turbine starts up. It allows the rotor to accelerate up to approximately 57% of nominal speed. At this constant speed, the torque slightly increases up to approximately 10% of nominal torque.

(2) At wind speeds between 5 m/s and 9 m/s the rotational speed increases up to nominal rotational speed, also the torque slightly increases.

(3a) In this region, rotational speed remains constant, and the torque further increases up to nominal torque. This occurs at wind speeds between 9 m/s and 12 m/s.

(4a) At wind speeds above 12 m/s, the wind turbine reaches rated conditions, producing maximum power. Both torque and speed are allowed to change slightly around this nominal operating point.

[1]The reasoning behind this low-noise operating curve is explained in section 2.4.2

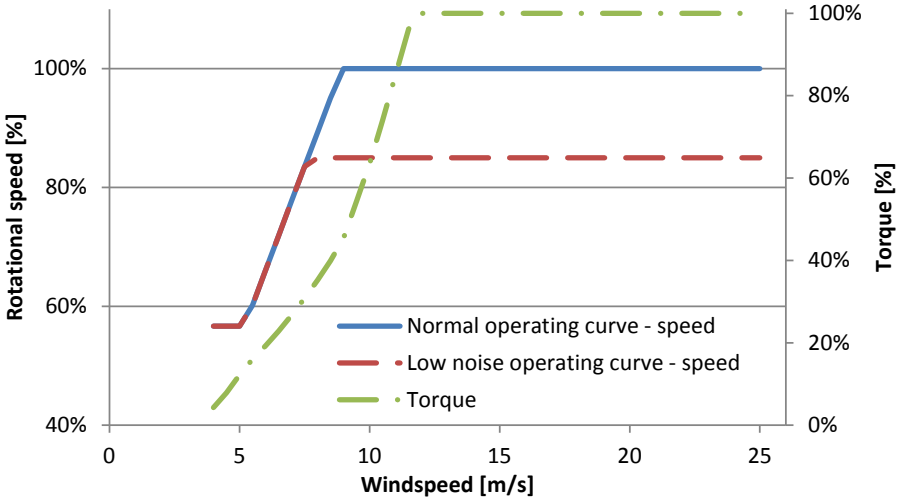

Figure 2.7: Typical operating curve of a fictional wind turbine with respect to wind speed.

In the low-noise operating curve (red curve), the rotational speed is only allowed to increase up to 85% of nominal speed, which is the maximum speed for this low-noise operating condition. At wind speeds between 7.5 m/s and 12 m/s, only the torque can increase (3b), to eventually reach the low-noise nominal operating conditions in (4b).

This very flexible operation of the wind turbine maximises the power output of the wind turbine. This requires however that the tonality behaviour of the wind turbine is optimised in this huge operating range in terms of rotational speed (from approximately 50% up to 100% of nominal speed), as possible mechanical tonalities of the wind turbine drive train are directly linked with the rotational speed.

2.4 Wind turbine noise

Since wind turbine noise differs significantly from other sources such as industry or traffic noise, a good understanding of the mechanisms causing wind turbine noise is essential. This section looks at wind turbine noise using two different approaches: looking how the noise from these noise sources can be characterised

and investigating the different noise sources. It also discusses how this wind turbine noise is perceived by human hearing, and how it is regulated.

2.4.1 Wind turbine noise characteristics

Wind turbine noise has several characteristics which distinguishes wind turbine noise from other noise sources such as industry or road noise. Main characteristics (besides the total sound power level) of wind turbine noise include:

- amplitude modulation (AM)
- tonality
- low frequency (LF) noise

Amplitude modulation

AM is the cyclic variation of the wind turbine noise over time. Residents living nearby wind turbines often describe this noise as pulsating. According to Van Den Berg [8] the AM is caused by the trailing edge noise and it has pulsation frequencies linked with the blade pass frequency. An in-depth literature study and data analysis at many wind turbines and wind farm sites in the UK by Stigwood et al. [158] revealed that

- AM is not limited to wind farms. All turbines including single turbines can cause AM.
- AM is caused by trailing edge noise.
- AM is affected by the meteorological conditions.
- AM is directional. It can mostly be found in cross wind and down wind conditions.
- AM should best be measured in the evening, at night or early in the morning when there is low cloud cover or high wind shear.
- The presence of AM leads to a higher awareness of the noise which eventually results in a higher annoyance.

Tonalities

A tonality is caused when the amplitude of a single frequency or of a small frequency band is significantly higher than the amplitude of its neighbouring frequencies, such as the sound of a whistle. The human hearing is very sensitive to tonalities. A noise with a tonality is considered much more annoying than an equally loud noise without tonality [84]. Figure 2.8 shows a typical wind turbine noise spectrum with two audible tonalities, one around 125 Hz and one around 250 Hz.

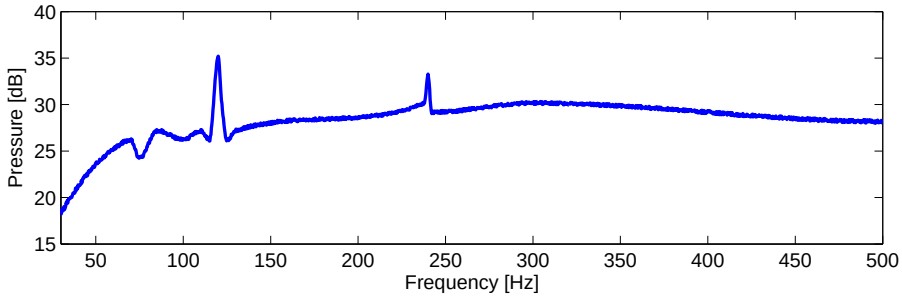

Figure 2.8: Typical noise spectrum of a wind turbine containing two audible tonalities.

Wind turbine tonalities are mostly caused by the gearbox, the generator and the wind turbine power electronics. The IEC 61400-11 standard [74] is used to measure, evaluate and report wind turbine noise and wind turbine tonality in an objective and reproducible manner. The first part of this standard handles instrumentation and measurements for both acoustic and non-acoustic quantities. It regulates microphone layout (see figure 2.9), data acquisition settings, required wind speed bins, wind speed measurements, minimum dataset required for further analysis, ...

The second part of this standard documents the procedure on how to evaluate total and tonal noise based on the measurements performed in the first part. For each wind speed bin possible tones are identified. For each possible tone, the background masking noise is calculated and subtracted. A tonal audibility criterion, taking into account that the human hearing is able to perceive some tones better than other tones, is also taken into account, resulting in a tonal audibility for each possible tone. If this tonal audibility is higher or equal than -3.0 dB, then this possible tone is considered as a relevant tone.

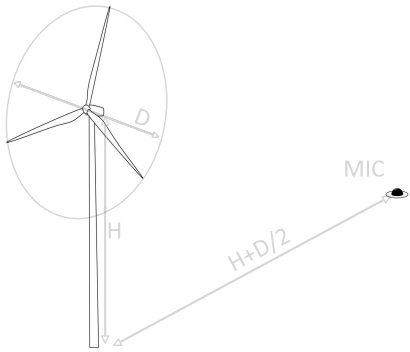

Figure 2.9: IEC setup showing microphone location at $H + \frac{D}{2}$ downwind of wind turbine.

The IEC 61400-11 procedure results in a document reporting the relevant tones of the wind turbine, each with their frequency at which they occur and the wind speed(s) when they are audible. The IEC 61400-11 standard however does not include any specific limit or penalty on audible tones. It leaves this penalisation and regulation up to other authorities.

Low frequency noise

LF noise is the noise of the wind turbine with frequencies linked with the blade pass frequency which are very close to the actual lower frequency hearing limit for humans. The emitted LF noise from wind turbines is currently a hot research topic whether or not it is audible or sensible and whether or not this LF noise can affect human health. As this noise has its origin in the aeroacoustic noise, it will not be further discussed.

2.4.2 Wind turbine noise sources

In general noise radiated from a wind turbine can be subdivided in two big categories:

1. aeroacoustic noise
2. mechanical noise

Aeroacoustic noise

Aeroacoustic noise originates from the aero-elastic interaction between the air and the blades, the tower and the nacelle. Aeroacoustic noise is airborne noise and is primarily broadband of nature. Aeroacoustic noise is considered as the main source of wind turbine noise [175]. Many noise mechanisms contribute to this aeroacoustic noise. Most important noise mechanisms include flow separation noise, turbulent layer trailing edge noise, leading edge noise and tip noise [15, 112, 137]. Figure 2.10 shows how these individual noise mechanisms contribute to an example A-weighted noise spectrum of a large modern wind turbine. The aeroacoustic noise is responsible for both the AM and the low frequency noise content of the wind turbine noise.

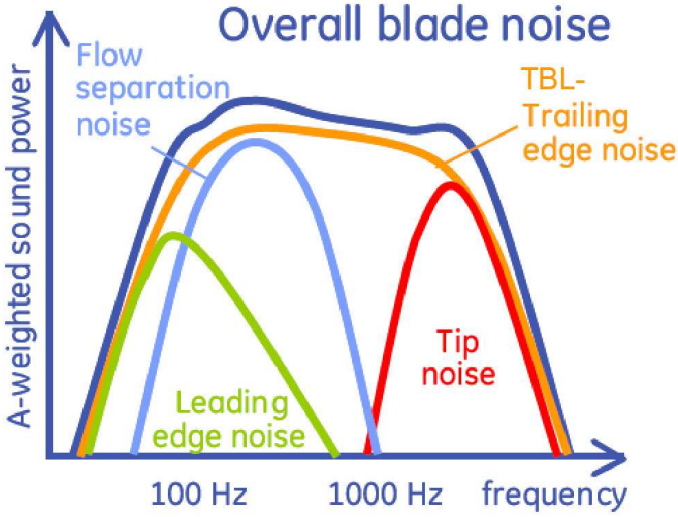

Figure 2.10: Contribution of individual noise mechanisms for an A-weighted noise spectrum of a large modern wind turbine. Reproduced from [137]

As the aeroacoustic noise is considered as the main source of the wind turbine noise, much effort is spent to lower this aeroacoustic noise. These optimisations can be divided in two groups based on their impact on the resulting energy output of the wind turbine:

1. *Approaches which achieve a noise reduction without a reduction in energy output of the wind turbine.* These approaches mainly focus on the blade

and the blade tip design [113, 137, 141] e.g. see figure 2.11 of a wind turbine blade with a serrated design to reduce the produced noise.

2. *Approaches which achieve a noise reduction but also result in lower energy output of the wind turbines.* These techniques include reducing the inflow velocity[2] or the local angle of attack of the blades.
   An implementation of such a technique is the usage of the so-called 'low-noise' operating modes. During these low-noise operating modes (see figure 2.6), torque is kept at nominal level, but the rotational speed of the wind turbine is lowered resulting in both reduced aeroacoustic noise levels and a reduced energy output. As a consequence, this operating mode is only utilised when absolutely necessary, e.g. for a wind turbine close by a residential area, during the evening and night.

Figure 2.11: Climber removing trips from serrated blade. Reproduced from [113]

[2]inflow turbulent noise and trailing edge noise both scale with approximately the fifth power of the local blade inflow velocity[11, 15, 112]

Mechanical noise

Mechanical noise originates from interaction between individual mechanical components such as gears. Mechanical noise sources include the gearbox, generator, cooling fans, yaw drives and hydraulics. Mechanical noise is initially propagating structure-born through mechanical structures, bearings and bushings to surfaces which will radiate the structure-born noise into airborne noise.

Mechanical noise most often has a tonal nature because mechanical machinery and also electronics tends to operate at fixed frequencies. Think of the rotational speed of a fan, the rotational speed of an electric motor, the rotational speed of a combustion engine, or the electrical frequency in a power converter, ...

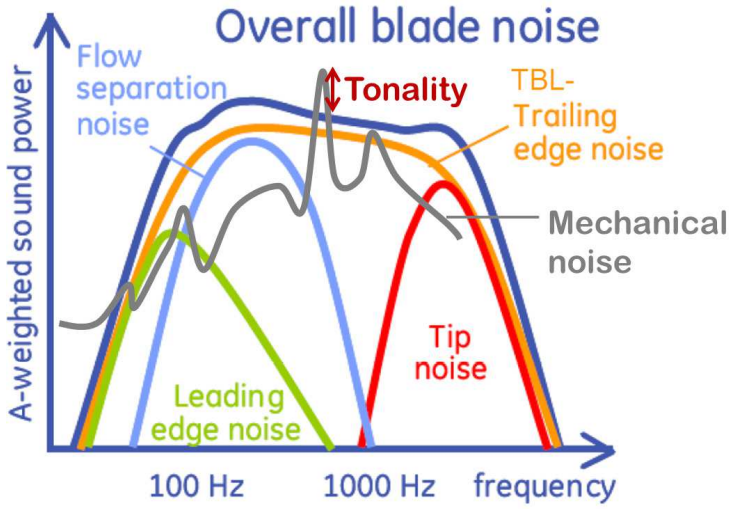

Figure 2.12: Contribution of individual noise mechanisms for an A-weighted noise spectrum of a large modern wind turbine including a typical mechanical noise spectrum. Partially reproduced from [137]

This mechanical noise is not considered to be the dominant source of wind turbine noise [175], but only becomes audible when these discrete tones rise above the aeroacoustic noise. Figure 2.12 shows this aeroacoustic noise and how the tonal mechanical noise can cause a tonality. The level of the tonality is defined in the IEC 61400-11 standard and relates with the level of the peak compared with the level of its neighbouring frequencies, indicated by the red

arrow in figure 2.12. The level of the tonality therefore depends on the level of the mechanical noise source, but also on the level of the aeroacoustic noise which serves as background noise. Reductions in this aeroacoustic noise, by optimised blade design or by the usage of so-called 'low-noise' operating modes, can have an adverse effect on the level of the tonalities and result in a slight reduction of the total wind turbine noise, but also in an increase in annoyance due to a higher tonal content.

2.4.3 Wind turbine noise perception and annoyance

Several studies have been performed to investigate how wind turbines and wind turbine noise is perceived by people living in the vicinity of one or multiple wind turbines [127, 128, 9, 129, 176, 80]. These studies investigated how a wind turbine and wind turbine noise affect the living environment of the residents. These studies were performed by handing out questionnaires to people living in a close vicinity of the wind turbines. These questionnaires were then linked with calculated noise levels caused by the wind turbines in the vicinity.

A common way to analyse such data is by calculating a so-called 'dose-response' relationship which also exists for other noise sources such as transportation noise [104, 106] or industry noise (stationary) [105]. These dose-response relationships express the percentage of the population being annoyed (%A) or highly annoyed (%HA) by a certain level of noise (typically expressed by L_{DEN}[3]) and are typically used as an important source of information when drafting regulations to impose limits on certain noise sources. As mostly calculated noise levels are used in these investigations instead of measured noise levels, no correlation can be drawn between the presence and level of noise characteristics such as AM and tonality and the amount of people annoyed by this noise. Figure 2.13 shows these dose-response relationships for wind turbine noise and transportation noise.

Main conclusions from these studies are:

- Wind turbines produce a specific noise which is perceived differently than for instance air, road or rail noise: a wind turbine noise level of 45 dBA L_{DEN} annoys or highly annoys many more people than an equally loud air, road or rail noise. This may be caused by the specific sound characteristics of wind turbine noise such as amplitude modulation and possible tonality.

[3] L_{DEN} is a noise metric which is defined as a weighted average of the A-weighted long-term L_{Aeq} during the **d**ay, **e**vening and **n**ight, and applies a 5dB penalty to noise in the evening and a 10dB penalty to noise during the night [106].

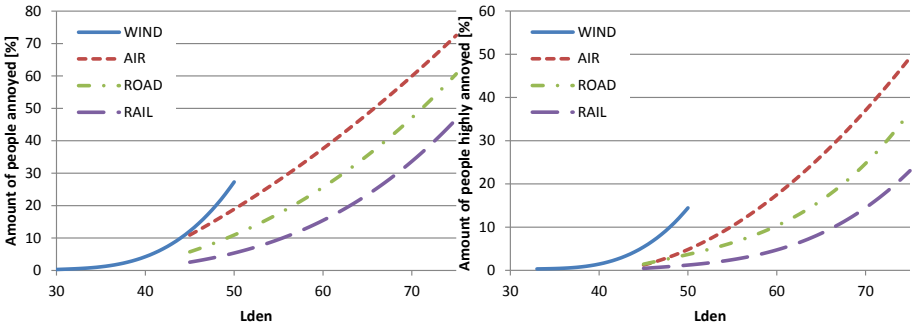

(a) Annoyed (b) Highly annoyed

Figure 2.13: Comparison of the percentage of residents annoyed or highly annoyed indoors due to wind turbine noise (wind) and due to transportation noise (air, road and rail).

- Although noise level has the highest impact on the percentage of residents annoyed or highly annoyed, other aspects, such as age, visibility of the wind turbines when indoor, economical benefit, environment (rural or built-up), noise sensitivity, ... have a significant effect on whether or not a resident is annoyed when exposed to a certain wind turbine noise level. Especially people who have economical benefit from the wind turbines and usually live closer to the wind turbines reported significantly less annoyance.

These studies have established a relationship between overall wind turbine noise using the L_{DEN} metric and annoyance. They recognise the effect of the typical wind turbine noise (amplitude modulation, tonality, low frequent noise) on this dose-response relationship which is implicitly included; however, they cannot take it quantitatively into account as it would require noise measurements to quantify these characteristics inside the dwellings of all residents who participated in these questionnaires. Reductions of the amplitude modulation or tonalities inside the wind turbine noise may therefore result in a lower percentage of the population being annoyed or highly annoyed making wind turbine noise more comparable with transportation noise.

2.4.4 Regulations on wind turbine noise

No European or American regulation on wind turbine noise exists. Instead, a big disparity exists on wind turbine noise regulations based on location. Regulations

can be imposed on state level (such as in the U.S.), on country level (such as in France), on regional level (such as in Belgium), on provincial level (such as in Canada) ... Other countries (such as Germany) do not have a specific wind turbine noise regulation at all and rely on their general noise guidelines to limit wind turbine noise [34].

The disparity between all regulations becomes quite clear when comparing the actual contents. All regulations limit the overall noise based on a specific metric such as L_{Aeq} or L_{DEN}. These limits often depend on land use designated areas (such as industrial area versus recreational area), time (such as day versus night) and existing background noise level. In some cases regulations also set limits on the level of individual octave bands, on LF noise, on impulsive noise, ...

In many regulations background noise is taken into account. Often, at sites with already increased background noise levels (such as industry sites) the noise limits are changed from the regulated values to the already existing background noise. This allows placing wind turbines in already loud areas if the noise from the wind turbines is significantly lower than the existing background noise.

If tonality is included in the regulations it is mostly taken into account by defining penalties on the overall level: when a tonality limit is exceeded a penalty is added to the overall noise level which is limited by the regulations. In some regulations such as in some provinces in Canada this penalty is always added (one assumes that all wind turbines have tonality), in other regulations these penalties should only be taken into account if the wind turbine prototype certification measurements (IEC 61400-11) showed tonalities. If tonality is not included in the wind turbine noise regulations (such as in Flanders), tonality limits are mostly defined by an applicable industry noise limit and also require wind turbine prototype certification measurements.

Tables 2.1 and 2.2 give an overview of the applicable wind turbine noise limits in Flanders, Belgium and the surrounding countries. A more global overview of international legislation and regulations can be found in [34].

Table 2.1: Noise level limits for wind turbines in Flanders, Belgium. (annex 5.20.6.1 of VLAREM)

Area	Noise level dB(A)		
	day (7am-19pm)	evening (19pm-22pm)	night (22pm-7am)
1a: Residential recreation areas	44	39	39
2a: Areas or parts of areas, other than residential areas, at a distance of less than 500 m of industrial areas	50	45	45
2b: Residential areas or part of residential areas, at a distance of less than 500 m of industrial areas	48	43	43
3a: Areas or parts of areas, other than residential areas or parts of residential areas, at a distance of less than 500 m of areas for small and medium-size companies, areas for the provision of services or excavation areas, during the excavation	48	43	43
3b: Residential areas or parts of residential areas at a distance of less than 500 m of areas for small and medium-size companies, areas for the provision of services or of land use areas, during the excavation	44	39	39
4: Residential areas	44	39	39
5: Industrial areas, areas for the provision of services and public utilities and land use areas, during the excavation	60	55	55
5bis: Rural areas	48	43	43
6: Recreation areas, other than residential recreation areas	48	43	43
7: All other areas, other than buffer areas, military areas and areas where in specific decisions noise levels are determined	44	39	39
8: Buffer areas	55	50	50
9: Areas or parts of areas at less than 500 m of gravel excavation areas, during the excavation	48	43	43

Table 2.2: Comparison of noise level limits in residential areas for wind turbines in some European countries [34].

Governing Jurisdiction	Noise Metric	Residential Area
Belgium - Flanders	L_{Aeq} at 95% of nominal power [dB(A)]	day: 44, evening & night: 39
Belgium - Wallonia	L_{Aeq} at all wind speeds [dB(A)]	45
France	L_{Aeq} at all wind speeds [dB(A)]	day: 5 dB(A) increase allowed with reference to background noise level, night: 3 dB(A) increase allowed
Germany	L_{r} (long time average noise level) at all wind speeds (dB(A))	day: 50-55, night: 35-40
The Netherlands	L_{DEN} & L_{night}	L_{DEN}:47, L_{night}:41

2.5 Wind turbine farm planning

Wind turbine farm planning is a complex process trying to maximise the economic output of a wind farm taking into account many constraints. The wind turbine farm planning processes consist of two big steps: site location and site layout.

2.5.1 Site location

During this initial step a location for a wind farm is sought. Key driver here is to maximise economic output. Optimum locations are therefore locations with a high mean wind speed. Mesoscale models of the atmosphere (see figure 2.14) are used to provide an estimate of the long term mean wind speed. However many constraints need to be taken into account when selecting possible site locations such as intended land usage, proximity to habitation, ecology (fauna and flora), accessibility for heavy and big parts during construction, a good electric grid connection, ... Based on this mesoscale model and all the influencing constraints a list of potential wind turbine sites is generated.

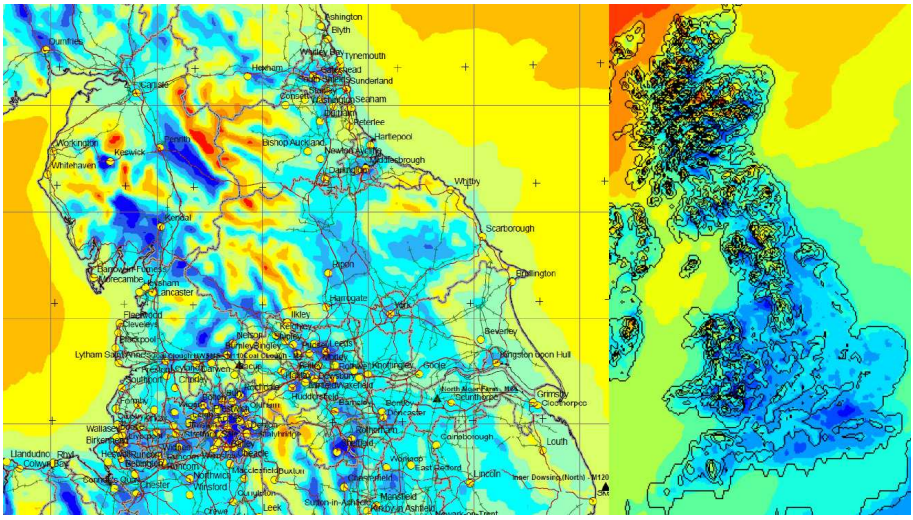

Figure 2.14: Mesoscale model for the UK. Reproduced from [17]

2.5.2 Site layout

Once an appropriate site location is selected the wind farm layout is determined. This optimisation process tries to gain from topographical effects and tries to minimise losses such as wake effects in order to maximise energy yield. Result of this optimisation process is an actual wind turbine farm layout: where to place the individual wind turbines. In contrast with the more global constraints when looking for an optimal site, the site layout planning takes more local constraints into account such as: visibility, proximity to habitation, shadow flicker induced by the rotating blades, electromagnetic effects, noise and other obstacles such as existing masts or electrical lines.

Unlike shadow flicker or setback distance constraints which can easily be plotted on maps to find possible wind turbine locations (see figure 2.15), constraints like noise levels require more advanced calculations. To verify that emitted noise levels stay below local regulations these regulations mostly specify a calculation method and parameters to use. Often an ISO 9613 (Acoustics - Attenuation of sound during propagation outdoors) [77] calculation is required. These calculations start from expected wind turbine noise sound power levels (measured using IEC 61400-11 and possibly including a tonality penalty) and take into account items such as terrain layout, background noise and ground absorption to determine noise pressure levels in the surroundings and at the

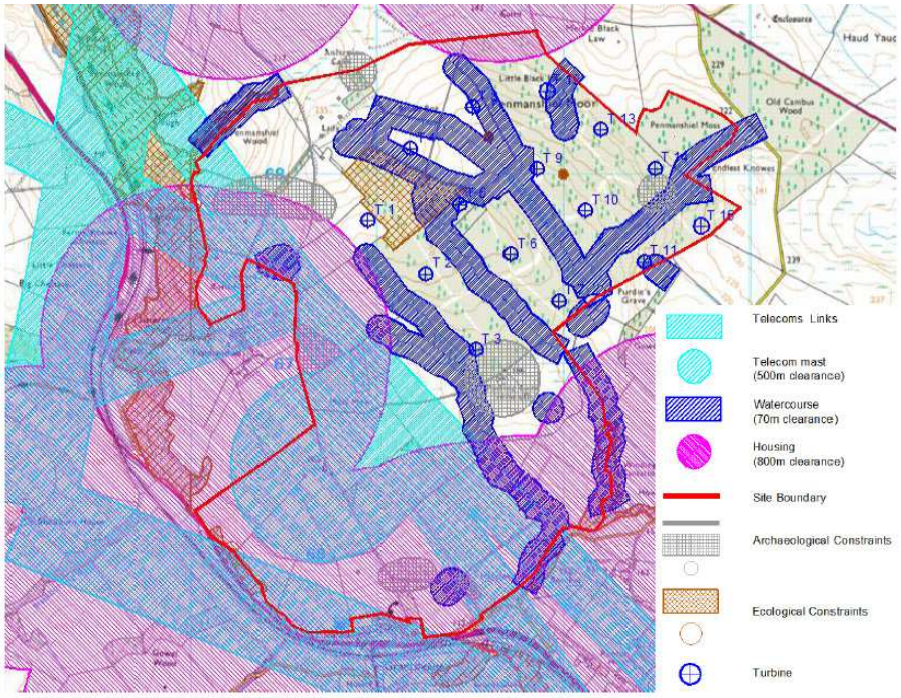

Figure 2.15: Example constraint map showing all constraints for a selected site. Reproduced from [17]

neighbours dwellings. Results of such a calculation can be seen in figure 2.16; it shows if a certain wind turbine farm configuration complies with local noise regulations, or if one or more wind turbines should be moved, removed or put in a low-noise operating mode during e.g. night-time. More information on wind turbine site assessment and wind turbine farm planning can be found in [21, 17].

2.6 Wind turbine gearboxes

2.6.1 Design

The wind turbine gearbox is an essential part in the drive train of a classical wind turbine. In this configuration the gearbox is used to increase to the rotational speed of the rotor (which is typically between 10 and 17 RPM) up to

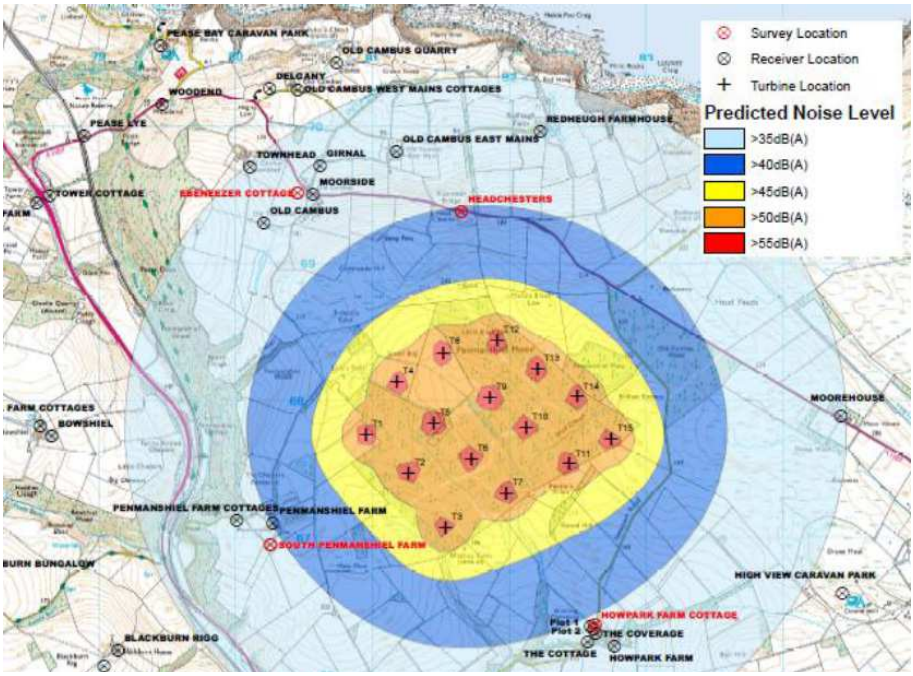

Figure 2.16: Example ISO 9613 results plot showing predicted noise levels for a selected site. Reproduced from [17]

rotational speeds suitable for the generator (which are typically in the range between 1000 and 1800 RPM). In total a gearbox ratio of approximately 100 is needed, which most often results in a gearbox with three gear stages. By increasing the rotational speed, also the rotor torque (typically in the range between 1 and 5 MNm) is reduced by the same amount. The wind turbine gearbox is connected to the main shaft or, in an integrated wind turbine layout, directly to the rotor hub at the low speed side. On the high speed side the gearbox connects to the generator using a generator coupling (see figure 2.5).

Figure 2.17 shows a sectional drawing of the gearbox used in this dissertation. It shows gearing layout, bearing locations and the names of the large cast parts, the rotating parts and the bearings according to the IEC 61400-4 standard [75]. Figure 2.18 gives some more information on some ZF Wind Power products to get a feeling with dimensions and weight of these wind turbine gearboxes.

Several concepts exist to mount the drive train (mainshaft, gearbox, generator) on the mainframe. Typical suspension types are the 3-point suspension (one main

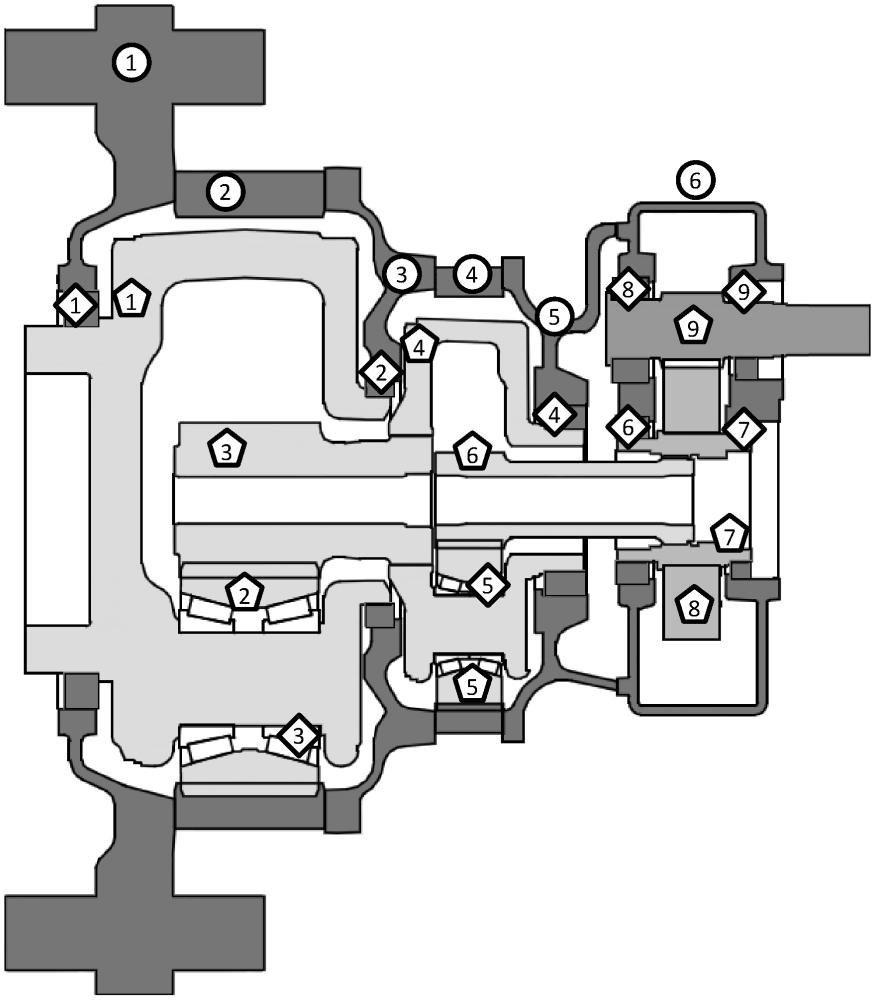

Structural components - stationary

(1) torque arm (TA)
(2) low speed ring wheel (LSRW)
(3) intermediate bearing housing, low speed side (IBH LSS)
(4) intermediate speed ring wheel (ISRW)
(5) Intermediate bearing housing, intermediate speed side (IBH ISS)
(6) High speed housing + main cover (HSH) + (MC)

Rotating components - Low speed planetary gear stage

(1) Low speed stage planet carrier (LSS-PC)

(2) Low speed stage planet (LSS-PG)

(3) Low speed sun (LSS-SU)

(2) Low speed ring wheel (LSRW)

Rotating components - Intermediate speed planetary gear stage

(4) Intermediate speed stage planet carrier (ISS-PC)

(5) Intermediate speed stage planet (ISS-PG)

(6) Intermediate speed sun (ISS-SU)

(4) Intermediate speed ring wheel (ISRW)

Rotating components - Parallel gear stage

(7) high speed intermediate shaft (HS-IS)

(8) high speed intermediate gear (HS-IG)

(9) high speed shaft (HSS)

Bearings

(1) low speed stage planet carrier bearing, rotor side (LSS-PC-RS)

(2) low speed stage planet carrier bearing, generator side (LSS-PC-GS)

(3) low speed stage planet bearing (LSS-PG-RS)

(4) intermediate speed stage planet carrier bearing, generator side (ISS-PC-GS)

(5) intermediate speed stage planet bearing (ISS-PG-RS)

(6) high speed intermediate shaft bearing, rotor side (HS-IS-RS)

(7) high speed intermediate shaft bearing, generator side (HS-IS-GS)

(8) high speed shaft bearing, rotor side (HSS-RS)

(9) high speed shaft bearing, generator side (HSS-GS)

Figure 2.17: Sectional drawing of the wind turbine gearbox used throughout this dissertation. Naming convention according to the IEC 61400-4 standard [75].

Generator power	1.5 MW	6.15 MW
Configuration	1 planetary stage 2 helical stages	2 planetary stages 1 helical stage
Approx. weight	12700 kg	63000 kg
Overall length	2100 mm	3973 mm
Picture		

Figure 2.18: Limited product overview of ZF Wind Power wind turbine gearboxes.

bearing and two connection points on the gearbox) and the 4-point suspension (two main bearings and two connection points on the gearbox). Depending on the number of suspension points and their physical implementation, the gearbox is loaded by only the wind torque or also by other components of the external wind loading such as the radial forces and bending moments which significantly affect the construction of the gearbox. It also determines the possible vibration isolation of the gearbox to the mainframe: a gearbox loaded in all directions should be connected rigidly to the mainframe in all directions while a gearbox only loaded by torque can be connected rigidly to the mainframe in only the torque direction and weak in all directions improving vibration isolation. More information about these different drive train concepts and their impact on noise and vibrations can be found in [72].

2.6.2 Excitation sources

Gears

A huge amount of research has been devoted over the last few decades to fully comprehend the underlying mechanisms responsible for gear noise. In general it can be said that gear noise originates from the non constant gear meshing forces. The best known component, the component of the gear meshing forces along the line of action, is called the transmission error (TE) force and is considered to be

the dominant gear noise mechanism. TE is defined as the difference between the actual position of the driven gear and the position that the driven gear would occupy if it were rigid and perfect [178]. TE has its origin in the compliance of gears and gear teeth, shafts, housing flexibility, ... all resulting in periodic varying gear mesh forces. Several tools exist to calculate and minimise this TE taking all these flexibilities into account by modifying gear macro and micro geometry. Next to TE forces (along the line of action), also other forces such as friction forces and shuttling forces (due to the axially changing contact location) contribute to the resulting gear noise, however, they are expected to be less dominant [13, 55, 1].

Due to the periodic nature of the gear meshing this gear noise mainly excites well defined frequencies, mainly based on the macro geometry of the mating gear pair. For each parallel gear stage the so-called gear excitation frequency can be calculated as:

$$f_z = \frac{N_{\text{shaft}} \times Z}{60} \tag{2.1}$$

with

- N_{shaft}: rotational speed of shaft [RPM]
- Z: number of teeth on gear [-]

However, due to the fact that this gear meshing force is not 100% sinusoidal, also higher harmonics of this frequency exist resulting in a discrete amount of excitation frequencies. The gear excitation frequency is often called the first order, the first harmonic (at $2 \times f_z$) is called the second order, and so on ...

Other effects, such as a slightly misaligned gear wheel on a shaft, result in a modulation of the gear meshing forces. In the frequency domain this modulation results in so-called 'sidebands' around the gear excitation frequency. For the slightly misaligned gear wheel this modulation is linked with the rotational speed of the shaft and results in additional sidebands spaced at $\frac{N_{\text{shaft}}}{60}$ Hz around the gear excitation frequency.

For a planetary gear stage with a fixed ringwheel this gear excitation frequency can be calculated as:

$$f_z = \frac{N_{\text{planetcarrier}} \times Z_{\text{ringwheel}}}{60} \tag{2.2}$$

with

- $N_{\text{planetcarrier}}$: rotational speed of the planet carrier [RPM]
- $Z_{\text{ringwheel}}$: number of teeth on the ring wheel [-]

Around this gear excitation frequency a lot of sidebands spaced at $\frac{N_{\text{planetcarrier}}}{60}$ Hz are present. The relative importance of the main gear excitation and these sidebands and whether or not this main gear excitation frequency or some sidebands are visible is determined by the actual configuration of the planetary stage: it is mainly influenced by the rotational spacing of the planets (equally or non-equally spaced) and the relative phase difference between the individual planets. More information on excitation frequencies of planetary gear stages can be found in [170].

In general this signifies that for a 3 gear stage wind turbine gearbox a lot of discrete gear excitation frequencies exist which can all excite an eigenmode leading to resonance and a tonal noise issue. Experience however learns that the excitation originating from the first few (typically the first two) orders of the second gear stage and the third gear stage are dominant and may generate wind turbine tonalities.

Bearings

Bearings, similar to gears, also generate excitations. These excitations, originating from imperfections in rollers and raceways such as waviness of the raceways, are lower in amplitude than gear excitations and are considered not to be contributing to wind turbine tonalities. In an exceptional case where bearing excitations would be higher in amplitude than the gear excitations, then this bearing should be considered faulty and be replaced which will solve the issue. More information about bearing excitation frequencies can be found in [111].

Other auxiliaries

For completeness it should also be mentioned that other auxiliaries such as electrical pumps or cooling fans can cause noise issues with frequencies related with the rotational speed of the pump or the blade pass frequency of the cooling fan.

2.7 Wind turbine noise transfer paths

A commonly used approach to look at noise and vibration issues is the so-called 'source - transfer path - receiver' approach. This approach subdivides a noise and vibration issue in a source which transmits its noise or vibrations over a certain transfer path to a receiver. A noise or vibration issue can be dealt with by modifying only the source, the transfer path or the receiver or a combination of both. Figure 2.19 utilises this approach on an entire wind turbine and takes both structure-born and airborne sound into account. Both gearbox and generator should be considered as noise sources, it is however more interesting to also take the individual gearbox and generator noise sources and transfer paths into account. Main sources of wind turbine noise include:

- Aeroacoustic noise by the interaction between the air and the blades, the tower and the nacelle.
- Mechanical noise by:
  - auxiliary systems such as: pumps, fans, cooling systems, ...
  - electrical systems such as: pitch drives, yaw drives, ...
  - gear noise originating from the wind turbine gearbox,
  - generator noise originating from the interaction of the generator with the grid and interaction between the rotor and the stator of the generator
  - ...

Noise from the wind turbine gearbox can propagate to the outside world in several ways. Most important transfer paths are:

1. Through rotating parts: structure-born from the gears, through all rotating parts including mainshaft to the blades, and airborne from the blades to a receiver outside.
2. Through non-rotating parts: structure-born from the gears, through some (or all) rotating parts, through the bearings and wind turbine gearbox housing to the wind turbine mainframe. From the mainframe it can propagate to the nacelle cover or the tower, and radiate airborne to a receiver outside.
3. Airborne: Airborne from the wind turbine gearbox housing, through the nacelle cover to a receiver outside.

The relative level of each transfer path compared with the other transfer paths at a certain frequency determines which transfer path is dominant.

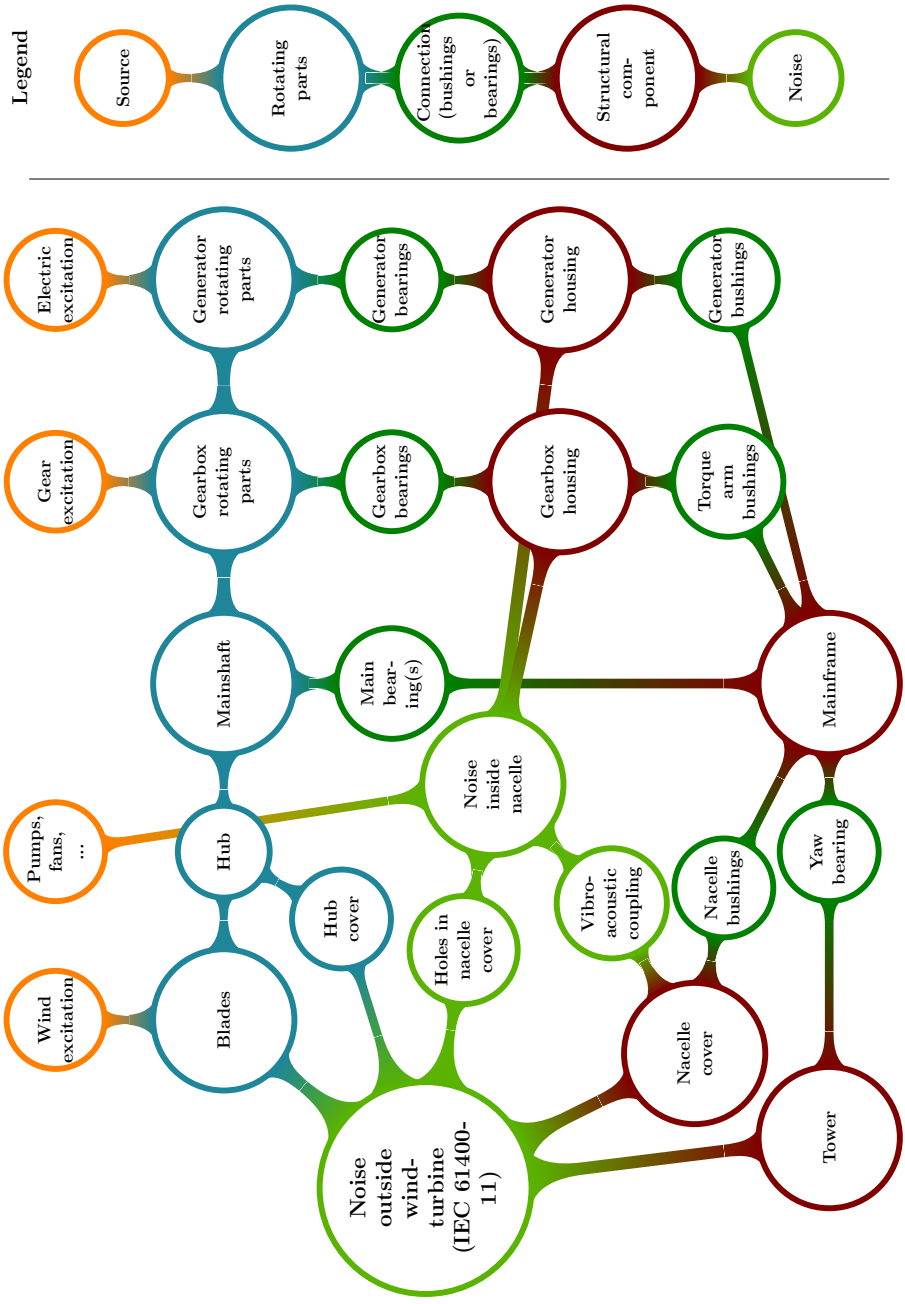

Figure 2.19: Graphical representation of paths how noise and vibrations can propagate throughout a wind turbine.

2.8 Conclusions

This chapter introduced wind turbines and the noise produced by the wind turbines. Based on the reports of the IPCC wind turbines can play an important role in mitigating the effects of the climate change, depending on how these proposals are translated into regulations.

The layout of a modern multi-megawatt wind turbine is discussed. Focus is put on the drive train layout, and on the complex and wide operating conditions of the wind turbine.

Wind turbine noise is firstly described by its main characteristics: amplitude modulation, tonality, and low frequency noise. Tonalities are visible in the noise spectrum as single tones or sharp peaks, and are perceived by the human hearing as very annoying. The IEC 61400-11 standard documents the way to measure and to evaluate these tonalities.

Secondly, wind turbine noise is characterised by its sources: aeroacoustic noise and mechanical noise. Aeroacoustic noise on the one hand originates from the interaction of the air and the blades, the tower and the nacelle. Aeroacoustic noise is airborne noise and is primarily broadband of nature. Aeroacoustic noise is considered as the main source of wind turbine noise and is responsible for both the amplitude modulation and the low frequency noise content of the wind turbine noise. Several methods exist to lower this aeroacoustic noise such as optimising blade layout, but also the so-called wind turbine low-noise operating mode. This low-noise operating mode reduces the operational speed which significantly reduces the aeroacoustic noise, but also the produced power. Mechanical noise on the other hand originates from the interaction between individual mechanical components such as gears. Mechanical noise sources include the gearbox, generator, cooling fans, yaw drives and hydraulics. Mechanical noise most often has a tonal nature because mechanical machinery and also electronics tends to operate at fixed frequencies. This mechanical noise is not considered to be the dominant source of wind turbine noise, however, when these discrete tones rise above the aeroacoustic noise it becomes audible and is perceived as very annoying.

Several studies have been performed to investigate how wind turbines and wind turbine noise is perceived by people living in the vicinity of one or multiple wind turbines. In general it can be concluded that wind turbine noise is perceived more annoying than another equally loud noise source such as transportation

noise. This difference in perception may be due to the specific wind turbine noise characteristics such as amplitude modulation and the presence of tonalities. Lowering the amplitude modulation and tonalities will reduce this annoyance.

An overview on regulations showed that a large disparity exists based on location. Typically limits are set on the overall level depending on land use, time and existing background noise levels. Tonality is mostly addressed by defining penalties on the overall level.

An overview on wind turbine gearbox design was given including a cross sectional drawing of the gearbox used in this dissertation. Gear noise, which is the main source of mechanical noise of the wind turbine gearbox, is characterised by defining its typical gear mesh frequencies. Furthermore, an in-depth overview is given of the possible transfer paths by which the mechanical gear noise can propagate (both structure-born and airborne) to the outside of the wind turbine and eventually result in tonalities if its level rises above the aeroacoustic noise.

Chapter 3

Wind turbine drive train modelling, an overview

This chapter describes the current state-of-the-art and state-of-the-use in wind turbine drive train modelling with a strong focus on predicting the dynamic behaviour of the wind turbine drive train. Two kinds of models are capable of capturing wind turbine drive train dynamics up to a certain extent: drive train design load models, and drive train noise and vibration models. Note that there is an overlap between those two kinds of models as some models are used for both load prediction but are also accurate enough to assess the NV behaviour. For both types of models an overview is given and the limitations and shortcomings of these models are discussed.

3.1 Wind turbine drive train design load models

At the very start of the development of a new wind turbine, specialised software is used to predict the drive train design loads. These codes take into account all relevant external conditions, combined with all possible operating and fault conditions of the wind turbine. Based on these predicted loads, the development of the individual drive train components such as the main shaft or the gearbox can start. All calculations to predict strength or durability of any component in the drive train are based on these load predictions. These codes are typically split up in several modules (see figure 3.1), each specialised in a certain aspect of the wind turbine or its environment. Some of the most known codes are GH Bladed [14, 27] FAST-AD [179], and Flex [118]. A more elaborate overview on

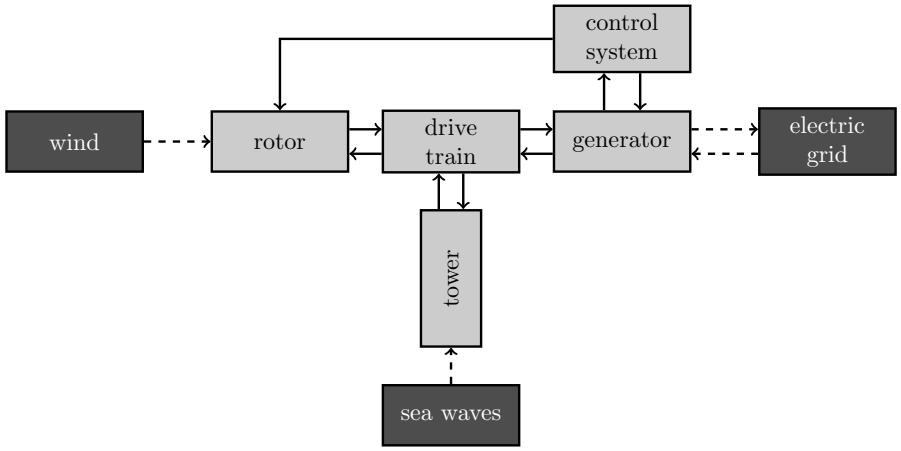

Figure 3.1: Schematic representation of the implementation of existing wind turbine design codes (dark grey: external modules, light grey: internal modules). Reproduced from [132].

these codes can be found in [132, 107, 145, 18].

The combination of the modules rotor, drive train, generator and tower form the structural model in these codes. Although no exact description for all these codes is made public, the concept of all these codes is believed to be more or less similar [132] and include 3 to 5 DOFs for tower deformations, 12 to 18 DOFs for blade deformation for a three bladed rotor, and 1 additional DOF to represent the deformation in the entire drive train. Figure 3.2 shows a graphical representation of such a model. This model is used to derive the equations of motion which are then coupled and combined with the governing equations describing the external load input (an aeroelastic model for the blades e.g.) and the equations describing the wind turbine controller resulting in a set of equations which describe the global wind turbine behaviour.

Typically these models are solved in the time domain and they require wind fields, sea wave excitations and grid events as input to obtain the deformation at these DOFs and the accompanying loads. However, these models can also be solved in the frequency domain, and eigenmodes can be extracted which describe the dynamic behaviour of the complete wind turbine. These eigenmodes include: first few tower bending modes, first few blade bending modes and the first torsional eigenfrequency of the drive train, ... The actual number

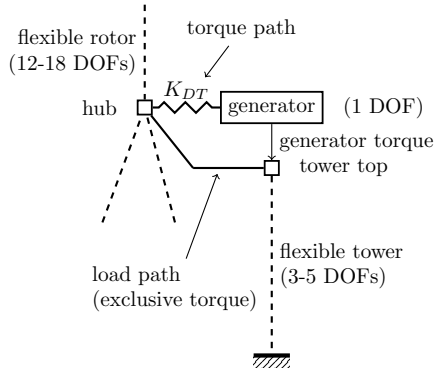

Figure 3.2: Schematic representation of the DOFs in a structural model of a three-bladed wind turbine in a traditional design code. Reproduced from [132]

of eigenmodes depends on the number of DOFs that are taken into account. Figure 3.3 shows some of the blade bending eigenmodes. A more elaborate overview of these eigenmodes for 7 different turbines can be found in [132].

The structural model utilised in these codes gives insight in the wind turbine dynamic behaviour in a frequency range between 0 and 10 Hz. This information is very valuable for the determination of the loading on the individual components of the drive train, and to avoid harmful resonances such as exciting a tower bending eigenfrequency with the dominant wind turbine excitation frequencies 1P[1] and the first multiples of 3P for a three bladed wind turbine. It however gives no insight in the dynamics of the wind turbine in the audible frequency range (typically assumed between 20 Hz and 20 kHz for an average person) where tonalities may occur and can therefore not be utilised to assess the dynamic behaviour of the wind turbine in the audible frequency range.

For certification however an assessment should be made regarding load increasing resonances in the main drive train components. For this purpose, a more detailed model is employed, typically with more torsional DOFs for the gearbox and other components of the drive train such as main shaft, shrink disks, brake, couplings, generator, ... [37]. Usage of these models however stays limited at determining torsional eigenfrequencies in the lower frequency range, and no insight is gained in the total dynamic behaviour of the complete wind turbine drive train.

[1] nP stands for n $\times$ the rotational speed of the rotor (in Hz)

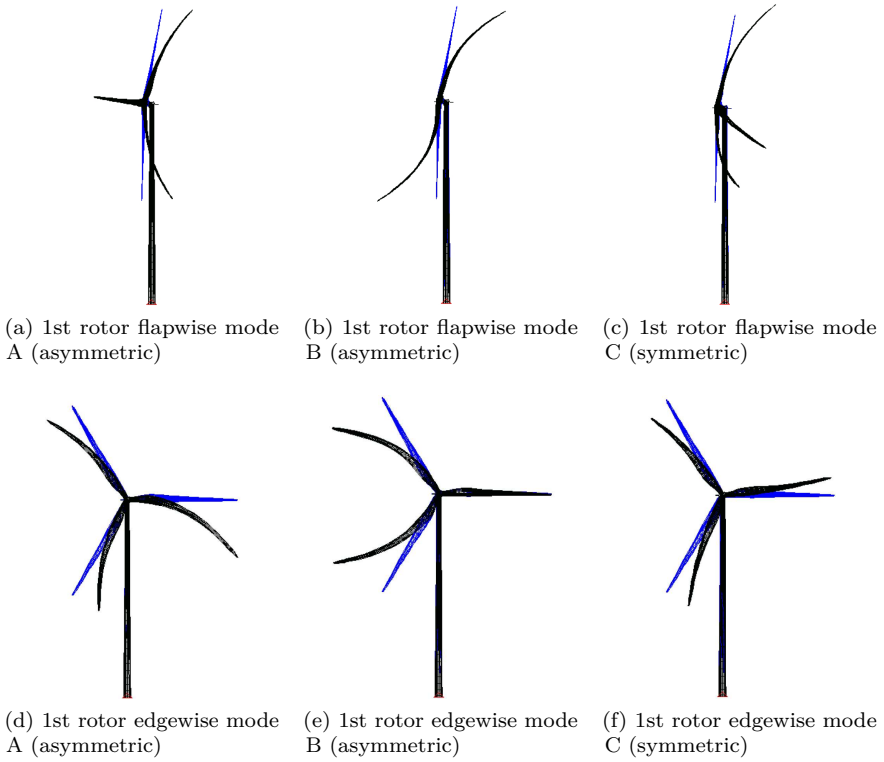

(a) 1st rotor flapwise mode A (asymmetric)
(b) 1st rotor flapwise mode B (asymmetric)
(c) 1st rotor flapwise mode C (symmetric)
(d) 1st rotor edgewise mode A (asymmetric)
(e) 1st rotor edgewise mode B (asymmetric)
(f) 1st rotor edgewise mode C (symmetric)

Figure 3.3: The 1st rotor modes of a wind turbine: side view for the flapwise modes and front view for the edgewise modes (undeformed and deformed models are shown). Reproduced from [132]

Peeters argued [132, 133, 134] that utilising a structural model with such a limited number of DOFs has several important limitations that could be overcome by increasing the detail in the structural model. These limitations mainly include lack of dynamic internal excitation (originating from the generator, gears and others), and the lack of detailed insight in component loading. Peeters proposed more accurate models of the drive train which include a large number of DOFs in contrast with the single DOF in the traditional or certification codes. Using these more detailed models, more insight can be gained in the static and dynamic behaviour of the drive train, resulting in a more accurate loading prediction for all components included in these models. Peeters suggested usage of the flexible MB technique as it allows simulating

complex linear or non-linear dynamics in the frequency range of interest with an acceptable computational effort. To state this case a model of a complete drive train was developed and analysed. His call for more DOFs was heard and now some traditional codes link in more complex models containing an arbitrary number of DOFs by using dynamically linked libraries (DLLs) [26]. Helsen [60] continued on the research of Peeters and investigated which components should be modelled flexible.

Next to some traditional codes which include more detail, general purpose commercial CAE codes utilising the MB and FE technique recently have been optimised to perform wind turbine loading calculations. Best known codes are Simpack [156, 51], LMS Virtual.LAB [87, 86] and Samcef [98]. These general purpose commercial CAE codes are coupled with aerodynamic codes to capture the interaction between the blades and the wind [54, 143]. Using these codes, numerous models of entire wind turbines or wind turbine drive trains have been generated to assess or to investigate wind turbine (drive train) loads:

- Dollhofer and Stache [28, 157] investigated the replacement of the traditional design load codes with these models.
- Heege et al. [58, 57] concluded that a complete wind turbine drive train model is necessary to accurately capture the resulting loads, especially in the wind turbine gearbox.
- Schlecht et al. [146, 149, 150, 147, 148] made numerous models of large drive trains, also including drive trains for wind turbines and concluded that flexible models with a large number of DOFs should be used to accurately predict the loading on a complete drive train as torsional models do not suffice. Furthermore Schlecht et al. used these models to investigate possible resonances inside the drive train and suggested that these resonances should be further investigated as they could be the cause for premature failures of the wind turbine drive train.
- Radovcic [140] demonstrated the use of flexible MB to compute load cases such as single blade assembly and investigate detailed bearing loads which cannot be assessed using the traditional codes.
- Viadero et al. [169] used flexible MB to assess the complex loading of suspension mooring lines which keep a floating wind turbine on its position.
- Jassman et al. [81] reduced the loads on the drive train by employing model predictive control.

- Helsen et al. [72] investigated the impact of the suspension conditions of the wind turbine gearbox on its loads.
- To significantly increase the insight in the loading of individual components of the wind turbine gearbox, the National Renewable Energy Laboratory (NREL) started the Gearbox Reliability Collaborative (GRC) project. Main goals of the GRC are to improve the design approach and to recommend practices and test methods which should result in an improved gearbox reliability. To achieve these goals, the GRC uses a combined approach of gearbox testing, modelling and analysis of condition monitoring data [109, 116, 95, 94] on a self owned 750 kW wind turbine. The gearbox of this wind turbine was retro fitted by the GRC to increase similarity with gearboxes of multi megawatt wind turbine drive trains. Several measurements on the wind turbine and on a drive train dynamometer were used to gain insight in the actual loading and the validity of several MB models of this drive train:
  - Oyague et al.[117, 115] investigated the modelling approach and the impact of the model refinement on the torsional behaviour of the gearbox model.
  - LaCava et al. [83] showed that torsional degrees of freedom do not suffice to predict the actual loading on a gearbox, and that flexible gearbox models have the highest correlation with the experimental validation cases.
  - Haastrup et al. investigated the effect of shaft flexibility [44], the necessary model approach to accurately model the deflections in the torque arm bushings [46], and the effect of planet carrier misalignment on gear lifetime reductions [45].
  - Guo et al. [42] investigated the impact of gravity, non-torque bending moments, torque load and bearing clearance on the load sharing between the individual planets of the planetary gear stage. Also the impact of bearing and gear clearances and gravity on tooth wedging, resulting in non-linear behaviour was investigated [41].

Furthermore, much effort is spent in advanced substructuring techniques such that these calculations can be performed in a computationally efficient way [174, 173, 110, 172].

Mainly driven by premature failures, a high amount of effort has been spent to improve these load predictions by experimentally validating these predictions. These initiatives include:

- the European FP7 project PROTEST which was conducted to increase the knowledge to specify and to measure the loads in the wind turbine drive train [73, 32];
- the building and exploitation of test rigs such as the test rig located at the Center for Wind Power Drives (CWD) in Aachen [90, 20] which are capable of testing a complete wind turbine nacelle, including the complete drive train;
- large research projects performing in-depth simulations and measurement campaigns such as the GRC which focusses primarily on the wind turbine gearbox; and
- the adaptation of well known experimental validation techniques for usage with wind turbines such as using experimental modal analysis to characterise the low frequent dynamic behaviour of a wind turbine [103, 120, 122, 121, 119] and using this information to validate a flexible MB model of this wind turbine [114, 101, 100].

All these modelling and validation initiatives significantly increased the insight in wind turbine load predictions. Although many of the models discussed above contain a sufficient amount of DOFs such that next to load prediction also prediction of the dynamic behaviour of the drive train is possible, they however give no insight in modelling approach and necessary model detail to accurately predict the dynamic behaviour in the audible frequency range, nor has any of these models been thoroughly validated beyond static or quasi static loading conditions.

3.2 Noise and vibration models

This section gives an overview on models developed to assess the dynamic behaviour of a gearbox. A distinction is made between non wind turbine gearbox models and wind turbine gearbox models.

3.2.1 Non wind turbine gearboxes

According to Nevzat Özgüven and Houser[123], who reviewed over 188 publications on mathematical models in gear dynamics, the first systematic efforts to analyse gear dynamics occurred around 1920. Since then, a huge amount of research was performed to investigate stresses, pitting, transmission efficiency, but also radiated noise, vibrations and natural frequencies. However,

most of these investigations were performed using lumped mass models only taking into account a limited amount of information and neglecting the influence of e.g. shafts, bearings, housing structures and supporting structure. The investigations building vibro-acoustic models of the entire gear system are sparse [55]. A limited overview of vibro-acoustics models that however do take the entire gear system into account with or without the gearbox housing are listed below.

Lim and Singh [91, 92] investigated the effect of vibration transmission through rolling element bearings. They proposed a bearing stiffness formulation which is capable of calculating the so-called off-diagonal stiffness elements resulting in a more accurate estimation of the bearing stiffness and thus also in the transfer path between gears and housing. Using this new bearing stiffness formulation Lim and Singh [93] modelled three different cases, the most complex being a model of the research gearbox of the National Aeronautics and Space Administration (NASA) in the Glenn Research Center. This gearbox includes a pair of spur gears mounted on two shafts, each shaft supported on two bearings, and both shafts supported in a flexible housing.

In his PhD thesis, Roosmalen [142] constructed a similar model as the model of Lim and Singh taking gears, shafts, bearings and a flexible housing into account. He noticed that although the predictions of the transfer functions of the empty housing agreed considerably well with the experimental measurements on the empty housing, the transfer functions of the gearbox including the gears, shafts and bearing agreed less with measurements. He concluded that further research is necessary to increase the accuracy of the coupling between the gearbox internals and the gearbox housing.

Hajžman et al. combined a component mode synthesis (CMS) reduction of flexible shafts and gears with a CMS reduction of a simple gearbox housing using the bearing stiffness values. The approximative averaged surface velocity (ASV) approach was employed to assess the radiated airborne noise.

Zhu et al. [182] investigated a heavy duty marine gearbox. An FE model of the complete housing was generated and coupled using an FE model of the shafts and gears using a simplified bearing model. For the gears a linear model was utilised and excitation from gear mesh stiffness variation and tooth impact was used as input. The calculated eigenmodes showed a significant coupling between dynamics of the shafts and gears and housing dynamics. A limited experimental validation campaign was performed showing acceptable correlation between

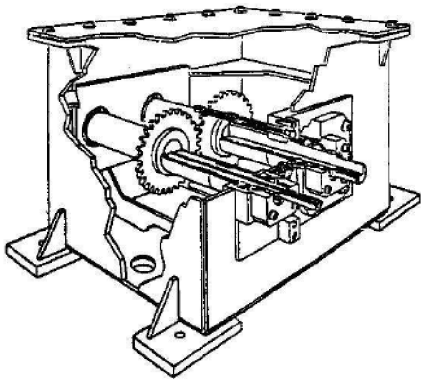

Figure 3.4: NASA GRC test gearbox. Reproduced from [49].

measurements and model.

Probably driven by the availability of experimental measurements, the dynamic behaviour of the NASA gearbox (see figure 3.4) at the Glenn Research Center is quite popular, and several models of this gearbox have been proposed and validated using these measurements:

- In [55] He et al. investigated the effect of sliding friction on the noise of the NASA gearbox. To perform this investigation he calculated the dynamic bearing forces using a lumped mass model of the gears, shafts and bearings, and introduced these bearing forces onto an FE model of the flexible housing. Using the Rayleigh integral technique he calculated the radiated sound and concluded that this technique is promising to predict gearbox airborne noise radiation.

- Hambric et al. [49, 48, 50] investigated the effect of the additional damping of journal bearings on the noise and vibrations based on coupled CMS reductions of shafts and housing. Both model and experimental measurement results showed that journal bearings may have a beneficial effect on the resulting vibrations, but this cannot be considered as a general conclusion as there were also frequencies at which the journal bearings transmitted more vibrations than the rolling element bearings.

- Parker, Guo et al. [126, 43] constructed both a lumped mass model and an FE contact model of this gearbox to predict the structural behaviour and an BE model of the gearbox to predict the noise radiation. They noticed a clear coupling between shafts, gears, bearings and housing, and a decoupling between the gearbox and its test rig. They validated both the analytical, the FE model, and the BE model based on the experimental measurements. They concluded that
  - bearing off-diagonal terms are necessary for accurate noise and vibration predictions, that
  - a wave journal bearing does not necessary produce less noise and vibrations even though it has significant higher damping than traditional roller element bearings, and that
  - gear dynamics significantly affect housing vibration and noise radiation. Housing and bearings themselves have however a limited effect on gear vibration.

Similarly as the research conducted by the NASA also the Forschungsvereinigung Antriebstechnik (FVA) investigates the gearbox noise radiation by combining MB models of the drive train, including a flexible housing, with an acoustic FE radiation model to predict the resulting radiated noise [88].

3.2.2 Wind turbine drive train noise and vibration modelling

In contrast with the vast amount of research dedicated to the loading of individual drive train components (by its low frequent dynamic behaviour), not much research has been performed to obtain insight in the NV behaviour of a wind turbine drive train which is determined by its high frequent dynamic behaviour.

Schlecht et al. [149, 148] developed several MB models to assess resulting loads, and concluded that 6 DOF models are necessary to capture all dynamic effects. They also investigated the eigenfrequencies of their flexible MB model of a complete wind turbine up to the audible frequency range and concluded that these possible resonances should be investigated as they might give rise to premature failures.

Schelenz and Jandray et al. [144, 79] performed dynamic measurements up to 30 Hz on a nacelle test rig and correlated these results with a MB model of this system. They furthermore investigated the impact of the flexibility of the

planet carrier and the connection between the planet carrier and the planet shaft on the resulting system dynamics.

Helsen et al. [70, 66, 63, 67] concluded that flexibility of the individual components of the gearbox and accurate bearing representations are absolutely necessary to accurately predict the dynamic behaviour of the wind turbine drive train, especially in the audible frequency range.

Augustino [5] proposed to use flexible MB to assess the noise and vibration behaviour in the audible frequency domain of a complete wind turbine. An application case was however not yet presented.

3.3 Limitations and shortcomings of current models to predict the NV behaviour

In this section, multiple papers and publications were reviewed to make an assessment of the current state-of-the-art and state-of-the-use concerning noise and vibration prediction of wind turbine drive trains. Two kinds of models were investigated, the so-called wind turbine drive train load models, and models with a strong focus on noise and vibration, for both wind turbine drive trains and other applications.

Load estimation models are crucial in the wind turbine design phase for the calculation of the loads on the drive train. Recently the accuracy and detail of these models got improved by significantly increasing the number of DOFs and by thorough experimental validation campaigns. Although some of these models have enough DOFs to predict the dynamic behaviour of the drive train in the audible frequency range, their main focus remains on load estimation, and the impact of model detail on the dynamic behaviour remains unknown. Furthermore, the thorough experimental validation campaigns mainly focus on global load variation, typically below the audible frequency range. It is therefore concluded that these models cannot be used directly to assess the noise and vibration behaviour of a wind turbine drive train.

On the other hand many models exist to predict the noise and vibration behaviour of gearboxes, varying from lumped mass models to full FE contact models. Some of these models, and mainly the models of the NASA gearbox have been experimentally validated. The approach used to model the NASA gearbox (fully coupled models, including bearing stiffness off-diagonal values

and taking both shaft and housing flexibility into account) seems the most appropriate to model a wind turbine drive train. Due to the huge difference in size, construction and weight between this NASA gearbox and a wind turbine drive train, there still remain several challenges that should be solved before this approach can be used in the design process of a wind turbine drive train, such as which components should be included in the model, and to which extent; what is the impact of the boundary conditions on the dynamic behaviour of the wind turbine; what is the expected resulting accuracy of the simulation model; can this approach be experimentally validated on an existing multi megawatt wind turbine drive train; ...

Next to these noise and vibration models of non wind turbine gearboxes, also some publications of noise and vibration models of wind turbine gearboxes were found. However no significant insight in the model and the impact of the model choices on the resulting dynamic behaviour is given. Moreover none of these models have been extensively validated with experimental measurements in the audible frequency domain.

Based on the identified limitations in the current state-of-the-art and state-of-the-use, the need for a methodology / modelling approach to accurately predict the dynamic behaviour of a wind turbine drive train becomes clear. This modelling approach should be experimentally validated such that the proposed models can be trusted and used in the design process to optimise the dynamic behaviour of a wind turbine drive train. Moreover, based on the identified state-of-the-art, this work can be considered unique as it is the first to give in-depth, thoroughly experimentally validated insight in the dynamic behaviour of a wind turbine gearbox.

Chapter 4

Modelling and experimental validation of individual wind turbine gearbox components

4.1 Introduction

This chapter describes how the most important individual components of the gearbox are modelled. These components are:

- gearbox housing,
- planet carriers,
- gears,
- bearings, and
- shafts

Components which have an important impact on the resulting modal behaviour of the complete gearbox are also experimentally validated. These individual components will then be used to build the MB model of the complete gearbox in Chapter 5. The results obtained by performing these analysis are specific for this wind turbine gearbox (shown in figure 2.17), however, the gained insight can be generalised for other wind turbine gearboxes of approximately the same

size, and the suggested approach can be followed when investigating other kinds of gearboxes or even other mechanical systems.

4.1.1 Multibody modelling

Both the FE and the MB modelling approach can be used to capture the dynamic behaviour of a complete gearbox including gears, bearings, shafts and gearbox housing. Due to the many contact phenomena inside the gearbox (contact between gears and contact between rollers and raceways inside the bearings), even in unloaded conditions, the wind turbine gearbox is a time variant system: the applied load changes the stiffness of gears and the stiffness distribution of the bearings, while the current state of the gearbox (positioning of planet carriers) determines where the gear contact forces are introduced inside the gearbox housing. Modelling this time variant system in FE would require a significant amount of contact elements, resulting in lengthy computation times making design optimisations infeasible. Even a linearisation of these contact elements into linear springs is impractical, especially for the gears. The MB approach overcomes these issues with specially developed non-linear force elements for both bearings and gears removing the need for contact elements. This results in acceptable computation times in both frequency and time domain which is necessary for design optimisation.

In this dissertation the MBS approach is used to simulate the dynamic behaviour of the gearbox. For some investigations and for the creation of flexible bodies inside the MB model the FE approach is used. The main goal of an MB model is thus to describe the static or dynamic behaviour of multiple connected rigid or flexible bodies. It can be used to calculate kinematic behaviour, dynamic behaviour (eigenmodes), static deformation under load, transient deformation under load, ... Main elements of such a MB model are bodies, forces and constraints.

Bodies in an MB model are physical bodies having mass and rotational inertia which can be rigid or flexible. In this dissertation, the commercial MBS code Simpack is used which uses the fixed axis floating frame of reference. Using this approach the global approximative rigid body motion of a flexible body is described by the position of its fixed axis floating frame of reference with respect to the global inertia reference frame. Deformations of this flexible body are included as a linear superposition of normal modes and static modes, are considered small with respect to the large global rigid body motion and are

expressed with respect to this floating frame of reference. More information on how flexible bodies are generated and included in the MB model is given in section 4.2.3.

With respect to coordinate formulations, two mainstream options exist: absolute coordinates and relative coordinates. With absolute coordinates the position and motion of a body is described with respect to the global inertial system. With a relative coordinate formulation however, which is used in this dissertation, the position and motion of a body is described with respect to the global inertial system or to another body. In both formulations each body has a joint. This joint describes which kind of motion is allowed, and thus what kind of position and motion is included as DOFs in the MB model. In the absolute coordinate formulation this joint is expressed with respect to the global inertia system and in most of the cases all motion is automatically allowed. In the relative coordinate formulation however, this joint is expressed with respect to the global inertia system or another body and the user can choose which motion to allow. This allows to directly connect different bodies together, often resulting in a lower DOF count.

Force elements are used to introduce any kind of force in the MB model. This includes an external force (such as wind loading or gravity) and an internal force between two bodies (such as a bearing or gear force). Many force formulations exist and the choice between them depends on what should be modelled (e.g. gear force, bearing force, damping force, ...).

Constraints are used to constrain or to tie together some DOFs between two different bodies.

More information on the MB approach can be found in [152, 177]. More information on the software package Simpack which is used to model the gearbox can be found in [155].

4.2 Gearbox housing

The gearbox housing is the outer enclosure of the gearbox. It is not a single component, but consists of many individual castings and one or more ring wheels which are bolted together (see section 2.6). The flexibility of this gearbox

housing has a dominant role on the overall gearbox dynamics [60]. An accurate model of the gearbox housing is therefore crucial for an accurate prediction of the dynamic behaviour of the entire gearbox.

This section describes how this gearbox housing is modelled and validated. In the final MB gearbox model it will be included as a single flexible body using a CMS reduction of its FE model. Emphasis is put on both the accuracy of the individual components, on the way these individual components are assembled to form the gearbox housing, and on how the assembled FE model is included in the MB model.

4.2.1 Individual components

Modelling

The geometry of each individual component of the gearbox housing is first simplified to remove small features such as little bore holes, small chamfers, small rounds, ... as they do not contribute to global dynamics and only slow down the CMS reduction procedure. The geometries of all these individual components are then assembled to form the geometry of the gearbox housing. Using this assembled geometry an FE mesh is generated for all individual parts. On the contacting surfaces between two different bodies an identical mesh is generated such that node merging can be used to combine the FE models of the individual parts to form the FE model of the complete gearbox housing in an efficient way. Table 4.1 gives an overview of the main individual components of the gearbox housing.

Table 4.1: Overview of individual components

Component	Mass [tonne]	Number nodes [kNodes]	Experimentally validated	Mesh
torque arm (TA)	3.1	119	Yes	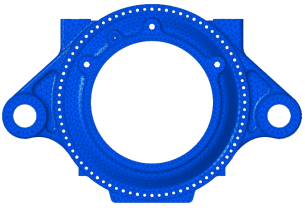
low speed ring wheel (LSRW)	2.7	115	Yes	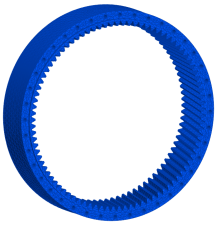
intermediate bearing housing, low speed side (IBH LSS)	2.2	70	Yes	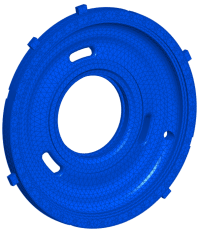
intermediate speed ring wheel (ISRW)	0.6	99	No	

Continued on next page

Table 4.1 – *Continued from previous page*

Component	Mass [tonne]	Number nodes [kNodes]	Experimentally validated	Mesh
intermediate bearing housing, intermediate speed side (IBH ISS)	1.2	81	No	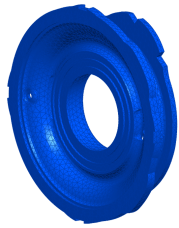
HSH	2.1	239	Yes	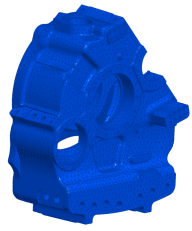
MC	0.3	27	Yes	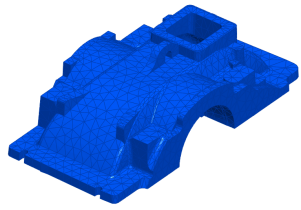
Others[1]	1.4	204		
Total	13.6	954	Yes [2]	

A mesh convergence study was performed to investigate the influence of the mesh density on the stability of the eigenfrequencies. In total 10 different meshes were generated with a node count between 80e3 and 1e6 nodes using both linear and 2nd order elements. For each mesh, the eigenfrequencies are compared with the eigenfrequencies of the mesh with the highest node count. Both an average frequency deviation and a maximum frequency deviation are calculated

[1] This mainly includes covers, brake arm, pump assembly, bearing outer rings, ...
[2] See section 4.2.2

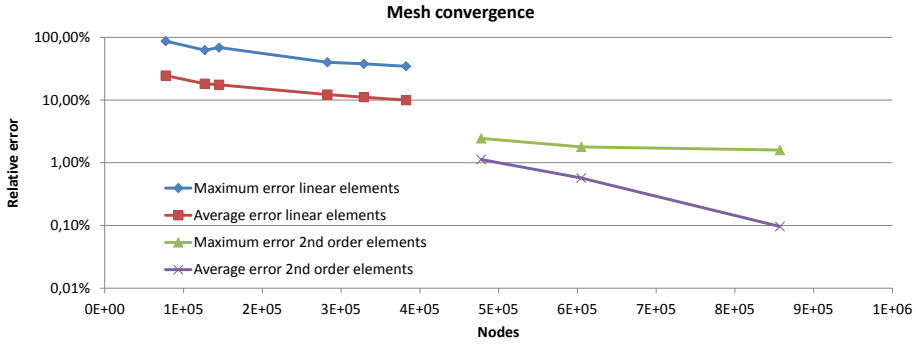

Figure 4.1: Mesh convergence study - average and maximum frequency error for all modes up to 2 kHz with respect to a model containing 1E6 nodes.

for each mesh (except for the finest mesh: 2nd order TET10 elements, approx 1e6 nodes) for all eigenfrequencies up to 2 kHz. Figure 4.1 shows these results.

The time necessary to compute the CMS reduction mainly limits the node count. Acceptable computational times are achieved by limiting the node count to approximately 1E6. Preferably high order elements should be used. An element size between 2 cm and 3 cm for the thin walled castings, such as the HSH, and an element size of around 5 cm for the thick walled castings, such as the TA produced acceptable results. Next to the node count, also the size of the multi point constraints(MPCs) used to introduce forces in the FE model (see section 4.4.2) should be limited as it significantly affects the required RAM memory to perform the CMS reduction.

Experimental validation

To obtain confidence in the FE models of these individual components, the FE models of 3 large castings (TA, IBH LSS and HSH + MC) and the LSRW are experimentally validated. Because mainly the modal behaviour and not the static behaviour is of interest, an experimental modal analysis (EMA) is used to characterise the dynamic behaviour of these individual components. For all these components a so-called 'pre-test' simulation is performed. Based on the FE model this pre-test searches optimal locations for both accelerometers and shaker to optimally identify the modal behaviour of the structure. The information from this pre-test is used as a guidance to select the used accelerometer locations: often accelerometer locations were added to improve the graphical representation of the measured modeshape.

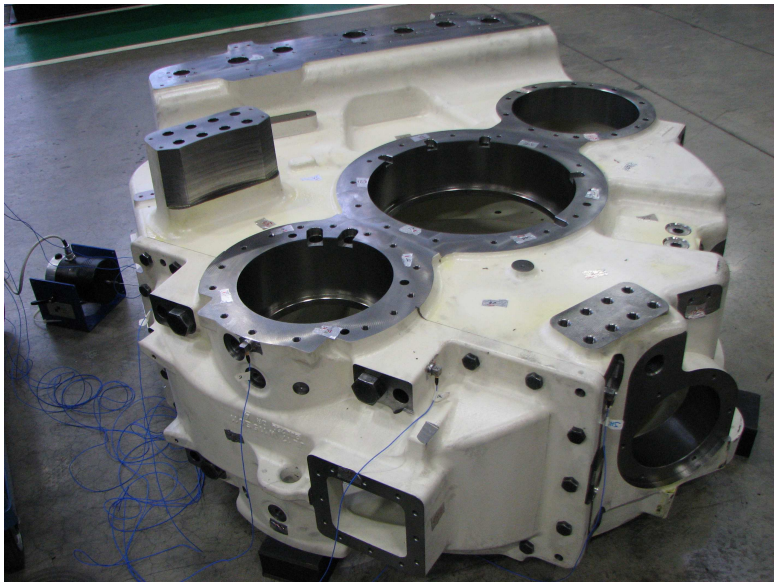

Figure 4.2: Measurement setup for HSH+MC

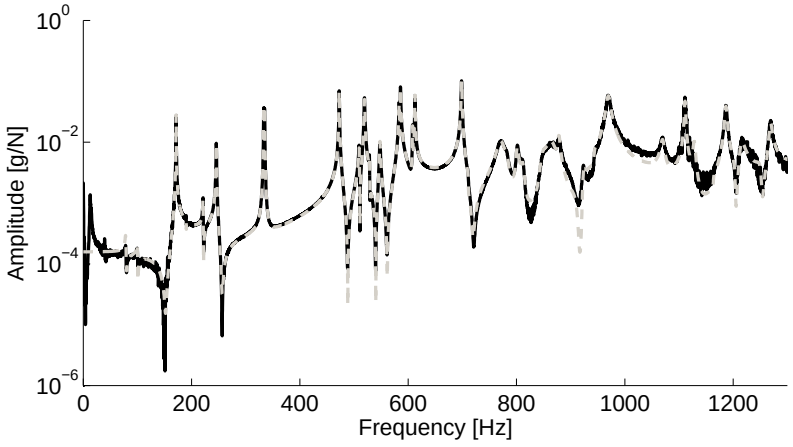

Figure 4.3: Typical FRF from TA: black: measured; gray: synthesized

Measurements To perform an EMA, the frequency response functions(FRFs) of the structure should be measured. All the measurements were performed using an LMS SCADAS III, LMS Test.Lab [97], a large electrodynamic shaker and 4 tri-axial accelerometers. Multiple runs, using different accelerometer

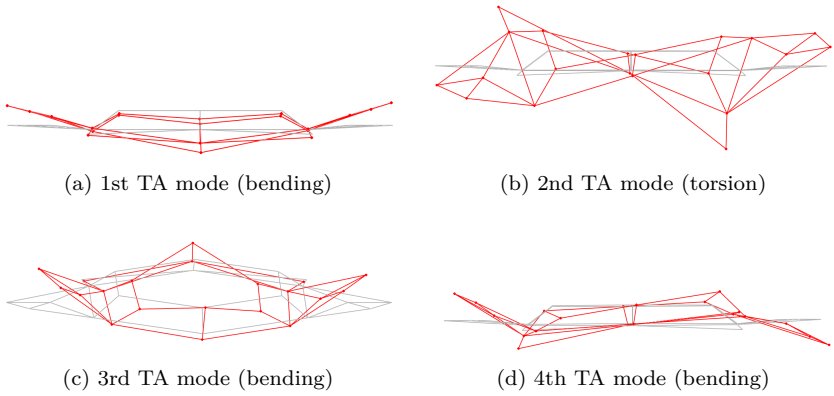

(a) 1st TA mode (bending)

(b) 2nd TA mode (torsion)

(c) 3rd TA mode (bending)

(d) 4th TA mode (bending)

Figure 4.4: First four experimentally obtained modeshapes of the TA.

locations were necessary to measure all locations determined during the pre-test. To simulate free-free suspension conditions, the components were put on flexible rubber blocks. The number of these blocks was determined in such a way not to exceed the load carrying capacity of the blocks, and to reduce the frequency of the rigid body modes as much as possible. Because only 1 shaker was used, it is impossible to detect all the double modes which are typical for rotation symmetrical structures such as the LSRW and the IBH LSS. Using the FE model it was afterwards determined whether the measured mode was a single or double mode.

Figure 4.2 shows this setup when measuring the HSH + MC. Figure 4.3 shows a typical measured FRF from the TA and its synthesized FRF as a result of the EMA. Note the rigid body modes below the first identified eigenfrequencies. Figure 4.4 displays the first four eigenmodes of the TA. More detailed information on these individual measurement campaigns, the used settings, the analysis and the results can be found in Appendix C.

Correlation Correlation between FE model and measurements was calculated using FEMTools [29]. Table 4.2 gives an overview on the correlation results of the individual components. It lists the number of measurement points, the number of eigenfrequencies that were measured, and how well the eigenmodes from the FE model correlate with the experimentally identified eigenmodes from the EMA. This correlation between FE model and EMA is given by the number of mode pairs below 1 kHz, their average modal assurance criterion

(MAC) value and their average absolute relative frequency difference[3]. Mode pairs consist of a measured mode shape and its corresponding simulated mode shape with a MAC value higher than 60%. Double modes are counted as two modes and the double FE modes are considered to be matched if one or both of the modes match with a measured mode shape. Figure 4.5 shows a typical mode shape pair of the TA.

Table 4.2: Overview of individual components - Initial correlation results

Component	Number of measurement points	Number of modes measured below 1kHz	Percentage of matched modes below 1 kHz	Average MAC	Average absolute relative frequency difference
TA	20	31	97%	86%	0.6%
LSRW	12	28	93%	86%	0.8%
IBH LSS	36	25	88%	89%	1.2%
HSH + MC	102	50	42%	79%	3.5%

Model updating For all individual components correlation is further improved in two steps: first, the global E-modulus of the part was changed to improve the material properties, and, afterwards, the E-modulus of the individual elements was changed to account for local effects. The average absolute relative frequency difference was used as objective function and was minimised in both update steps. Update step 1 was sufficient for all components except for the HSH+MC. The correlation of the complex HSH+MC improved drastically above 600 Hz with the second update step. Frequency differences between simulated and experimentally identified eigenmodes also dropped significantly for the entire frequency band of interest (see table 4.3). Table 4.4 summarises the results for all individual components, figure 4.6 shows the MAC matrix of the HSH+MC

[3]The average absolute relative frequency difference is defined as: $\sum_{i=1}^{N} \frac{1}{N} \left| \frac{f_{i,\mathrm{EMA}} - f_{i,\mathrm{FE}}}{f_{i,\mathrm{EMA}}} \right|$. An absolute value is used such that both positive and negative relative frequency differences would not average out to zero.

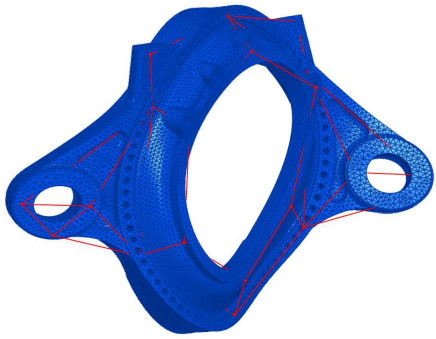

Figure 4.5: Torque arm mode shape pair. Blue: FE modeshape, red: experimental modeshape (EMA)

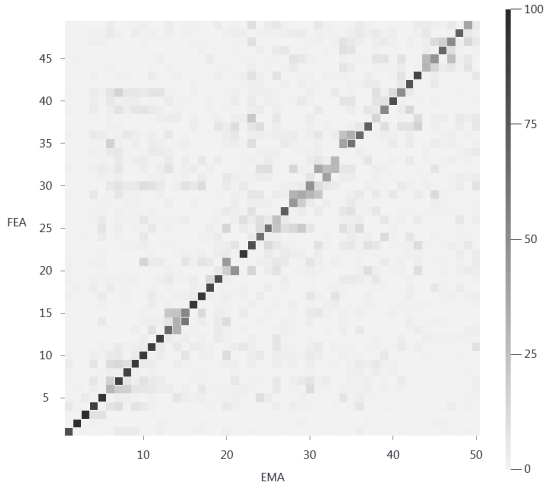

Figure 4.6: MAC matrix for HSH+MC

after the update and figure 4.7 shows the E-modulus of the HSH+MC after the update.

Note that corrections in the E-modulus of the material are in some places not physical: locally, a change more than doubling the E-modulus was observed. This suggests that a correction to the thickness of the casting in that area should be made. Performing an update on the thickness of the casting however is impractical as it requires moving the nodes which form the free surface of

Table 4.3: Overview correlated modes of HSH + MC: intial versus updated correlation results

Frequency band [Hz]	Number of identified modes	Initial			Updated		
		Number of correlated eigenmodes	Average MAC	Average absolute relative frequency difference	Number of correlated eigenmodes	Average MAC	Average absolute relative frequency difference
100 - 200	1	100%	82%	7.4%	100%	80%	5.3%
200 - 300	3	100%	94%	5.1%	100%	94%	0.2%
300 - 400	5	80%	82%	4.2%	80%	90%	0.0%
400 - 500	6	83%	73%	2.8%	83%	79%	0.0%
500 - 600	6	67%	83%	4.3%	67%	87%	0.0%
600 - 700	7	29%	74%	1.7%	71%	74%	0.0%
700 - 800	6	0%			0%		
800 - 900	8	0%			63%	72%	0.0%
900 - 1000	8	25%	67%	3.3%	38%	76%	0.0%

the casting. A combination of a 3D geometry scan to exactly quantify the geometry including casting deviations and a model update to compensate for local E-modulus differences would result in an optimal correlation [85]. However, as a model is desired which resembles as closely as possible all individual castings instead of one specific measured casting in particular, this is not done. Instead, multiple EMA measurements should be performed to assess the variability of the modal behaviour of these important large castings.

Table 4.4: Overview of individual components - Updated correlation results

Component	Initial			Updated		
	Percentage of matched modes below 1 kHz	Average MAC	Average absolute relative frequency difference	Percentage of matched modes below 1 kHz	Average MAC	Average absolute relative frequency difference
TA	97%	86%	0.6%	97%	88%	0.1%
LSRW	93%	86%	0.8%	100%	85%	0.8%
IBH LSS	88%	89%	1.2%	96%	90%	0.2%
HSH + MC	42%	79%	3.5%	60%	81%	0.1%

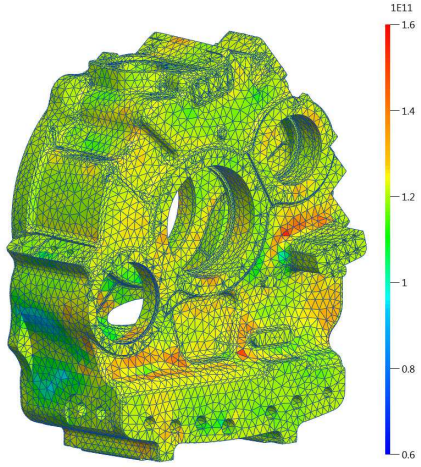

Figure 4.7: E-modulus of updated HSH+MC

Conclusions All components with exception of the HSH+MC showed initially or after slightly modifying the global material properties a very good correlation: more than 85% of all measured mode shapes were found in the FE models with correlations higher than 85% and with average absolute relative frequency differences lower than 1%. The HSH+MC needed both the material update and

an in-depth update cycle which addressed the E-modulus of individual elements to increase correlation at frequencies above 600 Hz. This lower correlation with measurements compared with the other components may be caused by the fact that the HSH+MC has:

1. a complex, relatively thin walled geometry leading to many eigenfrequencies in the frequency range of interest with rather complex mode shapes compared with the other measured parts; and / or
2. a low percentage of machined faces, and therefore large zones with casting tolerances (in the range of millimetres) which are more than an order of magnitude bigger than typical machining tolerances. These casting tolerances also have a bigger effect on a thin walled geometry compared with a rather thick massive component such as the TA for instance.

In general it can be concluded that, taking into account the updated material properties, the FE models of the individual components show a very good correlation with measurements below 600 Hz. If correlation in a higher frequency range is necessary, then focus should be put on the HSH+MC which has the most complex and relatively thin walled geometry of the complete gearbox.

4.2.2 Assembly of individual components

Modelling

The mesh of the complete gearbox housing is formed by joining the meshes of the individual components (including the meshes of the 4 updated components) (see figure 4.8). During the physical assembly of the gearbox, bolts and pins are used to join the individual parts. Due to the large number of bolt connections and their locations throughout the entire gearbox housing they may have a significant influence on the modal behaviour of the total gearbox. This assumption is verified by including a bolt model in the FE model of the gearbox housing. Several methods exist to include bolt connections in FE models, ranging from mesh merging two surfaces together up to modelling the individual bolts with pretension and friction between all contacting surfaces [108]. However, not all methods are appropriate to be linearised and to be used in a CMS reduction. Kim et al. [82] compared and validated different methods not only on the resulting stresses, but also on their applicability and correctness when performing a modal analysis. The most advanced model: the solid bolt model takes into account the bolt, the bolt pre-stress and the friction between the two contacting surfaces which makes this method difficult to be used in a CMS reduction.

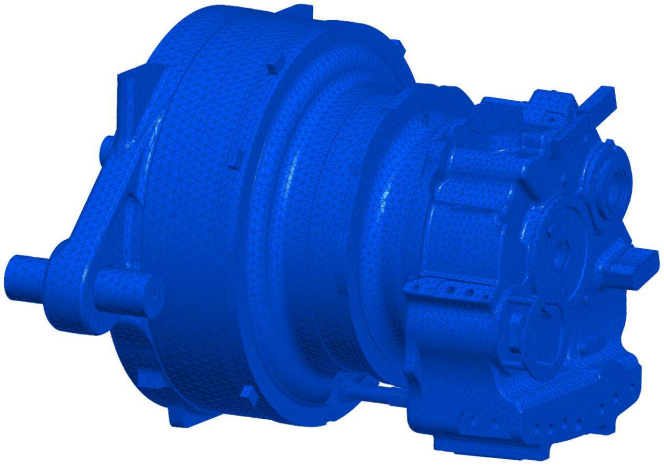

Figure 4.8: FE model of the complete gearbox

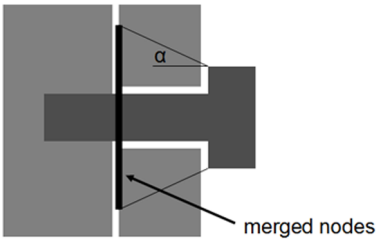

Figure 4.9: Influence of bolt pretension α on the merged nodes

In this dissertation a mesh merging technique derived from the solid bolt model is used. In this model, the bolt is taken into account by replacing the friction elements (which are used for stress calculations and consist of non-linear contact elements) with mesh merging, but only in the region underneath the bolt which undergoes compression due to the pretension of the bolt. This region, which has a typical conical shape, is defined by the α angle which typically ranges between 25° and 33° [153] (see figure 4.9). The influence of the pretension can be investigated by varying α: a bigger α corresponds with a larger connected zone and thus a larger bolt pretension. Several Ansys parametric design language (APDL) [4] scripts have been developed that automate this mesh merger in these zones underneath the bolts during the FE model generation phase.

A parameter variation case was performed to study the effect of this bolt

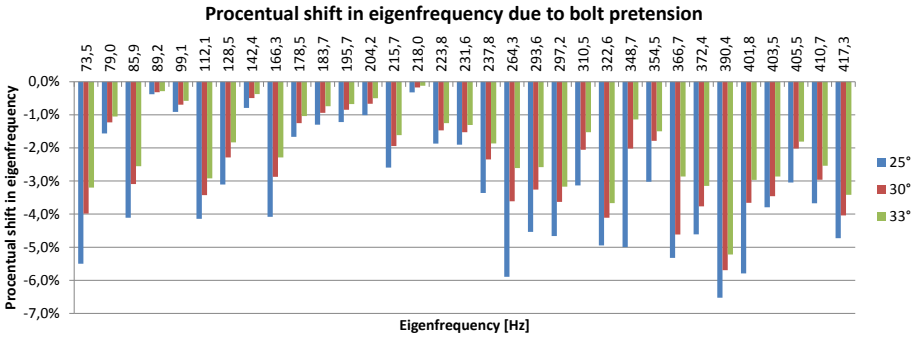

Figure 4.10: Influence of bolt pretension (expressed as α) on the eigenfrequencies of the empty gearbox housing. (Reference: $\alpha = 90°$)

pretension on the gearbox eigenfrequencies: 6 different bolting connections were investigated, containing in total approximately 250 bolts. Figure 4.10 shows the relative change of the eigenfrequencies when all 6 bolting connections are changed together. Four different cases are calculated: three physical cases $\alpha = 25°$, $\alpha = 30°$ and $\alpha = 33°$, and one theoretical case: $\alpha = 90°$. The theoretical case is in fact the case where both contact surfaces are entirely mesh merged (no bolts included) and is used as the reference case. Investigations on the individual bolting connections showed that the shifts in eigenfrequencies shown in figure 4.10 are mainly caused by two individual bolting connections: on the one hand the bolting connection between the IBH ISS and the HSH and on the other hand the bolting connection between the HSH and the MC. These connections have a considerably lower number of bolts and a thinner connection flange leading to a smaller ratio between merged surface and total contacting surface than the other connections. This low contact ratio highly dominates geometrical flexibility yielding a higher influence on the modal behaviour than connections with a high contact ratio.

Based on this sensitivity study 3 conclusions can be drawn:

1. Almost all eigenfrequencies are affected by introducing the bolting model; when neglecting the bolting model, the eigenfrequencies are overestimated.

2. The two bolting connections with the lowest ratio of merged surface to total surface have the highest impact on the eigenfrequencies.

3. The dependency on bolt pretension depends on the mode; some modes depend largely on the pretension and others do not.

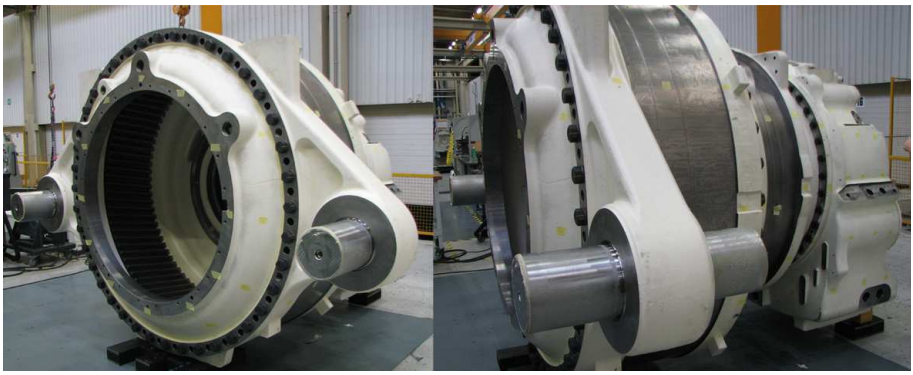

Figure 4.11: Measurement setup for the gearbox housing assembly.

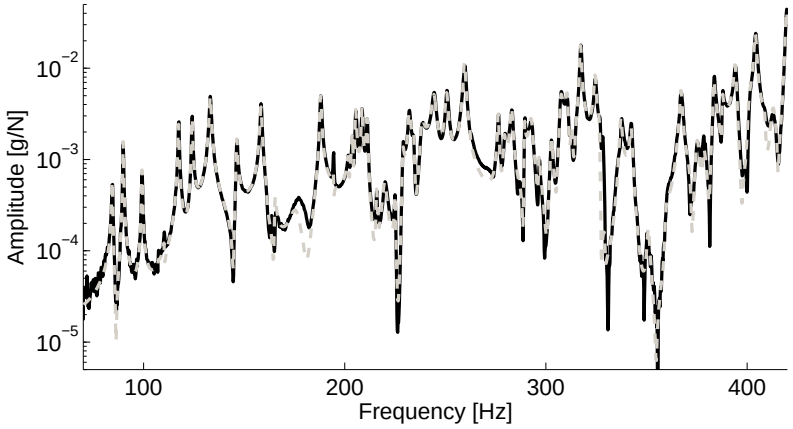

Figure 4.12: Typical FRF from assembly: black: measured; gray: synthesized

Validation

Measurements Similarly with validating individual components, the FRFs of the complete gearbox housing are measured and analysed using the EMA technique. The same equipment and rubber blocks were used. In total 276 points in 3 directions were measured during 69 measurement runs. These measurement points were determined from previous measurements and augmented by performing an additional pre-test analysis such that all expected mode shapes in the frequency band of interest can be distinguished from each other.

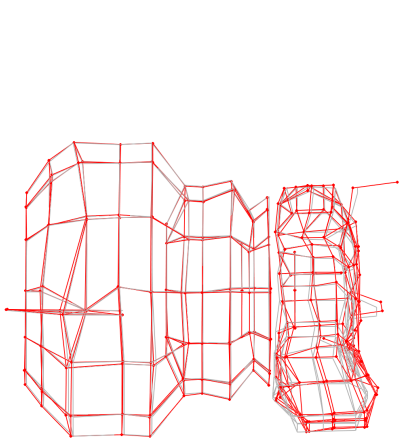

(a) 1st housing mode (brake mode)

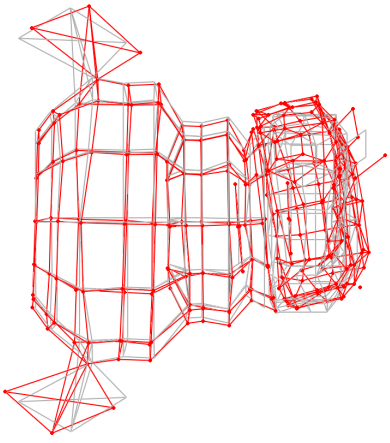

(b) 2nd housing mode (bending)

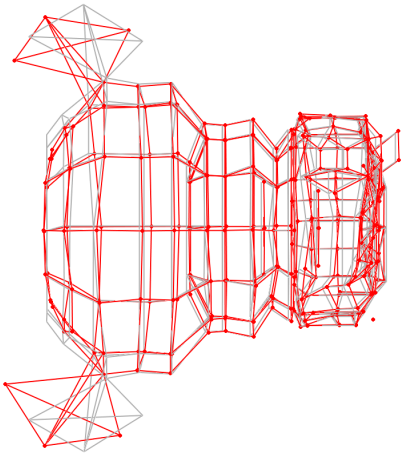

(c) 3rd housing mode (TA mode)

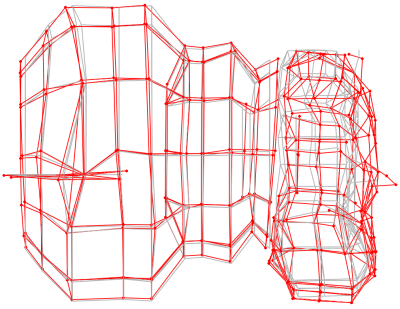

(d) 4th housing mode (HSH mode)

Figure 4.13: First four experimentally obtained modeshapes of the complete gearbox housing.

In total 90 eigenmodes were experimentally identified in the range from 0 Hz to 1 kHz. Although it was expected that the bolted interfaces would contribute significantly to the modal damping values, estimated damping values are quite low with an average of 0.2%. Figure 4.11 shows the measurement setup and figure 4.12 shows a typical FRF and the synthesized FRF as a result of the EMA processing. Figure 4.13 displays the first four experimentally obtained eigenmodes of this assembly.

Correlation and updating The measured mode shapes are correlated with multiple FE models: the initial FE model with the original material properties, the updated FE model with the updated material properties for the individual components, and FE models based on the updated FE model including the bolt model. Table 4.5 lists the correlation between the measurements and these FE models. Next to the average absolute relative frequency difference[4] also the average relative frequency difference[5] is given indicating which models systematically under- or overestimate the eigenfrequencies.

Table 4.6 gives insight in the up front accuracy of the FE model of the complete empty gearbox housing. It lists in frequency bands of 100 Hz, the number of experimentally identified eigenmodes, and for both the initial FE model, the updated FE model, and the updated FE model with bolts the number of correlated eigenmodes, the average MAC value, and the average absolute relative frequency difference between model and experiments.

[4]The average absolute relative frequency difference is defined as: $\sum_{i=1}^{N} \frac{1}{N} \left| \frac{f_{i,\text{new}} - f_{i,\text{old}}}{f_{i,\text{old}}} \right|$

[5]The average relative frequency difference is defined as: $\sum_{i=1}^{N} \frac{1}{N} \left(\frac{f_{i,\text{new}} - f_{i,\text{old}}}{f_{i,\text{old}}} \right)$

Table 4.5: Overview of gearbox assembly correlation results

Component	Percentage of matched modes below 1 kHz	Average MAC	Average absolute relative frequency difference	Average relative frequency difference
Original	26%	83%	1.5%	-0.7%
Updated	40%	84%	1.2%	0.6%
Updated + bolts ($\alpha = 60°$)	39%	82%	1.2%	0.7%
Updated + bolts ($\alpha = 55°$)	40%	82%	1.0%	0.5%
Updated + bolts ($\alpha = 50°$)	41%	82%	1.0%	0.4%
Updated + bolts ($\alpha = 45°$)	42%	81%	0.9%	0.2%
Updated + bolts ($\alpha = 40°$)	42%	80%	0.9%	0.0%
Updated + bolts ($\alpha = 35°$)	39%	80%	1.0%	-0.4%
Updated + bolts ($\alpha = 30°$)	34%	81%	0.9%	-0.5%
Updated + bolts ($\alpha = 25°$)	32%	79%	2.0%	-1.7%
Updated + bolts ($\alpha = 20°$)	26%	79%	3.0%	-2.9%

Table 4.6: Overview correlated modes of empty gearbox housing: initial versus updated versus bolted correlation results

Frequency band [Hz]	Number of identified modes	Initial			Updated			Updated + bolts		
		Number of correlated eigenmodes	Average MAC	Average absolute relative frequency difference	Number of correlated eigenmodes	Average MAC	Average absolute relative frequency difference	Number of correlated eigenmodes	Average MAC	Average absolute relative frequency difference
0 - 100	1	0%			100%	94%	6.1%	100%	93%	7.1%
100 - 200	5	100%	94%	1.4%	100%	96%	2.0%	100%	85%	1.3%
200 - 300	6	83%	87%	1.6%	100%	91%	1.4%	100%	87%	0.7%
300 - 400	6	67%	91%	1.1%	67%	92%	0.8%	67%	90%	0.6%
400 - 500	16	38%	72%	1.1%	75%	81%	0.6%	81%	80%	0.5%
500 - 600	10	20%	70%	0.7%	20%	72%	0.5%	30%	73%	0.5%
600 - 700	11	18%	72%	4.1%	45%	72%	0.9%	36%	71%	1.0%
700 - 800	10	0%			10%	69%	1.3%	20%	62%	0.7%
800 - 900	15	0%			0%			0%		
900 - 1000	10	0%			0%			0%		

Conclusions Three main conclusions can be drawn from the validation of the assembly model:

1. the eigenfrequencies identified using the EMA technique showed a lower damping value than expected. A modal damping value of 0.2% seems adequate to be used in MB models.
2. the large bolted connections have an influence on the modal behaviour of the gearbox. Without a bolt model the eigenfrequencies of the complete gearbox are slightly overestimated by approximately 1% which is very acceptable. A slightly better correlation with a higher number of matched modes and a lower frequency difference could be found by including a bolt model with $\alpha = 40°$.
3. The FE model of the gearbox housing can be considered up front to be quite accurate up to approximately 400 Hz. When accuracy is needed at higher frequencies an EMA should be performed on the HSH and MC which have the highest uncertainty.

4.2.3 Usage in MB model

CMS reduction

The number of DOFs required to accurately describe the complexity of the FE model presented in section 4.2.2 is too high to be included directly in the MB model. Therefore a CMS reduction technique is necessary to reduce the number of DOFs. Using a CMS reduced FE model consists of three steps:

1. generation pass
2. usage pass
3. expansion pass

Generation pass In the generation pass the full FE model is reduced. During this CMS reduction a transition is made from nodal DOFs to modal DOFs. This encompasses that deformations of the FE model are not expressed any more as a combination of individual nodal displacements, but as a combination of individual mode shapes. The amount by which an individual mode shape contributes to this deformation is called the modal participation factor (MPF). Typically all modeshapes in the frequency range from 0 Hz up to twice the maximum frequency of interest are included in the generation pass. These

modeshapes also do not include all nodes, but only a selected set of so-called 'master' nodes. Forces and displacements can only be introduced in these master nodes. Following locations are defined as master nodes:

- external force input locations, such as on the torque arms, on the first stage planet carrier or on the high speed shaft
- bearing locations
- gear force locations, such as the ring wheels
- locations where virtual accelerometers are placed

More elaborate information can be found in [19, 152].

Usage pass In the usage pass the reduced FE model is used inside another FE model or inside an MB model. When used in an MB model the MPFs and the derivatives of the MPFs are included as DOFs in the state vector of the MB model.

Expansion pass During the expansion pass the MPFs of the reduced FE model are used to obtain the nodal DOFs of the full FE model. An expansion pass is only necessary when information of the full FE model is necessary which was not included in the reduced FE model. This for instance includes positions of nodes which were not defined as master nodes, local strains, ...

Several APDL routines were developed and combined in an Ansys library to more efficiently create FE models of gearbox housings to perform a CMS reduction on. These routines mainly include an automatic setup of master nodes (for the introduction of forces, constraints, or virtual accelerometers) based on easy to use templates.

Table 4.7: Overview of planet carriers

Component	Mass [tonne]	Number nodes [kNodes]	Experimentally validated
low speed stage planet carrier (LSS-PC)	6.8	80	Yes
intermediate speed stage planet carrier (ISS-PC)	2.5	70	No

4.3 Planet carriers

4.3.1 Modelling

The planet carriers are large castings in which the planet shafts and thus the planets are mounted. The planet carrier including the planet shafts is considered as one flexible body inside the MB model. Similarly as the gearbox housing, the geometry of the planet carrier is first simplified to remove all small details. Using this simplified geometry of both planet carrier and planet shafts an FE model is made. The connection between planet carrier and planet shafts is considered to be bonded: both parts cannot separate nor slide with respect to each other. In operation however the size of this bonded contact changes [116]. This effect has an impact on static behaviour, but it is expected that it has a negligible effect on the dynamics of the entire gearbox. This bonded contact is implemented in the FE model by mesh merging: both interface surfaces of planet carrier and planet shaft utilise the same nodes.

Using the CMS technique described in section 4.2.3 the flexible bodies for both the first and the second stage planet carrier were generated. Table 4.7 gives an overview of the two planet carriers.

No mesh convergence study was performed on the planet carriers, instead a similar element size is used for both planet carriers which will, compared on the typical dimensions and thickness of the planet carriers result in a more than accurate enough estimation of the eigenfrequencies and modeshapes.

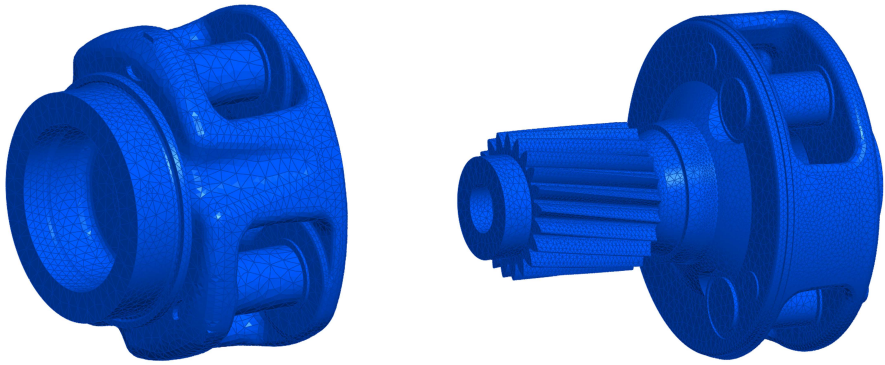

Figure 4.14: Planet carrier mesh. Left: LSS-PC, right: ISS-PC.

Note that the low speed stage sun (LSS-SU) and the ISS-PC are connected using a relatively stiff spline connection. To simplify the model and to reduce the number of bodies and flexible DOFs, these two bodies are combined and meshed together resulting in a single flexible body in the MB model. Figure 4.14 shows the FE models of these components. Master nodes (not visible) are included to connect planet bearings, planet carrier bearings, incoming torque, and virtual accelerometers.

4.3.2 Experimental validation

The FE model of the planet carrier of the first planetary stage without planet shafts is validated using an EMA. The measurement setup was identical to the measurement setup used for the measurements of the gearbox housing: the structure was placed on rubber blocks and attached to the shaker. FRFs were measured in 34 measurement points in 3 directions. In total 20 eigenmodes are identified in the range between 0 Hz and 1000 Hz. Figure 4.15 shows a measured FRF and its synthesis as a result of the EMA. Figure 4.16 shows the first 4 eigenmodes. Table 4.8 shows both initial correlation results and the correlation results after a global material update.

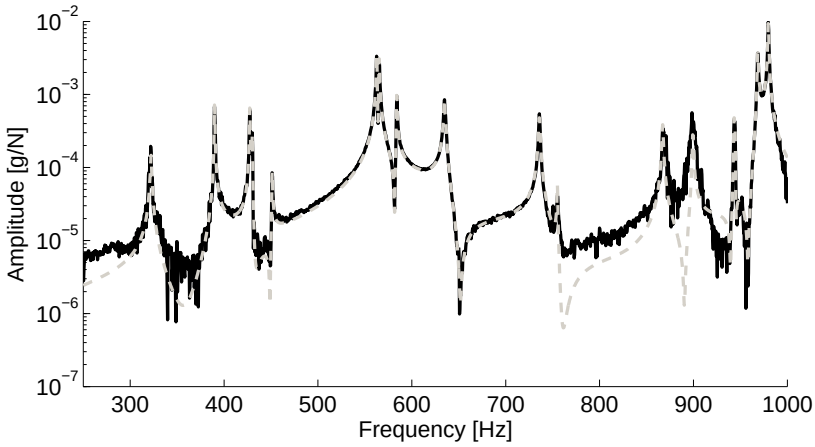

Figure 4.15: Typical FRF from PC: black: measured; gray: synthesized

Table 4.8: Validation of first stage planet carrier - Initial and updated correlation results

Component	Initial			Updated		
	Percentage of matched modes below 1 kHz	Average MAC	Average absolute relative frequency difference	Percentage of matched modes below 1 kHz	Average MAC	Average absolute frequency difference
LSS-PC	76%	91%	2.6%	86%	91%	0.3%

4.3.3 Conclusions

Experimental validation showed very good correlation between the experimentally obtained modeshapes and the modeshapes calculated by the FE model. Similarly with the gearbox housing, also the planet carrier has a relatively low modal damping. Due to the higher eigenfrequencies of the planet carriers (including planet shafts) compared with the gearbox housing (first eigenfrequency of LSS-PC: around 550 Hz, and first eigenfrequency of ISS-PC: around 440 Hz

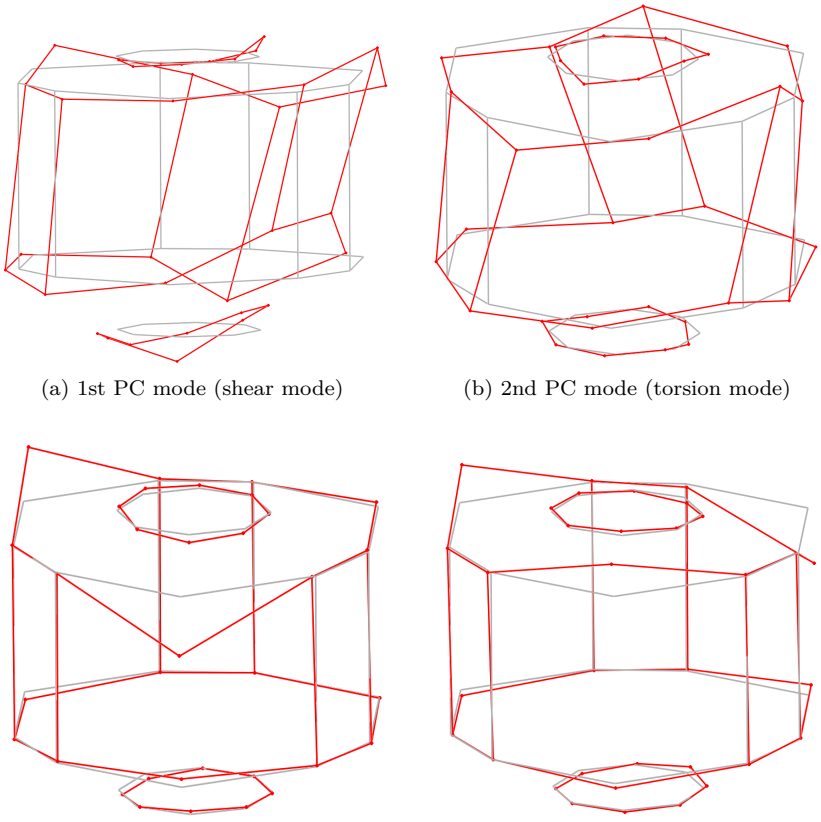

(a) 1st PC mode (shear mode)

(b) 2nd PC mode (torsion mode)

(c) 3rd PC mode (generator side flange mode)

(d) 4th PC mode (generator side flange mode)

Figure 4.16: First four experimentally obtained modeshapes of the low speed stage planet carrier.

[6]), it is expected that the flexibility of the planet carriers will have a smaller impact on global dynamics compared with the gearbox housing.

4.4 Bearings

4.4.1 Bearing stiffness determination

Many models with varying complexity exist to include bearings in large models of rotating mechanical systems. The simplest models just constrain the shafts in the gearbox housing. More complex models include the bearings by including radial (K_{yy} and K_{zz}) and possibly also axial (K_{xx}) stiffness values (see equation 4.1). Both Gargiulo [36] and Harris [52] derived formulas to calculate these stiffness values. However for an accurate investigation of the noise and vibration behaviour of the system a more accurate model is needed that also includes rotational stiffness values and the so-called off-diagonal values which couple the relative displacements with resulting moments and vice versa [91, 92, 63, 126] (see equation 4.2). Lim and Singh [91] proposed an analytical model based on Hertzian pressure to calculate, next to the radial, axial and torsional stiffness values also these off-diagonal values using a discrete summation over all rolling elements. Liew and Lim [89] extended this approach to also include the effect of varying stiffness by the changing number of rolling elements in contact during rotation, and thus taking a noise source effect of the bearing into account (see section 2.6.2). Guo [40] used a contact based finite element model to calculate the stiffness values and compared it with some of the models above.

[6] Although ISS-PC is constructed smaller, stiffer and lighter, the first eigenfrequency of the ISS-PC is lower than the first eigenfrequency of the LSS-PC due to the inclusion of the LSS-SU in the ISS-PC model.

$$\begin{bmatrix} F_x \\ F_y \\ F_z \\ F_\alpha \\ F_\beta \\ F_\gamma \end{bmatrix} = \begin{bmatrix} K_{xx} & 0 & 0 & 0 & 0 & 0 \\ 0 & K_{yy} & 0 & 0 & 0 & 0 \\ 0 & 0 & K_{zz} & 0 & 0 & 0 \\ 0 & 0 & 0 & 0 & 0 & 0 \\ 0 & 0 & 0 & 0 & 0 & 0 \\ 0 & 0 & 0 & 0 & 0 & 0 \end{bmatrix} \begin{bmatrix} X \\ Y \\ Z \\ \alpha \\ \beta \\ \gamma \end{bmatrix} \tag{4.1}$$

$$\begin{bmatrix} F_x \\ F_y \\ F_z \\ F_\alpha \\ F_\beta \\ F_\gamma \end{bmatrix} = \begin{bmatrix} K_{xx} & K_{xy} & K_{xz} & 0 & K_{x\beta} & K_{x\gamma} \\ K_{yx} & K_{yy} & K_{yz} & 0 & K_{y\beta} & K_{y\gamma} \\ K_{zx} & K_{zy} & K_{zz} & 0 & K_{z\beta} & K_{z\gamma} \\ 0 & 0 & 0 & 0 & 0 & 0 \\ K_{\beta x} & K_{\beta y} & K_{\beta z} & 0 & K_{\beta\beta} & K_{\beta\gamma} \\ K_{\gamma x} & K_{\gamma y} & K_{\gamma z} & 0 & K_{\gamma\beta} & K_{\gamma\gamma} \end{bmatrix} \begin{bmatrix} X \\ Y \\ Z \\ \alpha \\ \beta \\ \gamma \end{bmatrix} \tag{4.2}$$

These stiffness values depend on the actual position of bearing inner ring with respect to bearing outer ring, resulting in a load dependent (and thus non-linear) bearing stiffness values. Most important types of non-linearities in bearings are:

1. the non-linear individual rolling element load–deflection curve (Hertzian contact); and
2. the non-constant number of rolling elements in contact due to (external) loading.

Utilising bearings inside a MB model can be done in several ways:

1. calculate using a bearing model, or obtain from the bearing supplier, the 6×6 stiffness matrix at a certain operating condition and import those stiffness values in the MB model,
2. calculate and store, based on a bearing model, stiffness or force values at several bearing deflections in a lookup-table, and let the MB software interpolate in this lookup-table, or
3. include the bearing model by means of function expressions or user code in the MB software.

In the first approach only a linearised model of the bearings around the operating condition is available in the MB model. Therefore, depending on the amount of non-linearity of the bearings, only simulations around this operating condition can be considered as reliable and bearing deflections may be wrong. The second

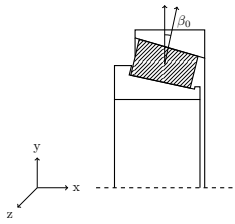

Figure 4.17: Tapered roller bearing.

and third approach do consider the bearing non-linearities inside the MB model and can thus be used in a wider range of operating conditions and can be considered as more accurate with respect to bearing deflections [162].

Impact of bearing design on the stiffness values

Several parameters determine the stiffness values of a bearing, most of them are design parameters such as dimensions, number of rollers, contact angle (see figure 4.17), but also operating parameters such as load and pre-stress will influence the resulting stiffness values. To investigate the impact of these design parameters on the resulting bearing stiffness values, an analytical parameter variation case is calculated. The HS-IS-RS (see figure 2.17) was selected and modelled using the approach formulated by Lim and Singh. Bearing inner ring - outer ring displacements were calculated using the complete MB model explained in Chapter 6. Using these initial displacements, individual roller forces are determined based on Hertzian pressure theory. These individual roller forces are then summed and differentiated to obtain all stiffness values. A detailed description including the mathematical formulation can be found in [91].

Two parameter variations are performed: a variation of the bearing contact angle β_0 and the pre-stress. Figures 4.18 and 4.19 show the evolution of 8 stiffness values from the 6×6 stiffness matrix: the axial and both radial stiffness values (K_{xx}, K_{yy} and K_{zz}), the two non zero rotational stiffness values ($K_{\beta\beta}$ and $K_{\gamma\gamma}$) and 3 off-diagonal values ($K_{x\gamma}$, $K_{y\gamma}$ and $K_{z\beta}$). Note that due to the initial displacement of inner ring with respect to the outer ring, the radial stiffness values K_{yy} and K_{zz} as well as the rotational stiffness values $K_{\beta\beta}$ and $K_{\gamma\gamma}$ are no longer identical.

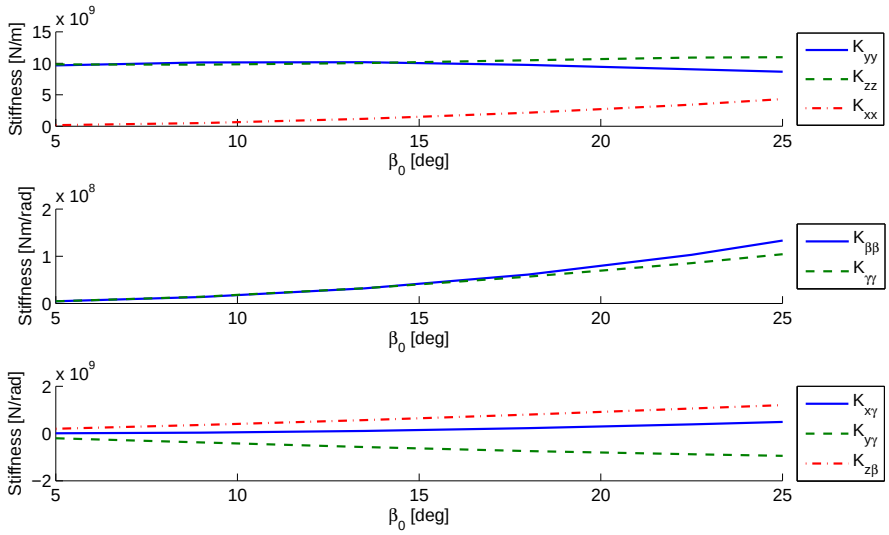

Figure 4.18: Change in bearing stiffness value due to changing contact angle. Original contact angle lies around 15°.

Following observations can be made:

1. a 2° increase of contact angle modifies
   - the axial stiffness by approximately 25%;
   - the radial stiffness values by approximately 1%;
   - the rotational stiffness values by approximately 25%; and
   - the off-diagonal stiffness values by approximately 10% to 35% depending on the direction.
2. inducing a pre-stress by offsetting the axial bearing position by 0.05mm results in a stiffness change of approximately 30% for axial, radial and rotational stiffness values, and in a stiffness change between 20% and 170% for the off-diagonal stiffness values.

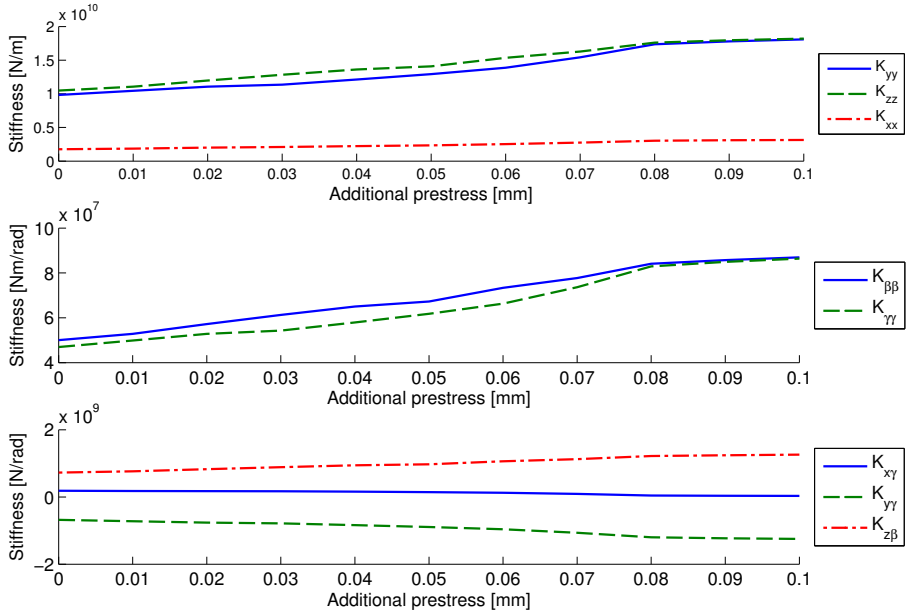

Figure 4.19: Change in bearing stiffness value due to addition of pre-stress.

4.4.2 Bearing force introduction

Regardless how the bearing force was calculated (using 6×6 stiffness matrices or advanced bearing models) it has to be introduced into both inner and outer ring. A common way to introduce a single force into an FE model is the usage of a so-called MPC which distributes the resulting bearing forces over a selected area in the FE model (such as the bearing seat). Two common implementations exist to achieve this goal: an RBE2 or an RBE3. Both those two coupling elements are specific implementations of an MPC. An RBE2 is an MPC which rigidly connects multiple nodes to one master node, whilst an RBE3 also connects multiple nodes to another node, but without introducing additional stiffness. Mathematically an MPC can be written in following form:

$$C_0 = \sum_{i=1}^{n} C_i U_i \tag{4.3}$$

with:

$$C_0 = \text{constant term}$$

$$U_i = \text{degree of freedom i}$$

$$C_i = \text{constant for degree of freedom i}$$

$$n = \text{number of terms in MPC}$$

When creating an RBE3 to couple one central node with many nodes, 6 MPCs are written; one for each degree of freedom of the central node (3 displacements and 3 rotations). Each MPC expresses how the position or rotation of the central node depends on the positions of the other nodes. An example of an RBE3 MPC is given below:

$$UX_{\text{centralnode}} = 0.25{\times}UX_{\text{node4}}{+}0.25{\times}UX_{\text{node45}}{+}0.25{\times}UX_{\text{node14}}{+}0.25{\times}UX_{\text{node7}} \tag{4.4}$$

When creating an RBE2 to rigidly couple one central node with N other nodes, many MPCs are written equalling the total number of DOFs of these N nodes, which typically comes down to 3 × N MPCs. Each MPC expresses how the position of one of the surrounding nodes depends on the position of the central node. An example of an RBE2 MPC is given below:

$$\begin{aligned} UX_{\text{node4}} &= UX_{\text{centralnode}} \\ UX_{\text{node45}} &= UX_{\text{centralnode}} \\ UX_{\text{node14}} &= UX_{\text{centralnode}} \\ UX_{\text{node7}} &= UX_{\text{centralnode}} \end{aligned} \tag{4.5}$$

To include an RBE3 in a CMS reduction care should be taken to properly define these MPCs [59]. The choice between RBE2 and RBE3 depends on the amount of stiffness which should be added to the model: an RBE3 does not add any additional stiffness into the flexible structure or shaft, while an RBE2 adds an infinite amount of stiffness to the flexible structure or shaft making that zone completely rigid. Figure 4.20 assesses the effect of this difference by comparing the modal behaviour of the complete gearbox housing when using an RBE2

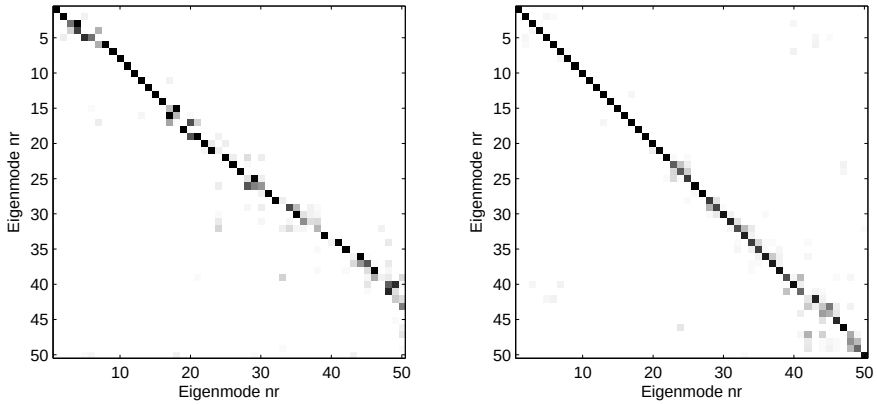

(a) LSS-PC-RS (b) HSS-RS

Figure 4.20: Comparison of structural eigenmodes when changing from RBE3 to RBE2. Vertical axis: RBE2, Horizontal axis: RBE3

or an RBE3 on an individual bearing seat. This comparison is made for both the low speed stage planet carrier bearing, rotor side (LSS-PC-RS) (diameter $\geq$ 1.2m) and the high speed shaft bearing, rotor side (HSS-RS) (diameter $\approx$ 0.3m) bearings. For each bearing a MAC matrix is computed between the complete gearbox housing using an RBE2 or RBE3 on that individual bearing position (all other bearing seats utilise an RBE3). This figure illustrates that the additional stiffness of the RBE2 introduced at the LSS-PC-RS bearing has a significant effect on the global eigenmodes: the model using the RBE2 has less eigenfrequencies in the same frequency range, and the MAC matrix between the eigenmodes of both models is no unity matrix, not even at the lower eigenfrequencies indicating a significant difference between the eigenmodes of the models using an RBE2 or an RBE3 on that bearing seat. The effect of the choice between RBE2 or RBE3 for the HSS-RS bearing however has no impact on the global eigenmodes: a MAC matrix between both sets of eigenmodes resembles the unity matrix closely.

By using such an RBE2 or RBE3 to introduce a bearing force in the flexible gearbox housing (but the same is similar when introducing a gear force in a ring wheel e.g.) implicitly 2 important assumptions are made:

1. forces which are introduced into the FE model are distributed over the entire connecting surface; and

2. deformations of the connecting surfaces of inner and outer ring do not influence each other.

When a shaft is introduced in a bearing seat it is clear however that this shaft (or planet carrier) stiffens this bearing seat: it becomes more difficult for the bearing seat to deform because both bearing and shaft (or planet carrier) counteract this deformation but it remains possible. This violates the second assumption. It is clear from figure 4.20 that this finite stiffness addition by introducing a shaft or a planet carrier has an effect on the LSS-PC-RS bearing while it does not have an effect on the high speed shaft bearing, generator side (HSS-GS) bearing in this frequency range of interest. To quantify this effect of adding a finite stiffness to the LSS-PC-RS bearing seat by inserting the planet carrier, a simple model is developed containing the TA, LSRW and the IBH LSS (see figure 4.21). Focus in this model is on both the so-called 'in-phase' and the 'out-of-phase' flapping modes (see figure 4.22). Both modes are important in the frequency range of interest and they may transfer vibrations through the torque arm interfaces to the rest of the structure. Furthermore, they both show significant deformation on the LSS-PC-RS bearing seat, indicated in red in figure 4.21).

Using this model 3 different analyses were performed:

1. Bearing LSS-PC-RS modelled as an RBE2
2. Bearing LSS-PC-RS modelled as an RBE3
3. Rolling elements of bearing LSS-PC-RS modelled as individual springs. Multiple analysis were performed switching on and off these individual springs simulating the angular position of the centre of the loaded zone and the width the loaded zone (see figure 4.23).

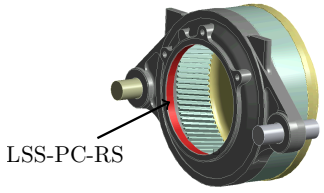

Figure 4.21: Graphical representation of the torque arm model.

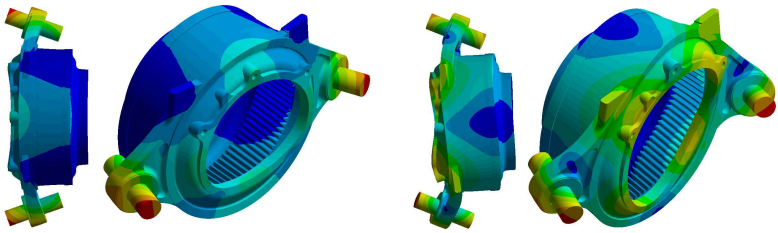

(a) In-phase flapping mode (b) Out-off-phase flapping mode

Figure 4.22: In-phase and out-off-phase flapping modes

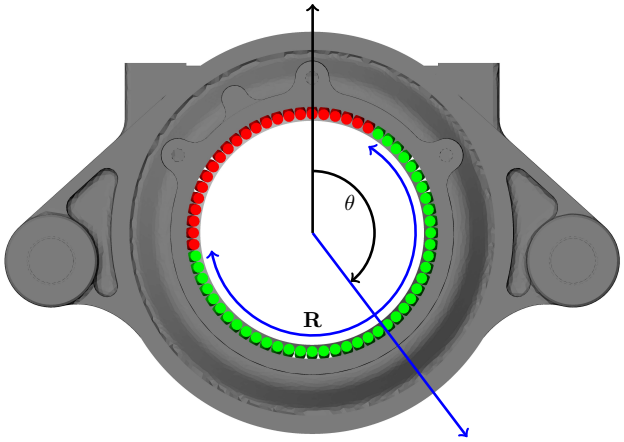

Figure 4.23: Gearbox housing with LSS-PC-RS bearing using roller based bearing model. LSS-PC is not shown for clarity reasons. Each roller represents an individual spring. Red rollers are inactive. Loaded zone at angle θ, width of loaded zone indicated by arc R.

Results

Table 4.9 lists the results from the simulations for the RBE2, RBE3, and the individual roller case with all roller elements in contact. The contour plot in figure 4.24 shows a graphical representation of the effect of the position and width of the loaded zone on both the in- and out-of-phase flapping mode eigenfrequencies. The radial dimension represents the size of the loaded zone (from 0% to 100%) while the angular dimension represents the angular position of the centre of the loaded zone.

The following conclusions can be made:

- The in-phase flapping mode is more affected by the RBE element choice than the out-of-phase flapping mode.
- The eigenfrequency corresponding to 100% rollers in contact is not equal to the eigenfrequency corresponding with the RBE2 element. If all rollers would have an infinite stiffness this should be the case.
- The eigenfrequencies from both modes, but especially the one of the in-phase-flapping mode, are significantly dependent on number of rollers in contact and the angular position of the centre of the loaded zone.

In general it can therefore be concluded that the in-phase flapping mode of the empty gearbox housing depends highly on the position and width of the loaded zone of the LSS-PC-RS bearing and thus on the actual loading condition such that a simplified representation of this bearing by an RBE2 or an RBE3 introduces a non negligible inaccuracy in the model. The effect of this non-linear bearing on its surrounding structure will be investigated in more detail using the complete gearbox model (see section 5.3.1).

Table 4.9: In- and out-of-phase TA flapping eigenfrequency.

Mode	RBE3	All rollers in contact	RBE2
In-Phase flapping mode	143.4 Hz	172.4 Hz	177.9 Hz
Out-of-Phase flapping mode	176.8 Hz	183.1 Hz	184.8 Hz

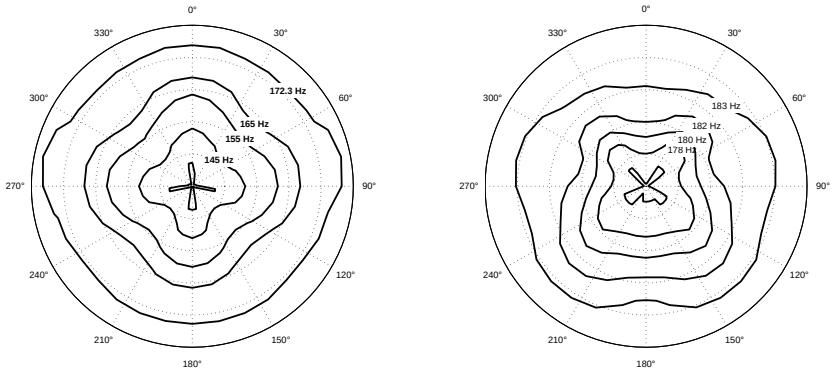

(a) In-phase flapping mode

(b) Out-off-phase flapping mode

Figure 4.24: Eigenfrequency using individual rolling element stiffness values. (Radial axis = number of rollers in contact from 0% to 100%; angular axis = angular position of the centre of the loaded zone)

4.5 Shafts and gears

4.5.1 Shafts

The gearbox used in this dissertation contains two shafts: the high speed intermediate shaft (HS-IS) and the high speed shaft (HSS). Similarly as with planet carriers and the gearbox housing, the shafts are modelled in FE using volume elements (beam elements are somewhat harder to use because the HSS also contains a pinion, and the HS-IS definitely cannot be called a slender shaft which is a necessary precondition to use beam elements). Components such as bearing inner rings are included in the FE mesh of the shaft to include both the additional mass and stiffness introduced by these components.

No experimental validation on these shafts is performed because:

- the first eigenmode is relatively high with respect to the other flexible components; and
- the geometry of the shafts is well defined as shafts are 100% machined. It is therefore expected that the FE model of both shafts is a very good up front

approximation of the dynamic behaviour not needing any experimental validation.

4.5.2 Gears

As the gears are the main source of wind turbine tonalities studied in this work (see section 2.6.2), it is important to have a good estimate of these gear excitation forces to calculate the resulting responses (vibration amplitudes or radiated acoustic noise). Two approaches are possible to calculate these responses: a calculation in the time domain or a calculation in the frequency domain. A calculation in the time domain requires a good force model capable of calculating the gear excitation forces (including the TE forces) based on the operating conditions (including actual gear positions and gear deformations). Although this is the most straightforward approach it has two important drawbacks:

1. a gearbox model is required which is capable of accurately determining the eigenfrequencies and eigenmodes, but also capable of accurately determining the static deformation to be able to make a good estimate of the gear excitation forces. Such a model requires more detail and it may slow down computations; and
2. a simulation in time domain should be performed. This requires a first step to reach the required operating conditions and a second step to perform a time simulation at this operating condition.

To overcome these drawbacks the usage of so-called transmission error frequency response functions(TE-FRFs) is proposed. These TE-FRFs are FRFs linking an output (such as an acceleration on the TA, radiated noise, ...) with a unit TE.

$$H_{\mathrm{TE}}(w) = \frac{Y(w)}{\mathrm{TE}}$$

with

$$H_{\mathrm{TE}}(w) = \text{frequency dependent TE-FRF}$$

$$Y(w) = \text{response}$$

$$TE = \text{unit TE}$$

As these TE-FRFs can be calculated in the frequency domain no lengthy time simulations are necessary. Next to that, also no advanced gear model capable of accurately calculating the TE is necessary in the MB model as the TE can be calculated using a dedicated gear software code and absolute results from the model can be obtained by multiplying the TE-FRFs with this pre-calculated TE. Note that next to TE-FRFs also FRFs can be calculated using e.g. sliding forces as input to also assess the impact of the sliding forces on the resulting NV.

Similarly with bearings also the individual gear forces should be introduced in both contacting gears. Using an RBE3 in this case seems adequate, however when using such an RBE3 implicitly the same 2 assumptions are made when using an RBE2 or RBE3 to introduce a bearing force into the flexible housing:

1. forces can be distributed over all nodes connected with the central node; and
2. deformations which do not result in displacement of the central node are not sensed by the MB model.

For gear wheels and pinions, which can be considered relatively stiff compared with the actual gear stiffness, this assumption does not have an influence on the accuracy of the results of the MB model. For a ring wheel, which is much more flexible than a pinion or a gear wheel this is not the case. For a ring wheel these two assumptions are:

1. planet gear forces are not introduced at the planet - ring wheel contact location, but introduced over the entire ring wheel; and
2. deformations of the ring wheel which do not result in displacement of the central node are not sensed by the MB model, or the ring wheel does not stiffen when introducing the planet-ring wheel contact.

First assumption - gear force introduction

Applying the individual gear forces to the centre of the gear wheel has no impact on the resulting acceleration at an arbitrary receiver point on the gearbox housing if this gearbox housing is rigid. However, for a flexible gearbox housing, this may have an impact on the resulting vibration amplitudes as the transfer paths from these individual contact locations to this arbitrary receiver point may alter both amplitude and phase of the applied force.

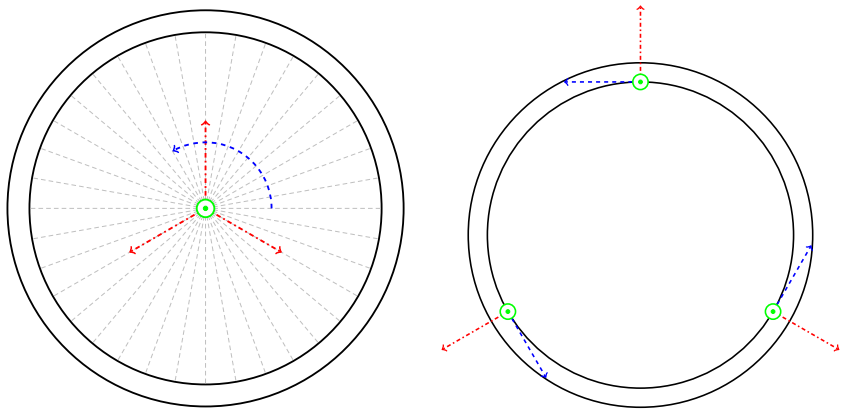

(a) RBE3 approach (b) Individual teeth

Figure 4.25: Forces applied on an internal ring wheel.
Legend: tangential force, radial force, axial force, RBE3.

This is verified using an FE model of the flexible gearbox housing, focussing on the second planetary gear stage. The gear tangential forces, the gear radial forces and the gear axial forces are applied on a central RBE3 or on the individual gear teeth (see figure 4.25). Vibration amplitudes are calculated for a point on the torque arm in vertical direction (which is considered to be one of the most important transfer paths for the transfer of gear excitation into the wind turbine) and a point located on the intermediate speed ring wheel. Figures 4.26 and 4.27 show these responses. Note that because all gear forces are considered equal and in phase, the response due to the radial forces for the RBE3 case has a zero amplitude and is therefore not visible.

In the case that the response from the tangential forces dominates the total response, then the RBE3 approach can be considered as a good approximation. When for instance the radial forces become dominant (higher frequency regions in figure 4.27), then the differences between the RBE3 and the teeth approach become more significant.

Using this approach, the potential of optimising the mesh phasing to mitigate the transmitted gear vibrations can also be investigated. In a planetary gear system with 1 sun, 3 planets and 1 ring wheel, 6 gear contacts exist. The total gear excitation force from this planetary gear stage depends on the relative phase of these individual gear contacts: do all planets of the planetary gear

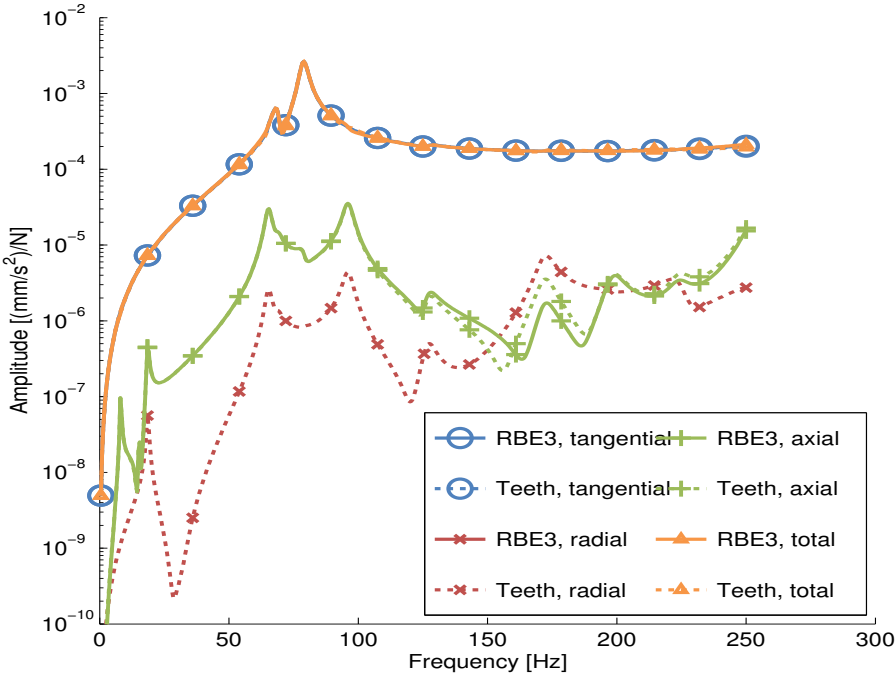

Figure 4.26: Comparison of vibration amplitudes on the torque arm (vertical direction) due to tangential (———), radial (———) and axial (———) gear forces. Full line: RBE3 approach, dashed line: individual teeth.

stage make a new contact with e.g. the ring wheel at exactly the same time, or is this spread out? One could compare this with summing 3 individual sinusoidal gear contact excitation functions at the same frequency in phase or out-of-phase to obtain a total gear excitation force. Several studies have been performed to derive the phase of the individual gear forces based on the design of the planetary gear stage [124, 76] and the possible effect of this gear phasing on the resulting vibrations, both theoretical [125, 3] and experimental [138]. These studies however neglect the impact of the flexibility of the gearbox housing on this possible reduction. Figure 4.28 shows the vibration amplitudes at the torque arm (vertical direction) due to the total gear force of the intermediate planetary gear stage. Contributions from the individual teeth forces are summed both in phase and 120° out of phase. This figure illustrates the huge potential of reducing the transmission of gear excitation into the wind turbine structure. This reduction is possible because the responses of the individual teeth forces are approximately equal in both magnitude and in phase. Mesh phasing results in a cancellation of the gear excitation in this case. Figure 4.29 however shows

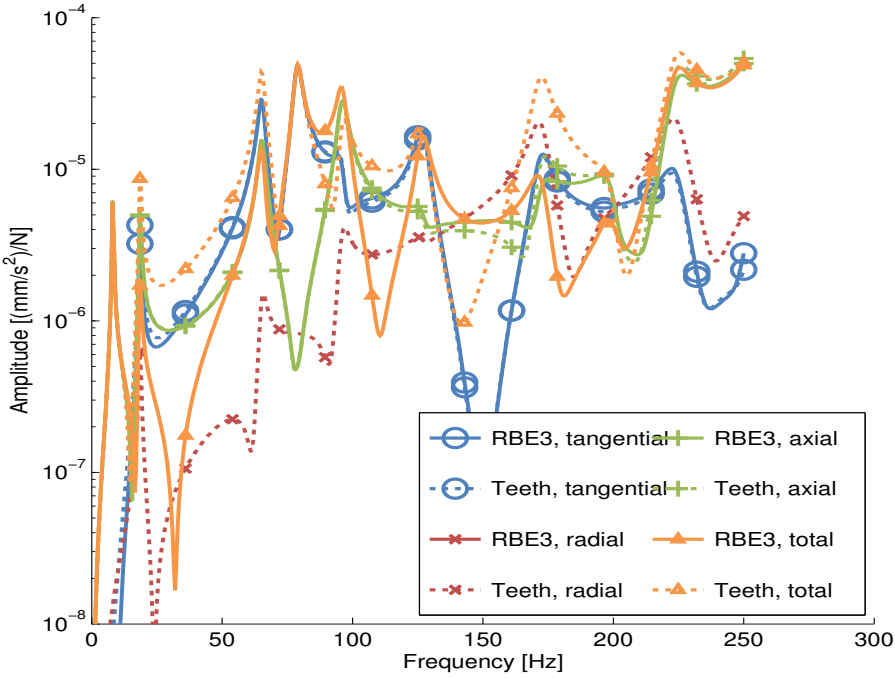

Figure 4.27: Comparison of vibration amplitudes on the intermediate speed ring wheel (vertical direction) due to tangential (———), radial (———) and axial (———) gear forces. Full line: RBE3 approach, dashed line: individual teeth.

a similar response on an arbitrary point on the gearbox housing. Because there is already an initial phase difference between the responses from the individual teeth forces, phase shifting does not cancel out the resulting response, but even amplifies it.

Second assumption - gear stiffness introduction

By summing and introducing the individual gear stiffness values to the centre of the ring wheel the additional radial stiffness introduced in the ring wheel which originates from the individual gear contacts with the ring wheel is neglected. Inserting a planet carrier and planets therefore does not have an impact on the eigenfrequency of eigenmodes such as an ovalisation eigenmode of the ring wheel. However joining the ring wheel with the other components of the flexible gearbox housing already stiffens the ring wheel radially, and the effect of the

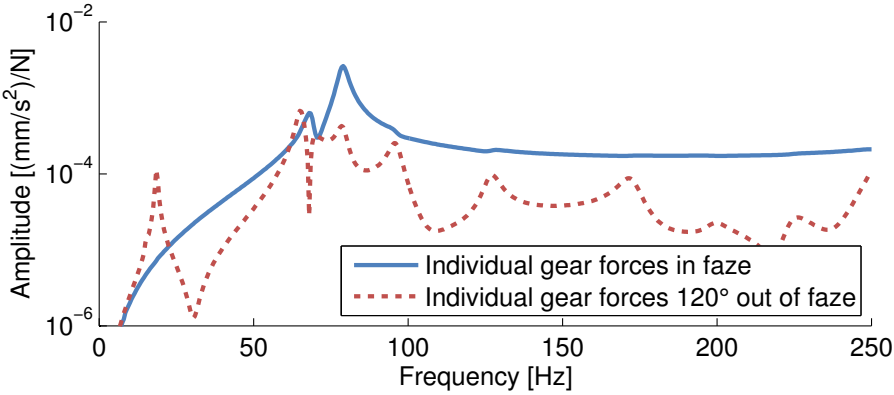

Figure 4.28: Resulting vibration amplitude on the torque arm (vertical direction). Full line: in phase, dashed line: 120° out of phase

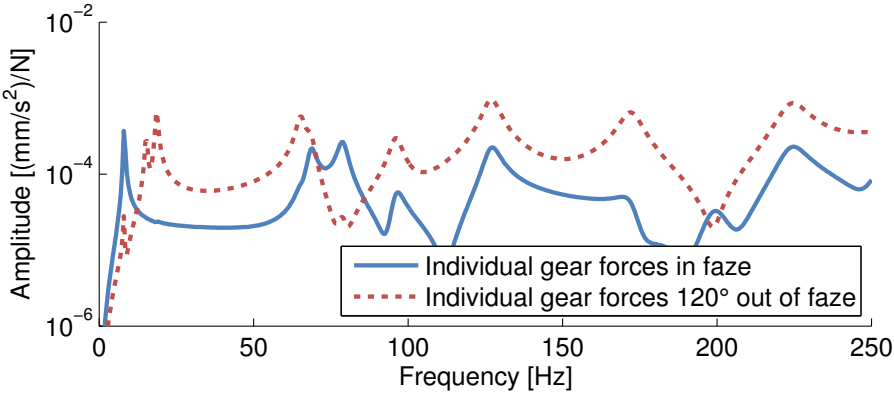

Figure 4.29: Resulting vibration amplitude on an arbitrary point on gearbox housing (axial direction). Full line: in phase, dashed line: 120° out of phase

additional stiffness introduced by the radial components of the individual planet ring wheel contact stiffness is negligible. This is verified by comparing the modal behaviour of the empty gearbox housing with the modal behaviour of the empty gearbox housing including 3 additional springs representing the radial stiffness of the gear contacts.

Conclusions

In general it can be concluded that using TE-FRFs in the frequency domain is a more efficient way to characterise the transfer path from gear excitations to accelerations or radiated noise compared with utilising a complex gear model capable of predicting the actual TE and performing simulations in time domain. Introducing the gear forces in the flexible gearbox housing using an RBE3 results in accurate global eigenmodes. However, acceleration results can only be considered accurate if the response by the radial gear forces can be neglected with respect to the response by the tangential gear forces which was the case for the torque arm in this example. If accurate acceleration or velocity results over the entire gearbox housing are required (e.g. for acoustical calculations), the gear forces should be introduced at their correct location. Furthermore it was shown that the effect of mesh phasing should be investigated taking the housing flexibility into account as it influences the results significantly.

4.6 Conclusions

Main goal of this chapter was to model the individual components of the wind turbine gearbox, to investigate the impact of the modelling approach, and if necessary to experimentally validate these individual components.

For the gearbox housing it was shown that the FE model of the gearbox housing can be considered up front to be quite accurate up to approximately 400 Hz. When accuracy is needed at higher frequencies an EMA should be performed on the assembly of the HSH and MC which has the highest uncertainty. Although this result is obtained by analysing only one specific gearbox, it is believed that this result can be generalised for gearboxes of similar size. Furthermore, it is expected that the dynamic behaviour of the flexible housing can be predicted accurately up front up to the frequency where the complex HSH starts to dominate the modal behaviour (around 400 Hz for this gearbox).

Furthermore, it should be noted that performing a 3D geometry scan or doing a modal update to try to match all eigenmodes may result in an extreme correlation with one individual gearbox housing, but not necessarily with another gearbox housing, as there is currently little or no knowledge on the variation of the modal properties when comparing multiple gearbox housings. Instead of further tuning the gearbox housing, future work should therefore include an investigation on the variability of the dynamic properties of the gearbox housing to determine an optimal level of correlation.

It was also shown that although bolts have an influence on the global dynamics, their impact is quite limited, and that modal damping of the complete gearbox housing is with 0.2% relatively low.

Both planet carriers and shafts are considerably stiffer than the flexible housing. As both shafts and planet carriers have their first eigenmode much higher than the housing, the impact of their flexibility on the global gearbox dynamics will be rather limited. Experimental validation of LSS-PC showed a good initial correlation.

For bearings it was shown that the choice between an RBE2 and an RBE3 has an impact on the global dynamics of the gearbox housing depending on whether or not the addition of the infinite stiffness of the RBE2 has an impact on the global dynamics of the gearbox housing in the frequency range of interest.

It was furthermore shown for the LSS-PC-RS bearing that introducing the individual roller forces (and stiffness values) on the correct location instead of summing these individual roller forces and evenly applying this sum over the entire bearing seat has a non negligible effect as it highly influences the so-called torque arm flapping modes. For these bearing locations, a more advanced bearing model, based on individual roller forces and correct force introduction should thus be used.

Usage of TE-FRFs in the frequency domain is proposed as they are a more efficient way to characterise the transfer path from gear excitations to accelerations or radiated noise compared with utilising a complex gear model capable of predicting the actual TE and performing simulations in time domain. Because radial gear stiffness values are less significant compared with the stiffness of the gearbox housing, introducing the gear forces in the ring wheel of the flexible gearbox housing using an RBE3 does not have a significant impact on the accuracy of the global eigenmodes. Acceleration results can only be considered accurate if the response by the radial gear forces can be neglected with respect to the response by the tangential gear forces. If accurate acceleration or velocity results over the entire gearbox housing are required (e.g. for acoustical calculations), the gear forces should be introduced at their correct location. Furthermore it was shown that the effect of mesh phasing should be investigated taking the housing flexibility into account as it influences the results significantly.

Chapter 5

Modelling and experimental validation of a wind turbine gearbox

5.1 Introduction

The model of the complete gearbox is built up by assembling all individual components (both bodies and forces) from previous chapter into one flexible MB model. Even though many components of the gearbox have been validated individually, a detailed investigation including an experimental validation of a complete assembled gearbox remains valuable as it mainly gives insight on the impact of the connection stiffness values which assemble the individual bodies such as gear and bearing forces into a complete gearbox model.

However, experimentally validating a complete gearbox introduces significant additional complexity compared with experimentally validating large castings. The reason for this is twofold. Observability of the gearbox becomes an issue: accelerometers can only be placed on the outside of the gearbox and on internal components which are accessible from the outside. Mode shapes such as the tilting of the second stage planet carrier can therefore not be measured directly but should be deduced from deformations of the gearbox housing. Secondly both gears and bearings introduce a significant amount of non-linearity. Stiffness of the bearings depends on both current loading conditions and pre-load settings.

Table 5.1: Modelling details of the HSH MC model - bodies

Bodies (5)	Approach
Parallel shafts	Flexible - CMS reduction up to 1 kHz
	Relative DOFs of HS-IS: 6 rigid, 0 flexible modes
	Relative DOFs of HSS: 6 rigid, 2 flexible modes
Gear wheel	LSS wheel: rigid body
	Pump wheel: rigid body
Housing	Flexible - CMS reduction up to 1 kHz
	Relative DOFs: 6 rigid, 49 flexible modes

Gear stiffness is even somewhat harder to assess in these conditions as it can, depending on the positioning of the gears, be completely zero when the gears are out of contact. Furthermore these stiffness values are not dependent any more on large global gearbox properties such as the geometry of the gearbox housing, but on small and local quantities such as gear backlash and bearing pre-load.

To facilitate the validation of this model and to increase the gained insight, this level is split up in two parts. The first part is a sub-assembly of the complete gearbox: HSH and MC including shafts and low speed gear wheel of the parallel gear stage is analysed and validated. Secondly the complete gearbox is analysed and experimentally validated. For both models the impact of the housing stiffness, the bearing stiffness values and in particular the actual bearing pre-load setting is investigated. As both models are experimentally validated in unloaded condition, the effect of the gear stiffness on the global dynamics is investigated with the test rig model in chapter 6.

5.2 HSH and MC

5.2.1 Model

Figures 5.1 and 5.2 show a graphical and a schematic representation of the model of the HSH and MC. Tables 5.1 and 5.2 give an overview of both the bodies and the forces which are used to build the model.

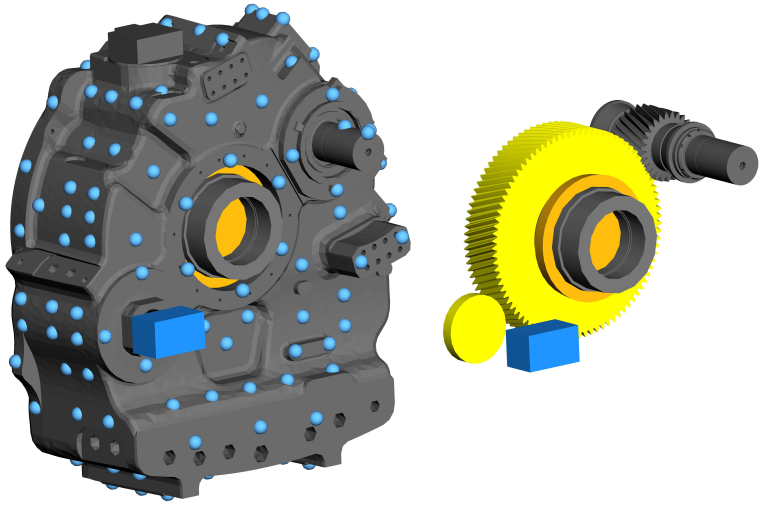

Figure 5.1: HSH MC model. Left: with flexible housing (blue dots: accelerometer locations for experimental validation). Right: without flexible housing

Table 5.2: Modelling details of the HSH MC model - forces

Forces (4)	Approach
Gear forces	None: gears are assumed out of contact in this model
Bearings (4)	6×6 fully populated stiffness and damping matrix or non-linear bearing model included in MB model.
Rubber blocks (4)	Rubber blocks used for EMA. Stiffness tuned to optimise correlation with rigid body modes of EMA

Sensitivity investigation

This subsection investigates how certain parameters dominate the modal behaviour. Following parameters are taken into account: housing stiffness, bearing stiffness, and high speed intermediate gear (HS-IG) inertia. For these parameters sensitivity values which indicate the impact of a certain parameter on the resulting eigenfrequencies have been calculated. A sensitivity value for a frequency band is calculated as the average of the relative frequency shifts of the eigenmode pairs in this frequency band due to this parameter change divided by the relative change of this model parameter. Sensitivities between different parameters can not be compared directly, as some parameters can be

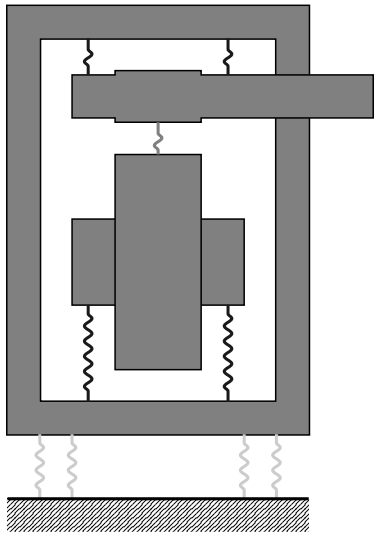

Figure 5.2: HSH MC schematic model overview Legend: bearings, gear force, rubber blocks.

altered more easily than others. To overcome this issue, the sensitivities are multiplied with an estimate of the relative upper bound of the parameter. For the stiffness of a flexible component this is +50%, for the stiffness of a bearing this is +25% and for the inertia of a wheel this is -30%.

$$s_{k,b} = \frac{1}{N_b} \sum_{i}^{N_b} \left(\frac{\frac{f_{i,b,\mathrm{new}} - f_{i,b,\mathrm{old}}}{f_{i,b,\mathrm{old}}}}{\frac{p_{k,\mathrm{new}} - p_{k,\mathrm{old}}}{p_{k,\mathrm{old}}}} \right) \frac{p_{k,\mathrm{UB}} - p_{k,\mathrm{old}}}{p_{k,\mathrm{old}}} \tag{5.1}$$

with

$$s_{k,b} = \text{sensitivity for parameter } k \text{ in frequency band } b$$

$$f_{i,b} = \text{eigenfrequency } i \text{ in frequency band } b$$

$$N_b = \text{Number of eigenmodes in frequency band } b$$

$$p_k = \text{model parameter } k$$

$$p_{k,\mathrm{UB}} = \text{upper bound of model parameter } k$$

Figure 5.3 summarises the results. The effect of these parameters on the rigid body modes is not taken into account. Following conclusions can be made: the large inertia of the gear wheel only has a significant impact on the first few eigenfrequencies in the lower frequency range. At higher frequencies this gear wheel behaves as if almost uncoupled from the rest of the model. The bearings have an impact on the modal behaviour over the entire frequency range, however their impact is biggest at the lower frequencies. The flexible gearbox housing has the highest impact on the modal behaviour in the complete frequency range.

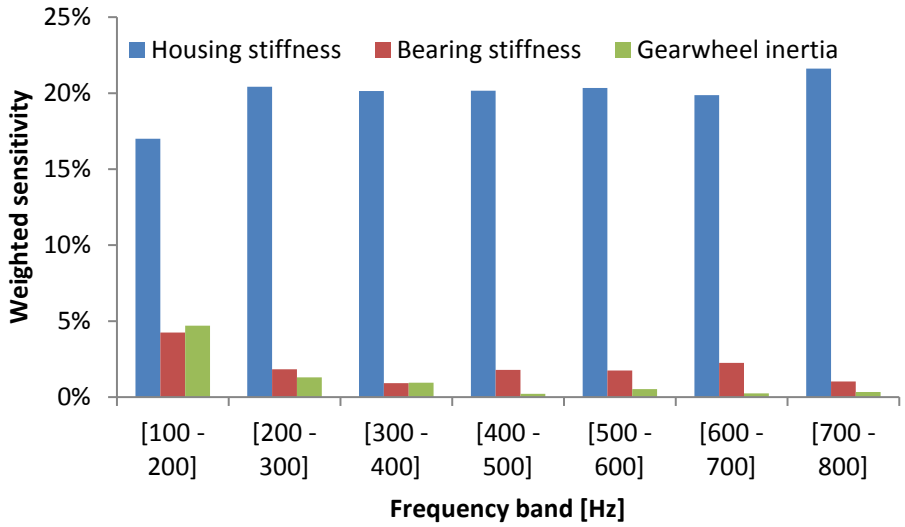

Figure 5.3: Weighted sensitivities for the HSH MC assembly.

Effect of pre-load

The actual pre-load setting of the bearings on a shaft or planet carrier is allowed to vary in a certain range. Because the actual bearing stiffness is highly dependent on this pre-load setting it may have an influence on the eigenfrequencies and mode shapes and thus on the correlation between the model and the experimental validation campaign. To assess this influence of the bearing pre-load on the eigenfrequencies and on the mode shapes, a parameter variation case on the bearing pre-load for both the HS-IS shaft and the HSS shaft is performed. Pre-load settings of both shafts were modified simultaneously. Figure 5.4 shows the change in eigenfrequency of the first 5 eigenmodes modifying the pre-load in an acceptable pre-load setting range. Several observations can be made:

- Most of the eigenfrequencies are affected by the pre-load.
- The impact of the pre-load on the eigenfrequencies is less significant at higher pre-loads.

It can be concluded that bearing pre-load has a significant effect on the eigenfrequencies of the HSH and MC. Eigenfrequencies can shift up to 15% when changing the pre-load setting from minimum allowable to maximum allowable setting. The impact of the pre-load on the eigenfrequencies is most pronounced on low pre-load settings and drops at higher pre-loads. Only the modeshape of the first eigenfrequency changes significantly by altering the pre-load. The modeshapes of the higher eigenfrequencies change only slightly. Furthermore, note that this pre-load setting will have an impact on the correlation between measurements and model.

5.2.2 Measurements

An EMA was performed on this sub-assembly of the gearbox containing the two large castings (HSH and the MC). This sub-assembly also contains both the HS-IS and HSS shafts, their pre-loaded bearings, the HS-IG, the pump assembly, heating system and lubrication system. To simulate free-free conditions, this sub-assembly was placed on rubber blocks. An electro mechanical shaker was used to excite this sub-assembly and accelerations were measured at 201 locations using 4 tri-axial accelerometers in 52 runs. During the eigenmode identification process 46 eigenmodes in the frequency range between 0 Hz and 1000 Hz were identified. Small, extremely low damped peaks, probably related with the tubings of the lubrication system, were ignored. Figure 5.5 shows

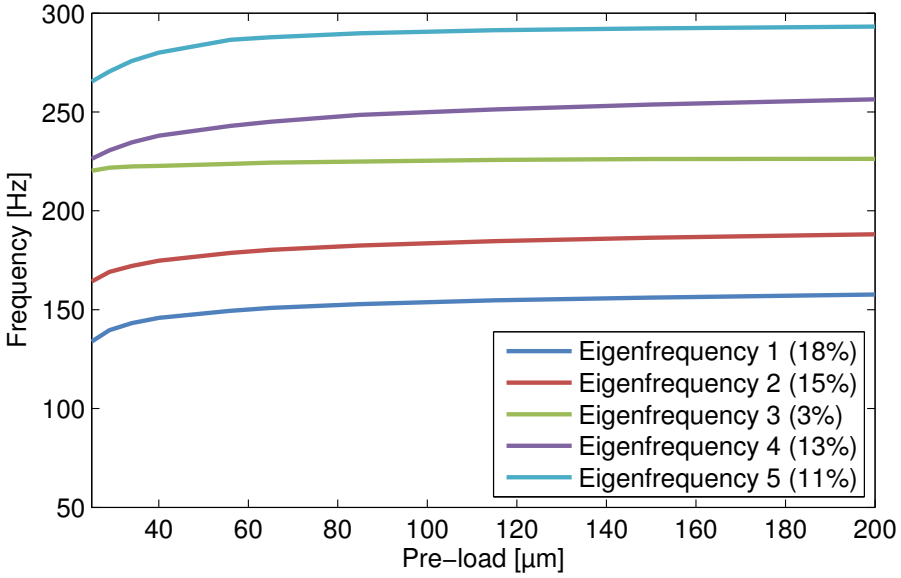

Figure 5.4: Effect of pre-load on frequency of the first 5 non rigid body modes.

this measurement setup. Figure 5.6 shows a typical measured FRF and its corresponding synthesized FRF as a result of the eigenmode identification process. Note that only 5 out of 6 rigid body modes could be identified, and that the modal damping ($\approx 2\%$) is significantly higher than the modal damping measured of the empty HSH and MC (see section 4.2.1).

5.2.3 Correlation

The MAC criterion is used to correlate the modeshapes from the model with the experimentally obtained modeshapes. Next to the high dependency of the imprecisely known bearing pre-load 2 other factors have a significant impact on the correlation:

1. the MB model does not fully represent the measurement setup: no detailed geometrical information is available for the heating system and the pump assembly, and due to the high complexity, and low relevance the lubrication system was not included in the MB model either. It is therefore likely that eigenmodes which are dominated by those missing parts are not correlated with a simulated eigenmode; and

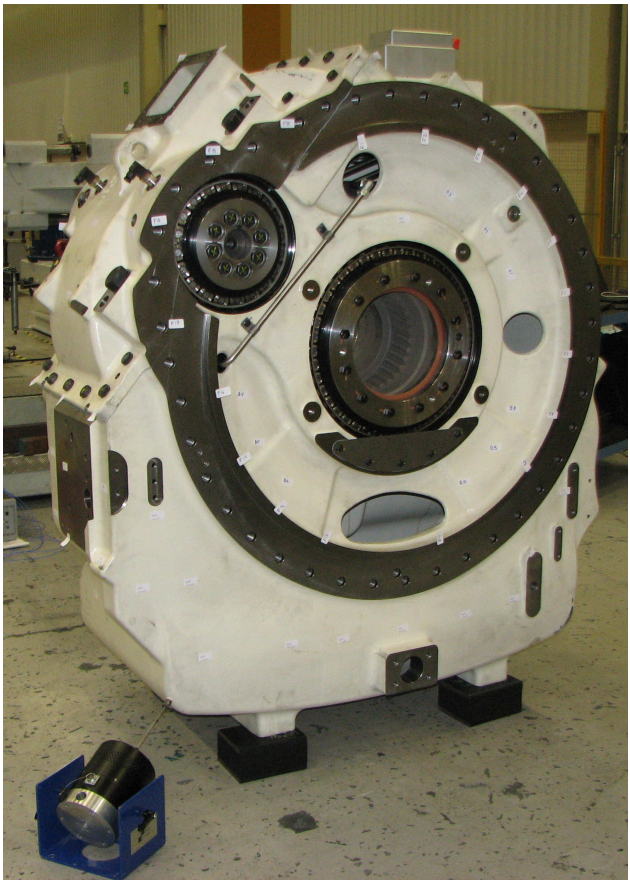

Figure 5.5: Measurement setup for HSH MC model

2. the correlation between the updated flexible HSH + MC housing and the experimentally obtained modeshapes of this individual component (see section 4.2.1, table 4.3) dropped significantly above 700 Hz. As the flexible housing is dominating the modal behaviour of the HSH + MC model, correlation above this frequency between the HSH + MC model and the experimentally obtained modeshapes is very unlikely.

Correlation is again calculated using FEMTools [29]. FEMTools' main purpose is to correlate FE models with experimental data. FEMTools is however highly customisable and was adapted using the built-in scripting language to also support reading Simpack models, modifying Simpack model parameters and

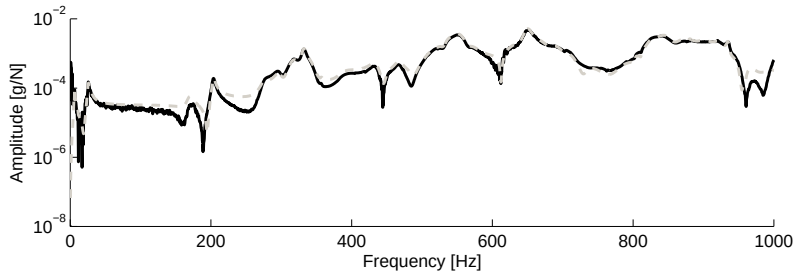

Figure 5.6: Typical FRF from HSH MC: black: measured; gray: synthesized

performing correlation with eigenmodes computed by Simpack. More details about these scripts are given in Appendix A.

Table 5.3 shows the correlation between the experimentally identified modes and the simulated eigenmodes based on the MAC criterion. All mode shape pairs with a MAC value above 40% are considered to be correlated. Typically a higher MAC value is desired to correlate simulation and experimental results. An additional visual comparison between the measured and simulated eigenmode for modepairs with a low MAC value however confirms the correlation. Following conclusions can be made:

1. An acceptable correlation exists between the modeshapes of the experimental measurement and the modeshapes of the MB model up to approximately 500 Hz.
2. The frequency difference between the experimental modeshapes and the modeshapes of the MBS model is mostly below 5% with only a few exceptions.

5.2.4 Conclusions

A model of the HSH + MC was built to gain more insight in the impact of the bearing stiffness values on the global dynamics. A sensitivity study showed that the flexible gearbox housing has the highest impact on the global dynamics. The effect of the bearing stiffness values is smaller and also more focussed on the lower frequency ranges. The effect of the HS-IG inertia on the global dynamics is almost negligible. A parameter variation case showed that the pre-load settings of the bearings (especially low pre-load settings) have a significant impact on the resulting eigenfrequencies.

Table 5.3: Mode correlation table between HSH + MC measurements and MB model

Frequency range [Hz]	Number of modes identified	Number of correlated eigenmodes	Average MAC	Average absolute relative frequency difference
0 - 100	5	100%	95%	6%
100 - 200	1	100%	92%	4%
200 - 300	3	100%	78%	12%
300 - 400	6	83%	63%	5%
400 - 500	4	75%	74%	3%
500 - 600	7	14%	61%	0%
600 - 700	5	80%	50%	7%
700 - 800	3	33%	52%	6%
800 - 900	7	14%	42%	4%
900 - 1000	5	0%		

Correlation with an experimental measurement campaign revealed overall an acceptable correlation up to approximately 500 Hz. Due to the quite accurate model of the HSH + MC up to 700 Hz (see section 4.2.1), the deviation between the experimentally identified eigenfrequencies and the model depends heavily on the used bearing stiffness values which have the second highest impact (after the flexible housing) on the resulting eigenfrequencies. Above 500 Hz correlation drops significantly which can be expected as the flexible housing of the HSH and MC, the most important component for this model, showed a similar behaviour with experimental measurements.

5.3 Full gearbox - Structural model

5.3.1 Model

Figures 5.7 and 5.8 show a graphical and a schematic representation of the structural gearbox model. Tables 5.4 and 5.5 give an overview of both the forces

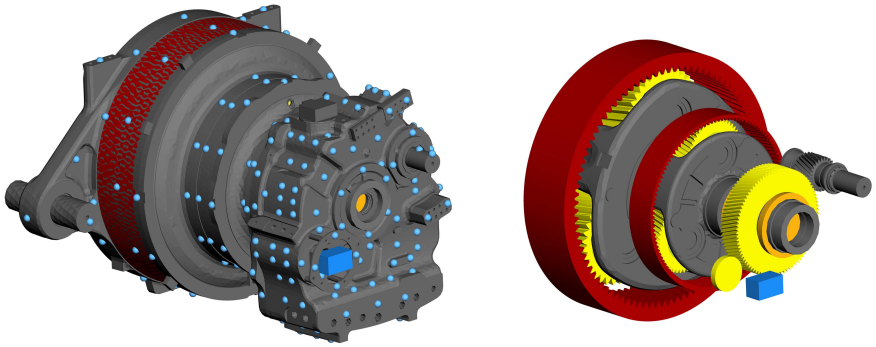

Figure 5.7: Gearbox model. Left: with flexible housing (blue dots are virtual accelerometers). Right: without flexible housing

and the bodies which are used to build the model.

Table 5.4: Modelling details of the full gearbox model - forces

Forces	Approach
Gear forces	Gear force element including varying stiffness, gear slicing, backlash, ... Note that this gear force element was switched off when performing correlations between this model and measurements on an unloaded gearbox.
Bearings	combination of 6×6 fully populated stiffness and damping matrix, bearing lookup table or roller based bearing depending on the analysis.
Rubber blocks	Rubber blocks used for EMA. Stiffness tuned to optimise correlation with rigid body modes of EMA

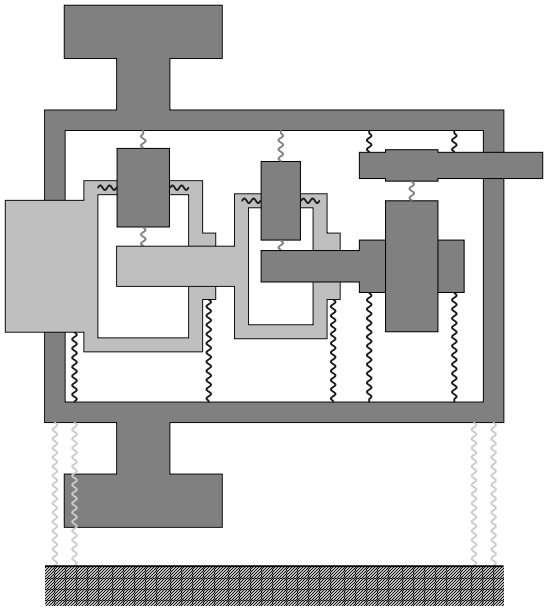

Figure 5.8: Gearbox schematic model overview, measurement setup.
Legend: bearings, gear force, rubber blocks.

Table 5.5: Modelling details of the full gearbox model - bodies

Bodies (15)	Approach
PC	Flexible - Component Mode Synthesis (CMS) reduction up to 1 kHz
	Relative DOFs PC 1: 6 rigid, 14 flexible
	Relative DOFs PC 2: 6 rigid, 8 flexible
Planet shafts	Flexible - CMS reduction up to 1 kHz
	Relative DOFs included in model PC
Planets	Rigid body
	Relative DOFs of all planets 6×6 rigid
Sun shafts	Flexible - CMS reduction up to 1 kHz
	Relative DOFs of Sun 1: 0 flexible - included in PC2
	Relative DOFs of Sun 2: 3 flexible
Parallel shafts	Flexible - CMS reduction up to 1 kHz
	Relative DOFs of Low speed shaft: 6 rigid, 0 flexible modes
	Relative DOFs of High speed shaft: 6 rigid, 2 flexible modes
Gear wheel	LSS wheel: rigid body
	Pump wheel: rigid body
Housing	Flexible - CMS reduction up to 1 kHz
	Relative DOFs: 6 rigid, 124 flexible modes

Sensitivity study

Similarly with the model of the HSH + MC a sensitivity study is performed to investigate the impact of model changes on the modal behaviour of the complete gearbox. For this sensitivity study the model of the gearbox is constrained at its LSS-PC, and 2 springs are used to simulate the gearbox suspension stiffness. This configuration resembles the actual configuration in the wind turbine more closely than a free free condition (see figure 5.9). Similarly with the model of the HSH + MC the sensitivities are multiplied with a relative bound of that parameter. Following sensitivities are calculated: bearing stiffness values (upper bound: +25%), the housing stiffness (upper bound: +50%), gear wheel inertia (lower bound: -30%), the stiffness of LSS-PC and ISS-PC (upper bound: +25%) and the mass of the LSS-PC and ISS-PC (lower bound: -15%).

Figure 5.10 shows the results from this sensitivity study. This sensitivity study again emphasises the importance of the flexible gearbox housing as it has the highest sensitivity resulting in the most dominant component over the entire

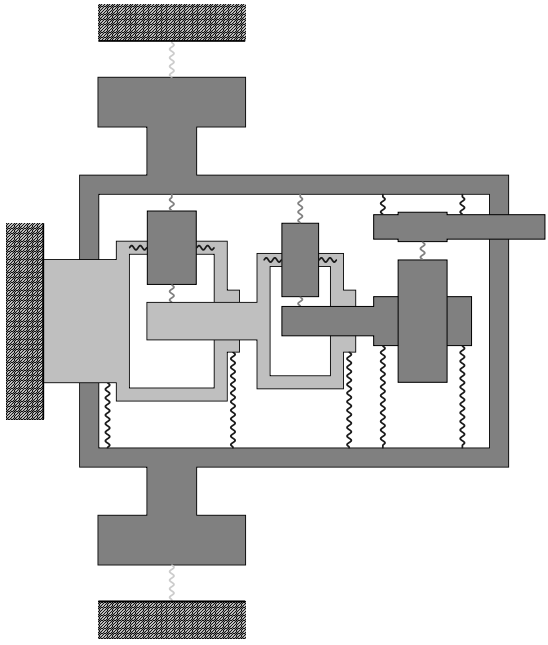

Figure 5.9: Gearbox schematic model overview, measurement setup.
Legend: bearings, gear force, torque arm suspension.

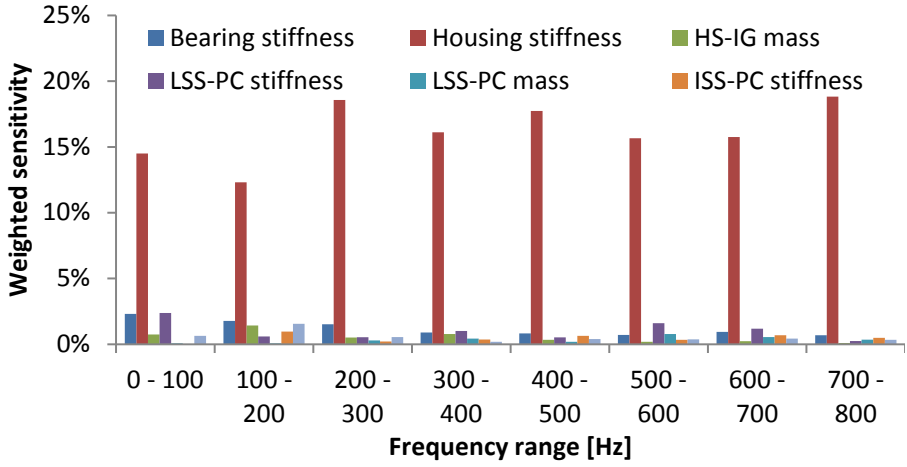

Figure 5.10: Weighted sensitivities for the gearbox assembly.

frequency range. Second most dominant are the bearing stiffness values in the lower frequency bands. The effect of the mass of the HS-IG and the mass and the stiffness of both planet carriers (LSS-PC and ISS-PC) is rather limited with only a few exceptions. More in-depth insight in the impact of the flexible gearbox housing design is gained by performing an additional sensitivity study on the most important individual components of the flexible housing. For all individual components sensitivities are calculated by changing the E-modulus of these components, which links directly with their overall stiffness. Figure 5.11 shows these sensitivities[1]. From these sensitivities it is clear that the overall stiffness of both ring wheels has a negligible effect on the modal behaviour of the complete gearbox. The TA has an impact on some frequency ranges while both intermediate bearing housings have a large impact on the more global mode shapes in the lower frequency ranges. The higher frequency range is dominated by the HSH + MC.

[1]These sensitivities can be compared directly and are not multiplied with an upper bound of the parameter.

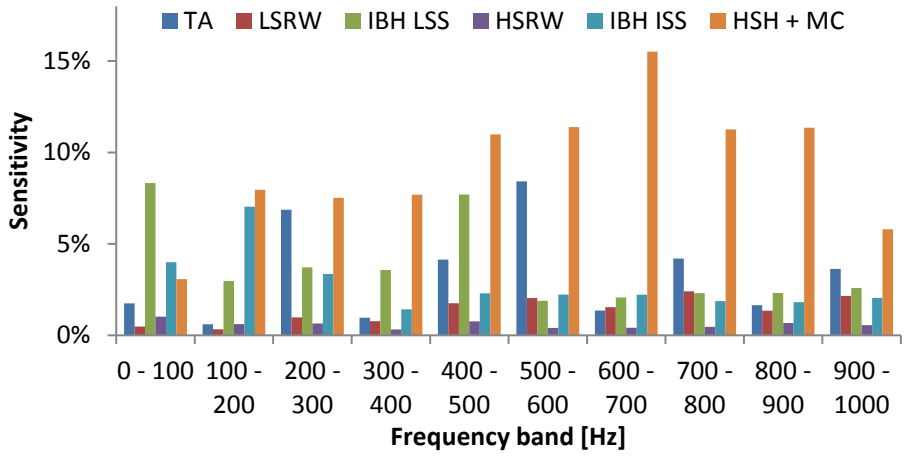

Figure 5.11: Sensitivities for the gearbox assembly, focus on individual components of the gearbox housing.

Effect of pre-load

Again the influence of the bearing pre-load on the eigenfrequencies is assessed for both shafts of the parallel gear stage and for the LSS-PC. For both, pre-load was changed in the allowable pre-load setting range. Note that for the investigation of the pre-load of the LSS-PC different boundary conditions are used (gearbox is suspended on its torque arm and its LSS-PC) to better represent the behaviour of the gearbox in the wind turbine. Figures 5.12 and 5.13 show the impact of this pre-load modification on the resulting eigenfrequencies. Eigenfrequencies which shift more than 5% are plotted with a thick full line.

Following observations can be made:

- variation of eigenfrequencies by pre-load modification of both HS-IS and HSS stay below 10%; and
- variation of eigenfrequencies by pre-load modification of LSS-PC stays limited to maximum 10% except for the low eigenfrequencies (<100 Hz) which shift with approximately 20%.

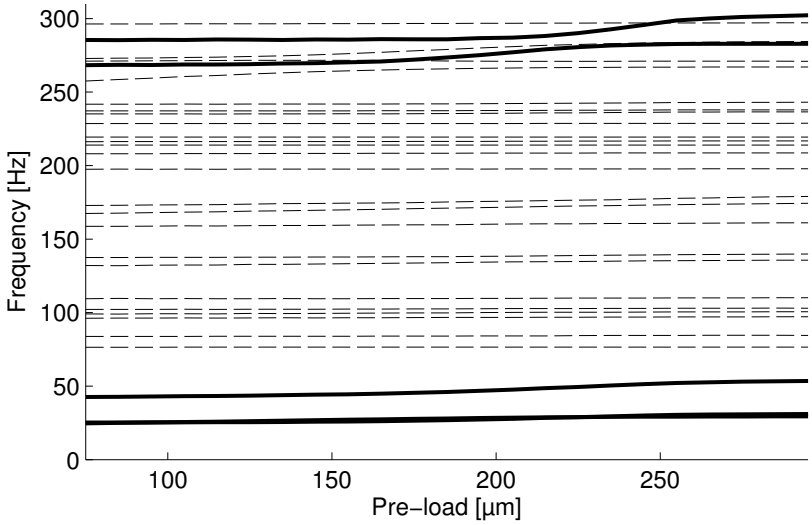

Figure 5.12: Effect of LSS-PC bearing pre-load on eigenfrequencies between 0 and 300 Hz. Eigenfrequencies which shift more than 5%: thick line; others: dashed normal line.

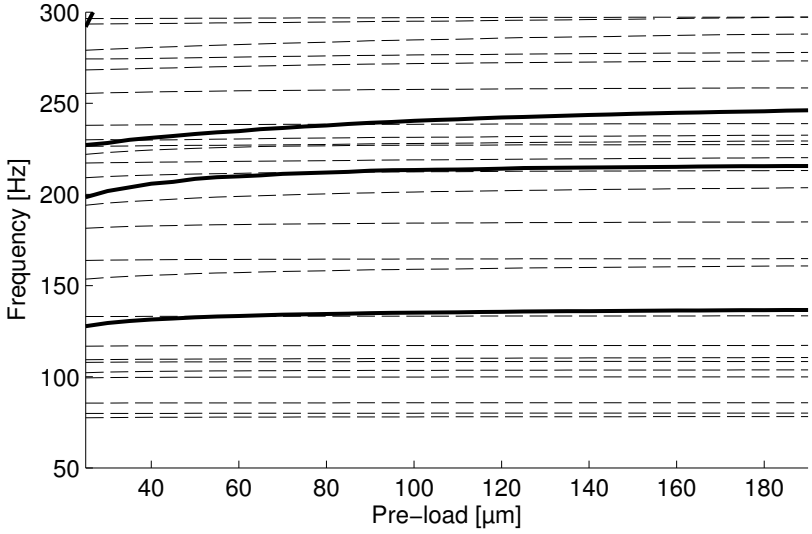

Figure 5.13: Effect of HS-IS and HSS bearing pre-load on eigenfrequencies between 50 and 300 Hz. Eigenfrequencies which shift more than 5%: thick line; others: dashed normal line.

Effect of bearings with non-constant stiffness

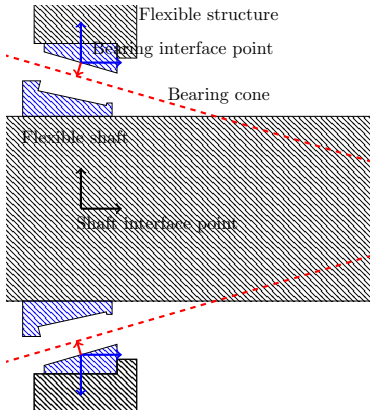

Figure 5.14: Advanced bearing model - overview.

Section 4.4.2 showed that for large bearings the number of rollers in contact and the actual location of the loaded zone can affect the so-called in-phase and out-of-phase flapping modes. This section describes how the implementation in section 4.4.2 using an FE model is translated to an implementation for the MB model. This implementation is complexer as it requires that the bearing inner ring can rotate with respect to the bearing outer ring. Instead of using simple springs to directly connect the inner ring with the outer ring of the bearing, springs are used between fixed locations on the outer ring, and a cone which represents the bearing inner ring. Figure 5.14 shows a graphical representation of this bearing model with:

- **Flexible structure**: the flexible supporting structure (gearbox housing or bearing outer ring).
- **Bearing interface point**: a position on the bearing outer ring which is an integral part of the flexible structure. There are as many bearing interface points as there are rolling elements in the bearing.
- **Shaft interface point**: central position on the rotating shaft. There is only one shaft interface point for each bearing. The shaft could be flexible or rigid.
- **Bearing cone**: a rigid cone, defined by the bearing outer ring raceway and fixed at the shaft interface point. In figure 5.14 this cone is offset for clarity reasons.

The calculation of the total bearing force can be described as follows:

For each roller i:

1. Calculate the shortest distance between bearing interface point i and the bearing cone. This distance is the compression of roller i.
2. Calculate the resulting (non-linear) roller force based on the roller compression
3. Introduce the force in bearing interface point and introduce the opposite force and accompanying moments in the shaft interface point.

Main assumptions:

- the rollers are stationary and fixed to the outer ring, they do not rotate when the inner ring rotates;
- the roller stiffness is not influenced by roller misalignment; and
- the bearing inner ring deformation is not taken into account, it is represented by a rigid cone.

Main advantages of the proposed method are:

- Accurate (non-linear) force calculation based on individual roller compression.
- Because individual forces are introduced in different points in the flexible structure the stiffening effect of the bearing on the flexible structure is correctly taken into account.
- The utilisation of the bearing cone, and the distance calculation between a fixed location on the flexible structure (bearing interface point) and the bearing cone allows rotational movement of the shaft or planet carrier. All other displacements such as tilt and axial offsets are also taken into account correctly.
- Pre-stress can easily be taken into account by offsetting the shaft interface point.
- Both the non-linear rolling element stiffness and the non-linearities caused by the non-constant number of rollers in contact are taken into account.

An in-depth description about the distance calculation and the stiffness calculation is given in Appendix B. The effect of this non-constant bearing stiffness is tested for the LSS-PC-RS, HS-IS-RS and HS-IS-GS bearings. The wind turbine environment is approximated by including the main shaft, main bearing and the TA suspension bushings (see figure 5.15). Two different load cases are calculated: firstly the impact of normal operating torque is investigated by gradually applying the normal operating torque from 20% up to 100%, and secondly the impact of the extreme non-torque bending moment is investigated by keeping the normal operating torque at 100% and gradually applying the extreme non-troque bending moment from 0% up to 100%. This bending moment results in a misalignment of the LSS-PC. Figure 5.16 shows how this external load has an impact on the number of rollers in contact of the bearing which leads to a shift in several global eigenfrequencies with more than 5% as shown in figure 5.17.

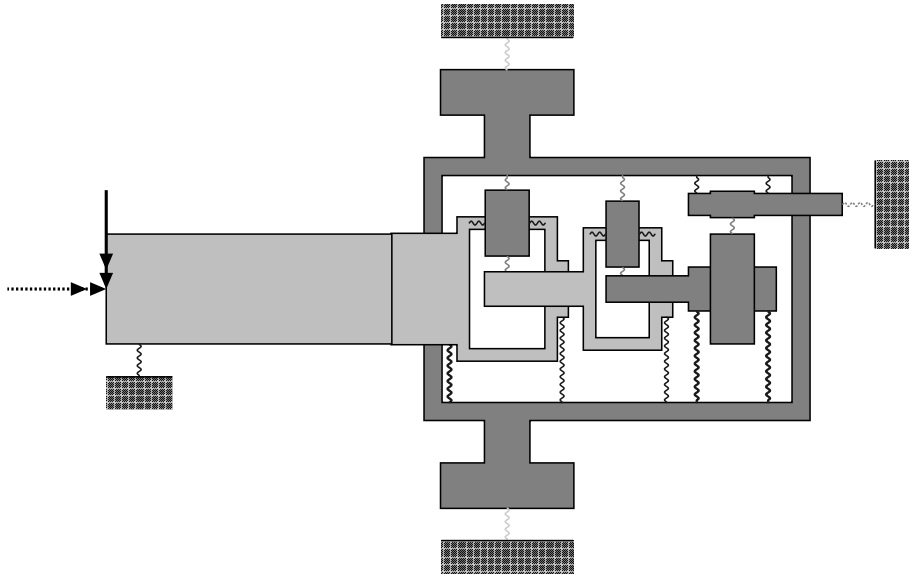

Figure 5.15: Gearbox model with advanced bearings, main shaft, main bearing and rubber supports.
Legend: bearing, roller based bearing, gear force, torque support, high speed shaft spring, input torque and bending torque.

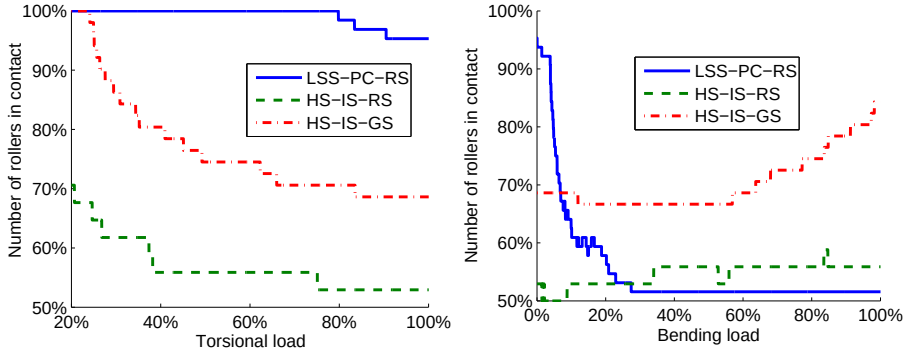

(a) Loadcase 1: only torsional load

(b) Loadcase 2: 100% torsional load and additional bending load

Figure 5.16: Number of rollers in contact due to changing external load

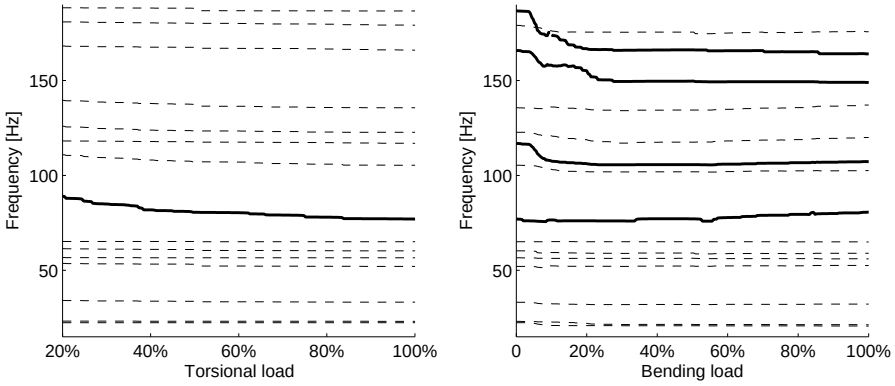

(a) Loadcase 1: only torsional load

(b) Loadcase 2: 100% torsional load and additional bending load

Figure 5.17: Shifting eigenfrequencies due to changing external load. Eigenfrequencies which shift more than 5%: thick line; others: dashed normal line.

5.3.2 Measurements

An EMA was performed on the complete assembled gearbox. The measurement setup (see figure 5.18) is identical with the measurement setup of the EMA of the sub-assembly with one exception: for this measurement two large electrodynamic shakers were used instead of one to be able to put enough energy in the gearbox modeshapes in the frequency band of interest. To simulate free-free suspension the gearbox was again placed on rubber blocks. In total accelerations at 305 measurement points are measured in 3 directions using 4 accelerometers during 78 runs.

Even though 2 electrodynamic shakers were used response levels stayed relatively low compared with the background noise (measurements took place in the testing hall of the ZF Wind Power Lommel factory). Energy input was acceptable up to approximately 400 Hz. Above 400 Hz energy input into the system dropped significantly resulting in lower quality FRFs. These lower quality FRFs complicated the eigenmode identification process. Eigenmodes below 400 Hz are considered accurate and physical eigenmodes above 400 Hz are considered less accurate. 86 Eigenmodes (including 3 rigid body modes) were identified in the frequency range between 0 Hz and 900 Hz.

5.3.3 Correlation

Table 5.6 gives insight in the correlation between the experimentally identified eigenmodes and the eigenmodes from the MB model.

Note that the number of modes of the flexible MB model exceeds the number of experimentally identified eigenmodes in the same frequency band. A visual inspection of these uncorrelated eigenmodes reveals that these uncorrelated eigenmodes are often dominated by movement of internal components such as the ISS-PC and its planets. This is expected as the EMA measurement setup violates the observation principle by not measuring on internal components, and excitation levels might not have significantly excited these internal eigenmodes.

5.3.4 Conclusions

The model of the complete gearbox was built and investigated. A sensitivity study showed that the flexible gearbox housing is the most dominant component controlling almost completely the gearbox dynamic behaviour. Second most important parameters are the bearing stiffness values. The effect of the mass

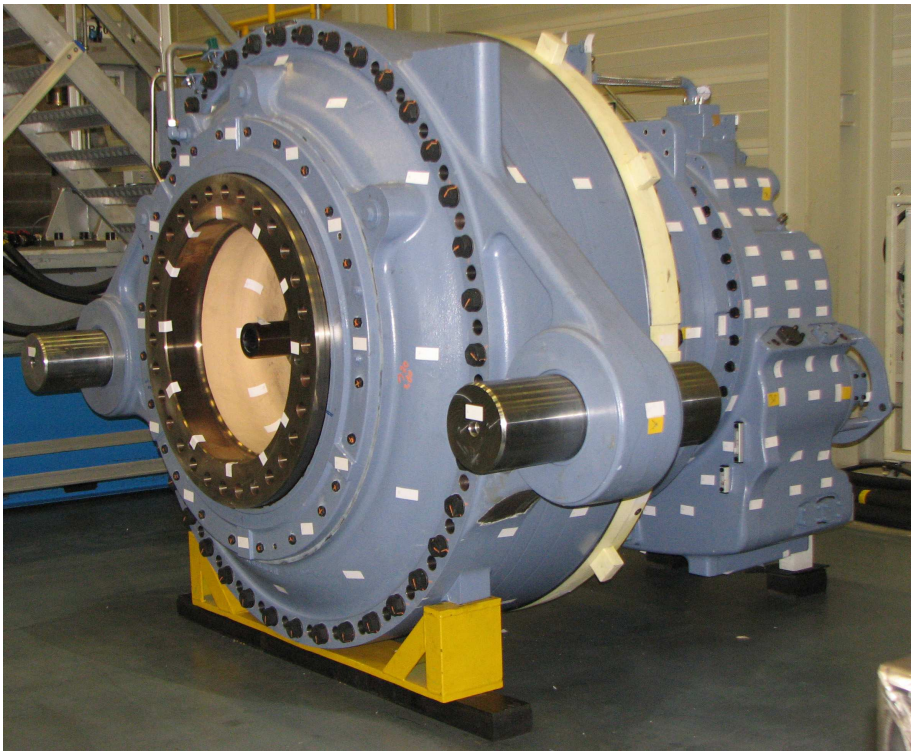

Figure 5.18: Measurement setup for the complete gearbox model

of the HS-IG, and the mass and the stiffness of both planet carriers is limited to a small number of eigenfrequencies and almost negligible for all others. A sensitivity study modifying the stiffness of the individual castings of the flexible gearbox housing revealed that the high frequency behaviour is dominated by the HSH and MC design. Lower frequency range behaviour is more determined by the intermediate bearing housings. The TA design has an impact over the entire frequency range of interest.

A parameter variation case assessing the effect of the bearing pre-load on the dynamics revealed that only few modes are affected by this pre-load setting, and that the impact of this pre-load for those few modes is as high as 10% on the HS-IS, the HSS and the LSS-PC with only a few exceptions in the lower frequency range for the LSS-PC which reach even up to 20%.

Table 5.6: Mode correlation table between GBX measurements and MBS model

Frequency range [Hz]	Number of modes identified	Number of correlated eigenmodes	Average MAC	Average absolute relative frequency difference
0 - 100	5	100%	94%	3%
100 - 200	5	100%	74%	2%
200 - 300	10	100%	76%	5%
300 - 400	15	67%	70%	3%
400 - 500	11	64%	61%	1%
500 - 600	9	33%	45%	9%
600 - 700	13	23%	67%	2%
700 - 800	7	14%	61%	7%
800 - 900	11	27%	54%	6%

Furthermore, an analysis using a roller based bearing model showed the impact of the external gearbox loading on the number of rollers in contact of several bearings leading to a shift in several global eigenfrequencies with more than 5%.

An in-depth experimental validation campaign revealed a very good correlation between experimentally identified eigenmodes and simulated eigenmodes up to approximately 300 Hz. Between 300 Hz and 500 Hz an acceptable correlation between model and experimental validation campaign was observed. Above 500 Hz this correlation drops significantly. This is expected due to lower quality of the FRFs above 400 Hz and a lower correlation between empty gearbox housing and measurements at higher frequencies.

5.4 Full gearbox - Acoustic model

5.4.1 Need for acoustic modelling

Acoustic models are frequency dependent and should be solved at each frequency of interest resulting in large calculation times. For these reasons some approaches exist to estimate the total radiated sound power without using an advanced acoustic model [47, 159]. The averaged surface velocity technique is such a method to estimate the total radiated sound power using a structural finite element model[171]. In general acoustic power can be calculated as:

$$W = \sigma \rho c S A S V \tag{5.2}$$

with

- W: acoustic radiated power [W]
- σ: radiation efficiency [-]
- ρ: density of air $[kg/m^3]$
- c: speed of sound in air $[m/s]$
- S: total radiating surface $[m^2]$
- $ASV = \frac{\sum_{i=1}^{n} S_i v_i^2}{S}$: averaged surface velocity, with S_i the surface of radiating panel i and v_i its surface normal velocity $[(m/s)^2]$

All the above quantities, with the exception of the radiation efficiency σ, can be calculated by structural FE software. In the cases that $\sigma \approx 1$ it can be neglected and the radiated power can be calculated using only structural FE software.

Jacobson and Singh measured and calculated this radiation efficiency for the research gearbox of the NASA in the Glenn Research Center [78]. The coincidence frequency (the frequency above which σ approximates 1) for their rather small and box shaped gearbox (see figure 3.4) lies somewhere above 2 kHz, indicating that the averaged surface velocity method cannot be used below 2 kHz in this case, and more advanced acoustic models are required to calculate the total radiated noise. As these results depend on the geometry

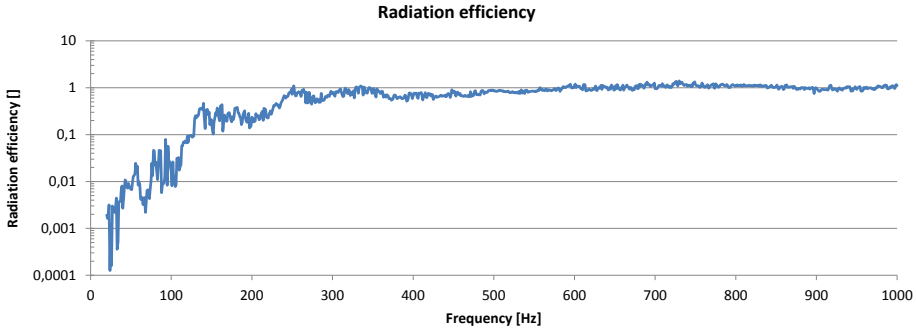

Figure 5.19: Radiation efficiency of the wind turbine gearbox between 20 and 1000 Hz.

of the gearbox, they cannot be used for a large complex shaped wind turbine gearbox.

The radiation efficiency of this wind turbine gearbox is calculated using the acoustic model of this gearbox (see section 5.4.2). Figure 5.19 shows that this radiation efficiency approaches unity above approximately 800 Hz which implies that an averaged surface velocity model cannot be used to accurately simulate the radiated acoustic power below this frequency, and that an advanced acoustic model should be used here.

5.4.2 Acoustic model

Figure 5.20 shows the acoustic FE model of the gearbox build using the LMS VL.Acoustics software [96]. Instead of meshing the radiating surface of the gearbox which is typical for an acoustic BE model, the air entrapped between the gearbox and an as small as possible convex wrap around the gearbox is meshed with volume elements. Maximum frequency was set to 1 kHz, resulting in a mesh size of 34 mm using 10 elements per wavelength, or in a total of 325 kNodes. Two types of boundary conditions are used; the first on the interface between the gearbox and the surrounding air to import the structural vibrations of the gearbox MB model into the acoustic model; and the second one on the outside of the acoustic mesh to prevent pressure waves from reflecting on the outer surface back to the gearbox. This second boundary condition is implemented in the model by using automatic matched layer (AML) elements [10, 168]. In this case mainly the total radiated sound power is of interest. To

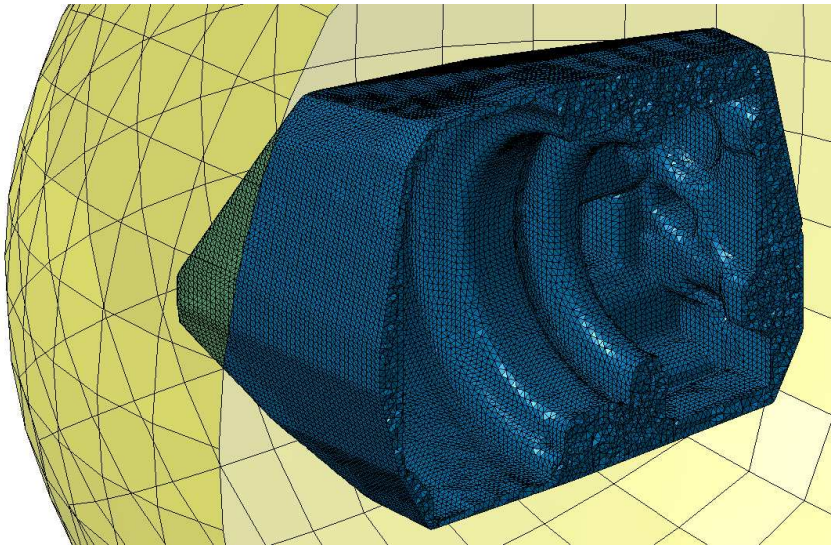

Figure 5.20: Acoustic FE mesh.

calculate this total radiated sound power, a spherical field point mesh (yellow mesh in figure 5.20) is placed around the acoustic FE mesh.

5.4.3 Structural - acoustic linking

Not much literature is published on the linking of multibody models with true acoustic models. Only recently similar simulations were performed on engine radiation [180, 154]. Older publications [159, 16, 56] often predict the radiated noise by using the ASV approach neglecting the radiation efficiency.

In order to calculate the total radiated sound power, the deformations of the flexible gearbox housing should be exported from the MB model into the acoustic model. Usually when calculating acoustics, the deformations are obtained through FE simulations and the deformations are available as displacements at each node. When using flexible multibody however, only the displacements at the master nodes and the MPFs are computed. One could use the MPFs to calculate the displacements at all the nodes of the FE model, but a more straightforward approach is to transform the acoustic model into modal coordinates such that the MPFs of the gearbox housing can be used directly

to calculate the radiated noise. This technique is known as modal acoustic transfer vectors(MATVs) which is the modal variant of the acoustic transfer vector (ATV) technique [164, 171].

The ATV technique has two major advantages. Firstly, because the ATVs are calculated on beforehand they do not depend on the actual structural deformation. This implies that they can be re-used when calculating the sound power for different load cases (such as an RPM runup) or different design variants (with limited changes on the exterior radiating surface). Secondly, when calculating exterior acoustics the ATVs are very smooth and can be frequency interpolated which will result in huge time savings. Instead of evaluating the ATVs at every frequency, the ATVs are only calculated at certain so-called 'master frequencies' and are interpolated at the so-called 'slave frequencies'. A rule of thumb exists to determine the distance between these master frequencies [163].

An ATV can be considered as an acoustic transfer function which relates the structural normal vibrating velocities v_{ns} with the sound pressure p at a single field point for each frequency $\omega/(2\pi)$:

$$p = \{ATV\,(\omega)\}^T \,.\, \{v_{ns}\,(\omega)\} \tag{5.3}$$

MATVs are the modal representation of the ATVs. ATVs and MATVs differ in the fact that each element of an ATV expresses the linear relation between vibration at a single vibrating element and the pressure in a single field point while each element of an MATV expresses the linear relation of a single mode shape and the pressure in a single field point.

The resulting pressure in the MATV approach is calculated by multiplying the MATVs with the MPFs:

$$p = \{MATV\}^T \,.\, \{MPF\,(\omega)\} \tag{5.4}$$

The usage of MATVs instead of ATVs has the advantage that the final acoustic evaluation is in the modal domain such that the results from the multibody model do not have to be transformed from the modal domain back to the nodal domain. Considering the sizes of the models, this results in huge savings in data transfer:

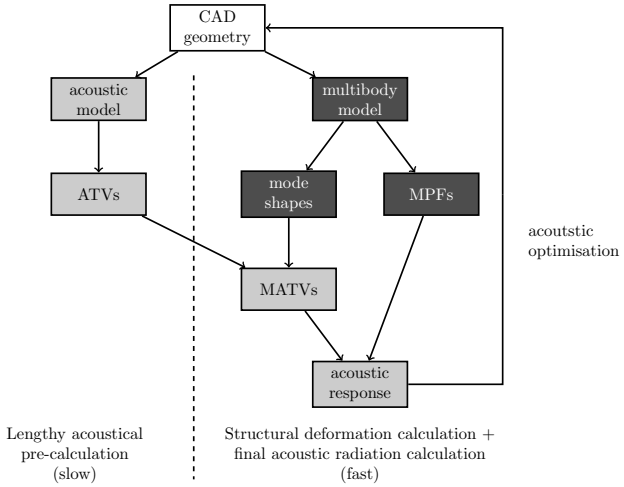

Figure 5.21: Global approach to calculate acoustics using the MATV technique.

- ATVs: 600kNodes × 3 DOFs/node × 120 sec × 4000 data samples / sec = 864E9 data points;
- MATVs: 150 MPFs × 120 sec × 4000 data samples / sec = 72E6 data points, or a data reduction with a factor of 12000 if the displacements of all FE nodes were to be translated back into the nodal domain.

Figure 5.21 shows the entire process from CAD data up to acoustic radiated power. Two clear paths should be separated, the left path which does the actual acoustic calculation of the ATVs and the right path which performs the structural deformation calculations using the multibody model and the mode calculation which will be used to transfer the ATVs into the modal domain. The final step is multiplying the MATVs with the MPFs to obtain the total radiated sound power.

5.4.4 Acoustic runup simulation

Using the multibody model (see figure 5.22) a time simulation of 120 seconds of an RPM runup from 0 RPM up to nominal RPM was performed. This was done by applying an input torque increasing from 0 Nm up to nominal torque. At the HSS a rotational dependent torque was used to simulate the generator torque. The variable time step solver SODASRT 2 was used with a

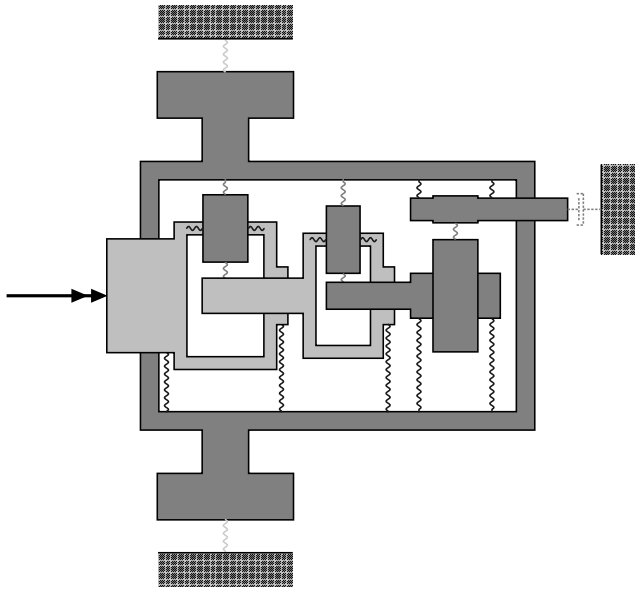

Figure 5.22: Gearbox model used for acoustic simulation.
Legend: bearing, gear force, torque support, high speed shaft rotative damper and input torque.

maximum time step size restriction of 0.00010 s, while output was generated at a sampling frequency of 4 kHz. This time simulation took approximately one day. Figure 5.23 shows some typical MPFs of the gearbox housing. All MPFs corresponding with eigenmodes with an eigenfrequency below 1 kHz were exported to Matlab. Matlab was used to cut the MPFs in 239 blocks of 1 second with 50% overlap. Using an fft with a Hanning window, these time blocks were converted to frequency spectra and exported to universal file format.

The ATVs of the acoustic model described in section 5.4.2 were calculated using the LMS Sysnoise software [160]. Master frequencies were in the range between 20 Hz and 1 kHz, using a frequency step of 15 Hz, resulting in 67 ATVs. This model was solved on a system with a dual Intel Xeon X5650 processor and 60 GB of RAM, and took almost 5 days. A further speedup of this calculation can be achieved by using the multiprocess support to assign different master frequencies to different cores. The ATVs were then converted to MATVs by using the same mode shapes that were used in the CMS reduction of the gearbox housing, and multiplied with the 239 sets of MPF spectra resulting in 239 acoustic solutions

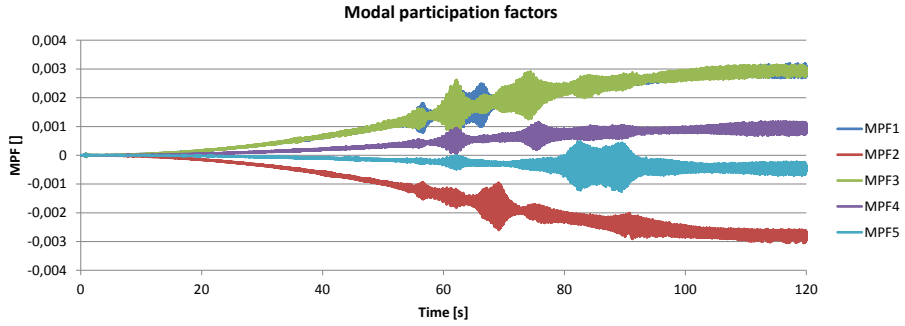

Figure 5.23: Typical modal participation factors of the gearbox housing during the RPM runup.

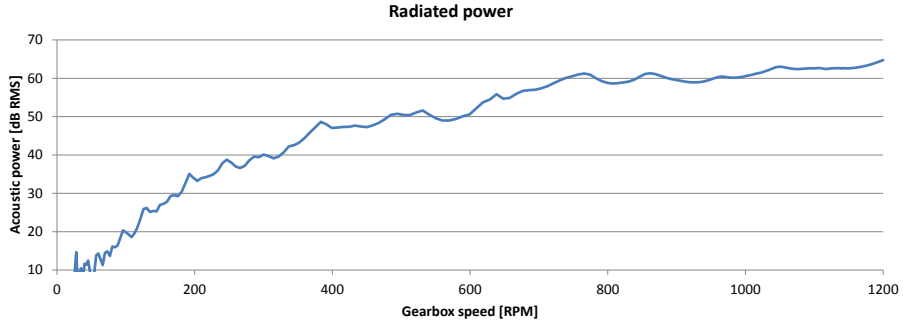

Figure 5.24: Acoustic radiated power versus gearbox speed.

at different RPMs.

Figure 5.24 shows the total sound power emitted at all 239 RPM load cases. The local maxima in this curve are due to structural resonances. Figure 5.25 shows a full Campbell diagram of these 239 RPMs as well as a low frequency zoom. In this low frequency zoom some structural eigenfrequencies can be seen.

Furthermore, during the calculation of the MATVs the radiating surface was subdivided in different panels belonging to the different main components of the gearbox. Figure 5.26 shows the frequency spectrum of the total acoustic power at nominal RPM and the contribution of all different panels. It shows that the high speed housing is contributing the most to the overall sound level,

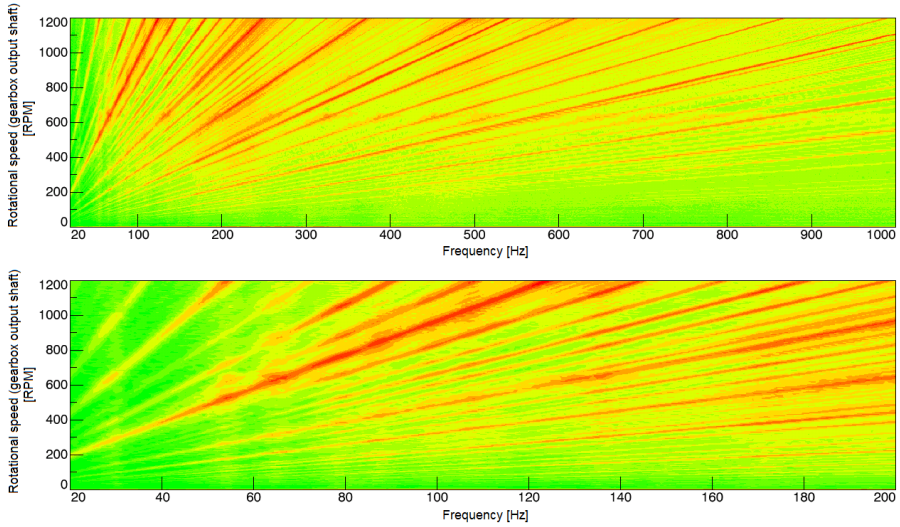

Figure 5.25: Campbell diagram of radiated power during RPM runup.

followed by the torque arm. The largest reduction in the overall level can be achieved when addressing those panels. This could be done by reducing the vibrational velocity of these panels, but also by reducing the radiating surfaces. It furthermore shows the low noise potential for gearboxes without a parallel gear stage (and high speed housing).

5.5 Conclusions

This chapter investigated the dynamic properties of the MB model of the complete gearbox model. To gain additional insight, this investigation was split in two parts firstly looking into the dynamic behaviour of the HSH + MC sub-assembly and secondly looking into the dynamic and acoustic behaviour of the complete gearbox.

A sensitivity study on the sub-assembly containing the HSH, the MC and the internals showed that the flexible housing of the HSH and the MC has the highest impact on the resulting dynamics of this sub-assembly. The impact of the bearing stiffness values is lower and mostly pronounced at the lower

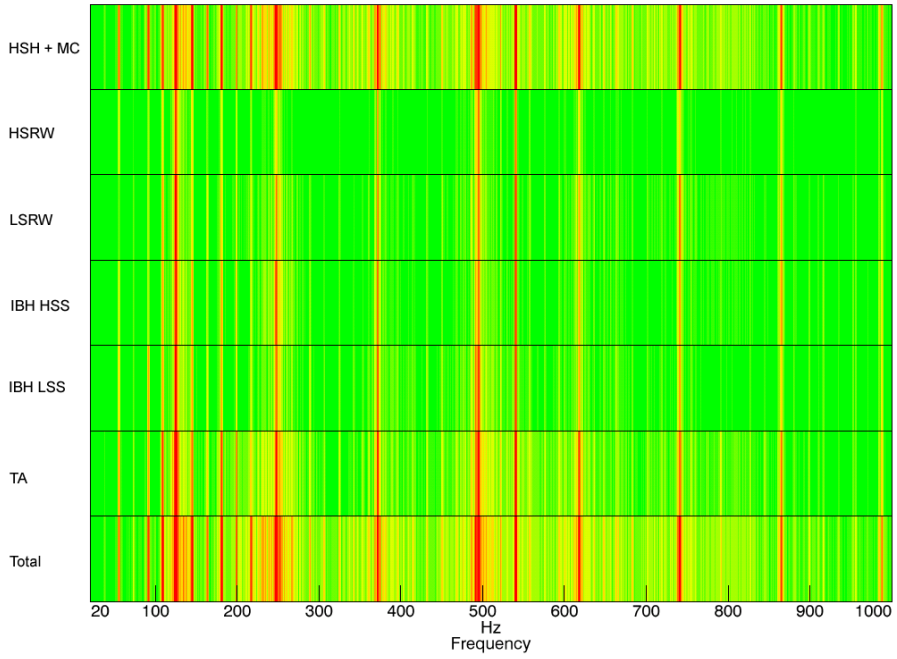

Figure 5.26: Panel contribution analysis at nominal speed.

frequencies, while the impact of the inertia of the HS-IG is almost negligible except for the first eigenfrequency. Very similar results are obtained for the sensitivity study on the complete gearbox housing revealing the highly dominant behaviour of the flexible gearbox housing on almost all eigenfrequencies over the entire frequency range. Bearing stiffness values can be considered as the second most important model parameter, while the effect of the mass of the HS-IG, and the mass and stiffness of the LSS-PC and the ISS-PC on the dynamic behaviour of the gearbox is limited to only a few eigenfrequencies and for all other eigenfrequencies it can almost be considered negligible.

To investigate the impact of the flexible gearbox housing on the modal behaviour of the gearbox in more depth, a sensitivity study modifying the stiffness of the individual components of the flexible gearbox housing was performed. This revealed that both intermediate bearing housings have a dominant role in the low frequent behaviour of the gearbox, while the design of the HSH and MC more dominates the high frequent behaviour of the gearbox. Impact of the TA is in several frequency bands, while the impact of both ring wheels is negligible.

The effect of the actual pre-load setting was investigated in further detail by performing a parameter variation calculation for both the sub-assembly of the HSH and the MC, and the complete gearbox. For the sub-assembly of the HSH and the MC this investigation showed an important dependency of almost all eigenfrequencies on this bearing pre-load which could result in a frequency shift of approximately 15%. Highest impact of the pre-load setting on the eigenfrequencies of this sub-assembly was observed at the low pre-load settings. The effect of the pre-load setting on the complete gearbox housing appeared to be less pronounced affecting fewer eigenfrequencies compared with the sub-assembly. This difference is likely related with the fundamentally different impact of the internals (shafts and planet carriers) and the bearings connecting the internals to the flexible housing on this flexible housing: for the HSH + MC sub-assembly the internals connect both sides of the flexible housing and will therefore have a large impact on the global dynamics of the flexible housing. The internals on the other hand of the complete gearbox housing do not connect both sides of the gearbox housing and can be considered to be mounted more locally resulting in a smaller impact on the global dynamics of the complete gearbox. This effect is also visible when comparing the sensitivity study of the sub-assembly with the sensitivity study of the complete gearbox. Smaller gearboxes such as industrial gearboxes and automotive gearboxes which have shafts connecting both sides of the casting are expected, especially when the utilised bearings are not or only slightly preloaded, to show a similar important dependency on the bearing pre-load.

Changing external loading on the gearbox causes changes in the number of rollers inside the bearings which contact both inner and outer ring. This changing number of rollers in contact has an impact on the resulting bearing stiffness and therefore also influences the resulting eigenfrequencies. By applying torsional and extreme bending loads some global eigenfrequencies shifted with more than 5%. This effect is expected to be most pronounced with large bearings as the external loading influences the bearing stiffness but also affects the stiffening effect of the bearing seat in the flexible supporting structure.

The accuracy and thus also the usability of these models to predict the dynamic behaviour was experimentally validated by performing an EMA on both structures. For both the sub-assembly and the complete gearbox this yielded similar results: a very good correlation between the experimentally identified eigenmodes and the simulated eigenmodes up to 300 Hz, and an acceptable correlation between 300 Hz and 500 Hz. For both models this correlation drops significantly above 500 Hz. Frequency deviations are higher for the sub-assembly

compared with the complete gearbox. This again agrees with the observation that the bearings (which are considered less accurate compared with the flexible housing) play a more important role on the global dynamics in the sub-assembly than in the complete gearbox. Although these results are based on a single gearbox, it is expected that these results can be generalised to wind turbine gearboxes of similar size. For other kinds of gearboxes, a similar approach should be followed to obtain similar insight.

Future measurement campaigns should furthermore consider measuring the dynamic behaviour of the gearbox internals such as the ISS-PC and its planets to gain additional insight on the dynamic behaviour of these internals when assembled in the gearbox.

An acoustic FE model of the flexible gearbox housing illustrated the need for advanced acoustic modelling as the coincidence frequency for this gearbox lies around 800 Hz rendering simplified acoustic methods based on structural FE below this frequency useless. Furthermore it was illustrated that ATVs and MATVs are an efficient way to firstly calculate the acoustic behaviour of the gearbox housing, and secondly to link the structural MB model with the acoustic FE model.

Based on these observations and the observations gathered in Chapter 4 it can be concluded that the flexible gearbox housing plays the most dominant role on the overall gearbox dynamics. Much effort should be spent in generating an accurate FE representation of the flexible gearbox housing as it will have a direct impact on the accuracy of the global gearbox dynamics. When significant modifications to the dynamic behaviour of the complete gearbox are necessary, focus should in most cases be put on altering the flexible gearbox housing rather than the internals. A bearing model capable of taking the non-linear effect of pre-load into account is preferred over using 6×6 stiffness matrices. If only 6×6 stiffness matrices are available, then special emphasis should be put when calculating these stiffness matrices on the actual pre-load setting such that representative stiffness matrices can be generated. It should furthermore be noted that the impact of the bearings becomes more dominant when those bearings are spanning the entire flexible housing, or when utilised in no load or in low pre-load conditions as the actual stiffness might vary significantly in different operating conditions.

Chapter 6

Modelling and experimental validation of two wind turbine gearboxes on the end of line test rig

6.1 Modelling

The test rig contains two gearboxes connected to each other on the low speed shaft side with the so-called low speed coupling, and they are mounted on a welded metal supporting structure (see figure 6.1). The high speed shafts of both gearboxes are connected using a cardan shaft to the motor unit which can either work as a motor or as a generator. More information about the capabilities of this test rig can be found in [63]. It is expected that this supporting structure has a very significant impact on the dynamic behaviour of the gearboxes on the test rig as this supporting structure can be considered quite flexible with its first eigenmodes well below 40 Hz.

Figures 6.1 and 6.2 show both a graphical and a schematical representation of the complete test rig model. It contains two identical gearboxes mounted on the supporting structure. Both the supporting structure and the low speed coupling are CMS reductions of FE models. The gearboxes are connected to the supporting structure using rubber bushings from which a static stiffness is

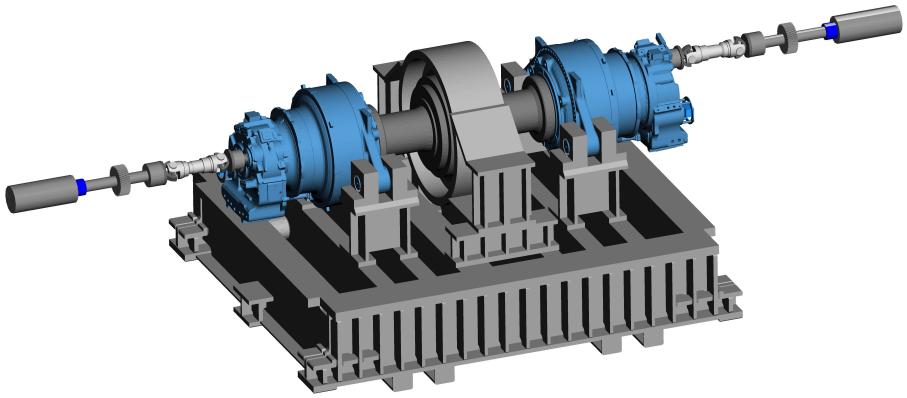

Figure 6.1: Multi body model of the two gearboxes on the test rig

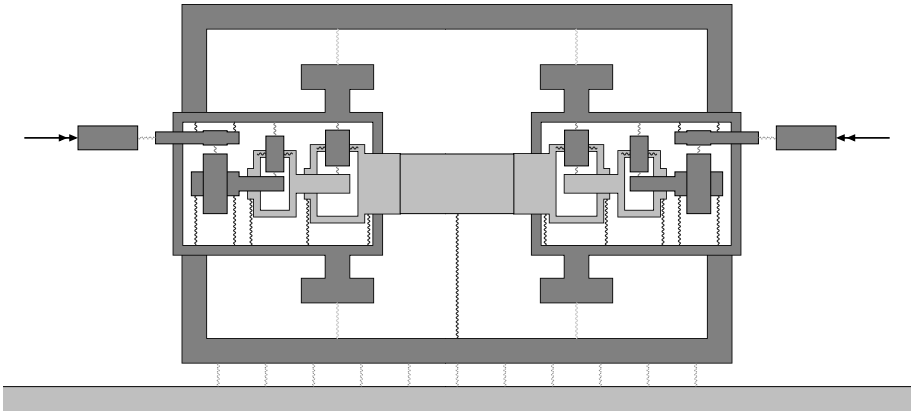

Figure 6.2: Multi body model of the two gearboxes on the test rig - Schematic view.
Legend: bearing, gear force, torque support, other spring and input and output torque.

measured and used. The high speed shafts from both gearboxes are connected using a shrink disk (modelled as a single rigid mass) and a cardan shaft (modelled as a flexible body) to the motor units. Because both gearboxes are connected to the motor units using cardan shafts and focus is on the two gearboxes, these motor units are modelled using only rotational DOFs.

6.1.1 Impact of the flexible supporting structure on the global dynamics

Dynamically the supporting structure can be considered quite flexible as it has its first free-free eigenfrequency well below 40 Hz. Static stiffness on the torque arm connection points on other hand is strongly direction dependent: both horizontal directions have a quite low stiffness (in the range of $10^8 \frac{N}{m}$), while the vertical direction has a high static stiffness (in the range of $10^{10} \frac{N}{m}$). When comparing these static stiffness values with the stiffness values of the rubber bushings, the test rig can be considered stiff in both axial and vertical direction, but very flexible in the lateral direction.

To assess the impact of this flexible supporting structure on the dynamic behaviour of the gearbox, eigenmodes of the test rig model utilising a flexible supporting structure are compared with the eigenmodes of the test rig model utilising a rigid supporting structure. The model with the rigid supporting structure is used as the reference model such that local eigenmodes of the supporting structure do not have an impact on the results. Based on these results (listed in table 6.1), it can be concluded that the flexible supporting structure has a significant impact on the dynamic behaviour of the test rig model, especially in the lower frequency range where next to the limited correlation also the highest frequency shifts occur.

6.1.2 Impact of load on the global dynamics

The change in stiffness between gears in contact or out of contact is the largest non-linearity in this model. To quantify this non-linearity a MAC is calculated between a loaded model and an unloaded model. Table 6.2 summarises the results. These results show the huge impact of the gear contact stiffness in all frequency bands on the dynamic behaviour of the gearbox on the test rig. The eigenmodes in the lowest frequency band (typically the rigid body motion of the gearbox in the test rig) seem to be less affected by the gear contact stiffness compared with eigenmodes in higher frequency bands as the number of correlated eigenmodes is often more than twice the number of correlated eigenmodes compared with other frequency bands. From these results it can be concluded that in order to accurately experimentally characterise the test rig by means of an EMA for instance, the test rig should be loaded.

Table 6.1: Impact of flexibility of supporting structure on global dynamics

Frequency band [Hz]	Number of matched modes	Average absolute relative frequency difference
0 - 100	61%	9.4%
100 - 200	72%	0.8%
200 - 300	65%	0.5%
300 - 400	69%	0.5%
400 - 500	72%	0.4%
500 - 600	70%	0.2%
600 - 700	93%	0.1%
700 - 800	66%	0.2%
800 - 900	87%	0.1%
900 - 1000	93%	0.2%

6.1.3 Sensitivity study

Similarly with the model of the complete gearbox, a sensitivity study is performed to investigate which model parameter dominates the modal behaviour of the test rig model. Similar with previous sensitivity studies, the sensitivities are weighted such that comparison becomes possible. Following sensitivities are calculated: gear stiffness (upper bound: 25%), supporting structure stiffness (upper bound: 50%), torque arm bushing stiffness (upper bound: 100%), low speed coupling stiffness (upper bound: 50%). Figure 6.3 shows the results.

From these results it can easily be deduced that the test rig has a huge impact on the global dynamics of the gearbox on the test rig: parameters linked to the test rig such as the supporting structure and low speed coupling have a significantly higher impact on global dynamics compared with e.g. the gear stiffness or the torque arm bushing stiffness. Based on these findings it can be stated that using the results from the test rig validation campaign to further validate the gearbox model is not straightforward as the test rig parameters,

Table 6.2: Impact of load on global dynamics

Frequency band [Hz]	Number of matched modes	Average absolute relative frequency difference
0 - 100	72%	1.3%
100 - 200	58%	0.9%
200 - 300	29%	0.5%
300 - 400	13%	0.4%
400 - 500	38%	1.4%
500 - 600	33%	0.4%
600 - 700	40%	0.3%
700 - 800	57%	0.2%
800 - 900	49%	0.1%
900 - 1000	65%	0.1%

the parameters with the highest uncertainty[1], also have the highest impact on global dynamics of the gearbox on the test rig over the entire frequency range of interest.

6.2 Measurements

As part of the ALARM project, an elaborate measurement campaign was set up:

1. to dynamically characterise the dynamic behaviour of the gearbox on the EOL test rig; and

[1]No parts of the test rig are individually validated, also the supporting structure-ground clamping stiffness is highly uncertain.

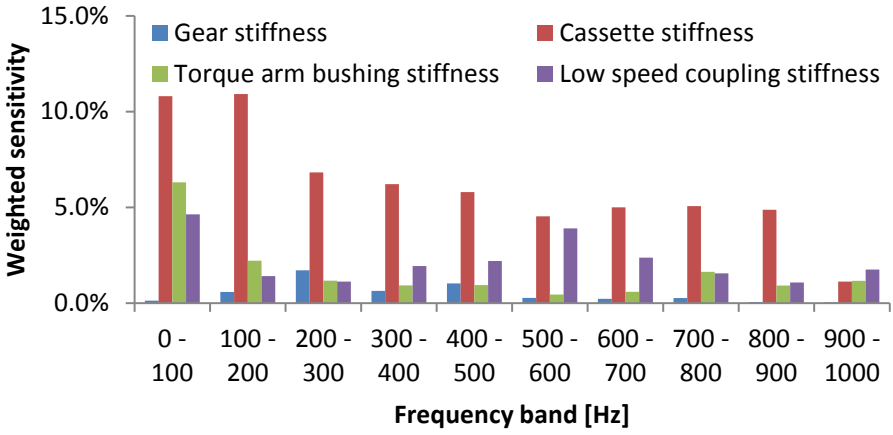

Figure 6.3: Weighted sensitivities for EOL test rig.

2. to try different methods and identify the method most capable of extracting the eigenfrequencies and eigenmodes of the gearbox, in loaded conditions on the EOL test rig. [2]

During these measurements, accelerations were measured in more than 250 points in 3 directions in multiple operating conditions. Accelerometers were placed on both gearboxes (with a strong focus on one of them: see left gearbox in figure 6.4) and on the test rig. Additionally two inertia shakers are mounted on the tested gearbox to insert a known input force into the test rig setup. Measurements were performed using a large LMS SCADAS III digital acquisition system and were analysed using the LMS Test.Lab software. Figure 6.4 shows an impression of this large measurement campaign.

Taking the additional difficulties of an operating gearbox into account, several processing techniques are tested:

1. operational deflection shapes (ODS) during steady state conditions;
2. operational deflection shapes (ODS) during a speed run-up;

[2]Note that this aspect of the ALARM project is not in the scope of this dissertation. More information on this aspect of the ALARM project: these measurements, the analysis of these measurements and the correlation between these different analysis methods can be found in [25, 23, 22, 24] and future work of these authors.

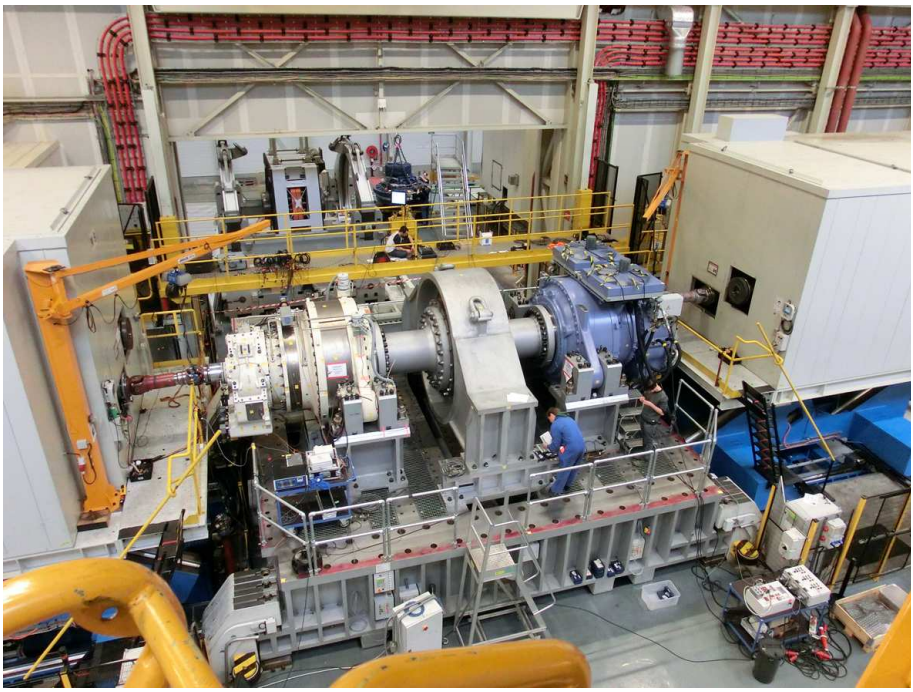

Figure 6.4: Measurement setup for the complete gearbox on the test rig

3. EMA using two inertia shakers on an unloaded test rig setup;
4. operational modal analysis (OMA) during a constant speed condition;
5. operational modal analysis (OMAX) during a constant speed condition with additional excitation input from the two inertia shakers; and
6. order based OMA during a speed run-up.

However, at the time of writing this dissertation, only the mode set obtained by using the two inertia shakers on the unloaded test rig setup was finished limiting the correlation between experiments and model to unloaded condition.

6.3 Correlation

A good correlation was found between the test rig (EMA, unloaded conditions) and the unloaded model up to approximately 150 Hz. Above this frequency the

correlation significantly decreased. Multiple possible reasons for this lower level of correlation exist:

- the flexible model of the supporting structure, the low speed shaft coupling and the connection stiffness between ground and flexible supporting structure are not validated and furthermore have a high impact on the modal behaviour of the complete assembly;
- the EMA measurements were performed in several runs and results were recombined afterwards using a reference signal. Quality of the extracted eigenmodes depends heavily on the used reference signal; and
- the eigenmodes at the test rig were extracted at standstill and unloaded conditions, it is therefore impossible to know which gears were in contact and which gears were not; furthermore, these conditions (in contact or out of contact) might have changed due to operational measurements in between the different EMA runs.

No further model updating steps were undertaken to improve the quality of this correlation because the parameters with the highest uncertainty are also the parameters with the highest impact on the model. Further model updating would not result in a more reliable gearbox model as multiple solutions with an increased correlation are possible. To significantly increase correlation between measurements and the test rig model, effort should be put in gaining more insight in the dynamic behaviour of the empty test rig (without any gearboxes mounted) by experimentally validating the empty test rig setup.

6.4 Conclusions

This chapter investigated the dynamic properties of two gearboxes mounted on the EOL test rig by developing and experimentally validating an MB model of this setup.

A first analysis showed the huge impact of the flexibility of the supporting structure on the global dynamics of the entire test rig. This flexible structure caused a large change in approximately 30% of the eigenmodes such that these eigenmodes could not be found back in the model with the flexible supporting structure. Furthermore this additional flexibility also results in frequency deviations, mainly in the lower frequency band between 0 and 100 Hz.

A second analysis investigated the impact of switching on or off the gear contact on the resulting eigenmodes. From these results it can be concluded that the difference between a loaded and an unloaded test rig is of such an order of magnitude that calculating eigenmodes from the test rig model or performing an EMA on the test rig in unloaded conditions is not representative for the dynamic behaviour of the gearbox on the test rig during normal operating conditions.

A sensitivity study showed the huge impact of the stiffness of the supporting structure and the low speed coupling compared with the stiffness of the torque arm bushings and the gear contacts.

An extensive measurement campaign was setup to dynamically characterise the dynamic behaviour of the gearbox on the test rig. A correlation between the experimentally identified eigenmodes using shaker excitation at standstill and unloaded conditions (this is currently the only mode set which is available) is of lower quality compared with the other experimental validation cases. This could be due to high uncertainty and huge impact of the test rig parameters, the uncertain condition of the gear contacts, and some issues with the EMA measurements. To gain additional insight in the dynamic behaviour of the gearbox on the test rig, and to be able to predict the dynamic behaviour of the gearbox on the test rig, effort should be put in on the one hand in the model by increasing the accuracy of the predicted eigenmodes by experimentally validating the empty test rig setup; and on the other hand effort should be put in methods capable of accurately identifying the modal parameters of the test rig setup in loaded operating conditions.

The lower correlation results however only have a small impact on the research objectives as the dynamic behaviour of the gearbox in the test rig environment is of much lower importance than the dynamic behaviour of the gearbox in the wind turbine environment. It furthermore highlights the need for a close cooperation between wind turbine manufacturer and wind turbine gearbox manufacturer as similarly with the test rig, the mainframe of the wind turbine will have a huge impact on the resulting eigenmodes.

Chapter 7

Virtual prototyping methodology to pro-actively avoid tonal wind turbine noise

The recent insights in the expected climate changes emphasise the need for energy sources with low- or zero-carbon emission. Renewable energy, and wind energy in particular is such a technology. As a consequence of this, more and more wind turbines are put up, not only in remote areas, but also within the vicinity of urban zones, and care should be taken that those newly installed wind turbines do not cause additional nuisance for the closely living habitants. Audible wind turbine mechanical tonalities cause annoyance and should be avoided. Regulations could oblige the wind turbine operator to shut down his wind turbine during the night and possibly also during the evening, to run the wind turbine in a suboptimal operating condition, or even to shut down the wind turbine completely, resulting in a very significant financial loss. Furthermore, the cost of troubleshooting and modifying a wind turbine or any of its components cannot be neglected. Therefore, mechanical tonalities should be avoided during the design phase of a wind turbine, reducing the risk of suboptimal usage resulting in a reduced energy yield, and removing the need for costly troubleshooting activities. This chapter discusses the virtual prototyping methodology that can be used to pro-actively avoid these mechanical tonalities.

7.1 Modelling method

Chapters 4, 5 and 6 investigated how the dynamic behaviour of a wind turbine gearbox can be predicted with acceptable accuracy. The numerous sensitivity studies and parameter variation cases revealed a huge dependency of the dynamic behaviour of the wind turbine gearbox on the design of its components, the manner how everything is pre-loaded, and its boundary conditions. These observations have two important implications:

1. A physical model based approach, requiring a lot of drive train details to be included in this model, will absolutely be necessary to obtain an accurate tonality prediction. Approaches, based on easy to use guidelines, will not be able to grasp the full complexity of the problem at hand.
2. This physical model based approach should cover the complete wind turbine drive train and its radiating surfaces. In most cases the resonances, that cause the mechanical tonalities, are drive train eigenmodes, influenced by the complete drive train, and not eigenmodes dominated by only one component such as the wind turbine gearbox. Attempts to analyse or to predict these eigenmodes should therefore focus on the entire drive train and not only on a subcomponent of it.

This section describes this virtual prototyping model necessary to predict mechanical tonalities.

7.1.1 Mechanical noise sources

Typically mechanical tonalities are excited by gear excitation, generator excitation (electric excitation) and excitation from auxiliaries. This dissertation focuses on mechanical tonalities excited by gear excitation originating from the gearbox, but excitation forces originating from other components could be included in a similar way.

One option is to include the physical phenomena lying at the origin of these gear excitation forces in the model. This is however not advisable as these noise mechanisms rely on very specific contact physics which are beyond the scope of this vibro-acoustic model. Instead, dedicated models should be utilised to predict these excitation forces which should then be used as input for this vibro-acoustic model.

7.1.2 Mechanical transfer paths

This part consists of the mechanical modelling of the drive train, and the surrounding structures that influence the dynamic behaviour of the drive train.

Mainframe

Similar to the supporting structure of the EOL test rig, the mainframe has a huge impact on the resulting dynamics of the entire drive train. Eigenmodes of this mainframe occur in the frequency range where the second gear stage is exciting. This mainframe should therefore be modelled as a flexible component. Furthermore, an EMA on this structure is advisable as this structure probably has a huge impact on the resulting accuracy of the wind turbine drive train model. Heavy components which do not introduce any additional stiffness into the mainframe, such as e.g. electrical cabinets, should be included in this model as single point inertias.

Mainshaft and main bearing(s)

Also the mainshaft and the main bearing(s) should be modelled and included in the mechanical model of the drive train. The mainshaft should be made flexible as it affects the bending modes of the drive train. An accurate estimation of the bearing stiffness should also be included, taking possible bearing pre-load or bearing clearance into account. Furthermore, an investigation should be performed if the resulting bearing forces can be introduced in a single point into the mainframe, or if a roller based approach should be utilised to correctly introduce these forces.

Gearbox

Chapters 4 and 5 discuss the required model in detail. Conclusions from these chapters lead to following summary:

- The gearbox housing has the highest impact on the resulting dynamics of the complete gearbox. Experimental validation on this wind turbine gearbox shows that the FE model of this gearbox housing can be considered to be accurate up to the frequency were the gearbox housing starts to show local deformation at the HSH and MC (approximately 400 Hz in this case). When accuracy is needed at higher frequencies, focus should

be on the models of the HSH and MC which have the most complex geometry resulting in the components of the gearbox housing with the highest uncertainty.

- Full bearing stiffness matrices are necessary that couple all DOFs. Ideally, a non-linear bearing model should be utilised such that the impact of the operating condition, including bearing pre-load, is automatically taken into account. If this is not available, 6×6 stiffness matrices should be generated taking operating conditions, bearing pre-load and gravity into account. Furthermore, the way that the bearing force is introduced into the flexible housing can affect the global eigenmodes, especially with large bearings. If accurate pro-active predictions are necessary, a roller based bearing model should be used which captures this effect.

- Constant gears stiffness values should be included. Gear excitation mechanisms however, can be omitted if these gear excitation forces are externally calculated, and introduced in this model. If the direct acoustic radiation of the gearbox housing is considered in the vibro-acoustic model, then special care should be taken to correctly introduce the planet-ring wheel gear forces. The common simplification to introduce these gear excitation forces at the centre of the ring gear instead of at each individual mesh between a planet and the ring gear results in inaccurate vibration velocity levels of the gearbox housing, required to assess the direct acoustic radiation.

- Shafts and planet carriers should be modelled flexible if they deform in the frequency range of interest.

Correlation of the model built in Chapters 4 and 5 with experimentally obtained eigenmodes shows very good correlation up to 300 Hz, and an acceptable correlation between 300 Hz and 500 Hz. Above 500 Hz this correlation drops significantly. Much effort should be spent in generating an accurate FE representation of the flexible gearbox housing as it will have a direct impact on the accuracy of the global gearbox dynamics. Experimental validation could be considered to further increase the accuracy of this model. When interested in higher accuracy in the lower frequency bands, up to $\approx$ 200 Hz, an EMA on the complete assembled gearbox is advised, as the inaccuracy of the bearings is considered higher than the inaccuracy of the gearbox housing in this frequency region. At higher frequencies, an additional EMA on the complete empty gearbox housing if possible, or on the HSH and the MC is advisable. Preferably multiple EMAs should be undertaken to assess the variance of this model.

Hub and blades

The hub and blades should definitely be included in the mechanical drive train model. It is however unsure up to which extent they should be included: this may go from one equivalent mass matrix up to flexible modelling of both hub and blades. A sensitivity study should be performed to investigate the impact of this choice on the resulting dynamic behaviour of the drive train. Furthermore, because the blades are also radiating the mechanical noise, the impact of this choice should also be assessed on the force excitation input into the hub.

Tower

Unlike the hub and blades, it is not known if the tower significantly affects the drive train behaviour. This should be investigated, and if not, it may be omitted in the mechanical drive train model. An (uncoupled) model of the tower however remains required to calculate the resulting vibration amplitudes as input for the radiation calculation of the tower.

Nacelle cover

The nacelle cover, typically a composite structure, is quite flexible and is probably not capable of significantly affecting the drive train behaviour. Only inertia and static stiffness should be taken into account in the drive train model. Similar to the tower, a model of the nacelle cover remains required to calculate the resulting vibration amplitudes as input for the radiation calculations.

7.1.3 Acoustic radiation

The vibrations on the entire wind turbine radiate noise to the surrounding. However due to their size only the tower, the nacelle cover and the blades are taken into account. This requires an acoustic model of these components. Using the approach described in section 5.4.3, the results from the mechanical drive train model can be linked with the acoustic radiation model. Further research should be performed to investigate which kind of acoustic model or approximation best serves this purpose.

Next to these external components, also the noise which is radiated directly from the gearbox housing may be taken into account if the gearbox airborne transfer path is of interest. This however requires much more effort as a coupled

acoustic simulation is required to take the insulation behaviour of the nacelle cover properly into account.

7.2 Required analysis

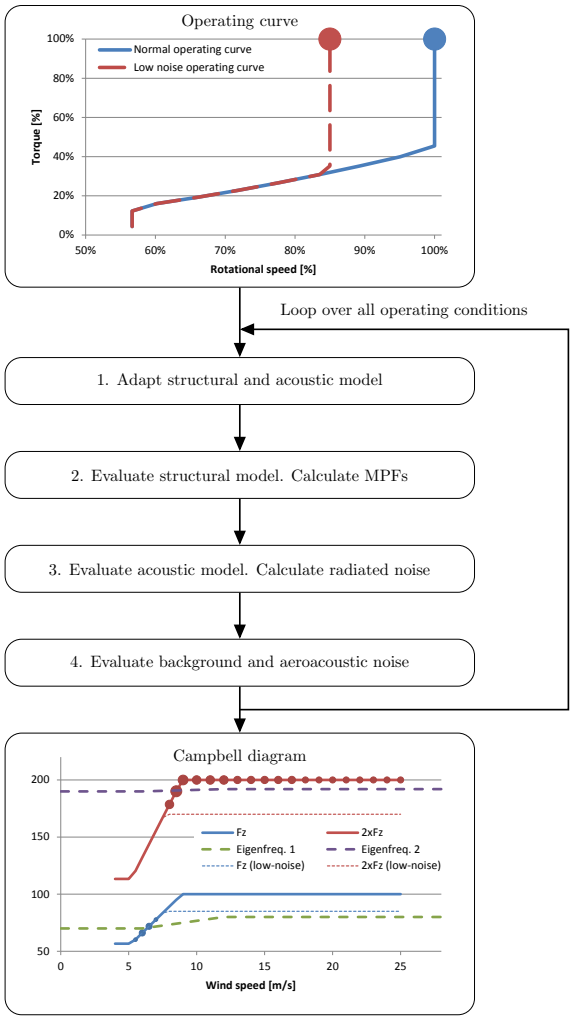

Figure 7.1: Tonality calculation methodology.

This section describes the approach to use this virtual prototyping model to assess the mechanical tonalities of the wind turbine. It consists of a loop with 4 steps, and 1 post-processing step afterwards (see figure 7.1):

Loop over all operating points of interest in the operating range of the wind turbine, preferably as a function of wind speed (see figure 2.7), including the low-noise mode. This loop contains following steps:

1. Firstly, both the structural and the acoustic model should be adapted to the current operating condition. This implies:
    - applying the correct load on the structural model which has an impact on e.g. bearing stiffness values;
    - computing the correct TE for each gear pair based on the current load and speed; and
    - setting the blade pitch angle in the acoustic model in the correct position.
2. Secondly, the mechanical model of the drive train should be evaluated. Preferably, this is done in the frequency domain by calculating for each gear pair TE-FRFs from this gear pair, towards the MPFs of the radiating components of the wind turbine (gearbox housing, tower, blades and nacelle cover). Each TE-FRFs should be multiplied with its corresponding TE spectrum to obtain the resulting MPFs. Note that because each TE spectrum only has significant components at its gear excitation frequencies, this multiplication should only be performed at those specific gear excitation frequencies. If a radiating component is not included in the mechanical model of the drive train (such as the nacelle cover), the interconnection forces should be calculated. Using these interconnection forces, the MPFs of these radiating components can be calculated using an FE model.
3. In this third step, the radiated noise is calculated. Each MPF should be multiplied with its corresponding MATVs to obtain an acoustic spectrum of the radiated noise originating from a certain gear pair. Again, this multiplication should only be performed at the gear mesh frequencies.
4. Lastly, an assessment should be made of the aeroacoustic noise produced by the wind turbine at this current operating condition. The radiated noise, originating from each gear pair, at is specific gear excitation frequencies, should be added to this, resulting in a total wind turbine noise spectrum.

In this final post-processing step, all wind turbine noise spectra should be analysed according to the IEC61400-11 [74]. Results from this analysis are

plotted in a Campbell diagram giving a complete overview of the tonal behaviour of the wind turbine. Figure 7.2 shows such a possible Campbell diagram. In this diagram the first and second order are plotted (Fz and 2×Fz) for the second gear stage. Both excitation orders cross an eigenmode (Eigenfreq. 1 and Eigenfreq. 2 respectively). The audibility of the tonality is indicated by the size of the dots. This results in two audible tonalities:

1. The first tonality occurs around 6 m/s, and disappears at higher wind speeds due to the changing rotational speed of the wind turbine. The eigenfreqeuncy of this eigenmode increases slightly due to the increasing load. In this case it should be investigated if the eigenfrequency can be shifted to a lower frequency such that it occurs out of the nominal operating range of the wind turbine. Shifting this eigenfrequency to higher frequencies will probably result in a tonality at higher wind speeds (if the masking noise at these higher wind speeds does not cover the mechanical tonality). Furthermore note that putting this turbine in low-noise mode (thin dashed lines in figure 7.2) results in tonal behaviour.

2. The second tonality occurs a bit before nominal rotational speed and at nominal rotational speed, resulting in an audible tone from around 8 m/s up to 25 m/s. Ideally, it this eigenfrequency should be shifted upwards to higher wind speeds (and thus more masking noise), or even higher, completely out of the nominal operating range. Putting this turbine in low-noise mode also removes this tone.

If however, no acoustic models are available, then two other possibilities exist to assess whether or not a resonance could become a tonality. Again using the structural model, eigenfrequencies should be calculated at all operating conditions, and should be put in a Campbell diagram together with the main excitation frequencies similar to figure 7.2 to detect the possible resonances. To assess if a resonance could become a mechanical tonality:

- resulting vibration values at blades, tower and nacelle can be used together with experience from previous tonalities to assess if this resonance may become a tonality; or
- based on experience, from previous troubleshooting, the particular eigenmode can be recognised, and considered as a potential risk to cause a mechanical tonality.

Either way, once the possible tonalities are identified, sensitivity studies should be performed:

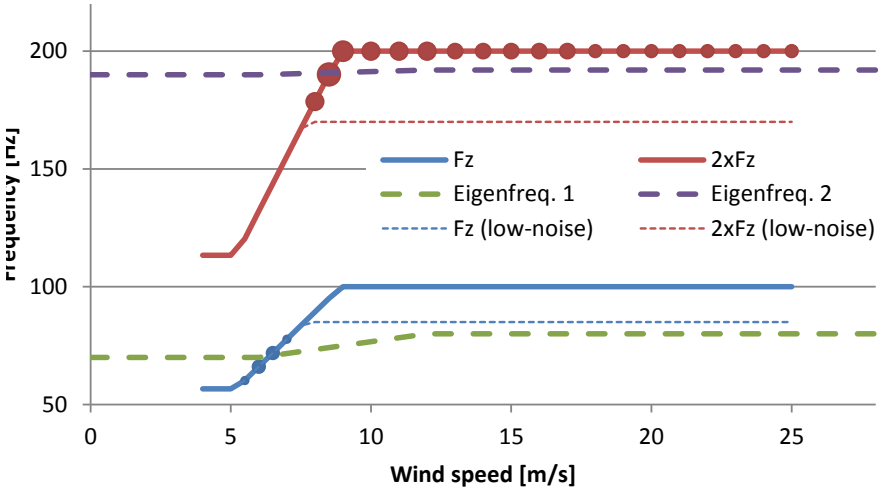

Figure 7.2: Campbell diagram indicating two possible tonalities.

- to try to remove the resonance out of the operating range of the wind turbine; or
- to try to uncouple the excitation forces, which originate from the resonance in the mechanical drive train, from the radiating surfaces, which may e.g. be achieved by modifying the rubber mounts between the mainframe and the nacelle cover.

7.3 Conclusions

This chapter described the virtual prototyping methodology to pro-actively predict tonal wind turbine noise. Firstly, based on the experience gained in previous chapters, the minimum model requirements necessary to accurately capture the mechanical resonances were discussed, as well as the requirements for the the acoustic model, necessary to calculate the resulting tonal levels. Secondly, the analysis strategy, necessary to obtain a tonality assessment in the complete operating range of the wind turbine was discussed, and a fictional example was given.

Chapter 8

Optimisation cases

This chapter uses the modelling approach proposed and validated in chapters 4, 5 and 6 to investigate possible design modifications on the gearbox to modify its dynamic behaviour. These cases are purely exemplary as only the wind turbine gearbox was taken into account. First optimisation looks at the effect of the individual bearings on the transmitted vibration amplitudes; the second optimisation modifies a wind turbine gearbox housing to shift a harmful resonance.

8.1 Optimisation case 1: Impact of bearings on the resulting wind turbine gearbox vibration amplitudes

This optimisation case focusses on the impact of bearings on the resulting gearbox vibration amplitudes. Firstly classical transfer path analysis (TPA) is used to investigate how the vibrations are transmitted through the individual bearings: does one bearing transmit more vibrations than another bearing? Secondly the effect of modifications (such as stiffness and damping, bearing positioning and bearing support stiffness) of individual bearings on the resulting vibration amplitudes are investigated and evaluated.

8.1.1 Using transfer path analysis to gain insight in the transmission of gear excitation through the different bearing positions

TPA is a collection of methods which are mainly used in the automotive industry to investigate how vibrations are transferred from source to receiver. Many variants of this technique exist. The choice of method mainly depends on which experimental data is at hand. In general all these methods separate the active parts (in automotive the engine, gearbox e.g.) from the passive part (in automotive the car body), and quantify how the vibrations are transmitted from the active parts to a receiver in the passive part (acceleration or pressure) [6, 35]. The locations where the active part connects with the passive part are called the interface locations and the functions which describe the relation between force input on an interface location to a receiver are called the transfer paths.

In the case of a coherent active part, the resulting accelerations in measurement point t, $\boldsymbol{a_{t_X}}$, $\boldsymbol{a_{t_Y}}$ and $\boldsymbol{a_{t_Z}}$ are calculated by summing all individual contributions to measurement point t. These individual contributions are calculated by multiplying the transfer paths $\boldsymbol{P_{t,i}}$ from interface i to measurement point t with the loads $\boldsymbol{F_i}$ (3 forces & 3 moments) acting on the interface point i:

$$\boldsymbol{a_t}(\omega) = \sum_{i=1}^{n} \boldsymbol{P_{t,i}}(\omega).\boldsymbol{F_i}(\omega) \tag{8.1}$$

with:

$$\boldsymbol{a_t}(\omega) = \begin{bmatrix} a_{t_X}(\omega) \\ a_{t_Y}(\omega) \\ a_{t_Z}(\omega) \end{bmatrix}$$

n = number of interfaces

$$\boldsymbol{P_{t,i}}(\omega) = \begin{bmatrix} TP_{t_X,i_X}(\omega) & TP_{t_X,i_Y}(\omega) & \dots & TP_{t_X,i_\beta}(\omega) & TP_{t_X,i_\gamma}(\omega) \\ TP_{t_Y,i_X}(\omega) & TP_{t_Y,i_Y}(\omega) & \dots & TP_{t_Y,i_\beta}(\omega) & TP_{t_Y,i_\gamma}(\omega) \\ TP_{t_Z,i_X}(\omega) & TP_{t_Z,i_Y}(\omega) & \dots & TP_{t_Z,i_\beta}(\omega) & TP_{t_Z,i_\gamma}(\omega) \end{bmatrix}$$

$$\boldsymbol{F_i}(\omega) = \begin{bmatrix} F_{i_X}(\omega) \\ F_{i_Y}(\omega) \\ F_{i_Z}(\omega) \\ F_{i_\alpha}(\omega) \\ F_{i_\beta}(\omega) \\ F_{i_\gamma}(\omega) \end{bmatrix}$$

These transfer paths can be obtained by measuring the FRFs from interface i to measurement point t with the active part removed. In total $3 \times 6 \times n$ FRFs should be measured for each measurement point. Figure 8.1 illustrates this approach using two interface locations ($i1$ and $i2$), and one measurement point ($t1$). During an operational measurement the forces F1 and F2 should be measured (left side of figure 8.1). Secondly, when the active parts are removed, the transfer paths from the interface points to the measurement point should be acquired (right side of figure 8.1). The individual contribution of each transfer path can then be assessed by multiplying the transfer paths with the forces.

Commonly the gearbox is considered as the active part. Similarly the described methodology can also be applied to the components of the gearbox. The rotating parts, (gears, shafts and planet carriers) which are considered as the active parts, transfer their vibrations through the bearings and ring wheels to the receivers. In this way, the individual contribution of the vibrations, originating from a gear pair, through each bearing on a receiver (accelerometer, total noise) can be investigated. This shows which bearing transmits the most vibrations from the gear to the outside world, and probably also which bearing (or bearing position) has most effect on reducing the noise.

Although TPA methods are widely used on a physical test set-up, they can also be used to gain additional insights in the MB model. In contrast with the use of TPA on a physical test set-up, the acquisition of all the structural FRFs and operational forces (even the rotational FRFs and the moments) is quite an easy

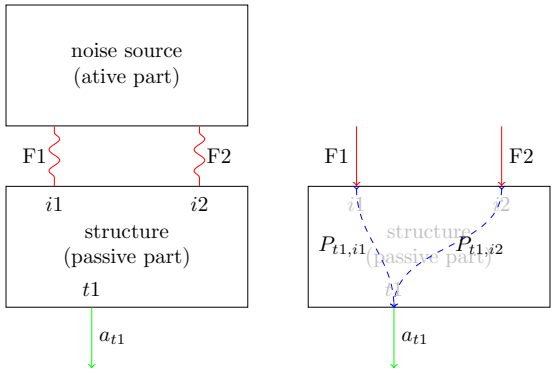

Figure 8.1: TPA measurement approach.

and straightforward job on an MB model.

Figure 8.2 shows a graphical representation of the internals of the gearbox. The hatched zones indicate the interface locations of the different transfer paths from the active zone (rotating parts) to the passive part (housing). These interface locations include both ring wheels and all bearings except the planet bearings. The bearing called intermediate speed stage planet carrier bearing, generator side (ISS-PC-GS) contains two physically separate bearings in a set. In the simulation model however they are considered as one bearing: one 6×6 stiffness matrix or one stiffness map. The virtual accelerometers are used as receiver points.

Following data are obtained by simulation:

- FRFs from the interface locations to the accelerometer positions. In total 1620 FRFs are calculated: 9 interface locations $\times$ 6 force components per interface location $\times$ 10 accelerometer positions $\times$ 3 directions per accelerometer position. For this FRF calculation all the active parts are removed.
- Forces (in 6 directions) in all the interface locations.
- Accelerations (in 3 directions) at all accelerometer locations.

Only results from the high speed mesh are reported. Similar analyses as those reported here can be performed on other gear meshes. All analyses were

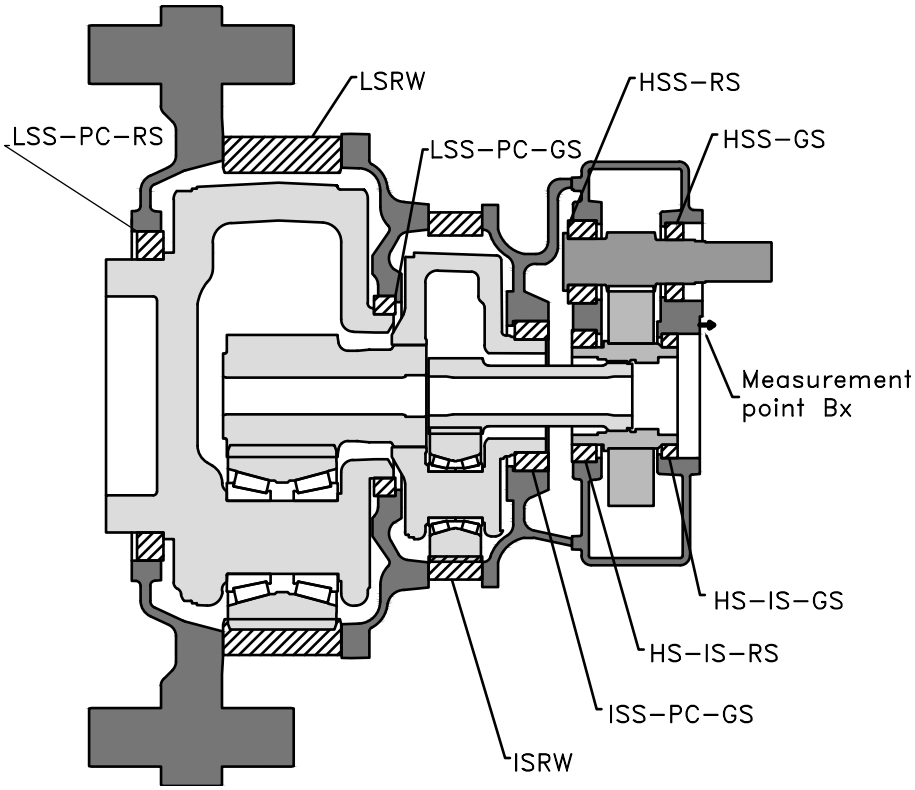

Figure 8.2: Sectional drawing of the wind turbine gearbox. Hatched zones are TPA interface locations.

performed at nominal speed which results in a high speed mesh frequency around 500 Hz. Figure 8.3 shows the acceleration spectrum at measurement point B in X direction (shown in figure 8.2). This measurement point has the highest vibrations at the high speed mesh frequency compared with the other measurement points. This is plausible because it is mounted very close to the HS-IS-GS and HSS-GS bearings which support the high speed gears. Figure 8.4 is a typical result of this TPA. At each frequency for all receiver locations such a figure can be made. Each path is graphically represented by an arrow indicating amplitude and phase. All these individual paths are summed in a vectorial way to obtain the total vibration amplitude (see equation 8.1). It shows how the gear excitation propagates through all bearing locations (amplitude and phase) in all directions (X, Y, Z, α, β, γ) to the receiver location. Figure 8.5 shows the same result, but with all directions of each transfer path combined. Both

figures reveal a large contribution of the high speed gear mesh excitation on the total amplitude through the bearings of the HS-IS shaft. This implies that for this gearbox, attempts to reduce the vibration levels at the high speed gear mesh frequency in measurement point B should focus on those bearings.

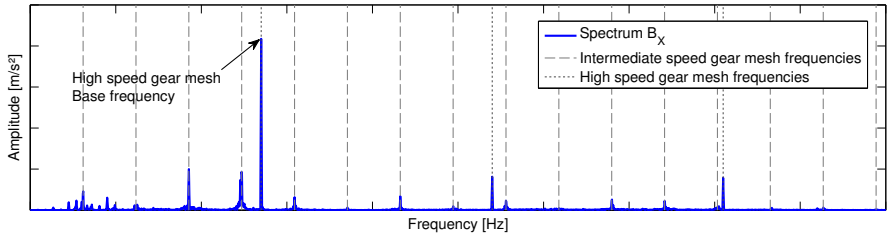

Figure 8.3: Simulated acceleration spectrum at measurement point B, X direction.

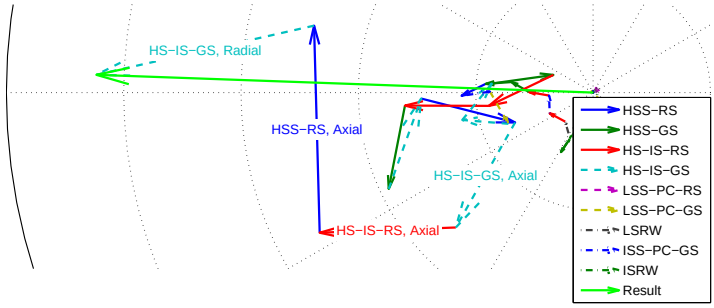

Figure 8.4: TPA vector contribution plot at measurement point B, X direction at high speed gear mesh frequency.

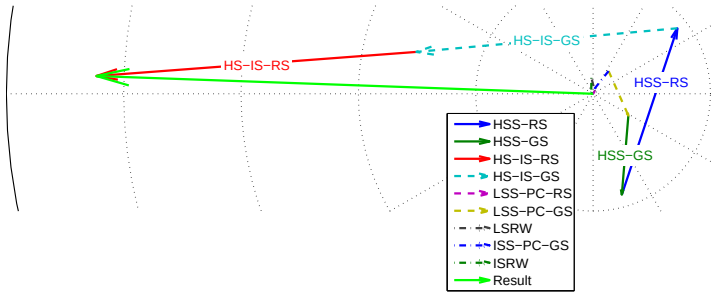

Figure 8.5: TPA vector contribution plot at measurement point B, X direction at high speed gear mesh frequency. Combined result.

8.1.2 Effect of bearing stiffness & damping values on the transmission of gear excitation

The impact of the bearing selection on the transmitted gear noise is investigated by:

1. changing the individual bearing stiffness values,
2. changing the surrounding structure that supports the bearing, and
3. changing the bearing damping.

Bearing stiffness variations Several parameters determine the stiffness values of a bearing, most of them are design parameters such as dimensions, number of rollers, contact angle, but also operating parameters such as load and pre-stress affect the resulting stiffness values. Both analytical (such as parameter variations on contact angle in section 4.4.1) and numerical (directly on the individual stiffness values) parameter variations can be used. In this optimisation case, a numerical parameter sensitivity analysis is performed on the stiffness values of the bearings to investigate their impact on the resulting vibration values. As a general remark it should be noted that this investigation is purely theoretical

and that bearings and their properties are mainly selected based on required bearing lifetime and not on noise and vibration characteristics.

It is expected that the results of the numerical sensitivity study are in agreement with the presented TPA analysis results. In this analysis constant 6×6 stiffness matrices are used and their stiffness values are subdivided in 4 categories:

1. axial stiffness,
2. radial stiffness,
3. rotational stiffness, and
4. off-diagonal terms.

For each bearing of the parallel gear stage (HS-IS-RS, HS-IS-RS, HSS-RS and HSS-GS) these bearing stiffness values are modified in a range of -50% to +50% to investigate the impact on the total resulting vibrations. Figures 8.6 and 8.7 show the resulting change in absolute vibration values at the high speed gear mesh frequency in measurement point B_x by a change in stiffness values for bearing HS-IS-RS and HS-IS-GS. Based on the results of all simulations, following conclusions can be made:

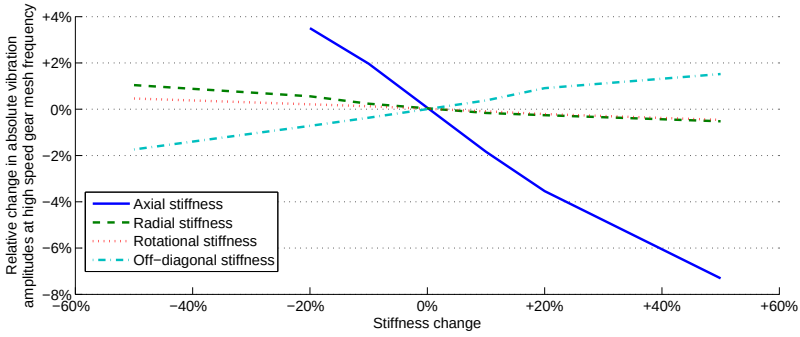

Figure 8.6: Change in absolute vibration amplitudes at high speed gear mesh frequency in measurement point B_x by changing stiffness values of HS-IS-RS bearing.

- For **HS-IS-RS**, the axial stiffness values affect the resulting vibration amplitudes the most, whilst the rotational stiffness values have the lowest impact on the resulting vibration amplitudes. For the point B_X as well as

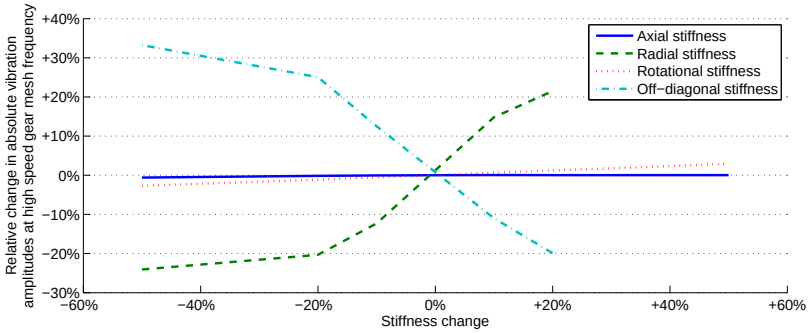

Figure 8.7: Change in absolute vibration amplitudes at high speed gear mesh frequency in measurement point B_x by changing stiffness values of HS-IS-GS bearing.

the other accelerometer points, this agrees with the findings of the TPA (see figure 8.4).

- For **HS-IS-GS**, both the radial and the off-diagonal stiffness values have a large influence on the resulting vibration amplitudes. The reason for this high dependency is explained in section 8.1.3. Similar to HS-IS-RS, the rotational stiffness values do not influence the resulting vibration values a lot.

- Only the axial stiffness values of **HSS-RS** have an influence on the resulting vibration values, which is similar to what was predicted by the TPA analysis for point B_X.

- For **HSS-GS** both axial, radial and off-diagonal stiffness values influence the total vibration results. Again, little to no influence of the rotational stiffness values.

Geometry modifications

Instead of modifying the stiffness by changing the bearings, also the stiffness of the supporting structure (which is already part of the passive part) can be modified. Based on the results from section 8.1.2 this is done for bearing position HS-IS-RS in the axial direction. Additional ribs were added to the structure to increase its stiffness. The main intent was to increase axial stiffness,

however, by the addition of these ribs, also the stiffness in other directions changed. Static stiffness values (calculated using an FE model as static force divided by static deformation) show an increase by approximately 20% for the axial direction and between 25% and 40% in radial and rotational direction according to the direction (ribs were not placed symmetrically). Figure 8.8 shows both the original geometry and the modified geometry with the additional ribs.

Results showed an average reduction in vibration amplitude of about 15%. Vibrations at measurement point B_x reduced with about 10%. 3 out of 32 measurement points showed an increase in vibration values, but their resulting vibration values are still considered to be low compared with measurement point B_x.

Figure 8.8: Mesh of finite element model of housing with left: original HS-IS-RS bearing support structure, and right: stiffened HS-IS-RS bearing support structure.

Damping variations

Next to stiffness values, also damping values of a bearing affect total noise and vibration behaviour. Damping of bearings can be modified by changing design parameters or lubricant. The highest change in damping however is not by changing bearing properties, but by changing the bearing from normal roller

bearings to journal bearings. This may lead to an increase of damping by a factor up to 1000 [49, 48]. In this investigation, only the influence of changing the damping of the bearings is investigated, stiffness values are left unchanged.

Results show an average overall reduction in vibration amplitudes of 6% and 21% by increasing the damping with a factor of 10 and 100 compared with a normal rolling element bearing. Consequently, switching from roller bearings to journal bearings may improve total noise and vibration behaviour.

8.1.3 Effect of bearing position on the transmission of gear excitation

Zhou [181] showed that the axial positioning of a bearing with respect to the gearbox housing could play a significant role in the resulting noise and vibrations. Figure 8.9 explains this phenomenon. The radial gear mesh forces, which are oscillating at the meshing frequency, will cause large or small bending moments on the housing depending on the bearing position i.e. further from or closer to the housing wall. These bending moments will cause out of plane vibrations of the housing wall.

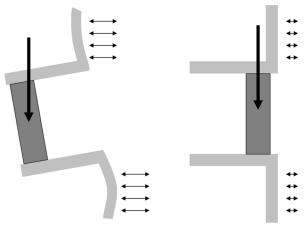

Figure 8.9: Schematic representation how the axial position of a bearing can influence the total noise and vibrations. Left: bearing positioned far from housing wall. Right: bearing positioned close to housing wall.

The effects of an axial offset of the bearings of the parallel gear stage are investigated in a range between ±50mm. Due to its large dependency on its axial position, HS-IS-GS was investigated in a wider range. Vibration amplitudes were extracted from the model when it was running at nominal load and at nominal speed. For this investigation constant 6×6 stiffness matrices were used.

Figure 8.10 shows how the averaged vibration amplitudes of all measurement locations change by modifying the axial position of a bearing. Figure 8.11 shows how the vibration amplitudes at measurement point B_X (the measurement point with the highest vibration amplitudes) change with modifying the axial position of a bearing. Most significant reduction in averaged vibration amplitudes (-25%) can be achieved by moving the HS-IS-GS bearing (which has the highest distance to the housing wall: see figure 8.2) towards the generator (and thus closer to the housing wall).

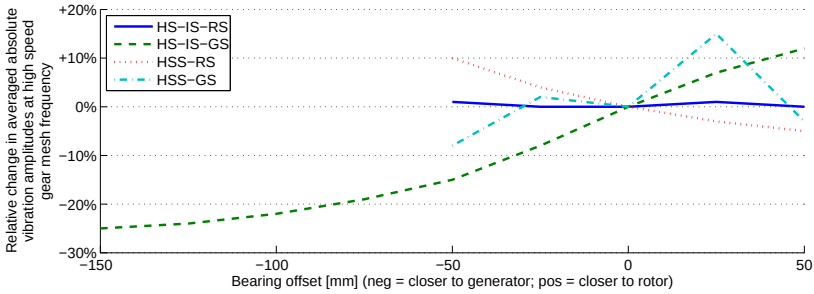

Figure 8.10: Relative changes in averaged absolute vibration amplitudes at high speed gear mesh frequency by changing the axial position of a bearing.

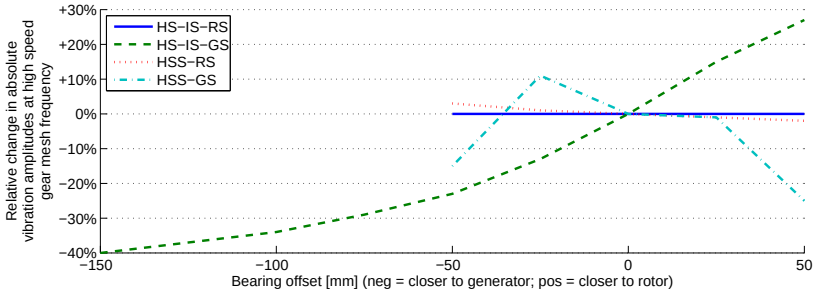

Figure 8.11: Relative changes in absolute vibrations amplitudes at high speed gear mesh frequency on measurement point B_X by changing the axial position of a bearing.

8.1.4 Conclusions

This optimisation case focussed on how the mechanical noise is transferred through the bearings to the outside by using the TPA approach. This approach

reveals which bearing transmits the highest excitation levels from the gears, which is a direct indication of where to optimise for vibration reduction.

In this optimisation case, the dominant transfer path (at the gear mesh frequency) consists of the HS-IS-GS and HS-IS-RS bearing. The effect of bearing stiffness variations on the transfer path is investigated using the flexible MB model. The conclusion is that the influence on the resulting vibration amplitudes can be significant (up to -20%). In addition, the same analysis method shows the important impact of the bearing damping on the resulting vibration amplitudes (up to -50% and more). Furthermore, bearings should be positioned aligned with the gearbox housing wall as this will also reduce vibration amplitudes (in this case up to 40% for measurement point B_X).

8.2 Optimisation case 2: Wind turbine gearbox housing bending modes

The bending mode of the wind turbine gearbox is one the first eigenmodes of the wind turbine gearbox. Based on experience from measurement campaigns on wind turbine gearboxes, it is known that this eigenmode should be assessed properly, because it typically lies close to the frequency range where the second gear stage is exciting and may cause a mechanical tonality. Figure 8.12 shows this global eigenmode. The frequency at which this bending occurs mainly depends on the design of the gearbox housing. This optimisation case therefore proposes a modification to the gearbox housing to shift this resonance out of the operating range.

The sensitivity study in section 5.3.1 showed (see figure 5.11) that mainly the IBH LSS and the IBH ISS dominate this low frequency range. As resonance with this eigenmode occurs almost at nominal rotational speed (see figure 8.14, it is chosen to stiffen the both the IBH LSS and the IBH ISS such that the eigenfrequency of this global bending mode increases and that it shifts out of the normal operating range. Lowering the frequency of this eigenmode would not be beneficial, as it would result in issues at lower wind speeds, typically also resulting in lower background noise making the tonality even more audible. Figure 8.13 shows both the original gearbox housing and the modified gearbox housing which has additional ribs at both the IBH LSS and the IBH ISS components.

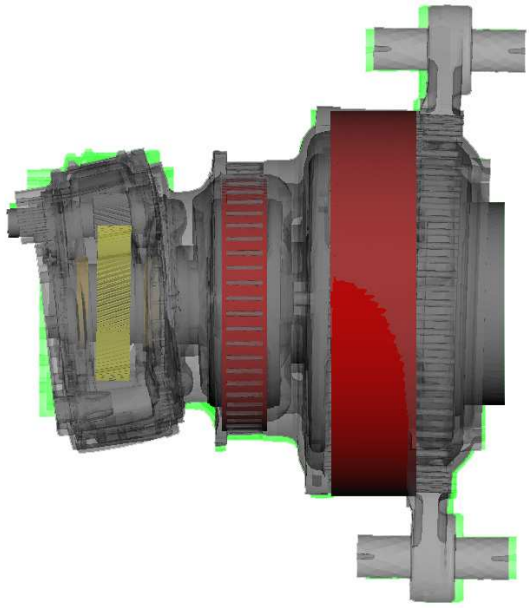

Figure 8.12: Bending eigenmode of the gearbox. Green background = undeformed model.

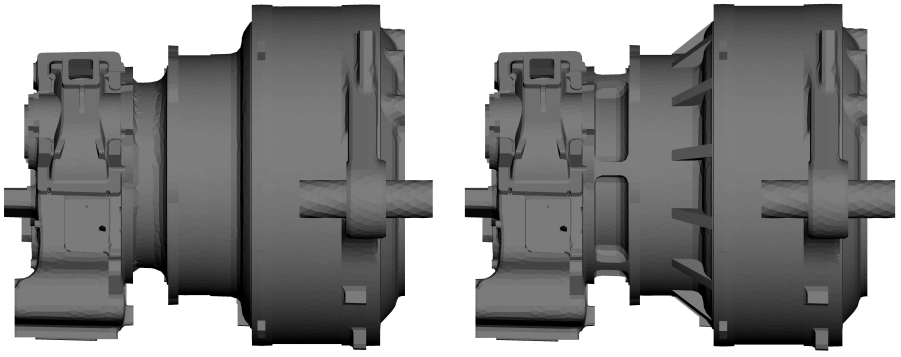

Figure 8.13: Additional ribs to stiffen the gearbox housing. Left: original housing, right: modified housing.

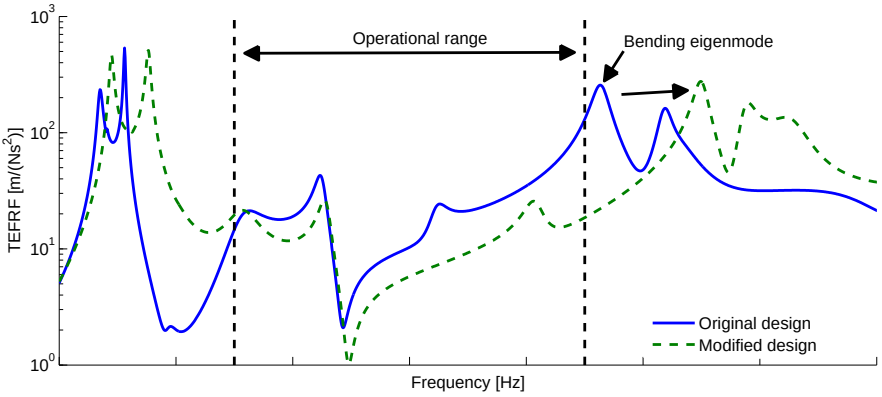

Figure 8.14: TE-FRFs calculated from planet-ring wheel gear excitation, second gear stage to acceleration on the torque arm in vertical direction for original and modified design.

To investigate the impact of this change, TE-FRFs are calculated from the second gear stage towards the gearbox mounting points. Figure 8.14 shows a clear shift (approximately 13%) of the bending eigenmode further away from the operational range resulting in a lower TE-FRF and thus a reduced propagation of the planet - ring wheel gear excitation of the second gear stage towards acceleration levels measured at the torque arm in vertical direction.

8.2.1 Conclusions

This optimisation case showed the impact of the housing design on the global eigenmodes of the complete gearbox. A slight modification to the design: the addition of only a few ribs resulted in a significant shift of a resonance, which potentially can lead to a tonality, out of the normal operating range. Although these results are not representative for the behaviour of the gearbox in the wind turbine, it clearly shows the impact of the gearbox housing on its dynamics, and the potential gains that can be achieved when optimising a design.

8.3 Conclusions

Although due to confidentiality reasons no real design improvement taking the complete wind turbine drive train into account could be performed, two design improvements on an isolated wind turbine gearbox were presented. First design improvement investigated the impact of the bearings (design, type and location) on the resulting vibration amplitudes. Second design improvement modified the flexible gearbox housing to shift a resonance, which could lead to a tonality, out of the normal operating range. Both these design improvements clearly illustrate the potential of pro-actively using virtual simulation models to optimise the noise and vibration behaviour of the wind turbine gearbox during its design.

Chapter 9

Conclusions

9.1 Overview and main contributions

Chapter 2 introduces wind turbines and wind turbine noise. It gives an overview on how the wind turbine noise is perceived by closely living habitants, how it is regulated, and how it is taken into account during the installation of a single wind turbine or a complete wind farm.

This first introductory chapter starts with a short introduction on the climate changes ahead of us, emphasizing the need for energy sources with zero- and low-carbon emission. All scenarios to mitigate the harmful impact of the climate changes include a significant increase of currently installed wind power.

The noise produced by wind turbines could mitigate this necessary increase. Wind turbine noise can be subdivided into two main categories:

1. aeroacoustic noise, which is the most dominant noise source of the wind turbine, broadband of nature and caused by the aero-elastic interaction between the air and the blades, tower and nacelle; and
2. mechanical noise, which is only audible when it rises above the aeroacoustic noise, is tonal of nature, and is caused by the mechanical components such as the gears in the gearbox.

Next to its overall level, other characteristics of the wind turbine noise, such as the amplitude modulation, the low frequency noise and the tonality mainly define the typical noise of a wind turbine.

A short overview on the specific regulations regarding wind turbine noise shows a big disparity based on location. Regulations could be on state level, on country level, on regional level, on provincial level, ... Some countries do not even have a specific regulation with regards to wind turbine noise and rely on their regulations regarding industry noise.

Main priority during the site selection phase where an individual wind turbine or a wind farm should be located is on maximising the energy yield of the individual wind turbine or wind farm. Constraints such as shadow flicker and wind turbine noise are addressed in a later phase. During this phase, the site layout phase, mostly an acoustic noise propagation calculation is necessary to guarantee that the resulting noise levels of the individual wind turbines stay below the regulatory limits.

A short introduction on wind turbine gearboxes includes a sectional drawing of the wind turbine gearbox used throughout this dissertation. Dominant excitation sources inside the wind turbine gearbox are the gears. The excitation frequency of these gears is linked with the rotational speed of the wind turbine. This excitation has multiple transfer paths to propagate towards noise at the exterior of the wind turbine. These transfer paths could amplify or attenuate the gear excitation forces. This behaviour is determined by the dynamic behaviour of the entire drive train in which the wind turbine gearbox is a component. The resulting noise levels could give rise to tonalities if the resulting noise levels rise above the aeroacoustic background noise.

Chapter 3 describes the state-of-the-art with respect to wind turbine drive train modelling with a strong focus on the models capable of calculating wind turbine drive train dynamics.

Wind turbine drive train design load models are used in the wind turbine industry to predict the loading on the components of the wind turbine. Traditionally, most of these drive train design load models are believed to be more or less similar [132] and include 3 to 5 DOFs for tower deformations, 12 to 18 DOFs for blade deformation for a three bladed rotor, and 1 additional DOF to represent the deformation in the entire drive train. Due to this low amount of DOFs, these

models are not usable to predict the dynamic behaviour of the wind turbine drive train in the audible frequency range. Recently also flexible MB is employed to more accurately predict the loading on individual components inside the gearbox such as on the gears or on the supporting bushings. Although these models are nicely documented and well validated in the quasi static domain, they cannot be used without further investigation to predict resulting noise and vibration amplitudes in the audible frequency range.

The first systematic efforts to analyse gear dynamics occurred around 1920 [123] and focussed mainly on lumped mass models taking only a limited amount of information into account, neglecting e.g. gearbox bearings and housing. The inclusion of these components, such as the gearbox housing, however, is absolutely necessary to accurately predict the dynamic behaviour in the audible frequency range [60]. The investigations building vibro-acoustic models of the entire gear system which take these components into account are rather sparse [55]. The investigations and experimental validations performed by various researchers on the research gearbox of the NASA at the Glenn Research Center provided most insight in complete gearbox dynamics again emphasizing the need to model the complete gearbox including the gearbox housing. Due to the huge discrepancy between this rather simple research gearbox and a multi-megawatt wind turbine gearbox, the results of these investigations cannot be translated directly and additional research is necessary.

Efforts to model more accurately the dynamics of the wind turbine drive train are quite limited, focus mainly on low frequency dynamics and lack thorough experimental validation.

Based on these identified limitations in the current state-of-the-art and state-of-the-use, the need for an experimentally validated modelling approach and methodology to accurately predict the dynamic behaviour of a wind turbine drive train becomes clear, justifying the research objectives of this dissertation:

1. develop a methodology / model approach to assess the vibro-acoustic behaviour of a wind turbine gearbox in the frequency area covering all relevant gear excitation frequencies. Focus of this methodology and modelling approach should be on the structural transfer path from the gears to the receiver, but not on the gear excitation itself;
2. experimentally validate this modelling approach;
3. get insight in which components are dominant for the dynamic behaviour;

4. get insight in which components are dominant for model accuracy;
5. use this methodology to shorten the trajectory to meet the noise and vibration requirements by a factor of 2; and
6. use this methodology to reduce the investment cost of reactive troubleshooting on existing product with a factor of 30%.

Chapters 4, 5 and 6 present the main contribution of the author and form the essence of this dissertation. This is the development and experimental validation of a modelling approach to accurately predict the dynamic behaviour of a wind turbine gearbox in the relevant audible frequency domain. A step-by-step approach is chosen to ensure the accuracy of each individual part of the complete model. Chapter 4 focusses on the individual components of the wind turbine gearbox, which are assembled in Chapter 5 to form the model of the complete gearbox. The impact of the EOL test rig on the dynamic behaviour of the gearbox is assessed in Chapter 6.

Based on the insights gathered in these chapters, it can be concluded that the flexible gearbox housing plays the most dominant role on the overall gearbox dynamics. Much effort should therefore be spent in generating an as accurate as possible FE representation of the flexible gearbox housing as it will have a direct impact on the accuracy of the global gearbox dynamics. When significant modifications to the dynamic behaviour of the complete gearbox are necessary, focus should in most cases be put on altering the flexible gearbox housing rather than the internals. Both intermediate bearing housings have a dominant role in the low frequent behaviour of the gearbox, while the design of the HSH and MC dominates the high frequent behaviour of the gearbox. Impact of the TA is limited to very specific eigenmodes in several frequency bands, while the impact of both ring wheels is almost negligible.

The multiple sensitivity studies revealed that bearing stiffness values have the second most important impact on the overall gearbox dynamics. Bearing models that couple all DOFs should be utilised. Due to its non-linear behaviour special care should be taken:

- The bearing model should produce the correct stiffness values taking both loading and bearing pre-load into account, or should only be used at that specific operating condition (also taking bearing pre-load into account) for which these stiffness values were calculated.

- For large bearings, summing the individual roller forces together and introducing them into the centre of the bearing results in inaccuracies in several eigenfrequencies. If these eigenfrequencies are of interest, a roller based bearing model should be used that introduces the individual roller forces into the outer ring.

Focus of this dissertation is on assessing and optimising the individual transfer paths from the gears to the outside, and not on optimising the gear contact behaviour. Therefore, instead of including a complex gear excitation model, the usage of so-called TE-FRFs is suggested. Using these TE-FRFs the relation between the TE of a gear pair and an arbitrary response such as acceleration at a certain location or an MPF can be calculated. As a result, changes from design modifications can be assessed without taking the gears into account. Therefore a simple gear force element taking the average gear mesh stiffness into account is sufficient. However when the acoustic radiation of the gearbox is of interest care should be taken to property introduce the planet - ring wheel gear excitation forces as the commonly used simplification of introducing these forces into the centre of the ring wheel will lead to inaccurate response levels.

Numerous EMAs were performed to assess the accuracy of the individual components, sub-assemblies and assemblies. For this gearbox model, a very good correlation up to 300 Hz, and an acceptable correlation between 300 Hz and 500 Hz was observed. It is expected that this will be somewhat similar in future gearbox models. To obtain an as accurate model as possible, much effort should be spent in generating an as accurate as possible FE representation of the flexible gearbox housing as it will have a direct impact on the accuracy of the global gearbox dynamics. Experimental validation could be considered to further increase the accuracy of this model. To increase the accuracy of the model in the lower frequency bands, up to $\approx$ 200 Hz, an EMA on the complete assembled gearbox is advised, as the inaccuracy of the bearings is considered higher than the inaccuracy of the gearbox housing in this frequency region. At higher frequencies, an additional EMA on the complete empty gearbox housing if possible, or on the HSH and the MC is advisable. Preferably multiple EMAs should be undertaken to assess the variance of these castings.

An acoustic FE model of the flexible gearbox housing illustrated the need for advanced acoustic modelling as the coincidence frequency for this gearbox lies around 800 Hz. Therefore, simplified acoustic methods based on structural FE models below this frequency are useless to assess the direct radiated noise from the gearbox housing. Furthermore it was illustrated that ATVs and MATVs are an efficient way to firstly calculate the acoustic behaviour of the gearbox

housing, and secondly to link the structural MB model with the acoustic FE model.

The analysis of the dynamic behaviour of the gearbox on the EOL test rig showed a very important dependency on its boundary conditions such as the supporting structure, low speed coupling, ... This strengthens the belief that the wind turbine gearbox cannot be assessed alone: although the excitation forces originate solely from the gears, it are the individual transfer paths determined by the dynamics of the complete wind turbine that attenuate this excitation or amplify it to a resonance which could lead to a mechanical tonality.

Chapter 7 discusses how the modelling approach investigated in previous chapters should be extended towards the full wind turbine, and how these models should be used to pro-actively predict mechanical tonalities.

Due to the high complexity and the high coupling of the individual components of the drive train, a model based approach is necessary. Furthermore, this model based approach should assess the global drive train eigenmodes using a model comprising this complete drive train. The insight generated by models of individual components is very limited due to the high dependency of these models on their boundary conditions.

A methodology is proposed to pro-actively assess mechanical tonalities originating from the wind turbine drive train based on a virtual prototyping model of the wind turbine drive train. Based on experience gained in previous chapters, the model requirements for this model are discussed, and an analysis approach to obtain an overview of the tonal behaviour of the wind turbine in its complete operating range is proposed.

Chapter 8 presents two optimisation cases to demonstrate the usability of these virtual simulation models.

Although due to confidentiality reasons no real optimisation case taking the complete wind turbine drive train into account could be performed, two optimisation cases on an isolated wind turbine gearbox are presented. First optimisation case investigated the impact of the bearings (design, type and location) on the resulting vibration amplitudes. Second optimisation case modified the flexible gearbox housing to shift a resonance, which could lead to

a tonality, out of the normal operating range. Both these optimisation cases clearly illustrate the potential of pro-actively using virtual simulation models to optimise the noise and vibration behaviour of the wind turbine gearbox during its design.

9.2 Recommendations for future research

This dissertation presented and experimentally validated a modelling approach and methodology to optimise a wind turbine drive train resulting in a reduced risk for tonalities. This section suggests several items to improve and extend this work. Similar to figure 2.19 this section is also organised in sources, transfer paths, and acoustic radiation (noise).

9.2.1 Sources

Although an accurate gear excitation model should not be included in the wind turbine drive train model, an accurate estimation of the gear excitation forces remains essential to predict resulting vibration or noise levels. Further research and experimental validation of models capable of accurately predicting these gear excitation forces therefore remains very important.

9.2.2 Transfer paths

All investigations to improve the accuracy of the individual transfer paths have a direct impact on the accuracy of the tonality predictions. Several improvements can be made:

- Sections 4.4.2 and 5.3.1 demonstrate how loading can influence the global gearbox eigenmodes by changing the stiffness of the rollers and the number of rollers in contact. This was investigated by employing both an FE and an MB model. The implementation in the MB currently requires a huge amount of user expressions to calculate the compression of each individual roller between a flexible outer ring (gearbox housing) and a rigid inner ring (planet carrier). This implementation should be optimised such that the time required for inserting such a roller based bearing model into the MB model and simulations in time domain with this roller based bearing model become feasible.

- Section 4.5.2 revealed that although the changing contact locations between ring wheel and planets have no effect on the global eigenmodes of the gearbox, it does influence the resulting acceleration amplitudes measured throughout the entire gearbox. Therefore to be able to accurately calculate vibration amplitudes on the gearbox, or to assess the direct wind turbine gearbox airborne sound radiation, additional research and development is necessary to practically implement this moving gear contact in MB models.
- The impact of the level of detail of the blades and the tower on the transfer paths should be assessed, resulting in a model of the wind turbine drive train which includes only the level of detail which is necessary to reach a certain accuracy.

Furthermore, all advances in experimentally characterising these components and assemblies will result in an increased insight on the dynamic behaviour of these components and assemblies, which leads to better models and to better tonality predictions. Possible improvements and extensions can be made:

- Experimental validation of the gearbox focussed on the global eigenmodes, measured at the exterior of the gearbox. To further increase the accuracy of these models, future measurements should therefore also focus on the internals or on sub-assemblies of the internal components such as a complete planet carrier with planets assembly.
- Experimental validation in this dissertation primarily focussed on correlating experimentally identified eigenmodes with eigenmodes computed from the model. A next step should also include validation of resulting vibration amplitudes.
- A huge amount of experimental measurements were performed to validate individual components, a sub-assembly of a gearbox, a complete gearbox and two gearboxes on an EOL test rig. All these measurements could only be performed on one test object instead of several test objects. Therefore no insight is gathered on the variability of the dynamic properties of these components or assemblies. Future work should include an investigation on the variability of these dynamic properties such that an optimal level of correlation or an uncertainty bound on the results can be obtained.
- Correlation between the experimentally identified eigenmodes of the complete gearbox and the gearbox model was performed in unloaded conditions. Therefore the impact of the gear contacts could not be in-depth investigated. It would be beneficial if a significant torsional load

could be applied on a single gearbox without modifying its dynamic response.

- This methodology relies on models to predict the individual transfer paths. Another approach could be the combination of these numerical models with experimentally identified modal models of the parts which are already available, e.g. a modal model of the mainframe. Care should be taken that the modal model representing this component only includes the dynamic behaviour of this component, and not its boundary conditions necessary for the experimental characterisation.
- Although the presented methodology focusses a complete wind turbine drive train, the underlying modelling approach has only been experimentally validated on a wind turbine gearbox and a wind turbine gearbox in an EOL test rig. Experimental validation of the ALARM wind turbine drive train model (including the wind turbine gearbox presented in this dissertation) remains therefore a key objective of the ALARM project.

9.2.3 Noise radiation

This dissertation only focussed on the noise radiation of the wind turbine gearbox. Although a similar approach could be followed for the complete wind turbine, further research is necessary to acquire a better insight in the noise radiation of a complete wind turbine.

- Although the noise radiation form the wind turbine gearbox was calculated, it is not yet clear if this transfer path from radiated noise from the gearbox housing, to vibrations induced on the nacelle cover, to noise radiated by the nacelle cover to the surroundings, is dominant over the structure-born transfer path. If this structure-born transfer path is dominant, then no acoustic simulation for the gearbox housing is necessary, nor any coupled vibro-acoustic models to calculate the noise transfer through the nacelle cover. If this transfer path is not dominant, simple measures to increase the sound insulation of the nacelle cover could be advised to lower the mechanical noise.
- The acoustic radiation calculation for the tower, blades and nacelle cover is not straightforward due the size of these components. Further research is necessary to make these computations practically feasible.

Appendix A

Femtools

Femtools has been extensively used during this dissertation for:

- correlating FE models with EMA
- correlating Simpack models with EMA
- calculating model sensitivities to track changes in model behaviour by varying parameters
- updating both FE and Simpack models to increase correlation with experiments

Although Femtools is designed to mainly operate on FE models, it is highly customisable and its build in scripting language allows to modify almost everything. Following sections give an overview of these modifications necessary to allow Femtools to use Simpack models instead of FE models. It was tried to alter Femtools as little as possible in order that functionality such as sensitivity calculations, MAC calculation, model updating, ... remains working as if it was working on an FE model.

A.1 Simpack model reader

The Simpack model reader allows importing a Simpack model in Femtools. The MB formulation of Simpack (using DOFs to represent global body movement and speed, and flexible modeshapes to represent global body deformation) is

not compatible using the FE oriented formulation of Femtools using nodes and elements. To overcome this issue virtual accelerometers are placed inside the Simpack model and correspond with nodes inside Femtools.

The virtual accelerometers are defined in Simpack as dummy (almost weightless) bodies connected rigidly to other bodies. When connecting to a flexible body, this flexible body should contain a master node at the location where the virtual accelerometer is placed such that elastic deformation can accurately be computed instead of roughly estimated based on neighbouring master nodes. By doing so, both the location of these virtual accelerometers, and the eigenmodes evaluated in these virtual accelerometers are exported to a so-called 'EVA' file.

Parsing of this 'EVA' file allows to insert nodes in Femtools. At least one dummy stiffness element should be created in Femtools such that it thinks a complete FE model is loaded and all functionality is unlocked. Although only one element is required, usage of several elements is advisable to introduce a mesh like geometry which enhances visual modeshape recognition.

A.2 Simpack model writer

The Simpack model writer allows modifying the Simpack model which is required to perform sensitivity calculations and model updates. Simpack models are saved to disk in a human readable (and modifiable) text based form. For the Simpack model writer, an approach using model variables was chosen. Inside the Simpack model, a variable is defined and assigned to some parameter (mass of a gear wheel or stiffness of a spring e.g.) and exported to a text file containing all parameters. Using a Femtools script this text file is parsed and so-called 'generic parameters' are defined in Femtools which can thereafter directly read and write the value from this fixed format text file.

A.3 Simpack solver & results reader

When importing a Simpack model in Femtools, the default Femtools solver is switched to a custom script based solver. For the eigenmodes, the Femtools script invokes the Simpack solver directly to firstly (if necessary) compute a steady state condition and afterwards the eigenmodes and eigenfrequencies. Afterwards the solver script calls the result reader to again parse this 'EVA' file and to import the displacement and phase of each virtual accelerometer for

each eigenfrequency.

When calculating FRFs, again initially a steady state computation can be performed. Afterwards the Simpack solver is invoked to calculate the so-called 'ABCD'-matrices and to export those matrices to a Matlab readable file. When completed, a Matlab session is started from within Femtools to read the ABCD-matrices and to calculate the requested FRFs from these ABCD-matrices in the requested frequency band. These calculated FRFs are exported to a file and parsed afterwards by the results reader.

Appendix B

Roller based bearing model

The force calculation of the roller based bearing model relies on

1. a calculation of the distance between the bearing cone and the bearing interface point i; and
2. a calculation of the roller force based on the compression of the roller

B.1 Distance calculation

Define a line: $\mathbf{X}(t) = \mathbf{P} + t\mathbf{D}$ for $t \in \Re$ (see figure B.1)

with:
P Bearing interface point
D Direction vector perpendicular on the bearing cone

and a cone: $\mathbf{A}.\left(\frac{\mathbf{X}-\mathbf{V}}{|\mathbf{X}-\mathbf{V}|}\right) = cos(\theta)$

with:
V origin of the cone;
A direction vector; and
θ angle between direction vector and outer edge.

The distance perpendicular on the bearing cone between the bearing interface point P and the bearing cone can be found as $\frac{t}{|\mathbf{D}|}$ when $\mathbf{X}(t)$ intersects the cone. The distance calculation can thus be transformed in the calculation of the

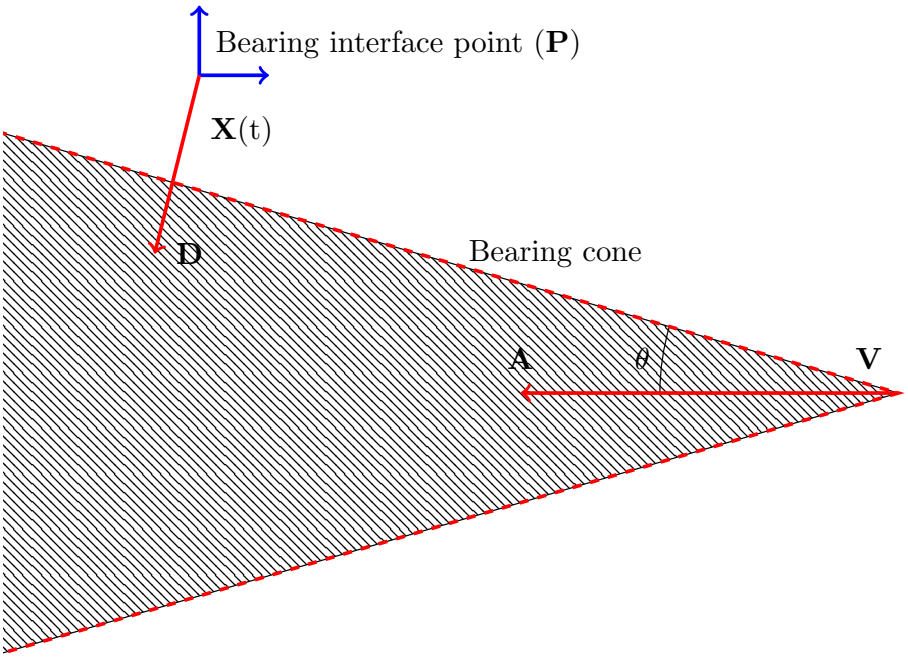

Figure B.1: Advanced bearing model - distance calculation.

intersection between $\mathbf{X}(t)$ and the bearing cone. The complete details about the intersection calculation between a line and a cone is well documented in [30] and are not repeated here.

The intersection point (and thus the distance) is calculated from:

$$c_2 t^2 + 2c_1 t + c_0 = 0$$

where

$$
\begin{aligned}
\gamma &= cos(\theta) \\
M &= (\mathbf{A}\mathbf{A}^T - \gamma^2 I) \\
\mathbf{\Delta} &= \mathbf{P} - \mathbf{V} \\
c_2 &= \mathbf{D}^T M \mathbf{D} \\
c_1 &= \mathbf{D}^T M \mathbf{\Delta} \\
c_0 &= \mathbf{\Delta}^T M \mathbf{\Delta}
\end{aligned}
$$

Following simplifications were made when implementing [30]:

- $\mathbf{A}$ is collinear with the X-axis. Therefore $\mathbf{A} = (1, 0, 0)$.
- All positions are calculated using $\mathbf{V}$ as origin, therefore $\mathbf{V} = (0, 0, 0)$.
- Because initially $\mathbf{X}(t)$ is perpendicular to the surface of the cone and only small offsets and rotations are expected, it is assumed that $\mathbf{X}(t)$ always penetrates the cone at two locations. Therefore $c_2 \neq 0$.

Using these assumptions above, the calculation of t can be simplified:

$$
\mathbf{A} = \begin{bmatrix} 1 \\ 0 \\ 0 \end{bmatrix}
$$

$$
\mathbf{V} = \begin{bmatrix} 0 \\ 0 \\ 0 \end{bmatrix}
$$

$$
\mathbf{P} = \begin{bmatrix} P_x \\ P_y \\ P_z \end{bmatrix}
$$

$$
\mathbf{D} = \begin{bmatrix} D_x \\ D_y \\ D_z \end{bmatrix}
$$

$$\mathbf{\Delta} = \mathbf{P} - \mathbf{V} = \begin{bmatrix} P_x \\ P_y \\ P_z \end{bmatrix}$$

$$M = (\mathbf{A}\mathbf{A}^T - \gamma^2 I) = \begin{bmatrix} -\gamma^2 + 1 & 0 & 0 \\ 0 & -\gamma^2 & 0 \\ 0 & 0 & -\gamma^2 \end{bmatrix}$$

$$\gamma = cos(\theta)$$

$$c_2 = \mathbf{D}^T M \mathbf{D} = -D_y^2\gamma^2 - D_z^2\gamma^2 - \left(\gamma^2 - 1\right)D_x^2$$

$$c_1 = \mathbf{D}^T M \mathbf{\Delta} = -D_y P_y \gamma^2 - D_z P_z \gamma^2 - \left(\gamma^2 - 1\right)D_x P_x$$

$$c_0 = \mathbf{\Delta}^T M \mathbf{\Delta} = -P_y^2\gamma^2 - P_z^2\gamma^2 - \left(\gamma^2 - 1\right)P_x^2$$

B.2 Roller force calculation

According to Harris et al. [53] the force in a cylindrical roller element can be expressed as follows:

$$Q = K_n \delta^n$$

$$K_n = \left[\frac{1}{\left(\frac{1}{K_i}\right)^{1/n} + \left(\frac{1}{K_o}\right)^{1/n}} \right]^n$$

with:

Q	Ball–or roller–raceway normal load	(N)
K_n	Total load–deflection factor (stiffness)	(N/mm^n)
δ	Roller deflection	(mm)
n	Load–deflection exponent ($n = 10/9$ for roller bearings)	
K_i	load–deflection factor for roller–inner raceway contact	(N/mm^n)
K_o	load–deflection factor for roller–outer raceway contact	(N/mm^n)

For roller-raceway contact (K_i and K_o) the following load deflection factor can be determined [53]:

$$K = 8.06E^4 l^{8/9}$$

with: l Roller length (mm)

Appendix C

Overview on experimental validation campaigns

This appendix gives more insight in the individual experimental validation campaigns that were performed to validate both FE and MB models.

C.1 Individual wind turbine gearbox components

C.1.1 Torque arm

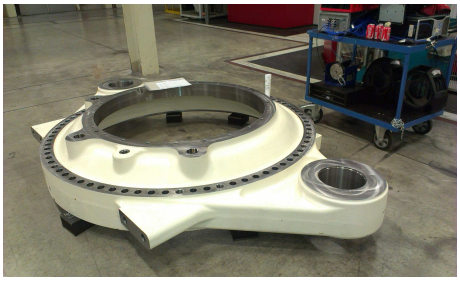

Figure C.1: Torque arm measurement setup.

Table C.1: Measurement settings for TA measurement campaign

Setup	
Number of measurement points	20
Response window	Exponential
Number of shakers	1
Excitation type	Burst random
Force window	Force exponential
Sample frequency	6400 Hz
Frequency resolution	0.195 Hz
Number of averages	25 linear averages
Analysis	
Modal parameter estimation method	PolyMAX
Results	
Average damping	0.3
Number of identified eigenmodes	
Total	31
Between 0Hz and 200Hz	4
Between 200Hz and 400Hz	4
Between 400Hz and 600Hz	8
Between 600Hz and 800Hz	6
Between 800Hz and 1000Hz	9

C.1.2 Low speed ring wheel

Table C.2: Measurement settings for LSRW measurement campaign

Setup	
Number of measurement points	12
Response window	Exponential
Number of shakers	1
Excitation type	Burst random
Force window	Force exponential
Sample frequency	6400 Hz
Frequency resolution	0.195 Hz
Number of averages	25 linear averages
Analysis	
Modal parameter estimation method	PolyMAX
Results	
Average damping	0.1%
Number of identified eigenmodes	
Total	17
Between 0Hz and 200Hz	3
Between 200Hz and 400Hz	2
Between 400Hz and 600Hz	1
Between 600Hz and 800Hz	8
Between 800Hz and 1000Hz	3

C.1.3 Intermediate bearing housing, low speed side

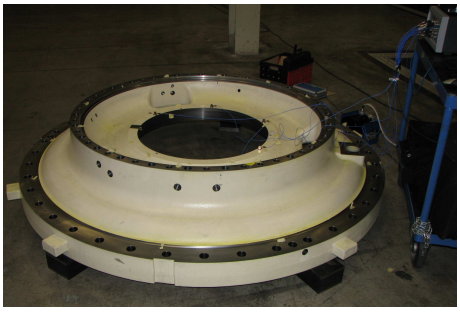

Figure C.2: Intermediate bearing housing, low speed side measurement setup.

Table C.3: Measurement settings for IBH-LSS measurement campaign

Setup	
Number of measurement points	36
Response window	Exponential
Number of shakers	1
Excitation type	Burst random
Force window	Force exponential
Sample frequency	6400 Hz
Frequency resolution	0.195 Hz
Number of averages	25 linear averages
Analysis	
Modal parameter estimation method	PolyMAX
Results	
Average damping	0.3%
Number of identified eigenmodes	
Total	25
Between 0Hz and 200Hz	2
Between 200Hz and 400Hz	4
Between 400Hz and 600Hz	8
Between 600Hz and 800Hz	5
Between 800Hz and 1000Hz	6

C.1.4 High speed housing and main cover

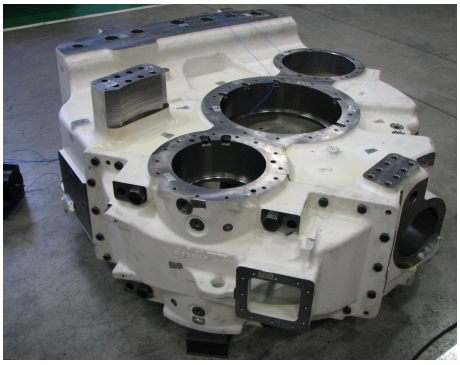

Figure C.3: High speed housing and main cover measurement setup.

Table C.4: Measurement settings for HSH + MC measurement campaign

Setup	
Number of measurement points	102
Response window	Exponential
Number of shakers	1
Excitation type	Burst random
Force window	Force exponential
Sample frequency	6400 Hz
Frequency resolution	0.195 Hz
Number of averages	30 linear averages
Analysis	
Modal parameter estimation method	PolyMAX
Results	
Average damping	0.3%
Number of identified eigenmodes	
Total	50
Between 0Hz and 200Hz	1
Between 200Hz and 400Hz	8
Between 400Hz and 600Hz	12
Between 600Hz and 800Hz	13
Between 800Hz and 1000Hz	16

C.1.5 Assembled gearbox housing

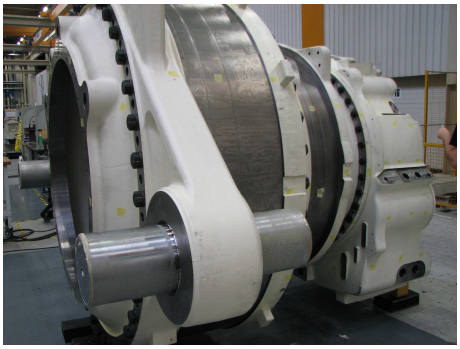

Figure C.4: Assembled gearbox housing measurement setup - 1.

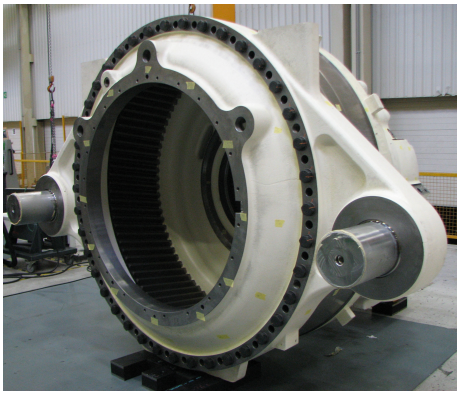

Figure C.5: Assembled gearbox housing measurement setup - 2.

Table C.5: Measurement settings for empty gearbox housing measurement campaign

Setup	
Number of measurement points	276
Response window	Exponential
Number of shakers	1
Excitation type	Burst random
Force window	Force exponential
Sample frequency	12800 Hz
Frequency resolution	0.391 Hz
Number of averages	30 linear averages
Analysis	
Modal parameter estimation method	PolyMAX
Results	
Average damping	0.2%
Number of identified eigenmodes	
Total	90
Between 0Hz and 200Hz	7
Between 200Hz and 400Hz	12
Between 400Hz and 600Hz	26
Between 600Hz and 800Hz	21
Between 800Hz and 1000Hz	24

C.2 Assembled gearbox

C.2.1 High speed housing and main cover

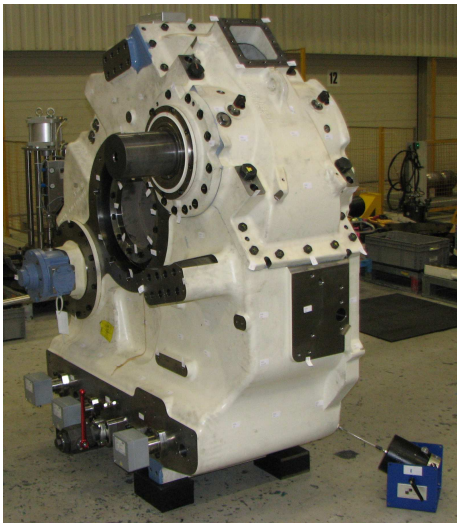

Figure C.6: Assembled high speed housing, main cover and internals - measurement setup.

Table C.6: Settings for measurement campaign of HSH + MC sub-assembly

Setup	
Number of measurement points	201
Response window	Exponential
Number of shakers	1
Excitation type	Burst random
Force window	Force exponential
Sample frequency	6400 Hz
Frequency resolution	0.391 Hz
Number of averages	40 linear averages
Analysis	
Modal parameter estimation method	PolyMAX
Results	
Average damping	0.2%
Number of identified eigenmodes	
Total	46
Between 0Hz and 200Hz	6
Between 200Hz and 400Hz	9
Between 400Hz and 600Hz	11
Between 600Hz and 800Hz	8
Between 800Hz and 1000Hz	12

C.2.2 Complete gearbox

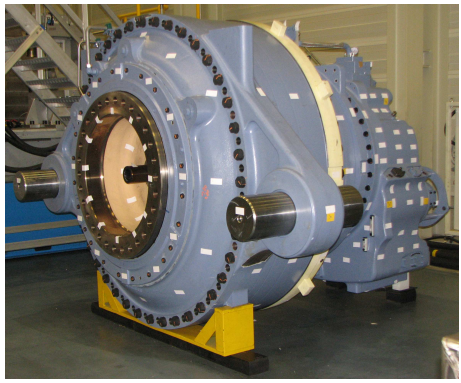

Figure C.7: Assembled Gearbox - measurement setup - 1.

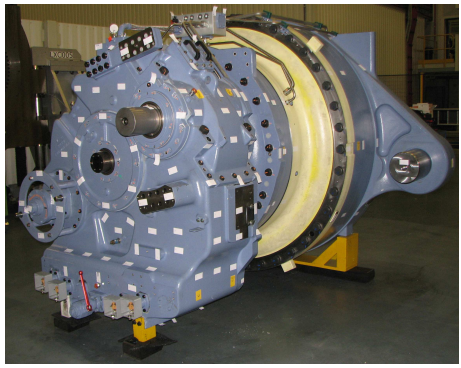

Figure C.8: Assembled Gearbox - measurement setup - 2.

Table C.7: Settings for measurement campaign of complete gearbox assembly

Setup	
Number of measurement points	305
Response window	Exponential
Number of shakers	2
Excitation type	Burst random
Force window	Force exponential
Sample frequency	6400 Hz
Frequency resolution	0.195 Hz
Number of averages	30 linear averages
Analysis	
Modal parameter estimation method	PolyMAX
Results	
Average damping	0.8%
Number of identified eigenmodes	
Total	86
Between 0Hz and 200Hz	10
Between 200Hz and 400Hz	25
Between 400Hz and 600Hz	20
Between 600Hz and 800Hz	20
Between 800Hz and 900Hz	11

Bibliography

[1] M. Åkerblom. *Gear Noise and Vibration: A Literature Survey*. 2001 (p. 39).

[2] *ALARM - Eureka website*. URL: `http://www.eurekanetwork.org/project/-/id/7220` (p. 6).

[3] V. K. Ambarisha and R. G. Parker. "Suppression of planet mode response in planetary gear dynamics through mesh phasing". In: *Journal of Vibration and Acoustics* 128.2 (2006), pp. 133–142 (p. 100).

[4] ANSYS, Inc. *ANSYS Parametric Design Language Guide*. 15.0. ANSYS, Inc. 275 Technology Drive, Canonsburg, PA 15317, Nov. 2013 (p. 73).

[5] R. Augustino. "Drivetrain simulation: optimization through flexible multibody simulation". In: *Proceedings of IQPC Bremen*. July 2014 (p. 57).

[6] H. Van der Auweraer, P. Mas, S. Dom, A. Vecchio, K. Janssens, and P. Van de Ponseele. "Transfer path analysis in the critical path of vehicle refinement: the role of fast, hybrid and operational path analysis". In: *SAE Technical Paper 2007-01-2352* (2007). DOI: `doi:10.4271/2007-01-2352` (p. 162).

[7] Barros, V.R., C.B. Field, D.J. Dokken, M.D. Mastrandrea, K.J. Mach, T.E. Bilir, M. Chatterjee, K.L. Ebi, Y.O. Estrada, R.C. Genova, B. Girma, E.S. Kissel, A.N. Levy, S. MacCracken, P.R. Mastrandrea, and L.L. White (eds.) *IPCC, 2014: Climate Change 2014: Impacts, Adaptation, and Vulnerability. Part B: Regional Aspects. Contribution of Working Group II to the Fifth Assessment Report of the Intergovernmental Panel on Climate Change*. Cambridge University Press, Cambridge, United Kingdom and New York, NY, USA, 2014 (p. 14).

[8] G. Van den Berg. "The beat is getting stronger: The effect of atmospheric stability on low frequency modulated sound of wind turbines". In: *noise notes* 4.4 (2005), pp. 15–40 (p. 22).

[9] G. Van den Berg, E. Pedersen, J. Bouma, and R. Bakker. "Project WINDFARMperception: visual and acoustic impact of wind turbine farms on residents". In: *Final report, June* 3.2008 (2008), p. 63 (p. 28).

[10] H. Bériot and M. Tournour. "On the locally-conformal perfectly matched layer implementation for Helmholtz equation". In: *Proceedings of NOVEM Noise and Vibration: Emerging Methods*. 2009 (p. 131).

[11] W. Blake. "Mechanics of flow-induced sound and vibration". In: *Academic, New York* (1986) (p. 26).

[12] B. Blockmans, J. Helsen, F. Vanhollebeke, and W. Desmet. "Dynamic Response of a Multi-megawatt Wind Turbine Drivetrain under Voltage Dips using a Coupled Flexible Multibody Approach". In: *Proceedings of the ASME 2013 International Design Engineering Technical Conferences & Computers and Information in Engineering Conference, Portland, Oregon*. DETC2013-12458. Aug. 2013 (p. 229).

[13] J. Borner, D. Houser, and S. of Automotive Engineers. "Friction and bending moments as gear noise excitations". In: *SAE transactions* 105 (1996), pp. 1669–1676 (p. 39).

[14] E. A. Bossanyi. *GH Bladed theory manual*. 13th ed. Garrad Hassan and Partners Limited. Bristol, UK, 2005 (p. 47).

[15] T. F. Brooks, D. S. Pope, and M. A. Marcolini. *Airfoil self-noise and prediction*. Vol. 1218. National Aeronautics, Space Administration, Office of Management, Scientific, and Technical Information Division, 1989 (pp. 25, 26).

[16] A. Carrarini. "Acoustic postprocessing for multibody simulations including flexible bodies". In: *Proceedings of the ECCOMAS International Conference on Multibody Dynamics*. 2009 (p. 132).

[17] M. Cassidy, A. D'Souza, and J. Bass. "How Does Noise Influence the Design of a Wind Farm?" In: *Proceedings of 5th International Conference on Wind Turbine Noise*. 2013 (pp. 33–35).

[18] A. Cordle and J. Jonkman. "State of the art in floating wind turbine design tools". In: *Proceedings of the 21st International Offshore and Polar Engineering Conference, Maui, Hawaii*. National Renewable Energy Laboratory (NREL), 2011 (p. 48).

[19] R. R. Craig Jr. "A review of time-domain and frequency-domain component mode synthesis method". In: *Proceedings of the joint mechanics conference. Albuquerque, USA*. 1985 (p. 81).

[20] *CWD - Center for Wind Power Drives*. URL: `https://www.cwd.rwth-aachen.de/home/` (p. 53).

[21] L. Dewilde, Y. Cabooter, K. De Ridder, J. Van Ypersele, and C. Tricot. *Improved prediction of wind power in Belgium - Part 1: sustainable production and consumption patterns*. Tech. rep. Scientific Support Plan for a Sustainable Development Policy (SPSDII), 2006 (p. 34).

[22] E. Di Lorenzo, S. Manzato, F. Vanhollebeke, S. Goris, B. Peeters, W. Desmet, and F. Marulo. "Dynamic characterization of wind turbine gearboxes in operational conditions". In: *Proceedings of 9th International Conference on Rotor Dynamics (IFToMM 2014), Milan, Italy*. Sept. 2014 (pp. 146, 228).

[23] E. Di Lorenzo, S. Manzato, F. Vanhollebeke, S. Goris, B. Peeters, W Desmet, and F. Marulo. "Dynamic characterization of wind turbine gearboxes using Order-Based Modal Analysis". In: *Proceedings of 26th International Conference on Noise and Vibration Engineering (ISMA 2014), Leuven, Belgium*. Sept. 2014 (pp. 146, 228).

[24] E. Di Lorenzo, S. Manzato, M. A., B. Peeters, and W. Desmet. "Order-Based Modal Analysis vs. standard techniques to extract modal parameters of operational wind turbine geraboxes". In: *Submitted for 33rd International Modal Analysis Conference (IMAC 2015), Orlando, FL, USA*. Feb. 2015 (p. 146).

[25] E. Di Lorenzo, S. Manzato, J. Houben, F. Vanhollebeke, S. Goris, and B. Peeters. "Wind Turbine Gearbox Dynamic Characterization using Operational Modal Analysis". In: *Proceedings of 32nd International Modal Analysis Conference (IMAC 2014), Orlando, FL, USA*. Feb. 2014 (pp. 146, 228).

[26] DNV GL. *Bladed - ADVANCED TRANSMISSION INTERFACE MODULE*. URL: `http://www.gl-garradhassan.com/assets/img/content/ENG-Bladed_Advanced_Transmission_Interface_Module-ENGLISH-email-(SECURED)-Sep10.pdf` (p. 51).

[27] DNV GL. *Bladed: Product information*. 2014. URL: `http://www.gl-garradhassan.com/en/software/GHBladed.php` (p. 47).

[28] J. Dollhofer and F. Stache. "Smooth migration from FLEX5 to modern Multi-Body-Simulation: Comparison SIMPACK vs. FLEX5". In: *Proceedings of EWEA*. 2012 (p. 51).

[29] Dynamic Design Solutions NV. *FEMTools (TM) - Version 3.7*. Interleuvenlaan 64, 3001 Leuven, Belgium (pp. 67, 114).

[30] D. Eberly. *Intersection of a Line and a Cone*. Tech. rep. Ceometric Tools, LLC, 2008 (pp. 192, 193).

[31] Edenhofer, O., R. Pichs-Madruga, Y. Sokona, E. Farahani, S. Kadner, K. Seyboth, A. Adler, I. Baum, S. Brunner, P. Eickemeier, B. Kriemann, J. Savolainen, S. Schlömer, C. von Stechow, T. Zwickel and J.C. Minx (eds.) "IPCC, 2014: Summary for Policymakers". In: *Climate Change 2014, Mitigation of Climate Change. Contribution of Working Group III to the Fifth Assessment Report of the Intergovernmental Panel on Climate Change*. IPCC, 2013. URL: `http://report.mitigation2014.org/spm/ipcc_wg3_ar5_summary-for-policymakers_approved.pdf` (p. 15).

[32] *EU FP7 Project PROTEST*. URL: `http://www.protest-fp7.eu/` (p. 53).

[33] Field, C.B., V.R. Barros, D.J. Dokken, K.J. Mach, M.D. Mastrandrea, T.E. Bilir, M. Chatterjee, K.L. Ebi, Y.O. Estrada, R.C. Genova, B. Girma, E.S. Kissel, A.N. Levy, S. MacCracken, P.R. Mastrandrea, and L.L. White (eds.) *IPCC, 2014: Climate Change 2014: Impacts, Adaptation, and Vulnerability. Part A: Global and Sectoral Aspects. Contribution of Working Group II to the Fifth Assessment Report of the Intergovernmental Panel on Climate Change.* Cambridge University Press, Cambridge, United Kingdom and New York, NY, USA, 2014 (p. 14).

[34] K. Fowler, E. Koppen, and K. Matthis. "International Legislation and Regulations for Wind Turbine Noise". In: *Proceedings of 5th International Conference on Wind Turbine Noise*. 2013 (pp. 30, 32).

[35] P. Gajdátsy. "Advanced Transfer Path Analysis Methods (Geavanceerde transfer pad analysemethodes)". PhD thesis. Arenberg Doctoral School of Science, Engineering & Technology, 2011 (p. 162).

[36] E. Gargiulo. "A simple way to estimate bearing stiffness". In: *Machine design* 52 (1980), pp. 107–110 (p. 86).

[37] GL. *Guideline for the Certification of Wind Turbines*. Germanishcer LLoyd (GL), 2010 (p. 49).

[38] S. Goris, J. Peeters, F. Vanhollebeke, B. Marrant, W. Meeusen, J. Helsen, D. Vandepitte, and W. Desmet. "A validated approach for multibody models of megawatt wind turbine gearboxes". In: *Proceedings of Dresdner Maschinenelemente Kolloquium-DMK*. 2009 (p. 230).

[39] S. Goris, F. Vanhollebeke, A. Ribbentrop, M. Markiewicz, L. Schneider, S. Wartzack, W. Hendrickx, and W. Desmet. "A validated virtual prototyping approach for avoiding wind turbine tonality". In: *Proceedings of 5th International Conference on Wind Turbine Noise*. 2013 (pp. 6, 229).

[40] Y. Guo and R. Parker. "Stiffness matrix calculation of rolling element bearings using a finite element/contact mechanics model". In: *Mechanism and Machine Theory* 51 (2012), pp. 32–45. DOI: 10.1016/j.mechmachtheory.2011.12.006 (p. 86).

[41] Y. Guo, J. Keller, and R. Parker. "Dynamic analysis of wind turbine planetary gears using an extended harmonic balance approach". In: *Proceedings of the International Conference on Noise and Vibration Engineering ISMA 2012*. Leuven, Belgium, Sept. 2012, pp. 4329–4343 (p. 52).

[42] Y. Guo, J. Keller, and W. LaCava. "Combined effects of gravity, bending moment, bearing clearance and input torque on wind turbine planetary gear load sharing". In: *AGMA fall technical meeting, Dearborn*. 2012 (p. 52).

[43] Y. Guo, T. Eritenel, T. M. Ericson, and R. G. Parker. "Vibro-acoustic propagation of gear dynamics in a gear-bearing-housing system". In: *Journal of Sound and Vibration* 0 (2014), pp. –. ISSN: 0022-460X. DOI: http://dx.doi.org/10.1016/j.jsv.2014.05.055. URL: http://www.sciencedirect.com/science/article/pii/S0022460X14004878 (p. 56).

[44] M. Haastrup, O. Ø. Mouritsen, and M. R. Hansen. "Effect of introducing flexible bodies in multi body dynamics". In: *The Nordic Seminar on Computational Mechanics*. 2009, pp. 193–196 (p. 52).

[45] M. Haastrup, R Hansen, M. K. Ebbesen, and O. Ø. Mouritsen. "Modeling and parameter identification of deflections in planetary stage of wind turbine gearbox". In: *Modeling, Identification and Control* 33.1 (2012), pp. 1–11 (p. 52).

[46] M. Haastrup, M. R. Hansen, and M. K. Ebbesen. "Modeling of wind turbine gearbox mounting". In: *Modeling, Identification and Control* 32.4 (2012), pp. 141–149 (p. 52).

[47] M. Hajžman and V. Zeman. "Modelling of gearbox vibration and noise". In: *PAMM* 5.1 (2005), pp. 93–94 (p. 130).

[48] S. Hambric, M. Shepherd, and Campbell. "Modeling vibration transmission in gearbox/shafting systems using an augmented component mode synthesis approach". In: *NOVEM*. 2012 (pp. 55, 171).

[49] S. Hambric, A. Hanford, M. Shepherd, R. Campbell, and E. Smith. *Rotorcraft Transmission Noise Path Model, Including Distributed Fluid Film Bearing Impedance Modeling*. NASA Contractor Report NASA/CR-2010-216812. NASA, 2010 (pp. 55, 171).

[50] S. A. Hambric, M. R. Shepherd, R. L. Campbell, and A. D. Hanford. "Simulations and Measurements of the Vibroacoustic Effects of Replacing Rolling Element Bearings With Journal Bearings in a Simple Gearbox". In: *Journal of Vibration and Acoustics* 135.3 (2013), p. 031012 (p. 55).

[51] J Harms. "DLC Calculations with SIMPACK Scripting". In: *Proceedings of SIMPACK Conference Wind & Drivetrain, Hamburg, Germany*. Sept. 2012 (p. 51).

[52] T. Harris. *Rolling bearing analysis*. Vol. 6. Wiley, 1966 (p. 86).

[53] T. A. Harris and M. N. Kotzalas. *Essential concepts of bearing technology*. CRC press, 2006 (pp. 194, 195).

[54] S. Hauptmann, D. Matha, and T. Hecquet. "Aeroelastic Load Simulations and Aerodynamic and Structural Modeling Effects". In: *Proceedings of SIMPACK Conference Wind & Drivetrain, Hamburg, Germany*. June 2010 (p. 51).

[55] S. He, R. Singh, G. Pavic, et al. "Effect of sliding friction on gear noise based on a refined vibro-acoustic formulation". In: *Noise Control Engineering Journal* 56.3 (2008), pp. 164–175 (pp. 39, 54, 55, 179).

[56] A. Heckmann, I. Kaiser, and A. Carrarini. "Bridging the Gap from Multibody Simulations to Acoustic Analysis". In: *Noise and Vibration Mitigation for Rail Transportation Systems* (2012), pp. 107–115 (p. 132).

[57] A. Heege, J. Betran, and Y. Radovcic. "Fatigue load computation of wind turbine gearboxes by coupled finite element, multi-body system and aerodynamic analysis". In: *Wind Energy* 10.5 (2007), pp. 395–413 (p. 51).

[58] J. Heege A.and Hemmelmann. "UPWIND FP6 Integrated Project: SAMCEF Mecano model validation of GE 1.5MW wind turbine". In: *Proceedings of first SAMCEF for Wind Turbines Conference, Hamburg, Germany*. Nov. 2007 (p. 51).

[59] G. H. Heirman and W. Desmet. "Interface reduction of flexible bodies for efficient modeling of body flexibility in multibody dynamics". In: *Multibody System Dynamics* 24.2 (2010), pp. 219–234 (p. 91).

[60] J. Helsen. "The Dynamics of High Power Density Gear Units with Focus on the Wind Turbine Application". PhD thesis. KULeuven, 2012 (pp. 51, 62, 179).

[61] J. Helsen, F Vanhollebeke, and W Desmet. "Assessment of the effect on gearbox dynamics of wind turbine upscaling by means of flexible multibody models." In: *Proceedings of the SIMPEP FVA Kongress, Veitshöchheim, Germany*. 2011 (p. 229).

[62] J. Helsen, D. Vandepitte, W. Desmet, J. Peeters, S. Goris, F. Vanhollebeke, B. Marrant, and W. Meeusen. “From torsional towards flexbile 6 DOF models for dynamic analysis of wind tubine gearboxes”. In: *Proceedings of the European Wind Energy Conference and Exhibition (EWEC)*. 2009 (p. 230).

[63] J. Helsen, F. Vanhollebeke, F. De Coninck, D. Vandepitte, and W. Desmet. “Insights in wind turbine drive train dynamics gathered by validating advanced models on a newly developed 13.2 MW dynamically controlled test-rig”. In: *Mechatronics* 21.4 (2011), pp. 737–752 (pp. 57, 86, 141, 228).

[64] J. Helsen, F. Vanhollebeke, B. Marrant, D. Vandepitte, and W. Desmet. “Multibody modelling of varying complexity for modal behaviour analysis of wind turbine gearboxes”. In: *Renewable Energy: An International Journal* 36 (2011), pp. 3098–3113 (p. 228).

[65] J. Helsen, D. Brandolisio, B. Peeters, F. Vanhollebeke, J. Peeters, D. Moens, and W. Desmet. “Rated life potential of gearbox model based force estimates”. In: *Proceedings of IMAC XXXII conference*. 2014 (p. 229).

[66] J. Helsen, F. Vanhollebeke, B. Marrant, F. De Coninck, D. Vandepitte, and W. Desmet. “Updated flexible multibody wind turbine drivetrain model to determine excitation inputs for acoustic calculations”. In: *ECCOMAS Multibody Conference, Brussels*. July 2011 (pp. 57, 229).

[67] J. Helsen, B. Marrant, F. Vanhollebeke, F. D. Coninck, D. Berckmans, D. Vandepitte, and W. Desmet. “Assessment of excitation mechanisms and structural flexibility influence in excitation propagation in multi-megawatt wind turbine gearboxes: Experiments and flexible multibody model optimization”. In: *Mechanical Systems and Signal Processing* 40.1 (2013), pp. 114 –135. ISSN: 0888-3270. DOI: http://dx.doi.org/10.1016/j.ymssp.2012.12.001. URL: http://www.sciencedirect.com/science/article/pii/S0888327012004700 (pp. 57, 227).

[68] J. Helsen, F. Vanhollebeke, B. Marrant, D. Berckmans, D. Vandepitte, and W. Desmet. “Experimental assessment of gear meshing excitation propagation throughout multimegawatt gearboxes”. In: *Proceedings of IMAC, Jacksonville*. 2011 (p. 230).

[69] J. Helsen, F Vanhollebeke, and W Desmet. “How the upscaling trend in wind turbine design affects dynamic behaviour of the drive train”. In: *Proceedings of 53rd AIAA/ASME/ASCE/AHS/ASC Structures, Structural Dynamics and Materials Conference*. 2012 (p. 229).

[70] J. Helsen, F. Vanhollebeke, D. Vandepitte, and W. Desmet. "Optimized inclusion of flexibility in wind turbine gearbox multibody model in view of model updating on dynamic test rig". In: *Proceedings of the 1st international conference on multibody system dynamics*. May 2010 (pp. 57, 230).

[71] J. Helsen, F. Vanhollebeke, D. Vandepitte, and W. Desmet. "Some trends and challenges in wind turbine upscaling". In: *Proceedings of ISMA International Conference On Noise And Vibration*. 2012 (p. 229).

[72] J. Helsen, P. Peeters, K. Vanslambrouck, F. Vanhollebeke, and W. Desmet. "The Dynamic Behavior Induced by Different Wind Turbine Gearbox Suspension Methods Assessed by Means of the Flexible Multibody Technique". In: *Renewable Energy* 69 (2014), pp. 336–346. ISSN: 0960-1481. DOI: http://dx.doi.org/10.1016/j.renene.2014.03.036. URL: http://www.sciencedirect.com/science/article/pii/S0960148114002006 (pp. 38, 52, 227).

[73] J. Holierhoek, H Korterink, R. van de Pieterman, H Braam, L. Rademakers, D. Lekou, T Hecquet, and H Söker. "Recommended Practices for Measuring in Situ the Loads on Drive Train, Pitch System and Yaw System." In: *Energy Research Center of the Netherlands (ECN), deliverable report* (2010) (p. 53).

[74] IEC. *Wind turbines - Part 11: Acoustic noise measurement techniques*. 3.0. Geneva, Switzerland: International Electrotechnical Commission, 2012 (pp. 23, 157).

[75] IEC. *Wind turbines - Part 4: Design requirements for wind turbine gearboxes*. 1.0. Geneva, Switzerland: International Electrotechnical Commission, 2012 (pp. 35, 37).

[76] M. Inalpolat and A Kahraman. "A theoretical and experimental investigation of modulation sidebands of planetary gear sets". In: *Journal of Sound and Vibration* 323.3 (2009), pp. 677–696 (p. 100).

[77] ISO 9613-2. *Acoustics – Attenuation of sound during propagation outdoors – Part 2: General method of calculation*. ISO, 1996 (p. 33).

[78] M. F. Jacobson, R. Singh, and F. Oswald. "ACOUSTIC RADIATION EFFICIENCY MODELS OF A SIMPLE GEARBOX". In: *Proceedings of Seventh International Power Transmission and Gearing Conference, San Diego, California*. Oct. 1996 (p. 130).

[79] H. Jandrey and Schelenz. *Vorläufiger Abschlussbericht AG MKS FVA-Projekt 652 I Antriebsstrangdynamik*. Tech. rep. FVA, 2014 (p. 56).

[80] S. A. Janssen, H. Vos, A. R. Eisses, and E. Pedersen. “A comparison between exposure-response relationships for wind turbine annoyance and annoyance due to other noise sources”. In: *The Journal of the Acoustical Society of America* 130.6 (2011), pp. 3746–3753 (p. 28).

[81] U Jassmann, J Berroth, D Matzke, R Schelenz, M Reiter, G Jacobs, and D Abel. “Model predictive control of a wind turbine modelled in Simpack”. In: *Journal of Physics: Conference Series* 524.1 (2014), p. 012047. URL: http://stacks.iop.org/1742-6596/524/i=1/a=012047 (p. 51).

[82] J. Kim, J. Yoon, and B. Kang. “Finite element analysis and modeling of structure with bolted joints”. In: *Applied mathematical modelling* 31.5 (2007), pp. 895–911 (p. 72).

[83] W. LaCava, Y. Xing, Y Guo, and T. Moan. “Determining wind turbine gearbox model complexity using measurement validation and cost comparison”. In: *European Wind Energy Association annual event, Copenhagen* (2012) (p. 52).

[84] U. Landström, E. Åkerlund, A. Kjellberg, and M. Tesarz. “Exposure levels, tonal components, and noise annoyance in working environments”. In: *Environment International* 21.3 (1995), pp. 265–275 (p. 23).

[85] T. Lauwagie, F. Vanhollebeke, B. Pluymers, R. Zegels, P. Verschueren, and E. Dascotte. “The impact of high-fidelity model geometry on test-analysis correlation and FE model updating results. ” In: *Proceedings of the International Conference on Noise and Vibration Engineering ISMA 2010*. Leuven, Belgium, Sept. 2010, pp. 2679–2688 (pp. 70, 230).

[86] G. Lethé, D. Kinne, and I. Terna. “Dynamic simulation of a windturbine system calculating vibrations, loads, durability and acoustic response in a single cae environment”. In: *European Wind Energy Conference and Exhibition*. 2009 (p. 51).

[87] G. Lethé, J De Cuyper, J Kang, M. Furman, and D. Kading. “Simulating dynamics, durability and noise emission of wind turbines in a single CAE environment”. In: *Journal of mechanical science and technology* 23.4 (2009), pp. 1089–1093 (p. 51).

[88] M. Liesegang. *Sachstandsbericht AK Geräusche FVA 587 II project: Prognose der Luftschallabstrahlung von Getrieben*. Tech. rep. FVA, 2014 (p. 56).

[89] H. Liew and T. Lim. “Analysis of time-varying rolling element bearing characteristics”. In: *Journal of sound and vibration* 283.3 (2005), pp. 1163–1179 (p. 86).

[90] C. Liewen, G. Jacobs, and D. Bosse. “Full size nacelle testing on two different test benches”. In: *Proceedings of IQPC - Wind Turbine Simulation, Testing and Validation*. 2014 (p. 53).

[91] T. Lim and R. Singh. “Vibration transmission through rolling element bearings, part I: Bearing stiffness formulation”. In: *Journal of Sound and Vibration* 139.2 (1990), pp. 179–199 (pp. 54, 86, 88).

[92] T. Lim and R. Singh. “Vibration transmission through rolling element bearings, part II: system studies”. In: *Journal of sound and vibration* 139.2 (1990), pp. 201–225 (pp. 54, 86).

[93] T. Lim and R. Singh. “Vibration transmission through rolling element bearings. Part III: Geared rotor system studies”. In: *Journal of sound and vibration* 151.1 (1991), pp. 31–54 (p. 54).

[94] H Link, J Keller, Y Guo, and B McNiff. *Gearbox Reliability Collaborative Phase 3 Gearbox 2 Test Plan*. Tech. rep. National Renewable Energy Laboratory (NREL), Golden, CO., 2013 (p. 52).

[95] H Link, W LaCava, J Van Dam, B McNiff, S Sheng, R Wallen, M McDade, S Lambert, S Butterfield, and F Oyague. *Gearbox reliability collaborative project report: findings from phase 1 and phase 2 testing*. Technical Report NREL/TP-5000-51885. NREL, 2011 (p. 52).

[96] LMS. *The LMS FEM Acoustics manual*. LMS. 2009 (p. 131).

[97] LMS International NV. Interleuvenlaan 68, 3001 Leuven, Belgium (p. 66).

[98] LMS Samtech. *SAMCEF Wind Turbines - Product brochure*. URL: `http://www.plm.automation.siemens.com/en_us/products/lms/samtech/samcef-wind-turbines.shtml` (p. 51).

[99] J. F. Manwell, J. G. McGowan, and A. L. Rogers. *Wind Energy Explained: Theory, Design and Application*. John Wiley & Sons, 2010 (p. 18).

[100] S. Manzato, B. Peeters, A. Toso, R. Osgood, Y. Lemmens, and H. Van der Auweraer. “Full-scale multibody modeling of a wind turbine based on experimental data”. In: *Proceedings of the International Conference on Noise and Vibration Engineering ISMA 2010*. Leuven, Belgium, Sept. 2010, pp. 3845–3858 (p. 53).

[101] S. Manzato, B. Peeters, A. Toso, R. Osgood, and Y. Lemmens. “Optimization of a full-scale multibody model of a wind turbine based on experimental data.” In: *Proceedings of the 2nd International Conference on Engineering Optimization, Lisbon, Portugal*. Sept. 2010 (p. 53).

[102] B. Marrant, F. Vanhollebeke, and J. Peeters. “Comparison of multibody simulations and measurements of wind turbine gearboxes at Hansenś 13 MW test facility”. In: *Proceedings of the European Wind Energy Conference and Exhibition (EWEC), 20-23 April 2010, Warsaw, Poland*. 2010 (p. 230).

[103] F. Meng, M. Ozbek, D. Rixen, and M. van Tooren. "Comparison of System Identification Techniques for Predicting Dynamic Properties of Large Scale Wind Turbines by Using the Simulated Time Response". English. In: *Structural Dynamics and Renewable Energy, Volume 1*. Ed. by T. Proulx. Conference Proceedings of the Society for Experimental Mechanics Series. Springer New York, 2011, pp. 339–349. ISBN: 978-1-4419-9715-9. DOI: 10.1007/978-1-4419-9716-6_31. URL: http://dx.doi.org/10.1007/978-1-4419-9716-6_31 (p. 53).

[104] H. M. Miedema and H. Vos. "Exposure-response relationships for transportation noise". In: *The Journal of the Acoustical Society of America* 104 (1998), pp. 3432–3445 (p. 28).

[105] H. M. Miedema and H. Vos. "Noise annoyance from stationary sources: Relationships with exposure metric day–evening–night level (DENL) and their confidence intervals". In: *The Journal of the Acoustical Society of America* 116 (2004), pp. 334–343 (p. 28).

[106] H. Miedema and C. Oudshoorn. "Annoyance from transportation noise: relationships with exposure metrics DNL and DENL and their confidence intervals." In: *Environmental health perspectives* 109.4 (2001), pp. 409–416 (p. 28).

[107] D.-P. Molenaar. "Cost-effective design and operation of variable speed wind turbines". PhD thesis. Delft, The Nedtherlands: Delft University of Technology, 2002 (p. 48).

[108] J. Montgomery. "Methods for modeling bolts in the bolted joint". In: *ANSYS User's Conference, 22-24 April 2002, Pittsburgh, Pennsylvania*. 2002 (p. 72).

[109] W. Musial, S. Butterfield, and B. McNiff. "Improving wind turbine gearbox reliability". In: *European Wind Energy Conference, Milan, Italy*. 2007, pp. 7–10 (p. 52).

[110] B. Nortier, S. Voormeeren, and D. Rixen. "Application of Residual Vectors to Superelement Modeling of an Offshore Wind Turbine Foundation". English. In: *Topics in Experimental Dynamics Substructuring and Wind Turbine Dynamics, Volume 2*. Ed. by R. Mayes, D. Rixen, D. Griffith, D. De Klerk, S. Chauhan, S. Voormeeren, and M. Allen. Conference Proceedings of the Society for Experimental Mechanics Series. Springer New York, 2012, pp. 149–163. ISBN: 978-1-4614-2421-5. DOI: 10.1007/978-1-4614-2422-2_15. URL: http://dx.doi.org/10.1007/978-1-4614-2422-2_15 (p. 52).

[111] M. P. Norton and D. G. Karczub. *Fundamentals of noise and vibration analysis for engineers*. Cambridge university press, 2003 (p. 40).

[112] S. Oerlemans, P Sijtsma, and B Méndez López. "Location and quantification of noise sources on a wind turbine". In: *Journal of sound and vibration* 299.4 (2007), pp. 869–883 (pp. 25, 26).

[113] S. Oerlemans, M. Fisher, T. Maeder, and K. Kögler. "Reduction of wind turbine noise using optimized airfoils and trailing-edge serrations". In: *AIAA journal* 47.6 (2009), pp. 1470–1481 (p. 26).

[114] R. Osgood, G. Bir, H. Mutha, B. Peeters, M. Luczak, and G. Sablon. "Full-scale modal wind turbine tests: comparing shaker excitation with wind excitation". English. In: *Structural Dynamics and Renewable Energy, Volume 1*. Ed. by T. Proulx. Conference Proceedings of the Society for Experimental Mechanics Series. Springer New York, 2011, pp. 113–124. ISBN: 978-1-4419-9715-9. DOI: 10.1007/978-1-4419-9716-6_11. URL: http://dx.doi.org/10.1007/978-1-4419-9716-6_11 (p. 53).

[115] F. Oyague. *Gearbox modeling and load simulation of a baseline 750-kW wind turbine using state-of-the-art simulation codes - Technical Report NREL/TP-500-41160*. Tech. rep. National Renewable Energy Laboratory, 2009 (p. 52).

[116] F. Oyague, D Gorman, and S. Sheng. "NREL gearbox reliability collaborative experimental data overview and analysis". In: *Windpower Conference and Exhibition*. 2010 (pp. 52, 82).

[117] F. Oyague, D Gorman, and S Sheng. "Progressive dynamical drive train modeling as part of NREL gearbox reliability collaborative". In: *Windpower 2008 Conference and Exhibition*. 2008 (p. 52).

[118] S Øye. "FLEX4. Simulation of wind turbine dynamics". In: *Proceedings of the 28th IEA Meeting of Experts "State of the Art of Aeroelastic Codes for Wind Turbine Calculations"*. Technical University of Denmark, Lyngby, Denmark, Apr. 1996, pp. 71–76 (p. 47).

[119] M. Ozbek and D. J. Rixen. "Operational modal analysis of a 2.5 MW wind turbine using optical measurement techniques and strain gauges". In: *Wind Energy* 16.3 (2013), pp. 367–381. ISSN: 1099-1824. DOI: 10.1002/we.1493. URL: http://dx.doi.org/10.1002/we.1493 (p. 53).

[120] M. Ozbek and D. Rixen. "Optical Measurements and Operational Modal Analysis on a Large Wind Turbine: Lessons Learned". English. In: *Rotating Machinery, Structural Health Monitoring, Shock and Vibration, Volume 5*. Ed. by T. Proulx. Conference Proceedings of the Society for Experimental Mechanics Series. Springer New York, 2011, pp. 257–276. ISBN: 978-1-4419-9427-1. DOI: 10.1007/978-1-4419-9428-8_21. URL: http://dx.doi.org/10.1007/978-1-4419-9428-8_21 (p. 53).

[121] M. Ozbek, D. J. Rixen, O. Erne, and G. Sanow. “Feasibility of monitoring large wind turbines using photogrammetry”. In: *Energy* 35.12 (2010). The 3rd International Conference on Sustainable Energy and Environmental Protection, {SEEP} 2009, pp. 4802 –4811. ISSN: 0360-5442. DOI: http://dx.doi.org/10.1016/j.energy.2010.09.008. URL: http://www.sciencedirect.com/science/article/pii/S0360544210004871 (p. 53).

[122] M. Ozbek, F. Meng, D. Rixen, and M. van Tooren. “Identification of the Dynamics of Large Wind Turbines by Using Photogrammetry”. English. In: *Structural Dynamics and Renewable Energy, Volume 1*. Ed. by T. Proulx. Conference Proceedings of the Society for Experimental Mechanics Series. Springer New York, 2011, pp. 351–359. ISBN: 978-1-4419-9715-9. DOI: 10.1007/978-1-4419-9716-6_32. URL: http://dx.doi.org/10.1007/978-1-4419-9716-6_32 (p. 53).

[123] H. N. Özgüven and D. Houser. “Mathematical models used in gear dynamics. A review”. In: *Journal of Sound and Vibration* 121.3 (1988), pp. 383 –411. ISSN: 0022-460X. DOI: http://dx.doi.org/10.1016/S0022-460X(88)80365-1. URL: http://www.sciencedirect.com/science/article/pii/S0022460X88803651 (pp. 53, 179).

[124] R. Parker and J Lin. “Mesh phasing relationships in planetary and epicyclic gears”. In: *ASME 2003 International Design Engineering Technical Conferences and Computers and Information in Engineering Conference*. American Society of Mechanical Engineers. 2003, pp. 525–534 (p. 100).

[125] R. G. Parker. “A physical explanation for the effectiveness of planet phasing to suppress planetary gear vibration”. In: *Journal of Sound and Vibration* 236.4 (2000), pp. 561–573 (p. 100).

[126] R. G. Parker, Y. Guo, T. Eritenel, and T. M. Ericson. *Vibration Propagation of Gear Dynamics in a Gear-Bearing-Housing System Using Mathematical Modeling and Finite Element Analysis*. NASA Contractor Report NASA/CR-2012-217664. NASA, 2012 (pp. 56, 86).

[127] E. Pedersen and K. Waye. “Perception and annoyance due to wind turbine noise. A dose-response relationship”. In: *The Journal of the Acoustical Society of America* 116 (2004), p. 3460 (p. 28).

[128] E. Pedersen and K. P. Waye. “Wind turbine noise, annoyance and self-reported health and well-being in different living environments”. In: *Occupational and Environmental Medicine* 64.7 (2007), pp. 480–486 (p. 28).

[129] E. Pedersen, F. van den Berg, R. Bakker, and J. Bouma. "Response to noise from modern wind farms in The Netherlands". In: *The Journal of the Acoustical Society of America* 126 (2009), p. 634 (p. 28).

[130] B. Peeters, H. Van der Auweraer, F. Vanhollebeke, and P. Guillaume. "Operational modal analysis for estimating the dynamic properties of a stadium structure during a football game". In: *Shock and Vibration* 14.4 (2007), pp. 283–303 (p. 228).

[131] B. Peeters, F. Vanhollebeke, and H. Van der Auweraer. "Operational PolyMAX for estimating the dynamic properties of a stadium structure during a football game". In: *Proceedings of the IMAC conference*. Vol. 23. 2005 (p. 231).

[132] J. Peeters. "Simulation of dynamic drive train loads in a wind turbine". PhD thesis. KULeuven, 2006 (pp. 19, 48–50, 178).

[133] J. Peeters, S. Goris, F. Vanhollebeke, B. Marrant, and W. Meeusen. "A need for advanced and validated multibody models as a basis for more accurate dynamic load prediction in multi-megawatt wind turbine gearboxes". In: *Proceedings of the International Conference on Noise and Vibration Engineering ISMA*. 2008, pp. 2097–2112 (pp. 50, 231).

[134] J. Peeters, D. Vandepitte, and P. Sas. "Flexible multibody model of a three-stage planetary gearbox in a wind turbine". In: *Proceedings of the International Conference on Noise and Vibration Engineering ISMA, Leuven, Belgium*. 2004, pp. 3923–3941 (p. 50).

[135] J. Peeters, S. Goris, F. Vanhollebeke, B. Marrant, J. Helsen, D. Vandepitte, and W. Desmet. "Insights in multimegawatt wind turbine gearbox dynamics using a validated multibody modeling approach". In: *ATK*. 2009 (p. 230).

[136] P. Peeters, T. Tamarozzi, F. Vanhollebeke, and W. Desmet. "A robust approach for substructure decoupling". In: *Proceedings of the International Conference on Noise and Vibration Engineering ISMA 2014, 15–17 September*. Leuven, Belgium, Sept. 2014, pp. 3907–3921 (p. 228).

[137] B Petitjean, R Drobietz, and K Kinzie. "Wind Turbine Blade Noise Mitigation Technologies". In: *Proceedings of Wind Turbine Noise, Rome, Italy*. 2011 (pp. 25–27).

[138] R. Platt and R. Leopold. "A study on helical gear planetary phasing effects on transmission noise". In: *VDI BERICHTE* 1230 (1996), pp. 793–808 (p. 100).

[139] T. J. Price. "James Blyth–Britain's first modern wind power pioneer". In: *Wind engineering* 29.3 (2005), pp. 191–200 (p. 17).

[140] Y. Radovcic. “Structural Simulation Validation at AREVA Wind”. In: *Proceedings of IQPC Bremen*. July 2014 (p. 51).

[141] R. Ramachandran, G. Raman, and R. Dougherty. “Wind Turbine Field Measurements With Compact Microphone Array Using Advanced Beamforming Methods”. In: *18th AIAA/CEAS Aeroacoustics Conference (33rd AIAA Aeroacoustics Conference)*. 2012 (p. 26).

[142] A. v. Roosmalen. “Design tools for low noise gear transmissions”. PhD thesis. Eindhoven University of Technology, Faculty of Mechanical Engineering, Power Transmissions and Tribology Laboratory, Eindhoven, 1994. DOI: 10.6100/IR423648. URL: http://dx.doi.org/10.6100/IR423648 (p. 54).

[143] F. Savenije and K. Boorsma. “Multi body simulations at ECN wind. Coupling of ECN software”. In: *Proceedings of SIMPACK Conference Wind & Drivetrain, Hamburg, Germany*. June 2010 (p. 51).

[144] R. Schelenz, F. Barenhorst, and L. Bi. “Messung und Modellvalidierung an einem 1 MW WEA Gondelsystemprüfstand im Hinblick auf zukünftige Zertifizierungsprozeduren”. In: *Proceedings of the VDI-Fachtagung Schwingungen von Windenergieanlagen, Bremen, 19-20 February 2013*. 2013 (p. 56).

[145] J. Schepers, J. Heijdra, D. Foussekis, S. Øye, R. Rawlinson Smith, M. Belessis, K. Thomsen, T. Larsen, I. Kraan, B. Visser, I. Carlen, H. Ganander, and L. Drost. *Verification of European wind turbine design codes, VEWTDC: final report*. Energy Research Centre of the Netherlands (ECN), 2003 (p. 48).

[146] B. Schlecht and T. Schulze. “Simulation of Drive Trains in Wind Turbines with SIMPACK”. In: *SIMPACK Users Meeting*. 2003 (p. 51).

[147] B. Schlecht, T. Rosenlöcher, and T. Schulze. “Efficient Strategies To Determine Reliable Load Assumptions For Wind Turbine Components”. In: *Proceedings of the European wind energy conference (EWEC), Warsaw*. 2010 (p. 51).

[148] B. Schlecht, S. Mtauweg, and T. Rosenlöcher. “Ermittlung realistischer Lastannahmen für das Pitchsystem und Festlegung der Regelungsstrategie einer Windenergieanlage mittels Mehrkörpersimulation”. In: *Proceedings of VDI-Tagung: Schwingungen von Windenergieanlagen, Bremen, Germany*. Feb. 2011 (pp. 51, 56).

[149] B Schlecht, T Shulze, and T. Hähnel. “Multibody-System-Simulation of Wind Turbines for Determination of Additional Dynamic Loads”. In: *SIMPACK Users Meeting*. 2004, pp. 09–10 (pp. 51, 56).

[150] B. Schlecht, T. Rosenlöcher, and T. Hähnel. “Strategy for User Orientated Simulation of Large Drive Trains to Calculate Realistic Load Conditions”. In: *Proceedings of the International Conference on Noise and Vibration Engineering ISMA, Leuven, Belgium*. 2008, pp. 2129–2142 (p. 51).

[151] Senvion. *The perfect choice for your location. The Senvion 3.XM series. - Senvion 3.XM Series Product Brochure*. Accessed on 23 August 2014 from `http://www.senvion.com/fileadmin/user_upload/02_WindPowerSolutions/ProductBrochures/Senvion_3.XM_Brochure_EN.pdf` (p. 19).

[152] A. A. Shabana. *Dynamics of multibody systems*. Fourth edition. Cambridge University Press, New York, 2013. ISBN: 9781107337213. URL: `http://dx.doi.org/10.1017/CBO9781107337213` (pp. 61, 81).

[153] J. Shigley, C. Mischke, R. Budynas, X. Liu, and Z. Gao. *Mechanical engineering design*. Vol. 89. McGraw-Hill New York, 1989 (p. 73).

[154] D. Siano and F. Bozza. “Noise Prediction of a Multi-Cylinder Engine Prototype Using Multi-Body Dynamic Simulation”. In: *Proceedings of 10th International Conference on Engines & Vehicles, Naples, ITALY, Session: Noise*. Sept. 2011. DOI: `10.4271/2011-24-0216` (p. 132).

[155] Simpack AG. *SIMPACK User Manual*. Simpack AG. Friedrichshafener Strasse 1, D-82205 Gilching, Germany, 2012 (p. 61).

[156] Simpack AG. *Simpack Wind - Product brochure*. URL: `http://www.simpack.com/industrial_sectors_wind.html` (p. 51).

[157] F. Stache. “The Use of Simpack in Wind Turbine Development”. In: *Proceedings of SIMPACK Conference Wind & Drivetrain, Hamburg, Germany*. Sept. 2012 (p. 51).

[158] M. Stigwood, S. Large, and S. D. “Audible amplitude modulation - results of field measurements and investigations compared to psycho-acoustical assessment and theoretical research”. In: *Proceedings of 5th International Conference on Wind Turbine Noise*. 2013 (p. 22).

[159] S. Sun, Y. Zheng, G. Ni, and J. ZHANG. “Multi-body dynamics analysis and low noise optimization of X6170ZC diesel”. In: *Transactions of Tianjin University* 13 (2007), pp. 297–302 (pp. 130, 132).

[160] *SYSNOISE Rev 5.5 Userś Manual*. LMS International. 2000 (p. 135).

[161] T.F. and D. Qin and G.-K. Plattner and M. Tignor and S.K. Allen and J. Boschung and A. Nauels and Y. Xia and V. Bex and P.M. Midgley. “IPCC, 2013: Summary for Policymakers”. In: *Climate Change 2013: The Physical Science Basis. Contribution of Working Group I to the Fifth Assessment Report of the Intergovernmental Panel on Climate Change*. IPCC, 2013. URL: `http://www.climatechange2013.org/images/report/WG1AR5_SPM_FINAL.pdf` (p. 14).

[162] K. Tietzel and T. Hahn. “Enhanced Modeling of Rolling Bearings”. In: *SIMPACK News* December (Dec. 2012), pp. 7–9. URL: http://www.simpack.com/fileadmin/simpack/doc/newsletter/2012/Dec_2012/SN-2-Dec-2012_Schaeffler_Modleing_rolling_Bearings.pdf (p. 88).

[163] M. Tournour, S. Dessart, and C. McCulloch. “On the accuracy of vibro-acoustic solutions using the ATV method”. In: *Proceedings of the International Conference on Noise and Vibration Engineering ISMA, Leuven, Belgium*. Sept. 2002 (p. 133).

[164] M. Tournour, J. Rossion, L. Bricteux, and C. McCulloch. “Speeding-up acoustic predictions”. In: *Proceedings of IMAC-XXII: Conference & Exposition on Structural Dynamics - Linking Test to Design* (p. 133).

[165] F. Vanhollebeke, J. Helsen, J. Peeters, D. Vandepitte, and W. Desmet. “Combining multibody and acoustic simulation models for wind turbine gearbox NVH optimisation”. In: *Proceedings of the International Conference on Noise and Vibration Engineering ISMA, Leuven, Belgium*. 2012 (p. 229).

[166] F. Vanhollebeke, P. Peeters, J. Helsen, E. Di Lorenzo, S. Manzato, J. Peeters, D. Vandepitte, and W. Desmet. “Large scale validation of a flexible multibody wind turbine gearbox model”. In: *Accepted for: Journal of Computational and Nonlinear Dynamics - Special Issue on Wind Turbine Modeling and Simulation* (2014) (p. 227).

[167] F. Vanhollebeke, J. Peeters, D. Vandepitte, and W. Desmet. “Using transfer path analysis to assess the influence of bearings on structural vibrations of a wind turbine gearbox”. In: *Wind Energy* (2014). DOI: 10.1002/we.1729 (p. 227).

[168] K Vansant, R Hallez, H Bériot, M Tournour, G Massa, S Donders, and H Van der Auweraer. “Simulating acoustic engine performance over a broad frequency range”. In: *Symposium on International Automotive Technology*. 2011 (p. 131).

[169] F Viadero, A Fernández, M Iglesias, A de Juan, E Liaño, and M. Serna. “Non-stationary dynamic analysis of a wind turbine power drivetrain: Offshore considerations”. In: *Applied Acoustics* 77 (2014), pp. 204–211 (p. 51).

[170] C. M. Vicuña. “Vibration characteristics of single-stage planetary gear transmissions.” In: *INGENIARE-Revista Chilena de Ingeniería* 22.1 (2014), pp. 88–98 (p. 40).

[171] O. Von Estorff. “Efforts to Reduce Computation Time in Numerical Acoustics An Overview”. In: *Acta acustica united with acustica* 89.1 (2003), pp. 1–13 (pp. 130, 133).

[172] S. N. Voormeeren, P. L. C. van der Valk, B. P. Nortier, D.-P. Molenaar, and D. J. Rixen. "Accurate and efficient modeling of complex offshore wind turbine support structures using augmented superelements". In: *Wind Energy* 17.7 (2014), pp. 1035–1054. ISSN: 1099-1824. DOI: 10.1002/we.1617. URL: http://dx.doi.org/10.1002/we.1617 (p. 52).

[173] S. Voormeeren. "Dynamic Substructuring Methodologies for Integrated Dynamic Analysis of Wind Turbines". PhD thesis. TUDelft, 2012. DOI: doi:10.4233/uuid:f45f0548-d5ec-46aa-be7e-7f1c2b57590d. URL: http://dx.doi.org/10.4233/uuid:f45f0548-d5ec-46aa-be7e-7f1c2b57590d (p. 52).

[174] S. Voormeeren, P. van der Valk, and D. Rixen. "Practical Aspects of Dynamic Substructuring in Wind Turbine Engineering". English. In: *Structural Dynamics and Renewable Energy, Volume 1*. Ed. by T. Proulx. Conference Proceedings of the Society for Experimental Mechanics Series. Springer New York, 2011, pp. 163–185. ISBN: 978-1-4419-9715-9. DOI: 10.1007/978-1-4419-9716-6_16. URL: http://dx.doi.org/10.1007/978-1-4419-9716-6_16 (p. 52).

[175] S. Wagner, R. Bareiss, G. Guidati, and . Wagner-Bareiß-Guidati. "Wind turbine noise". In: (1996) (pp. 25, 27).

[176] C. R. Warren and M. McFadyen. "Does community ownership affect public attitudes to wind energy? A case study from south-west Scotland". In: *Land Use Policy* 27.2 (2010), pp. 204–213 (p. 28).

[177] T. M. Wasfy and A. K. Noor. "Computational strategies for flexible multibody systems". In: *Applied Mechanics Reviews* 56.6 (2003), pp. 553–613 (p. 61).

[178] D. Welbourn. *Fundamental knowledge of gear noise: a survey.* Tech. rep. 1979 (p. 39).

[179] R. E. Wilson, S. N. Walker, and P. Heh. *Technical and user's manual for the FAST-AD advanced dynamic code.* Department of Mechanical Engineering. Oregon State University, Corvallis, US, 1999 (p. 47).

[180] C. Xia and Z. Zhang. "Simulation Analysis on Engine Radiated Noise". In: *Advanced Materials Research* 421 (2012), pp. 354–359 (p. 132).

[181] H. Zhou, M. Kato, K. Inoue, and K. Shibata. "Influence of bearing positions on sound radiation of single-stage spur gear system". In: *JSME international journal. Series C, dynamics, control, robotics, design and manufacturing* 40.1 (1997), pp. 128–134 (p. 171).

[182] C. Zhu, B Lu, C. Song, and D. Qin. "Dynamic analysis of a heavy duty marine gearbox with gear mesh coupling". In: *Proceedings of the Institution of Mechanical Engineers, Part C: Journal of Mechanical Engineering Science* 223.11 (2009), pp. 2531–2547 (p. 54).

List of publications

International peer reviewed journal articles

F. Vanhollebeke, P. Peeters, J. Helsen, E. Di Lorenzo, S. Manzato, J. Peeters, D. Vandepitte, and W. Desmet. "Large scale validation of a flexible multibody wind turbine gearbox model". In: *Accepted for: Journal of Computational and Nonlinear Dynamics - Special Issue on Wind Turbine Modeling and Simulation* (2014)

F. Vanhollebeke, J. Peeters, D. Vandepitte, and W. Desmet. "Using transfer path analysis to assess the influence of bearings on structural vibrations of a wind turbine gearbox". In: *Wind Energy* (2014). DOI: 10.1002/we.1729

J. Helsen, P. Peeters, K. Vanslambrouck, F. Vanhollebeke, and W. Desmet. "The Dynamic Behavior Induced by Different Wind Turbine Gearbox Suspension Methods Assessed by Means of the Flexible Multibody Technique". In: *Renewable Energy* 69 (2014), pp. 336–346. ISSN: 0960-1481. DOI: http://dx.doi.org/10.1016/j.renene.2014.03.036. URL: http://www.sciencedirect.com/science/article/pii/S0960148114002006

J. Helsen, B. Marrant, F. Vanhollebeke, F. D. Coninck, D. Berckmans, D. Vandepitte, and W. Desmet. "Assessment of excitation mechanisms and structural flexibility influence in excitation propagation in multi-megawatt wind turbine gearboxes: Experiments and flexible multibody model optimization". In: *Mechanical Systems and Signal Processing* 40.1 (2013), pp. 114 –135. ISSN: 0888-3270. DOI: http://dx.doi.org/10.1016/j.ymssp.2012.12.001. URL: http://www.sciencedirect.com/science/article/pii/S0888327012004700

J. Helsen, F. Vanhollebeke, B. Marrant, D. Vandepitte, and W. Desmet. "Multibody modelling of varying complexity for modal behaviour analysis of wind turbine gearboxes". In: *Renewable Energy: An International Journal* 36 (2011), pp. 3098–3113

J. Helsen, F. Vanhollebeke, F. De Coninck, D. Vandepitte, and W. Desmet. "Insights in wind turbine drive train dynamics gathered by validating advanced models on a newly developed 13.2 MW dynamically controlled test-rig". In: *Mechatronics* 21.4 (2011), pp. 737–752

B. Peeters, H. Van der Auweraer, F. Vanhollebeke, and P. Guillaume. "Operational modal analysis for estimating the dynamic properties of a stadium structure during a football game". In: *Shock and Vibration* 14.4 (2007), pp. 283–303

Full papers in proceedings of international conferences

P. Peeters, T. Tamarozzi, F. Vanhollebeke, and W. Desmet. "A robust approach for substructure decoupling". In: *Proceedings of the International Conference on Noise and Vibration Engineering ISMA 2014, 15–17 September*. Leuven, Belgium, Sept. 2014, pp. 3907–3921

E. Di Lorenzo, S. Manzato, J. Houben, F. Vanhollebeke, S. Goris, and B. Peeters. "Wind Turbine Gearbox Dynamic Characterization using Operational Modal Analysis". In: *Proceedings of 32nd International Modal Analysis Conference (IMAC 2014), Orlando, FL, USA*. Feb. 2014

E. Di Lorenzo, S. Manzato, F. Vanhollebeke, S. Goris, B. Peeters, W Desmet, and F. Marulo. "Dynamic characterization of wind turbine gearboxes using Order-Based Modal Analysis". In: *Proceedings of 26th International Conference on Noise and Vibration Engineering (ISMA 2014), Leuven, Belgium*. Sept. 2014

E. Di Lorenzo, S. Manzato, F. Vanhollebeke, S. Goris, B. Peeters, W. Desmet, and F. Marulo. "Dynamic characterization of wind turbine gearboxes in operational conditions". In: *Proceedings of 9th International Conference on*

Rotor Dynamics (IFToMM 2014), Milan, Italy. Sept. 2014

J. Helsen, D. Brandolisio, B. Peeters, F. Vanhollebeke, J. Peeters, D. Moens, and W. Desmet. "Rated life potential of gearbox model based force estimates". In: *Proceedings of IMAC XXXII conference.* 2014

B. Blockmans, J. Helsen, F. Vanhollebeke, and W. Desmet. "Dynamic Response of a Multi-megawatt Wind Turbine Drivetrain under Voltage Dips using a Coupled Flexible Multibody Approach". In: *Proceedings of the ASME 2013 International Design Engineering Technical Conferences & Computers and Information in Engineering Conference, Portland, Oregon.* DETC2013-12458. Aug. 2013

S. Goris, F. Vanhollebeke, A. Ribbentrop, M. Markiewicz, L. Schneider, S. Wartzack, W. Hendrickx, and W. Desmet. "A validated virtual prototyping approach for avoiding wind turbine tonality". In: *Proceedings of 5th International Conference on Wind Turbine Noise.* 2013

J. Helsen, F. Vanhollebeke, D. Vandepitte, and W. Desmet. "Some trends and challenges in wind turbine upscaling". In: *Proceedings of ISMA International Conference On Noise And Vibration.* 2012

J. Helsen, F Vanhollebeke, and W Desmet. "How the upscaling trend in wind turbine design affects dynamic behaviour of the drive train". In: *Proceedings of 53rd AIAA/ASME/ASCE/AHS/ASC Structures, Structural Dynamics and Materials Conference.* 2012

F. Vanhollebeke, J. Helsen, J. Peeters, D. Vandepitte, and W. Desmet. "Combining multibody and acoustic simulation models for wind turbine gearbox NVH optimisation". In: *Proceedings of the International Conference on Noise and Vibration Engineering ISMA, Leuven, Belgium.* 2012

J. Helsen, F. Vanhollebeke, B. Marrant, F. De Coninck, D. Vandepitte, and W. Desmet. "Updated flexible multibody wind turbine drivetrain model to determine excitation inputs for acoustic calculations". In: *ECCOMAS Multibody Conference, Brussels.* July 2011

J. Helsen, F Vanhollebeke, and W Desmet. "Assessment of the effect on gearbox

dynamics of wind turbine upscaling by means of flexible multibody models." In: *Proceedings of the SIMPEP FVA Kongress, Veitshöchheim, Germany.* 2011

J. Helsen, F. Vanhollebeke, B. Marrant, D. Berckmans, D. Vandepitte, and W. Desmet. "Experimental assessment of gear meshing excitation propagation throughout multimegawatt gearboxes". In: *Proceedings of IMAC, Jacksonville.* 2011

T. Lauwagie, F. Vanhollebeke, B. Pluymers, R. Zegels, P. Verschueren, and E. Dascotte. "The impact of high-fidelity model geometry on test-analysis correlation and FE model updating results. " In: *Proceedings of the International Conference on Noise and Vibration Engineering ISMA 2010.* Leuven, Belgium, Sept. 2010, pp. 2679–2688

J. Helsen, F. Vanhollebeke, D. Vandepitte, and W. Desmet. "Optimized inclusion of flexibility in wind turbine gearbox multibody model in view of model updating on dynamic test rig". In: *Proceedings of the 1st international conference on multibody system dynamics.* May 2010

B. Marrant, F. Vanhollebeke, and J. Peeters. "Comparison of multibody simulations and measurements of wind turbine gearboxes at Hansenś 13 MW test facility". In: *Proceedings of the European Wind Energy Conference and Exhibition (EWEC), 20-23 April 2010, Warsaw, Poland.* 2010

J. Helsen, D. Vandepitte, W. Desmet, J. Peeters, S. Goris, F. Vanhollebeke, B. Marrant, and W. Meeusen. "From torsional towards flexbile 6 DOF models for dynamic analysis of wind tubine gearboxes". In: *Proceedings of the European Wind Energy Conference and Exhibition (EWEC).* 2009

S. Goris, J. Peeters, F. Vanhollebeke, B. Marrant, W. Meeusen, J. Helsen, D. Vandepitte, and W. Desmet. "A validated approach for multibody models of megawatt wind turbine gearboxes". In: *Proceedings of Dresdner Maschinenelemente Kolloquium-DMK.* 2009

J. Peeters, S. Goris, F. Vanhollebeke, B. Marrant, J. Helsen, D. Vandepitte, and W. Desmet. "Insights in multimegawatt wind turbine gearbox dynamics using a validated multibody modeling approach". In: *ATK.* 2009

J. Peeters, S. Goris, F. Vanhollebeke, B. Marrant, and W. Meeusen. “A need for advanced and validated multibody models as a basis for more accurate dynamic load prediction in multi-megawatt wind turbine gearboxes”. In: *Proceedings of the International Conference on Noise and Vibration Engineering ISMA*. 2008, pp. 2097–2112

B. Peeters, F. Vanhollebeke, and H. Van der Auweraer. “Operational PolyMAX for estimating the dynamic properties of a stadium structure during a football game”. In: *Proceedings of the IMAC conference*. Vol. 23. 2005

FACULTY OF ENGINEERING SCIENCE
DEPARTMENT OF MECHANICAL ENGINEERING
PRODUCTION ENGINEERING, MACHINE DESIGN AND AUTOMATION (PMA)
Celestijnenlaan 300
B-3001 Heverlee
frederik.vanhollebeke@zf.com